Bell Laboratories

FINAL REPORT ON

REDUCTION AND ANALYSIS OF PARTICLE DATA FROM EXPLORER XV AND EXPLORER XXVI

by
W. L. Brown, L. J. Lanzerotti, et. al.

Contract NAS 5-3058

FEBRUARY 28, 1971

Period Covered September 1962 - August 1970

prepared by
Radiation Physics Research Department
Bell Telephone Laboratories, Incorporated
Mountain Avenue, Murray Hill, New Jersey 07974
Dr. W. L. Brown — Principal Investigator
on behalf of
Western Electric Company, Incorporated
83 Maiden Lane, New York, N.Y. 10038
for
Goddard Space Flight Center
Greenbelt, Maryland 20771
Mr. L. R. Davis — Technical Monitor

1. Report No.	2. Government Accession No.	3. Recipient's Catalog No.

4. TITLE AND SUBTITLE FINAL REPORT ON REDUCTION AND ANALYSIS OF PARTICLE DATA FROM EXPLORER XV AND EXPLORER XXVI	5. Report Date February 28, 1971
	6. Performing Organization Code
7. Authors W. L. Brown, L. J. Lanzerotti, et. al.	8. Performing Organization Report No.
9. Performing Organization Name and Address Bell Telephone Laboratories, Incorporated Murray Hill, New Jersey 07974 on behalf of Western Electric Company, Incorporated New York, New York 10038 Dr. W. L. Brown - Principal Investigator	10. Work Unit No.
	11. Contract or Grant No. NAS 5-3058
	13. Type of Report and Period Covered Final Report
12. Sponsoring Agency Name and Address National Aeronautics and Space Administration Goddard Space Flight Center Greenbelt, Maryland 20771 Mr. L. R. Davis - Technical Monitor	14. Sponsoring Agency Code
15. Supplementary Notes	

16. Abstract

This report consolidates material prepared by investigators who participated in the analysis of particle data acquired by Bell Laboratories particle detection equipment on Explorer XV and Explorer XXVI satellites. Results of studies contained in this report concern the distribution of charged particles trapped in the radiation belts around the earth which were traversed by the two satellites. This material has been presented at meetings in the form of talks and papers and in articles appearing in scientific journals. This report does not contain information included in the final report on Explorer XV dated June 30, 1964.

17. Key Words Explorer Particle Data Analysis Particles in Radiation Belts-Analysis Electrons and Protons during Geomagnetic Storms	18. Distribution Statement

19. Security Classif. (of this report)	20. Security Classif. (of this page)	21. No. of Pages	22. Price

PREFACE

This is the last of two final reports on a program which was initiated in 1962 to design and fabricate particle detection equipment for the Explorer XV and Explorer XXVI satellites and to provide data reduction and analysis services for particle data obtained from the equipment. Explorer XV was launched October 27, 1962 and acquired useful data for approximately one-hundred days. Explorer XXVI successfully acquired useful data from December 21, 1964 when it was launched until May 25, 1967 when it was turned off by NASA/GSFC. The preceding final report entitled "Final Report on Bell Telephone Laboratories Experiments on Explorer XV, Project SERB, Study on the Enhanced Radiation Belts, Contract NAS5-3058," dated June 30, 1964, was furnished to NASA/GSFC in July 1964.

The data reduction and analysis work carried out under this contract consisted of two tasks. The first task involved a study of the angular distribution and energy spectra of electron and proton fluxes in the earth's radiation zones. Both Explorer XV and Explorer XXVI were involved in this task. However, Explorer XV placed emphasis on studying the electrons artificially introduced into the inner radiation zone by high altitude nuclear explosions occurring in 1962. The second task, involving only Explorer XV, was an investigation of radiation damage to solar cells due to the exposure to charged particles in space.

Material presented in this report primarily concerns analysis of Explorer XXVI data. However, some Explorer XV results are included that were not available when the previous Explorer XV final report was prepared. Some of the results of work on Telstar I data, not covered by this contract but considered to be relevant, have also been included.

In accordance with original plans, all scientifically significant information derived from the data reduction and analysis work has been disseminated. This has been accomplished by means of talks at scientific meetings and articles presented in scientific publications. This report contains all such Bell Laboratories presentations encompassed by this contract. The authors of the various chapters of this report are Dr. W. L. Brown, Dr. C. S. Roberts, Dr. L. J. Lanzerotti, Dr. A. Hasegawa, Miss C. G. Maclennan, and Dr. J. G. Gabbe, all of Bell Laboratories; Dr. L. J. Cahill of the University of New Hampshire, Mr. L. R. Davis of NASA/GFSC, Dr. C. E. McIlwain of the University of California, and Dr. M. Schulz of the Aerospace Corporation.

TABLE OF CONTENTS

TABLE OF CONTENTS (continued)

TABLE OF CONTENTS (continued)

LIST OF TABLES

LIST OF ILLUSTRATIONS

CHAPTER 1

STUDIES OF TRAPPED RADIATION BY THE TELSTAR I AND EXPLORER XV SATELLITES

W. L. BROWN

Bell Telephone Laboratories, Inc., Murray Hill, N.J.

1. Introduction

This paper on particles in the trapped radiation belts might seem to be out of place at a conference on plasma space science. It does not deal at all directly with the structure of the solar wind or the boundary of the magnetosphere or with the aurora or the ionosphere. On the other hand, plasmas interact extremely broadly with particles and fields and there are important connections between the natural plasmas in space and the particles trapped within the magnetosphere. This paper will point to a few specific cases of this kind in which present understanding is extremely primitive if it exists at all. In addition this paper will deal with the consequences of the special plasmas created by nuclear explosions in space. These sources of new particles, controversial as they are in many respects, have provided some extremely interesting geophysical information on trapping in the radiation belts.

All of the observations of the Telstar I and Explorer XV satellites with which this paper is concerned have been made well within the magnetosphere at maximum radial distances of about 4 earth radii and at latitudes of less than 50°. This is a region in which the motion of charged particles is controlled by the magnetic field of the earth. In order to organize data on these trapped particles McIlwain (1961) devised a coordinate system which in effect maps the stable but irregular magnetic field of the earth on a dipole field with the same dipole moment, using the adiabatic invariants of the particle motion. His B,L-coordinate system is illustrated in Figure 1. The magnetic field lines are labelled with L, a coordinate specifying the radial distance of the crossing of the field line through the equatorial plane, and B, the magnetic field intensity on a given L line, a minimum at the equator and increasing in magnitude toward either pole. Position in the equivalent dipole space can be specified by B and L or alternatively by R and λ, the radial distance and dipole latitude as shown in the figure. Results in an R-λ representation are more easily visualized because of the pseudogeographic character of these coordinates. In the R-λ space the surface of the earth is extremely irregular since the magnetic field now serves as the frame of reference.

Charged particles move in spiral paths around the magnetic field lines and bounce between mirror points at magnetic field intensity B_m. In addition, the particles drift in longitude as a result of the radial gradient of the magnetic field and the curvature of the magnetic field lines. In this drift, particles stay on lines of constant L and fill

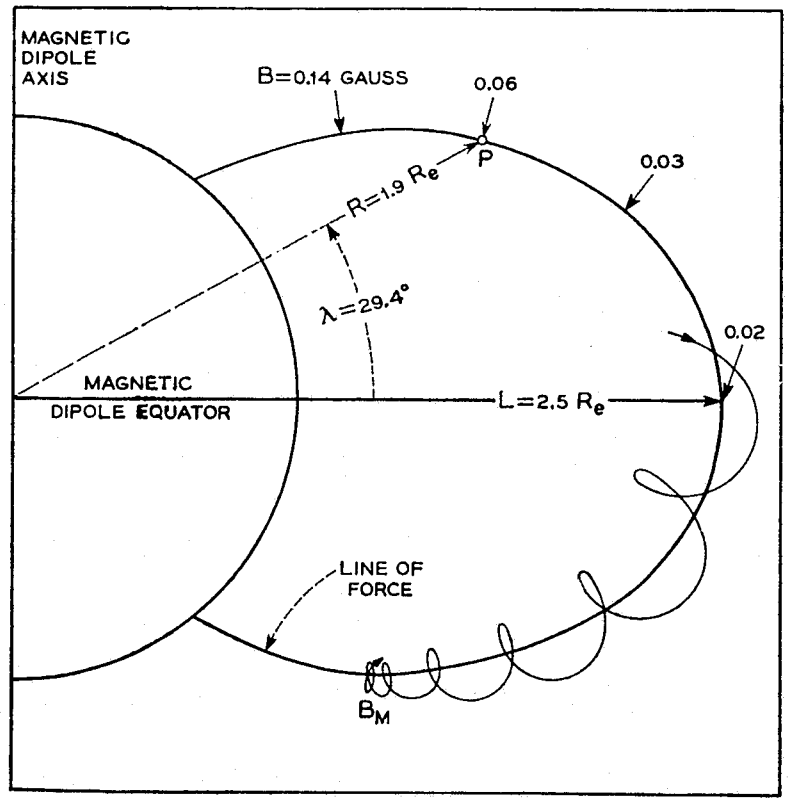

Fig. 1. The B, L and R, λ coordinate system of McIlwain.

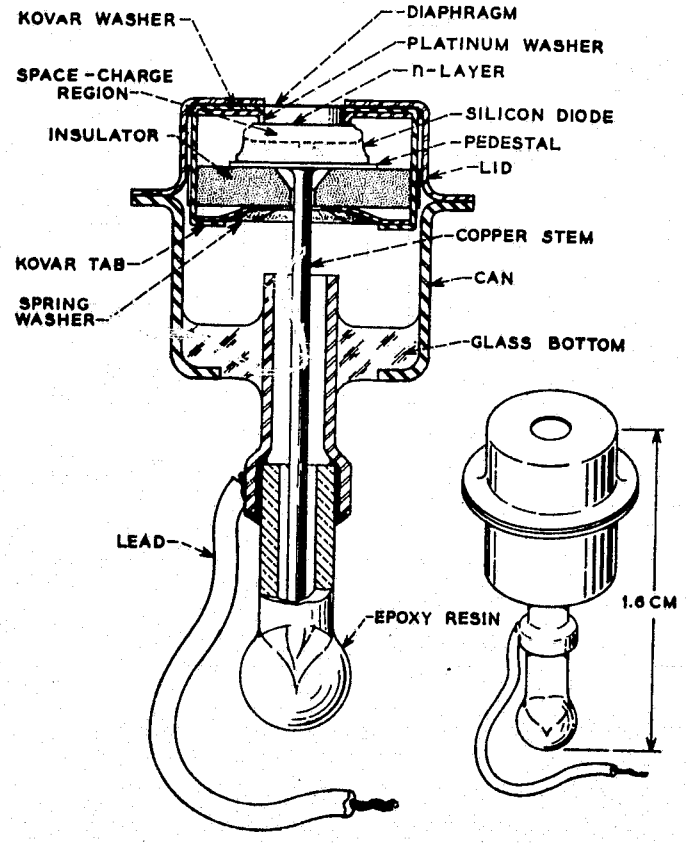

Fig. 2. The cross-section of a silicon p-n junction particle detector as used in experiments on the Telstar I and Explorer XV satellites.

out a magnetic shell labelled with L. Positively charged particles drift to the west and negatively charged particles to the east at a rate which depends upon the mass and energy of the particles, but which in all cases is very slow in comparison with the period of rotation of the particles around the magnetic field line and the bounce period of the particles between their mirror points.

All of the experimental results from the Telstar I and Explorer XV satellites have been obtained using semi-conductor p–n junction particle detectors. (BUCK *et al.*, 1964; also BROWN *et al.*, 1963). One of these devices is shown in Figure 2. The active volume is a disc shaped space charge region about 2 mm in diameter and 0.4 mm thick. This region contains a high electric field which separates holes and electrons created in the silicon by an incident charged particle and produces a pulse which is proportional to the amount of energy deposited by the particle in the active volume. The proportional response of the device is important in distinguishing between protons and electrons due to their very different rates of energy loss in material. By altering the condition for pulse height discrimination in the detector, by changing the thickness of the space charge region, and by varying the geometry of the shielding which surrounds the detector it has been possible to study protons and electrons over a relatively extensive energy region.

The results from these experiments have been treated in a variety of ways, one of which is illustrated in Figure 3 and 4 (BROWN *et al.*, 1963b). In Figure 3 an array of points is shown in R-λ space representing all points at which data was obtained from an electron detector in Telstar I during a particular five day period in August, 1962. These points trace out various classes of orbits of the satellite during this period and they are spread in the magnetic coordinate space because of the irregularities of the

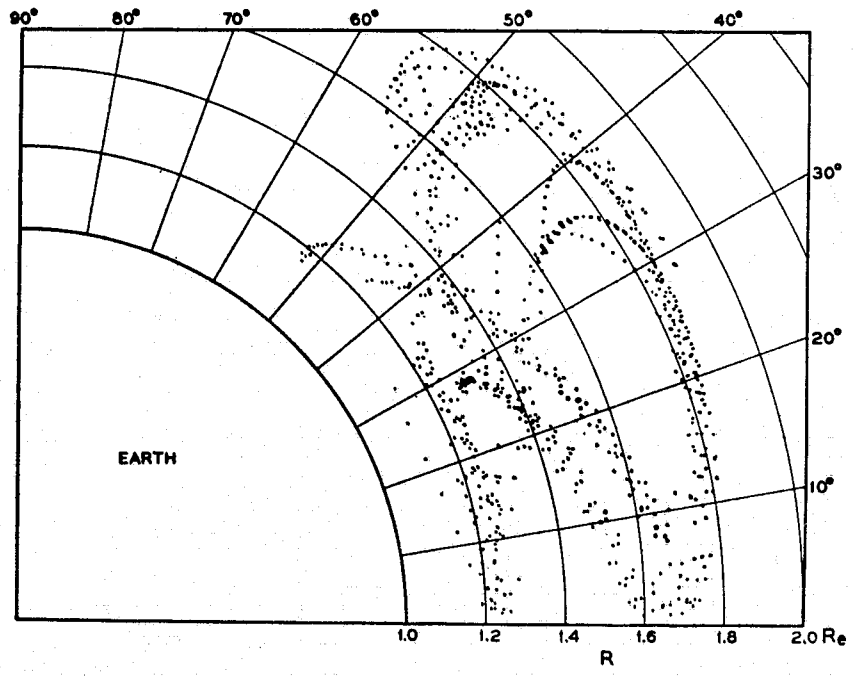

Fig. 3. Points in R-λ space at which data from an electron detector on Telstar I was collected during a five day interval. Individual orbits and sets of orbits are clearly visible.

magnetic field. Figure 4 shows only those points from Figure 3 at which the counting rate of the detector and hence the flux of the particles incident upon it fell within a chosen range. Contours of equal flux have been drawn through successively selected collections of points such as these to produce maps of the flux distribution. Examples will be shown in following sections for both protons and electrons as measured by Telstar I. We can of course also examine the time dependence of the flux in a par-

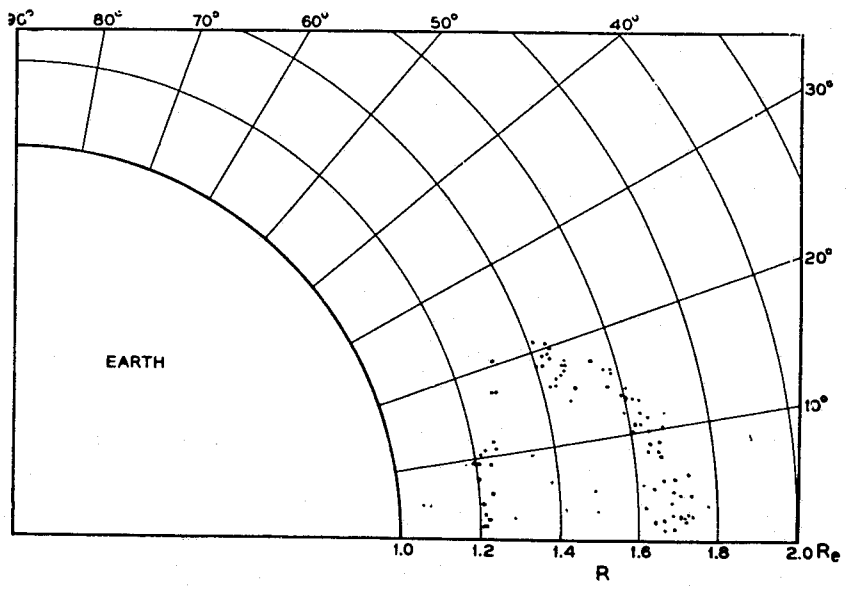

Fig. 4. A. portion of the points in Figure 3 selected to fall in a particular counting rate range.

ticular region of space by sorting the data not on intensity as is the case in Figure 4, but on B and L or R and λ and displaying it against time. Examples of this sort will also be illustrated in connection with electrons measured by the Telstar satellite.

2. Protons

Figure 5 is a set of flux contours for a detector on Telstar I measuring protons between 26 and 34 MeV (BROWN *et al.*, 1963b). The contoures have been produced as described in the preceding paragraph and are drawn five to a decade. The logarithm of omni-directional proton flux is indicated on the contours, the highest corresponding to a flux of approximately 2.5×10^4 protons/cm^2 sec. This value agrees quite well with earlier measurements by VAN ALLEN (1959) and by MCILWAIN (1963). The flux distribution is characteristic of the inner Van Allen belt. It shows a single maximum at approximately 1.6 earth radii and on the equator. The contours are limited at about 1.9 to 1.95 earth radii by the apogee of Telstar I's orbit.

Figure 6 compares the equatorial flux profile as determined by the 26–34 MeV detector of Figure 5 with those from other proton detectors on Telstar I and Explorer XV. The very much higher apogee of Explorer XV is clearly evident. In all cases there is a single equatorial maximum, but there is a systematic increase of both

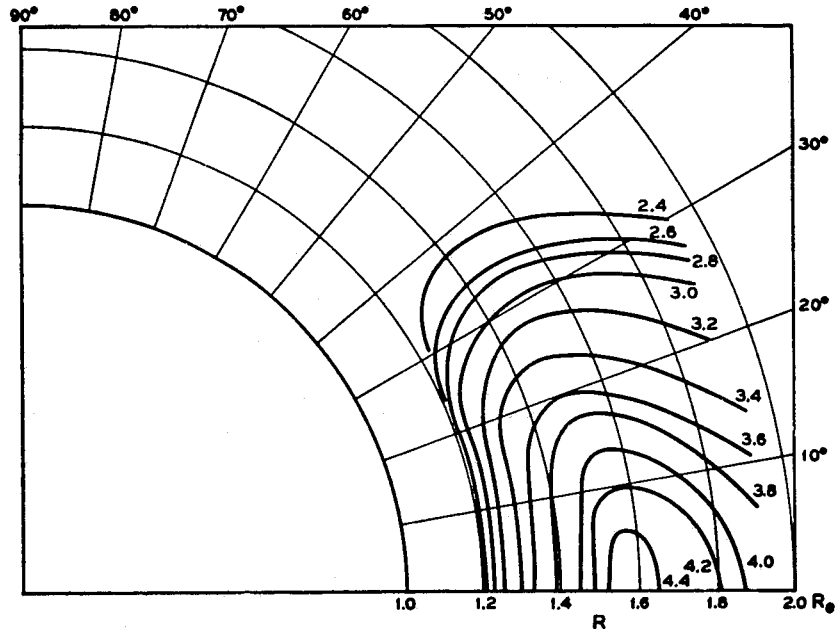

Fig. 5. Contours of equal flux of protons in the 26–34 MeV energy range as measured by Telstar I. The curves are labelled with the logarithm of the omnidirectional particle flux.

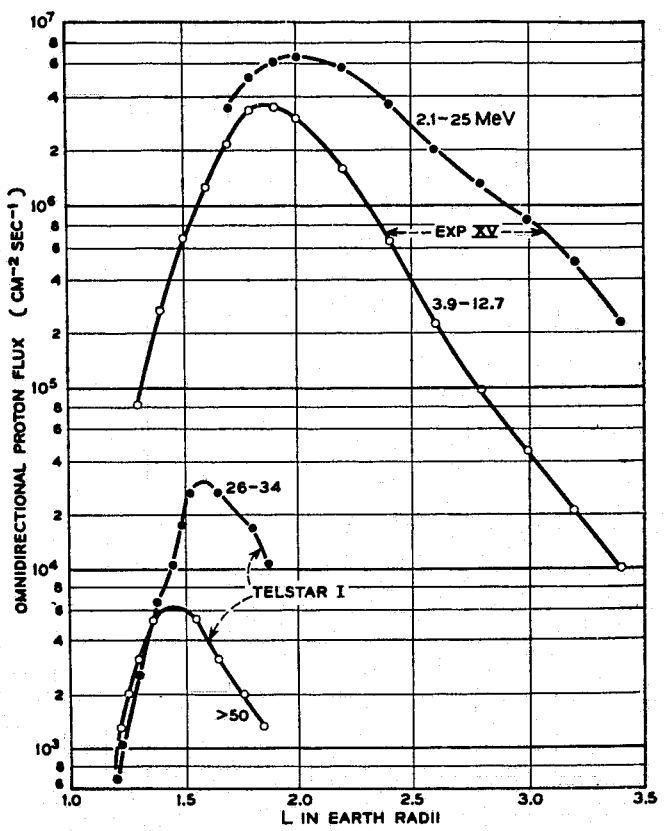

Fig. 6. The equatorial variation of omnidirectional proton flux from two detectors on Telstar I and two on Explorer XV.

maximum proton flux and the radial distance at which the maximum occurs with a decrease in proton energy. This same trend continues to still lower energies as measured by DAVIS and WILLIAMSON (1963). The distributions as determined by Telstar I and Explorer XV were quite stable over periods of several months. They represent thus an essentially steady state between particle source and loss mechanisms. There seems to be no doubt that a major source for the higher energy protons is provided by the decay of albedo neutrons produced by galactic cosmic rays and solar protons reacting with the earth's atmosphere (SINGER, 1960). There also seems to be no doubt that the atmosphere serves as the dominant loss mechanism controlling the very rapid fall off in the proton flux at low altitudes (RAY, 1960). The source for the low energy protons, however, and the mechanism which controls the upper altitude fall off in the flux are still uncertain. It has been suggested that the protons are lost above the flux maximum by scattering with hydromagnetic waves in the plasma (DRAGT, 1961), the waves perhaps arising at the magnetospheric boundary. It is also possible that acceleration mechanisms exist as a result of magnetic field fluctuations associated with boundary variations and that the lower energy protons of Figure 6 were once a part of the low temperature plasma. The importance of unravelling the details of such possibilities is quite evident.

3. Electrons

The distribution and stability of the electrons differ very markedly from the protons discussed in Section 2. Telstar I was observing the particles starting almost immediately after the United States high altitude nuclear explosion of July 9, 1962, the

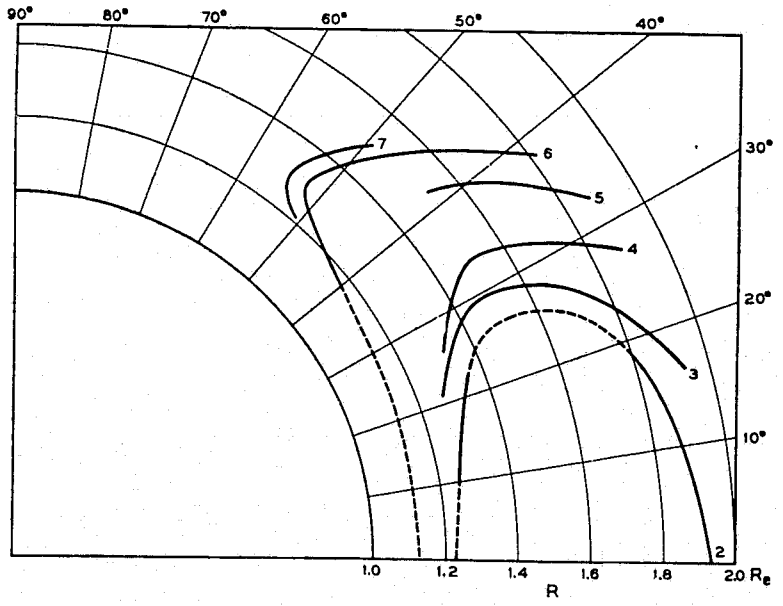

Fig. 7. Contours of equal omnidirectional counting rate for electrons from Telstar I in the time period from Day 193–197, 1962. The contours are two to a decade as follows: 2 – 6.6 × 10^7/cm² sec; 3 – 2.1 ⁄ 10^7; 4 – 6.6 ⁄ 10^6, etc. The omnidirectional counting rate is related to the omnidirectional flux of particles by the efficiency factor of the detector.

Starfish event (*Collected Papers*, 1963). Explorer XV was launched just before the second of the group of three Russian high altitude nuclear tests that took place in October and November of 1962. A great many new electrons were added to the belts in these events and possibly even a redistribution of already existing electrons took place as well. Figure 7 is a flux map from Telstar I (BROWN *et al.*, 1963b) for the earliest time period in which there is sufficient data to construct a meaningful map. Starfish occurred on Day 191 and Figure 7 spans the five day interval from Day 193 through 197. The contours were constructed in the way described in Section 1 from data in this case obtained by a detector dominantly measuring electrons of about

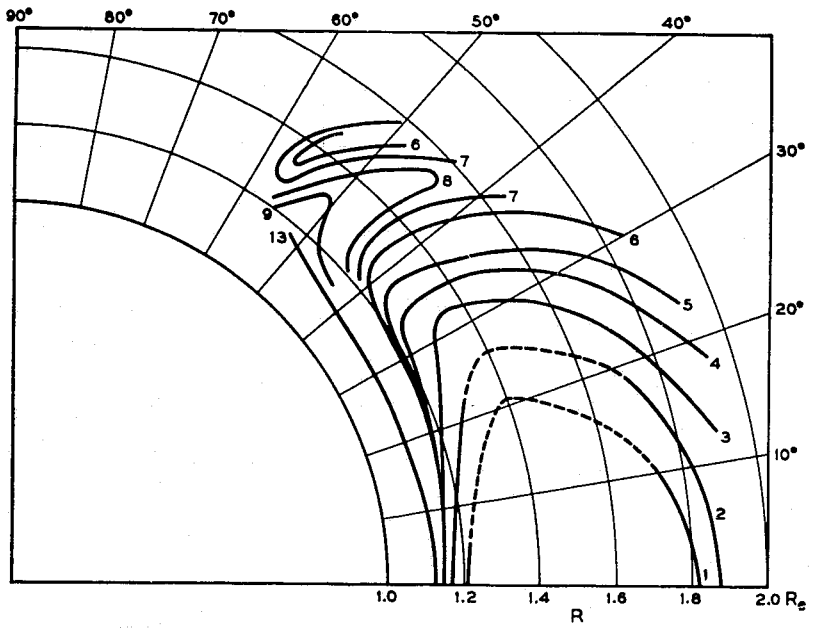

Fig. 8. Contours of equal omnidirectional counting rates for Days 203–207, 1962. The contour labelling is the same as in Figure 7 except that Contour 1 with an omnidirectional counting rate of 1.5×10^8 is now in evidence. This contour is slightly out of the normal two-to-a-decade order.

0.5 MeV. The contours are two to a decade, the highest shown, Contour 2, corresponding to an omnidirectional counting rate of approximately $7 \times 10^7/\text{cm}^2$ sec. The labelling of the curves has reserved Contour 1 for a still higher flux region not evident in this earliest case because of the orbit of the satellite. Notice that in Figure 7 there is only one maximum in the electron distribution up to dipole latitudes of about 50° and notice that Contour 2 crosses the $R = 1.8$ earth radii line at about 18°.

Figure 8 shows the situation about two weeks after Starfish during Days 203 to 207. Contour 3 now crosses $R = 1.8$ earth radii at 18° instead of Contour 2. There has thus been a decay in the observed particle flux in this region by about a factor of 3 in a ten-day period. A second maximum in the distribution is now evident as a result of an even more substantial loss of particles in the 40° to 50° region. This secondary maximum is the tip of the outer Van Allen belt, previously indistinguishable from the inner belt because of particles substantially filling the intervening space. Contour 1

is now observed at low latitudes, near crossings of the equator at both high and low altitudes. The satellite orbit has not yet precessed sufficiently to complete the contour as indicated by the dashed portions of the curve. Contour 1 has an omnidirectional counting rate of 1.5×10^8 counts/cm^2 sec. Because of the detector sensitivity as a function of electron energy the over-all efficiency of the detector in the presence of an electron spectrum produced by nuclear fission is approximately 0.2. The highest flux contour thus represents a total electron flux, if the spectrum is that of fission beta particles, of approximately 8×10^8/cm^2 sec.

Figure 9 shows the flux distribution in October just before the first of the Russian

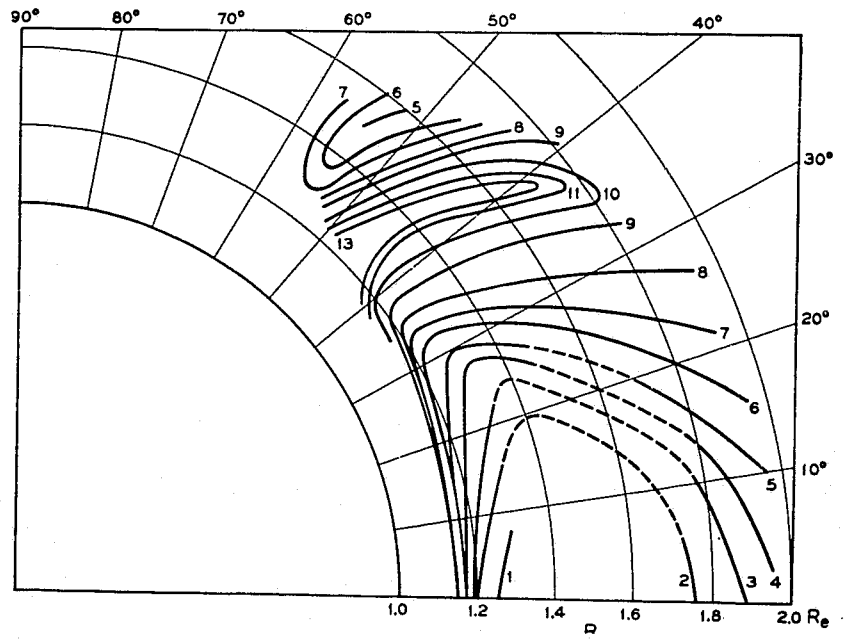

Fig. 9. Contours of equal omnidirectional counting rate for Days 288–294, 1962. The contour designations are as in Figures 7 and 8.

tests. The slot between the inner and outer belts is now extremely deep. The electron flux has decreased by about a factor of 300 at the deepest point. The position of Contour 2 at $R = 1.8$ earth radii $\lambda = 18°$ on Day 193–197 now falls between Contours 5 and 6 on Days 288–294, a decay of about a factor of 60.

Figure 10 shows the flux as a function of time in several small regions of space as indicated by the B-L values on the figure. The clusters of points along the lines reflect the times at which data was observed in each of these regions. On $L = 2.5$ the decay is fast and over-all very large as observed in connection with Figure 9. On $L = 1.7$ the decay is slow and only amounts to about a factor of 2 over the three month period. The decays are not exponential. If they were the curves would be straight lines on this semilogarithmic plot and would approach a final steady state value with a rather sharp corner. However, assuming the initial decay is approximately exponential, a time constant has been associated with the initial slope of these curves and others like them throughout the space in which Telstar I collected data. The time constants are themselves plotted in R-λ space in Figure 11. Notice that at the lowest altitudes the

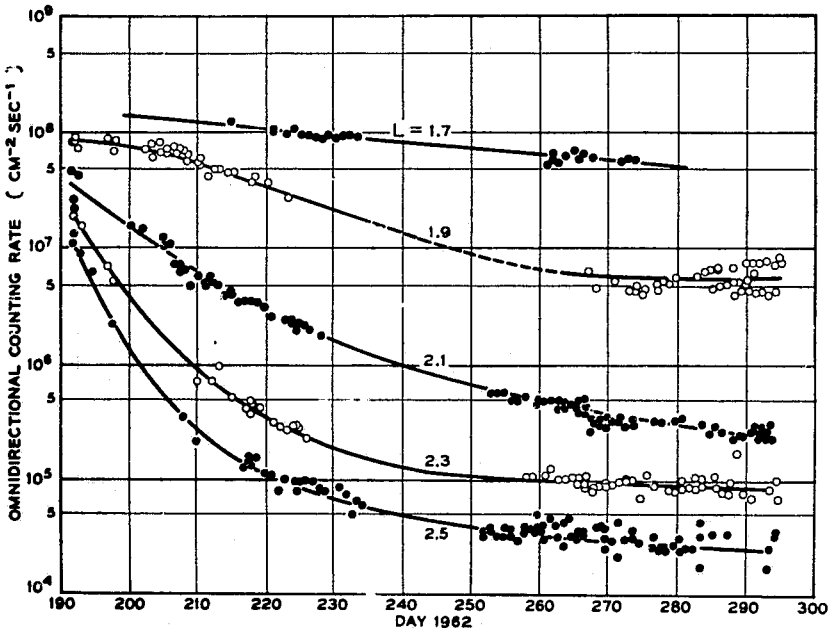

Fig. 10. The time dependence of the counting rate in several small regions of B, L space.

decay times are short as noted by VAN ALLEN *et al.* (1963). At intermediate altitudes near the equator the decay time is relatively long and at the highest altitudes and in the slot the time is once again short. The lightly dashed lines in the figure attempt to connect regions of approximately equal decay time. The shape of these lines is very roughly equivalent to the shape of the inner belt itself as seen in Figure 9. Clearly the rates of decay of the particles are closely related to the number of particles to be

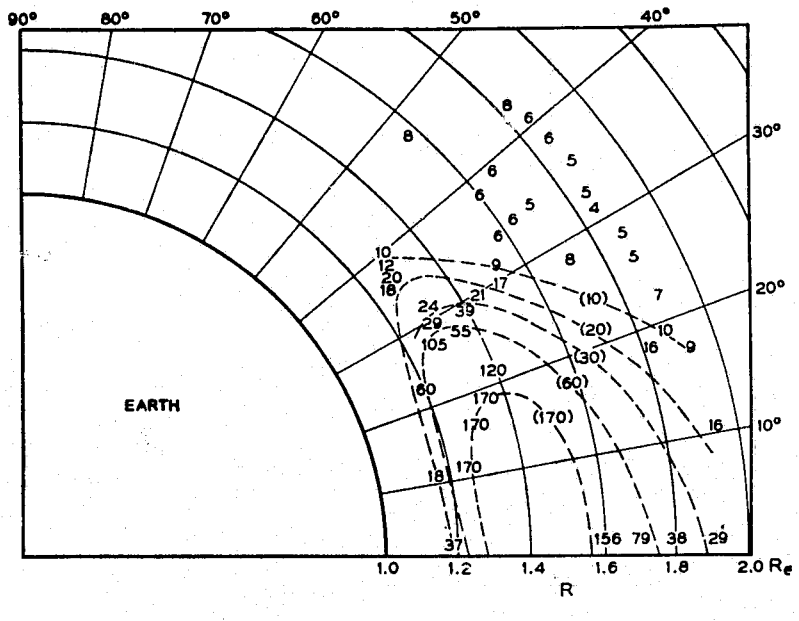

Fig. 11. The initial time constants from data such as in Figure 10 displayed in R-λ space. The decay times are in days. The dashed lines connect regions of equal decay times as indicated by the numbers in parentheses.

found in different regions. This is to be expected in a steady state case and in a case of a still decaying transient following a broad injection of new particles.

The question of the loss mechanism responsible for the results above is of very substantial importance, because these same mechanisms will be operative with respect to naturally occurring electrons as well as to electrons artificially introduced as in this case. At low altitudes (on L lines below about 1.3 earth radii) there seems to be no question but that loss is produced by interaction of the electrons with the earth's atmosphere (WELCH *et al.*, 1963; WALT *et al.*, 1963). Walt is calculating these decays in detail and is finding that his predictions agree quite well with the experimental observations. This correspondence is much more completely displayed with Van Allen's results from the Injun satellite (VAN ALLEN and LIN, 1964) than with results from Telstar I because of Injun's data coverage at low altitudes.

The atmospheric scattering process becomes less and less effective on higher altitude L lines as a result of the decreasing atmospheric density. On the other hand, Telstar I observations show the decay time becoming short again. Atmospheric scattering is certainly not producing the decay times of the order of a week, in the region of the slot. There has been considerable speculation concerning this process. One suggestion is that a Saturn-like ring of dust exists in space in the region of the slot and serves to remove electrons by scattering and energy loss. Such a dust ring would be tremendously effective in removing protons of a few MeV. The fact that the region of the slot is just where the maximum of the low energy proton distribution occurs (Figure 6) makes such a proposal exceedingly unlikely. It seems much more plausible that the loss is connected with some magnetic disturbance in this region of space. DUNGEY (1963) has just proposed the possibility that whistlers, interacting resonantly with the electrons in their cyclotron rotation around the magnetic field, are responsible for the rapid loss in the slot region. Whistlers are circularly polarized electromagnetic radiation produced by lightening discharges in the atmosphere. Dungey's proposal is an extremely interesting one which he will comment on in the discussion to follow. If this mechanism is correct it depends on the properties of the low energy plasma in the trapped particle space, because this plasma determines the propagation characteristics of whistler radiation.

On October 22, 28 and November 1 the Soviet Union carried out three nuclear tests which introduced new particles into the radiation belts in the region above $L=1.7$. Because of the character of the new particle distributions and the more extensive satellite instrumentation which was in space to observe them, these events added significantly in support and extension of information gained from the Starfish test. Figure 12 illustrates the observations of an instrument on the Explorer XV Satellite which measures electrons above 0.5 MeV. The data are for October 28, the day of the second Soviet test. The figure is a ϕ, L plot of the equatorial omnidirectional flux of particles, like Figure 6 for protons. The curve marked 1′ was obtained on the second half of the first orbit of Explorer XV as the satellite returned in its highly elliptical, nearly equatorial orbit from apogee at an L of approximately 4.4. This pass crossed $L=2$ at 0407 on October 28. Curve 1′ clearly shows the inner side of the

outer electron belt, the slot, and the rise toward the inner belt maximum. Curve 2 is the outgoing half of the next orbit and the particle distribution has radically changed with the addition of new electrons above $L=1.8$. This orbit crosses $L=2$ about one hour after the orbit 1′. The initial transient of new particles is not yet complete at

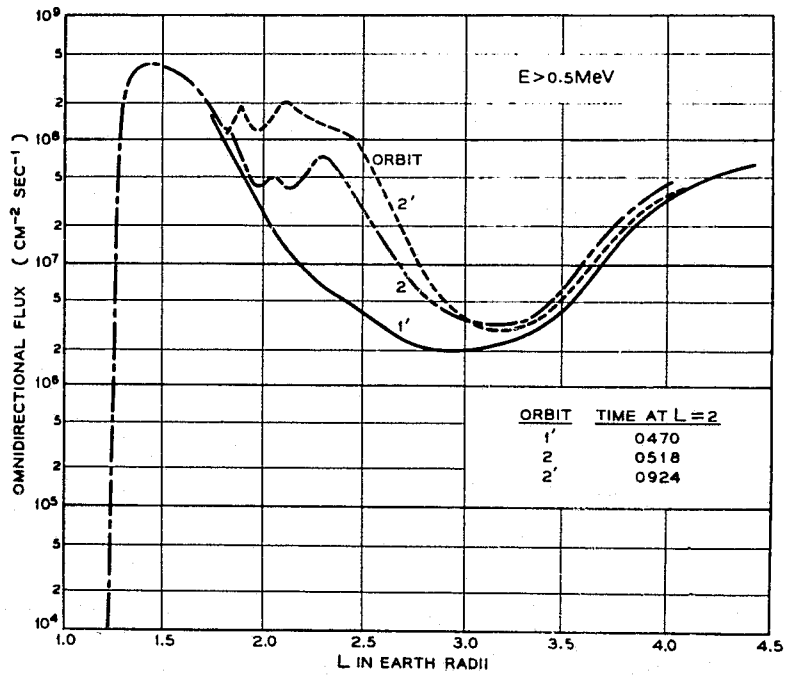

Fig. 12. The omnidirectional flux of electrons of >0.5 MeV for Explorer XV for the early passes on October 28, 1962. The satellite is nearly equatorial and the figure thus gives a nearly equatorial trace through the particle distribution.

this time as evidenced by the further increases in flux seen on the returning half of the second orbit some four hours later, curve 2′. The fortuitous observation of this transient illustrates the longitudinal drift of the magnetically trapped particles mentioned in Section 1. At $L=2$ on orbit 2 the satellite is over the Atlantic and observing electrons which have drifted eastward around the world from their injection by the explosion over Asia. For 0.5 MeV electrons the drift rate on $L=2$ is approximately 5.7 degree/minute (WELSH and WHITAKER, 1959). For the 270° of longitudinal drift required, the corresponding time is 47 minutes. On $L=3$ the drift rate is 3.8 deg/min. During the time between its passage across $L=2$ and 3, the satellite is moving eastward at approximately 1 deg/min. On all of the significant L shells the particles are thus drifting faster than the satellite and catching up with it on their first transit around the earth. From the drift rates on different L shells it is possible to deduce the time at which the injection of new particles took place to be consistent with the observations. This time cannot be determined with great precision because of the energy dependence of the drift rate, but it appears to have been 0440 ± 10 minutes. On orbit 2′ of Figure 12, the electrons have drifted at least five times around the earth and the distribution in various L shells should be longitudinally uniform.

Figure 13 shows the early results for a second detector on Explorer XV, this time

measuring electrons above 1.9 MeV. On orbit 1′ in this case there are two small spikes in electron intensity at about $L=1.85$ and 2.0. These seem to be the remnants from the first Soviet test six days earlier. There is no question but what much of the flux between $L=2$ and 3 is also left over from that earlier test since the slot region is not nearly as deep as it was observed by Telstar I to be just before the Soviet test series,

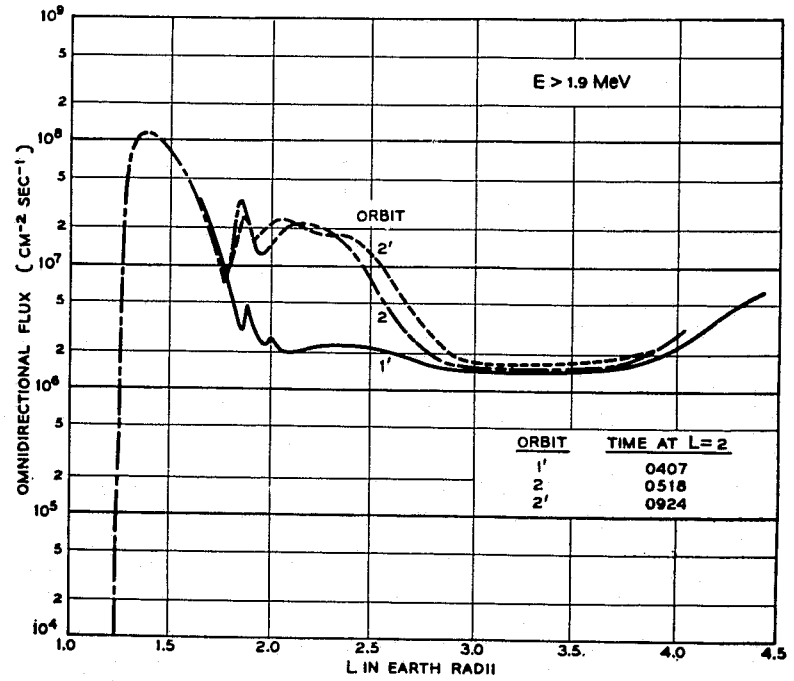

Fig. 13. The omnidirectional flux of electrons of > 1.9 MeV Explorer XV for the same period as that in Figure 12.

(Figure 9). In orbit 2 on Figure 13 the new electrons of greater than 1.9 MeV have clearly already arrived. In fact in comparison with orbit 2′ there are more electrons seen earlier than later. This does not seem to be a decay phenomena, but rather a decrease in flux associated with the longitudinal dispersion of the originally rather well clumped group of electrons. The drift rate for 1.9 MeV electrons on $L=2$ is approximately 20 deg/min. These particles are probably being observed on their second transit around the earth. If they were in their first transit the injection time would have to have been at about 0500, rather late for the lower energy particles seen in Figure 12. The structure in the electron distribution as observed on orbits 2 and 2′ is quite complex and can in principle at least be related to the motion of the radioactive fragments carried in the expanding plasma of the nuclear explosion.

In Figure 14, 15 and 16 results from three detectors measuring different energies are shown together for the first passes of the satellite to illustrate the L variation in the energy spectrum along the equator. The vertical spacings between these curves on the semilogarithmic plot give the relative spectral hardness of the electron distribution. From Figure 14 for orbit 1′ the residue of the first Soviet explosion is seen at greater than 1.9 and greater than 2.9 MeV, but is not distinguishable as sharp structure at greater than 0.5 MeV. In the outer belt region the detectors indicate fluxes approxi-

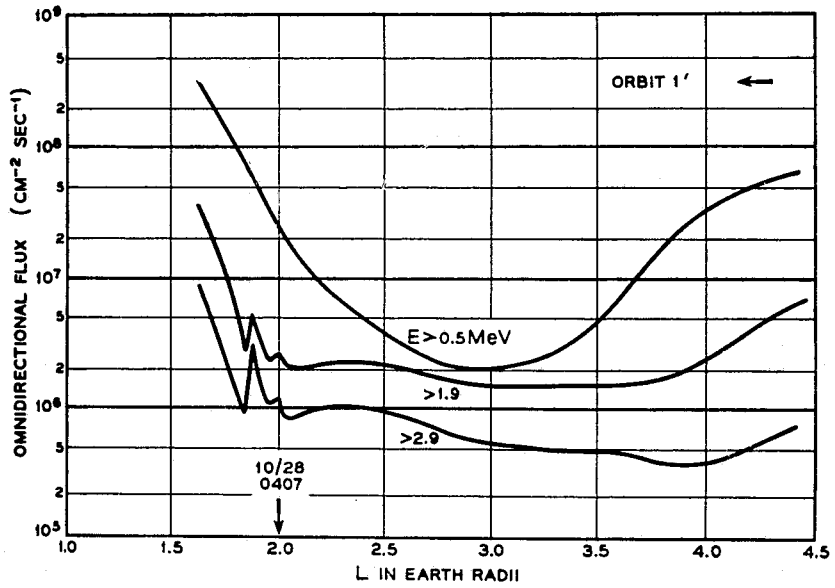

Fig. 14. The omnidirectional flux from three electron detectors on Explorer XV for the first returning pass from apogee on October 28. The variation in the vertical spacing of the curves in the semilogarithmic plot indicates the change in the spectral distribution of the electrons.

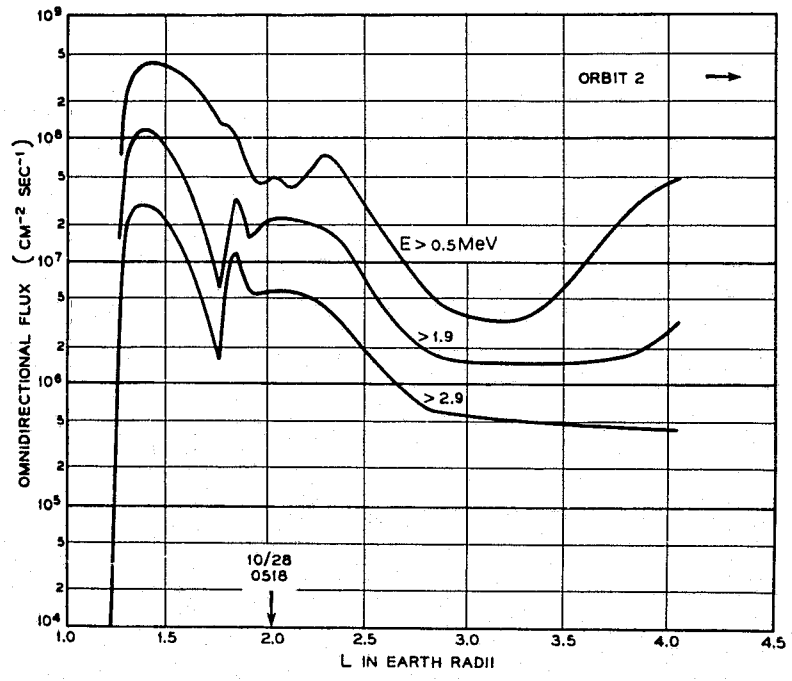

Fig. 15. The omnidirectional flux from the detectors of Figure 14 as for the second outgoing pass of Explorer XV. The time is very shortly after the second Soviet high altitude nuclear test.

mately in the ratio 1:0.1:0.01. In the bottom of the slot at about $L=3$ the ratios are 1:0.8:0.3 a very much harder spectrum. In Figure 15, orbit 2, the peak of the inner belt is seen to have ratios 1:0.3:0.09. These are in quite good agreement with the equilibrium spectrum of electrons created in fission beta decay. The electrons in the inner belt peak are dominantly those produced by the U.S. Starfish test, and in the

peak region they have not decayed very much between July and the end of October as discussed in connection with Figure 11. Between $L=1.8$ and $L\simeq 3$ the spectra in Figure 15 are confused by the transient of the newly added electrons in their drift around the world immediately after the second test. Figure 16 shows the electron distribution after it had time to disperse uniformly in longitude. Comparing these

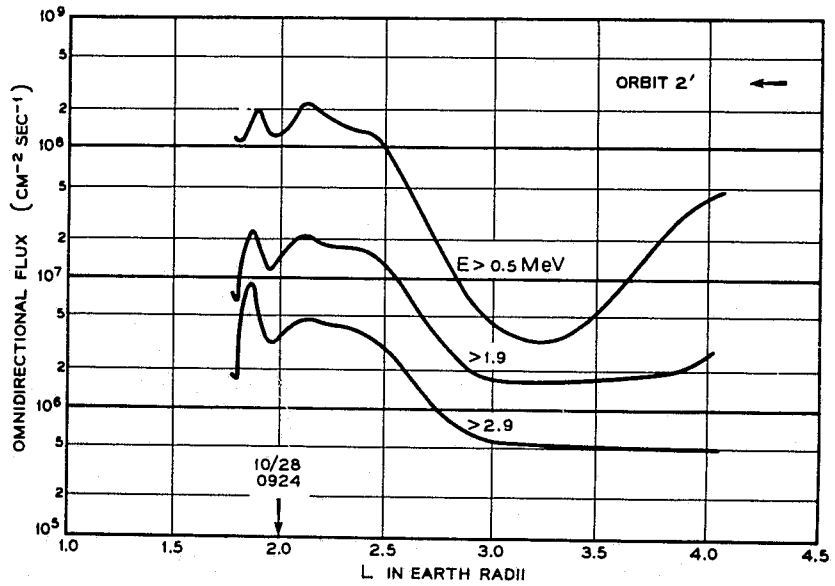

Fig. 16. The omnidirectional flux from the detectors of Figures 14 and 15 as for the second returning pass of Explorer XV. The newly injected electrons have now had time to disperse uniformly in longitude.

curves with those of Figure 14, it is clear that electrons of greater than 0.5 MeV have been added out to as far as $L=3.2$ or 3.3 whereas no significant number of the higher energy electrons has been added above $L=3$. This indication that the spectrum of added electrons is not everywhere the same is born out by comparisons over the whole L-region in which new particles have been added. Even at the maxima at $L=1.85$ and 2.15 in Figure 16 the spectra are different and in neither case are they what would be expected from β-decay of fission fragments. Somehow in the injection process the electron energies are reduced, possibly by the mechanism of Fermi deceleration in collision with the walls of the expanding plasma from the explosion as suggested by HESS (1963). Similar phenomena apparently occurred in Starfish as well, and served to produce a much softer spectrum of electrons at large L values than at small. Through such spectral differences and the difference in the detector response characteristics it is possible to account in a qualitative way for the apparent discrepancy between the Telstar I and Injun I measurements of the Starfish electron distribution in space (BROWN *et al.*, 1963c).

Figure 17 shows the situation on November 3 following the third Soviet test on November 1. The actual data are presented in the region between $L=1.5$ and 2 to illustrate how narrow and well defined the spike of injection was at about $L=1.78$. Unlike the earlier tests, the third test seems to have added no significant numbers of

electrons outside of the single narrow spike. At $L=1.85$ and above the electrons from the second test appear with decreased flux in comparison with Figure 16 because of particle decay over the week since their introduction. The decay of particles in the well-defined injection peaks from these two tests appears to occur by loss on the L shell, not by diffusion between L shells. That is, the peaks do not broaden substantially

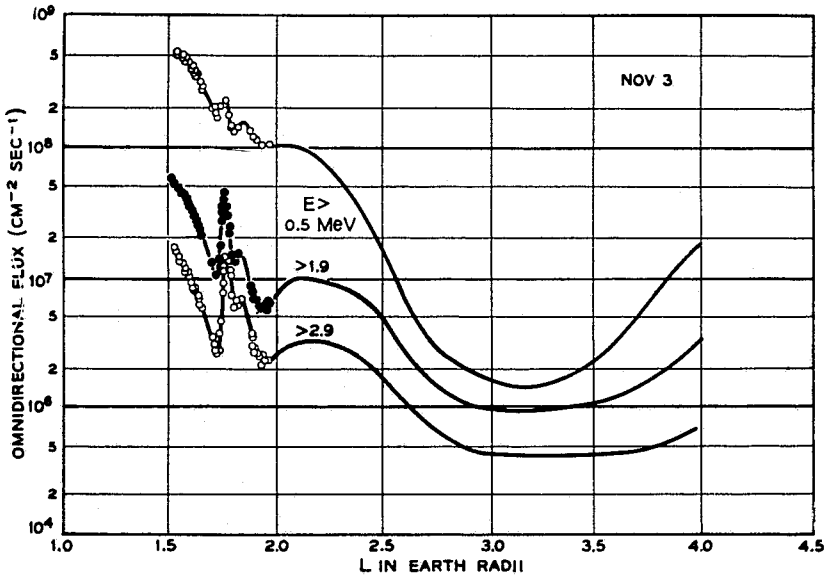

Fig. 17. The omnidirectional flux of electrons from the detectors of Figures 14, 15, 16 on Explorer XV following the third Soviet test on November 1, 1962. The spike of newly added electrons at $L = 1.75$ is extremely narrow.

as they decrease in magnitude with time. This is to be expected by Dungey's whistler loss mechanism but perhaps not by a mechanism which produces a general mixing of the different field lines due to broad magnetic disturbances.

In Figure 18 the electron distributions are shown as a function of B, along the $L=1.75$ line for several intervals of time. The minimum value of B in the figure corresponds to the equator on this field line. The orbit of November 3 in Figure 17 contributes one of the near equatorial points in Figure 18. The electron flux decreases with increasing B in all cases in the figure. This is the same as saying the flux decreases with increasing dipole latitude (Figure 2). It is also equivalent to saying that the distribution of mirror points is peaked at the equator. The triangles in Figure 18 which fall in with the solid circles of the December 14–18 time interval are those points measured before the third Soviet test. This region at $L=1.75$ has been essentially unaffected by the earlier tests so the triangles give enough data points to define a "before" particle distribution on this field line rather well. The new particles added on November 1 not only increase the equatorial flux as indicated in Figure 17 but also drastically alter the distribution of electrons in B. The very flat uppermost distribution that is produced, gradually loses its anomalous shape over the next few weeks and reassumes the approximately linear dependence of log ϕ on log B it had before the test. The whole distribution then decays together. More rapid disappearance of par-

ticles at large values of B and the decay of the distribution as a whole at long times are to be expected in processes controlled by diffusion of particle mirror points along field lines with ultimate particle loss in the atmosphere. This is the situation found by Hess (WELCH *et al.*, 1963) and by Walt (WALT *et al.*, 1963) for lower L values where the atmosphere controls the whole process. It should also be expected in the

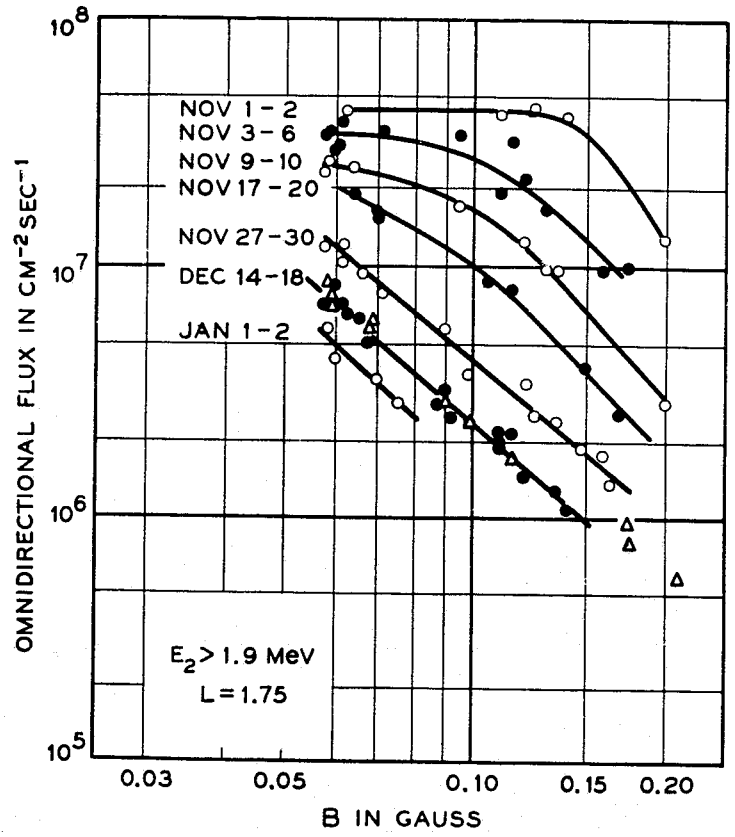

Fig. 18. The variation of the electron distribution along the $L = 1.75$ line as it changes with time. The triangles are points occurring before the third Soviet test on November 1.

whistler controlled diffusion of DUNGEY (1963). The fact that the flux in January in Figure 18 has dropped below the data of the triangles for late October is presumably due to a continuing decay of electrons either from the Starfish test or from the first Soviet test.

Figure 19 is analogous to Figure 18 but for $L=2.0$. There are now only two data points (triangles) before the test on October 28. One of these corresponds to the outgoing, the other to the incoming pass of the first orbit of Explorer XV. The equatorial point is that for orbit 1′ of Figure 14. The star marked "earliest point", is for orbit 2, at which time the high energy electrons had not dispersed in longitude. At $L=2.0$ the ϕ, B variation shows a maximum off the equator, an even more anomalous distribution than that on $L=1.75$. Such a distribution results from injection of new particles far off the equator. This shape rapidly disappeared and the decay process carries past the triangles of October 28 because of continuing decay of electrons from the first Soviet test. Results for a third field line, $L=2.4$, are shown in Figure 20. On

this line the injection is much less anomalous and a steady state linear dependence of log ϕ on log B is rapidly reassumed. Comparisons of Figure 18, 19 and 20 show two particular features. First, the decay is more rapid on the higher L lines. This is in agreement with the results of Telstar I shown in Figure 10 and observed by Telstar I for the Soviet tests as well. Second, the slope of the log ϕ, log B lines decreases with

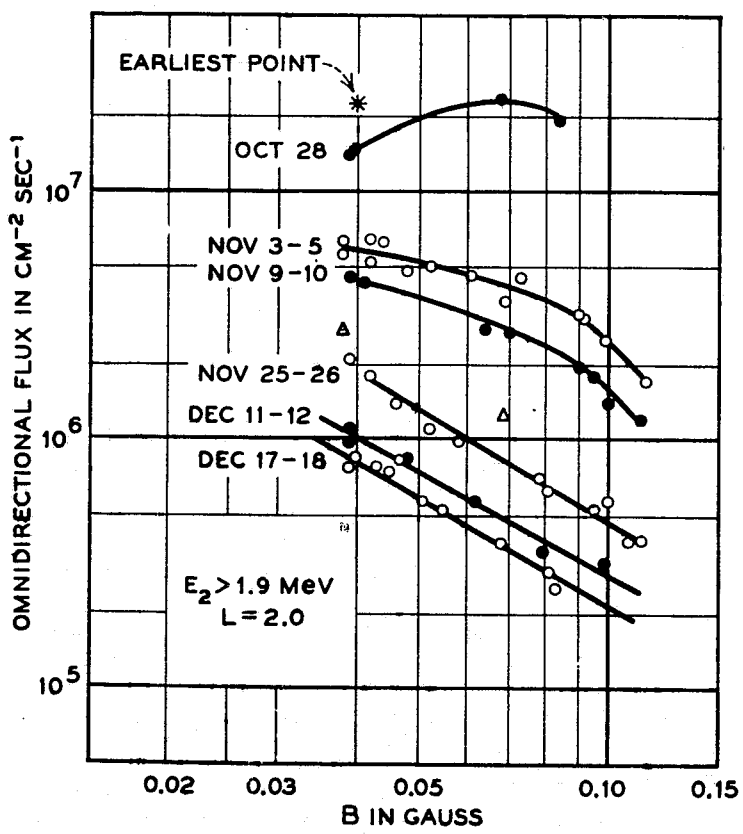

Fig. 19. The variation of the electron distribution along the $L = 2.0$ line as it changes with time. The triangles are the two points obtained before the second Soviet test on October 28. The star is the earliest point following the shot as in Figure 15.

increasing L. This is qualitatively consistent with the diffusion mechanism of particle loss because the ultimate sink for particles in the atmosphere is more remote for higher L lines.

Almost all of the discussion of electrons up to this point has been concerned with the distribution and the redistribution of the particles following artificially induced transients. In conclusion we will consider results for a region in which artificial effects have been unimportant in comparison with nature's own activity. Figure 21 shows the time record of greater than 0.5 MeV electrons from Explorer XV at $L=4$, in the outer electron belt. The two sets of points divide the data into near equatorial and off equitorial B-regions. There is very little B dependence as might be expected by extension of the decrease of the ϕ, B slope observed in Figure 18 through 20, for increasing L. Notice that there is a very rapid electron flux decline shown by the early data. It yields an approximately 5 day time constant. The two B-regions change

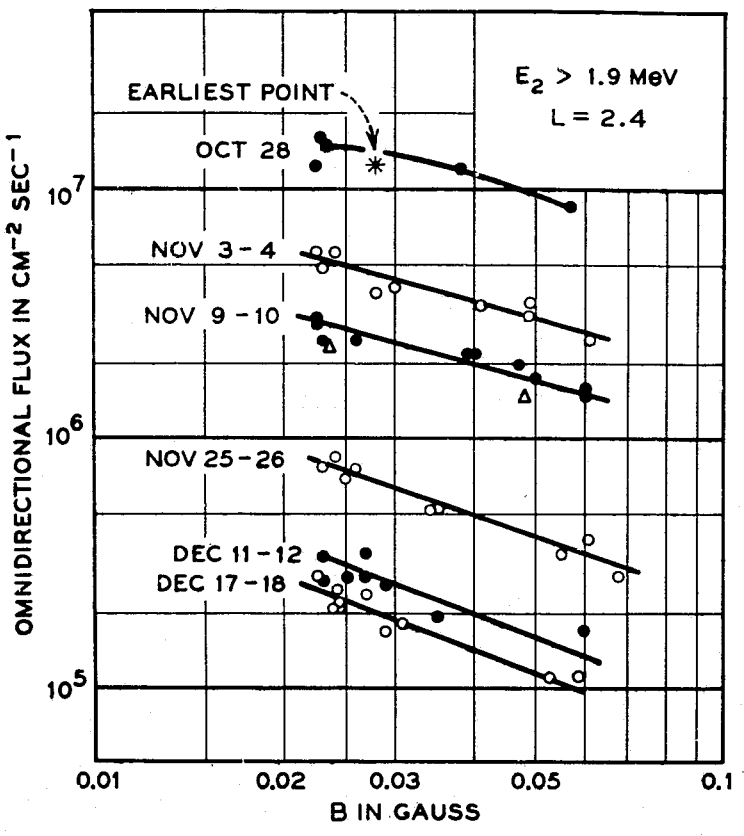

Fig. 20. The variation of the electron distribution along the $L = 2.4$ line as it changes with time. The triangles and the star have the same significance as in Figure 19.

together. Data is missing for about 12 days following day 314, but when the flux is measured on day 327, it is high again. There is a second decline with a similar but not identical decay time. Then on day 352, there is the start of a very large increase which in two days amounts to more than an order of magnitude. This phenomena occurs at the same time as SNYDER has reported observing very large disturbances in the plasma on the Mariner Spacecraft and large fluctuations in magnetic field on the earth (SNYDER *et al.*, 1963). On day 354, the flux reaches a peak and once again begins a rapid decline.

The situation for higher energy electrons is interesting in comparison. Figure 22 reproduces the curve drawn in Figure 21 to represent the shape of the 0.5 MeV data. This curve is superimposed on the greater than 1.9 MeV results with a factor of 10 scale change to make comparisons easier. The features of the two sets of data are similar, but note that the 1.9 MeV electrons rise before they decay in the approximately day 300 region and that the rise at approximately day 327 is visible after the data break whereas for the low energy electrons it was not. In the large rise on about day 352 the 1.9 MeV electrons again lag behind. The 0.5 MeV electrons have started to decline before the high energy electrons have reached their maximum. The increase for the 1.9 MeV electrons is about a factor of 40. These effects are certainly associated with plasma from the sun. Possibly magnetic disturbances initiated in interactions of

the solar wind plasma with the earth's field are responsible. It is tempting to believe the observations are showing an acceleration mechanism in operation. It goes on for several days, increasing the energy of very low energy electrons until they are measured by the 0.5 MeV detector and then later by the 1.9 MeV detector. One might also interpret the results as due to a time varying source of particles outside the magneto-

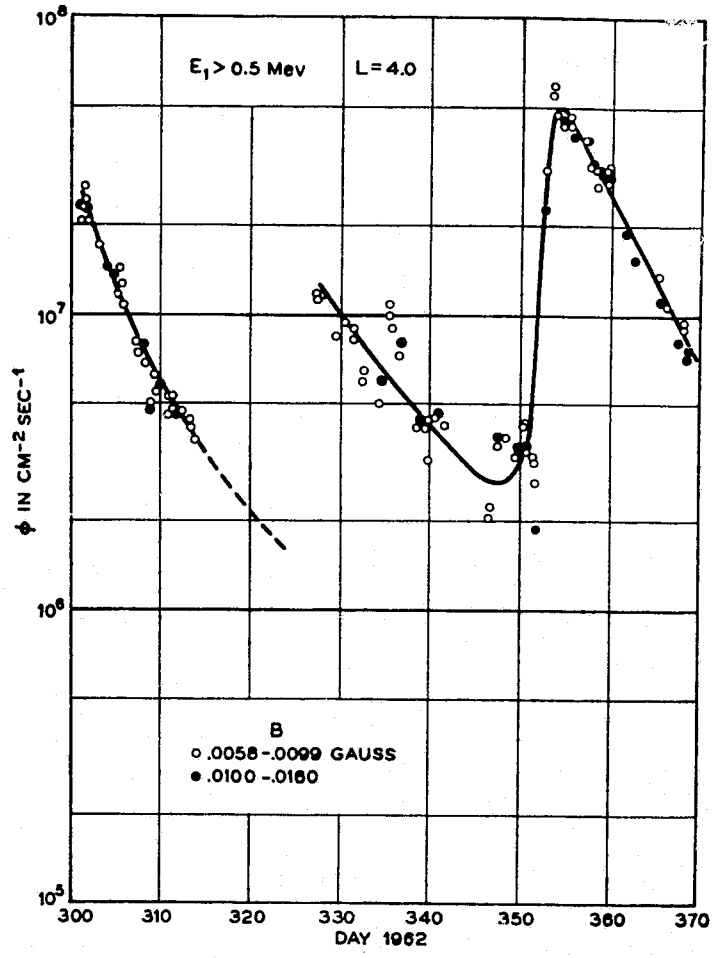

Fig. 21. The fluctuations in the > 0.5 MeV electrons in the outer electron belt at $L = 4.0$ from October 28, 1962 through January 4, 1963.

sphere, the source producing more high energy electrons later. There are difficulties of course in carrying out injection of such electrons through the magnetospheric boundary and there is no evidence for such energetic electrons from the sun. The interpretation of these effects is presently unknown. It seems almost certain to require a mechanism that involves the plasma from the sun in interaction with the earth's field, a topic that falls naturally into a symposium on plasma space science.

4. Summary

In summary there is evidence that for both protons and electrons in the trapped particle region around the earth, plasma, the low temperature plasma inside the mag-

netosphere, the high temperature plasma arriving from the sun, and the manmade plasma of nuclear explosions, is important in mechanisms of injection, acceleration, and particle loss. A great many intriguing suggestions have been made as possible interpretations of the observed phenomena but many, if not most, of the questions that can be asked remain unanswered in any satisfactory detail. We should, however,

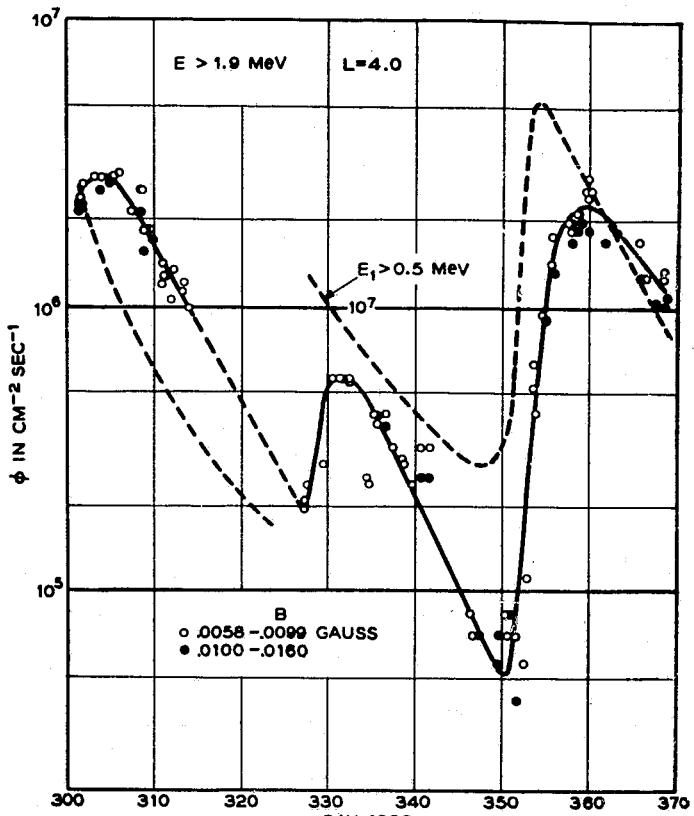

Fig. 22. The fluctuations in the $>$ 1.9 MeV electrons in the outer electron belts at $L = 4.0$ for the same time period as Figure 21. The totally dashed curve in the figure is reproduced from Figure 21 with a change in vertical scale of a factor of 10.

expect major advances in our understanding in the next few years with the increasingly sophisticated experiments that are being prepared and launched and with the theoretical effort that is examining these complicated geomagnetic effects.

References

Van Allen, J. A.: 1959, *J. Geophys. Res.* **66,** 1683.

Van Allen, J. A., Frank, L. A., and O'Brien, B. J.: 1963, *J. Geophys. Res.* **68,** 619.

Van Allen, J. A. and Lin, W. C.: 1964, *Trans. Amer. Geophys. Union* **45.**

Brown, W. L., Buck, T. M. *et al.*: 1963a, *Bell System Tech. J.* **42,** 899.

Brown, W. L., Gabbe, J. D., and Rosenzweig, W.: 1963b, *Bell System Tech. J.* **42,** 1505.

Brown, W. L., Hess, W. N., and Van Allen, J. A.: 1963c, *J. Geophys. Res.* **68,** 605.

Buck, T. M., Wheatley, G. H., and Rogers, J. W.: 1964, Proceedings of the Ninth Scintillation and Semiconductor Counter Symposium, March 1964, to be published *IEEE Trans. Nucl. Sci.*

Collected papers on the Artificial Radiation Belt for the July 9, 1962 *Nuclear Detonation, J. Geophys. Res.* **68,** (1963) 619.

DAVIS, L. R. and WILLIAMSON, J. M.: 1963, *Space Science Review* (ed. by W. PRIESTER), Interscience Publishers Inc., New York.
DRAGT, A. J.: 1961, *J. Geophys. Res.* **66,** 1641.
DUNGEY, J. W.: 1963, *Plan. Space Sci.* **11,** 591.
HESS, W. N.: 1959, *Phys. Rev. Letters* **3,** 11 and 145.
HESS, W. N.: 1963, *Bull. Amer. Geophys. Union,* p. 76.
MCILWAIN, C. E.: 1961, *J. Geophys. Res.* **66,** 3681.
MCILWAIN, C. E.: 1963, *Science* **142,** 3590.
RAY, E. C.: 1960, *J. Geophys. Res.* **65,** 1125.
SINGER, S. F.: 1960, *Space Research* **1** (ed. by H. KALLMANN-BIJL), North-Holland Publishing Company, Amsterdam.
SNYDER, C. W., NEUGEBAUER, M., and RAO, V. R.: 1963, *J. Geophys. Res.* **68,** 6361.
WALT, M., CRANE, G. E., and MACDONALD, W. M.: 1963, *Trans. Amer. Geophys. Union* **45.**
WELCH, J. A., JR. and WHITAKER, W. A.: 1959, *J. Geophys. Res.*, **64,** 909.
WELCH, J. A., JR., KAUFMAN, R. L., and HESS, W. N.: 1963, *J. Geophys. Res.* **68,** 685.

CHAPTER 2

SOME OBSERVATIONS OF THE DISTRIBUTION OF ENERGETIC PROTONS IN THE EARTH'S RADIATION BELTS BETWEEN 1962 AND 1964

J. D. GABBE and W. L. BROWN

Bell Telephone Laboratories, Inc., Murray Hill, New Jersey

Abstract. Flux distributions for protons with energies between 4 and 13 MeV, 18 and 27 MeV, 26 and 33 MeV, 50 and 135 MeV, and 49 and 145 MeV measured from July 1962 to September 1963 at geocentric distances in the range 1.01 to 3.4 earth radii are presented. Using data extending to June 1964, secular temporal changes are discussed, some effects of the magnetic storm of September 22, 1963 are described, and some aspects of the energy spectrum are noted.

1. Introduction

The purpose of this paper is to present several bodies of data on the proton distribution. These data were gathered between 1962 and 1964 by means of instruments on Telstar 1, Explorer XV, and Telstar 2.

Distributions in the form of log flux vs log B for various specified values of L are used to summarize the measurements. B is the magnetic induction in Gauss, and L is the magnetic shell parameter (McILWAIN, 1961). These coordinates and scales have been selected because they are well suited for making comparisons of flux values within and among the bodies of data in this paper and also between these results and those of other experimenters.

Some portions of these data have been published previously (BROWN, GAEBBE, and ROSENZWEIG, 1963; BROWN and GABBE, 1964; BROWN, 1965). This article collects the various distributions in one place, supplements them with previously unpublished information, and presents them all in the same coordinate system and on the same scale.

Extensive analyses of the data from the various instruments have been undertaken. During the course of this work, simple mathematical functions which give convenient and statistically accurate descriptions of the proton distributions have been evolved. Some of the analyses have been completed, others are still in progress. Because they are computationally so convenient, the formulae describing the Telstar 1 data are included in this article. The details of the completed analyses are in the process of publication elsewhere.

2. The Satellites

Information about the satellites is given in Table I, and the regions of R-λ (McIlwain, 1961) space accessible to the spacecraft are illustrated in Figure 1. As may be seen in the figure, the larger region of space explored by Telstar 2 includes almost all the smaller portion of space covered by Telstar 1. Explorer

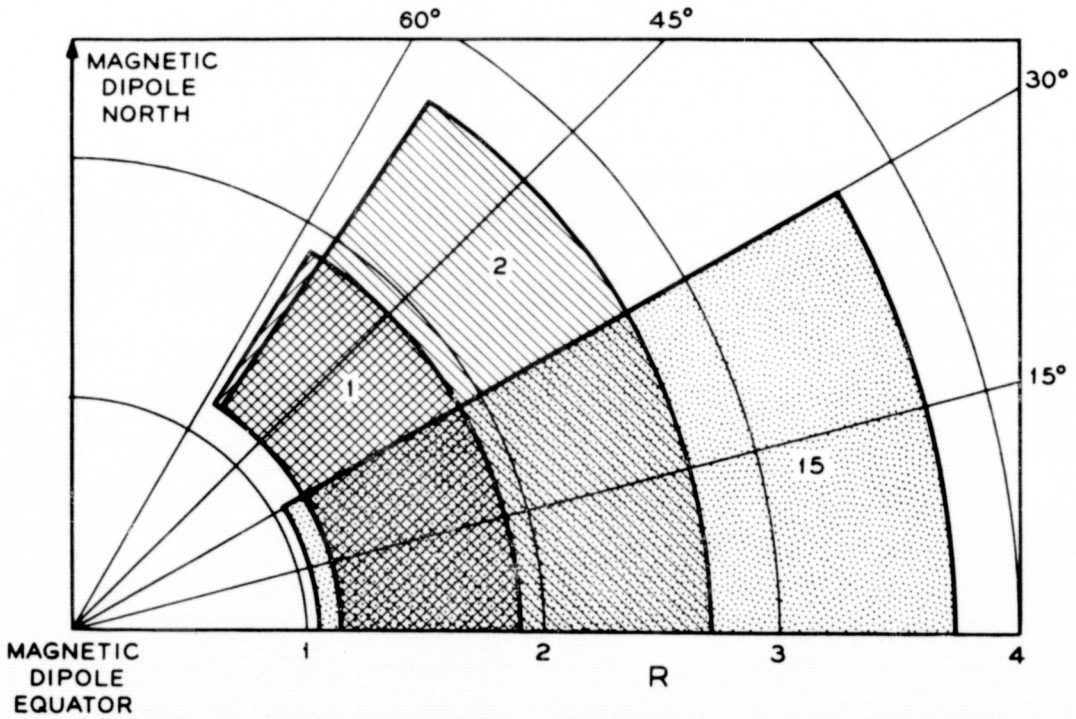

Fig. 1. The regions of R-λ space explored by Telstar 1 [1]; Telstar 2 [2]; and Explorer XV [15].

XV maps out higher altitude regions of space than the Telstar satellites, in addition to overlapping the portions covered by the Telstars at lower altitudes and latitudes. All the Explorer XV measurements were recorded during the active life of Telstar 1, but measurements from the two Telstar satellites do not overlap in time. The three vehicles were spin stabilized and all the detectors were mounted so that their symmetry axes lay in planes that were approximately perpendicular to the spin axes of their respective satellites.

3. The Instruments

The detecting elements in all of the instruments were semiconductor diodes made by diffusion of phosphorus into high resistivity p-type silicon. The sensitive

TABLE I

Satellites, Orbits, and Detectors

Satellite	*Period covered by data*		*Orbit***			*Spin Rate RPM*		*The detectors discussed here*			
	from	*to*	*Perigee in R_e*	*Apogee in R_e*	*Incl. deg.*	*Max*	*Min*	*Energy range MeV*	*Directional Characteristics*	*f*	*Counting interval sec*
Telstar 1 1962 $\alpha\varepsilon 1$	7/10/62–2/21/63		1.15	1.90	45	180	85	50–135	Omnidirectional	87	11
								26–33	Omnidirectional	1700	15
Explorer XV 1962 $\beta\lambda 1$	10/27/62–1/27/63		1.05	3.72	18	72	72	4–13	cone, 10° half-angle	4000	1.45
Telstar 2 1963 13A	5/ 7/63–	5/7/65*	1.15	2.70	43	180	65	49–145	Omnidirectional	76	11
								18–27	Omnidirectional	950	15

* Only data previous to 6/30/64 reported here.

** $R_e = 1$ earth radius $= 6371.2$ km.

regions of these diodes were disk shaped, about 2.9 mm in diameter and 0.4 mm in thickness at the nominal reverse bias voltage at which the diodes were operated. These devices have been described by BUCK *et al.* (1964) and the complete detector assemblies by BROWN *et al.* (1963). The energy range of the particles detected was determined by the shielding of the detector assemblies, the pulse height level set by the associated electronics, and the operating bias on the diodes. The conversion from the counting rate of the detectors to proton flux was made by multiplying the counting rate by the factors f in Table I. These constants take into account the geometric factors and the average efficiencies of the detectors. For a differential power-law spectrum of the form

$$J(E) \sim E^{-n} \tag{1}$$

where $J(E)$ is the flux of particles with energies between E and $E+\mathrm{d}E$, and the stated energy intervals, the quantities f deviate less than 5 per cent from those given in Table I for values of n between 0 and 7.5. Although the conversion factors are almost independent of the energy spectrum, variations in the conditions under which the detectors were made, assembled and operated lead to uncertainties of about 50 per cent in the absolute values of these constants for the several detectors.

4. The Data

The basic telemetered data are the number of counts recorded by a detector during a counting interval. The counting intervals for the various detectors are given in Table I. On the Telstar satellites the counting intervals occurred once a minute for both the detectors considered here. On Explorer XV the counting interval occurred approximately 5 times a minute. In all cases the date and universal time at which the data were recorded were inserted by the ground station. These times together with the ephemerides of the satellite allow one to associate the geographic position of the satellite with the data. The magnetic coordinates, B and L were calculated from the geographic position by means of McIlwain's FORTRAN computer program INVAR using the JENSEN and CAIN (1962) Epoch 1960 coefficients for the 48-term spherical-harmonic expansion of the earth's main magnetic field (MCILWAIN, 1962). In addition, bias voltages, satellite temperatures, and other housekeeping data appeared in the telemetry and were associated with the appropriate counting-rate data.

The Telstar detectors are intrinsically omnidirectional and the analyses performed have treated the data point by point. The Explorer XV detector is directional, and the data have been interpolated to specific L shells and corrected to equivalent omnidirectional flux using a method developed by ROBERTS (1965).

5. The flux vs B Contours

Figures 2 through 6 are presentations of the various proton distributions in the form of log J (where J is the omnidirectional flux) vs log B plots for selected L shells. For reasons connected with the equipment or analysis these presentations suffer from various small defects. Space does not allow a detailed discussion of these anomalies, but the most significant of them are mentioned in the text.

The results of the analysis of the data on protons with energies between 50 and 135 MeV taken with Telstar 1 are shown in Figure 2. The lines were produced from the equations and coefficients in Table II. The coefficients have

TABLE II

The Functional Fit to the 50–135 MeV Proton Data from Telstar 1

These expressions are valid only for $1.15 < L < 3.0$, $R < 1.95$ R_e*, and $J > 5$ proton/cm² sec.

$$C(B, L) \begin{cases} = A^2 \left[\dfrac{Z^2 - x^2}{Z^2(1-x^2)}\right]^{1/2} \left[1 - \left(\dfrac{x}{Z}\right)^2\right]^{2S}, x \leqslant Z \\ = 0, x > Z \end{cases} \quad \text{(a)}$$

where C = omnidirectional counting rate, counts/sec, of protons with energies above between 50 and 135 MeV; B = magnetic induction, Gauss; L = magnetic shell parameter; $x = \sqrt{1 - B_0/B}$; $B_0 = 0.311653/L^3$.

$$A \begin{cases} = \dfrac{A_1(L - L_0)}{A_2 + (L - A_3)^{A_4}}, L \geqslant L_0 \\ = 0, L < L_0 \end{cases} \qquad Z = \sqrt{1 - \left(\frac{Q}{L}\right)^3 \left[4 - \frac{3Q}{L}\right]^{-1/2}}$$

and $Q = L_0 + R_1(L - L_0) + R_2(L - L_0)^2 + R_3(L - L_0)^3$.

$$J(B, L) \approx 87\, C(B, L), J > 5 \quad \text{(b)}$$

where J = omnidirectional flux, protons/cm² sec, of protons with energies between 50 and 135 MeV.

$$j(u, L) \approx 87 \frac{A^2 \left[1 - \left(\dfrac{u}{Z}\right)^2\right]^{2S}}{2\pi Z \beta(\frac{1}{2}, 1 + 2S)} \quad \text{(c)}$$

where j is the equatorial unidirectional flux, protons/cm² sec ster, of protons with energies between 50 and 135 MeV

$u = \cos \alpha$

α = equatorial pitch angle

and $\beta(p, q) = \int_0^1 w^{p-1}(1 - w)^{q-1} dw$ is the beta function.

$L_0 =$	1.132792	$R_1 =$	0.2636094
$A_1 =$	10.197	$R_2 =$	−0.6011559
$A_2 =$	0.24662	$R_3 =$	0.4746468
$A_3 =$	0.74397	$S =$	0.32986
$A_4 =$	5.3565		

* 1 R_e = 6371.2 km

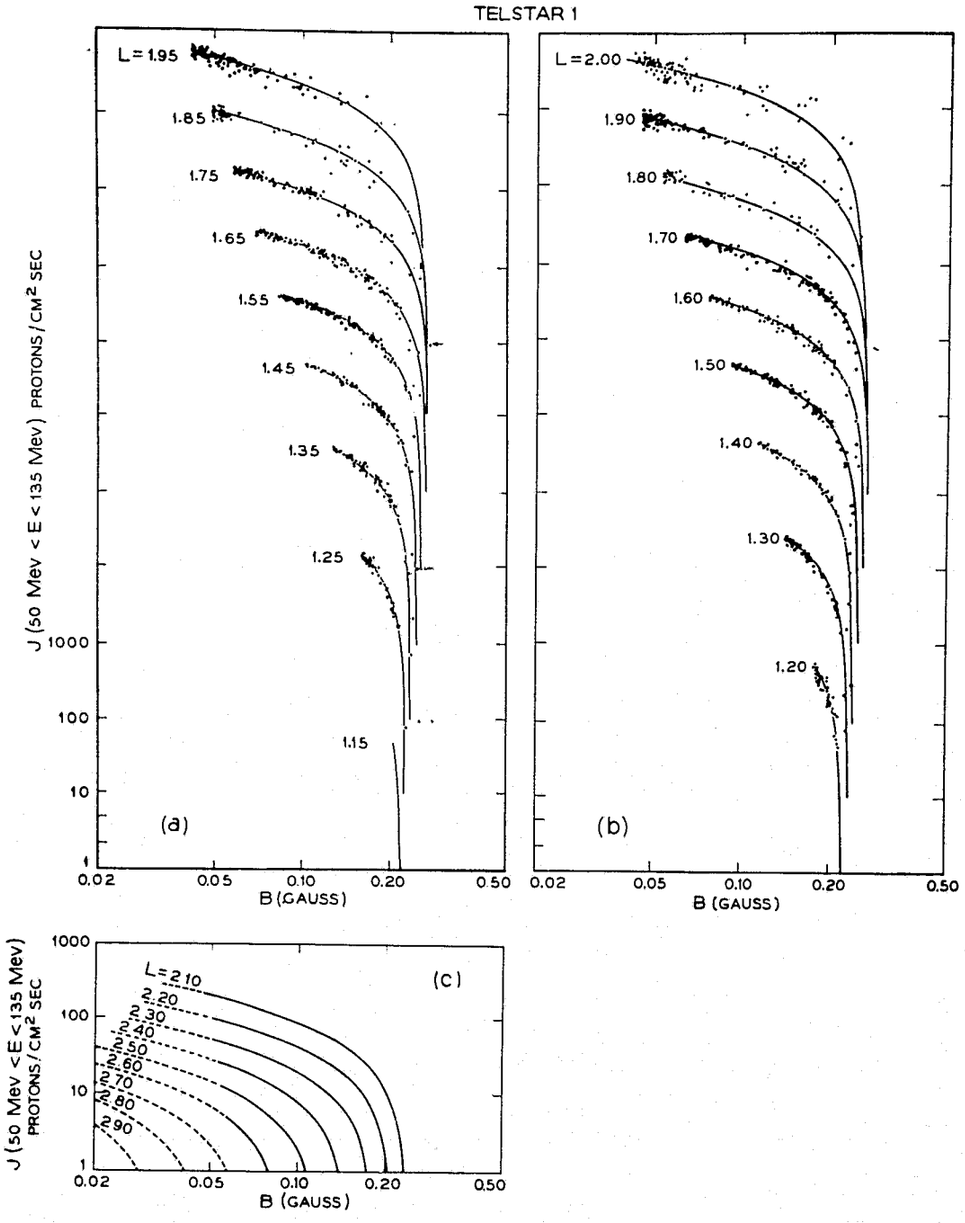

Fig. 2. Flux vs B contours for constant L for the 50–135 MeV protons measured on Telstar 1 (July 1962–February 1963). Adjacent contours are slipped one decade in J; and each contour rises from $J=1$. The points are data points near the appropriate L. Data points representing $J=0(\log J=-\infty)$ are plotted at $J=1$. The lines were generated from the model described in Table II. Dashes indicate extrapolations beyond the region in which data were acquired.

been determined by making a multidimensional least squares fit of the mathematical model in Table II to the data (GABBE, WILK, and BROWN, 1966). The model with the tabulated coefficients summarizes the distribution of these protons to an extent reasonably approaching expected statistical fluctuations. The points in Figure 2 are individual data points having L-values close to the L-values of the lines. How close depends on the density of the data, but the differences between the L-values of the points and that of the line is usually less than 0.005. These results should not be extended to fluxes below 5 protons/cm^2 sec, a value that approximately represents the lower limit of the sensitivity of the detector. The actual data points associated with L-lines having values greater than $L=2.0$, shown in section (c) of the figure, have been omitted. This has been done because the overlap among observations belonging to different L-lines that results from the statistical scatter at low counting rates tends to confuse the presentation when the points are included. The quality of the fit remains satisfactory.

The distribution of protons with energies between 26 and 33 MeV was also measured on Telstar 1, and is shown in Figure 3. The model described in Table III has been fitted to the 26–33 MeV measurements and the resultant coefficients appear in the table. The geometric factor of the detector was quite small and the instrument is effectively insensitive to fluxes below 100 protons/cm^2 sec.

Figure 4 is a presentation of the data on the 4–13 MeV protons measured on Explorer XV, as reduced to omnidirectional flux. The lines are the result of a preliminary least squares fit to the reduced data. They cannot realistically be extrapolated to values of flux beyond the data points. The points plotted in Figure 4 are only a representative sample of the existing data, but they cover the full range of observations.

The data from Telstar 2 have been divided into two time periods. The dividing line is the magnetic storm of September 22 (day 265) 1963, which substantially affected the proton distribution for $L \gtrsim 2.2$. The data preceding this storm were acquired between days 127 and 265, 1963 and this time will be referred to as "Summer 1963". The period extending from day 265, 1963 to day 182, 1964 (day 547, 1963) is "Winter 1964". Flux distributions from the summer of 1963 are shown in Figure 5 for 49–145 MeV protons and in Figure 6 for the 18–27 MeV protons. The points in Figures 5 and 6 are data which fall within thin L slices, i.e. ranges of L defined by $L \pm \Delta L$, where L is the nominal value for the measurements. The value of ΔL is usually 0.005. The curves for the Telstar 2 data are not least squares fits, but are hand drawn through the points. This procedure is somewhat uncertain at the high B end of the higher L lines, where the points are scattered because the fluxes are too small to give good counting statistics; and the detailed shape at this end of the line contains this uncertainty.

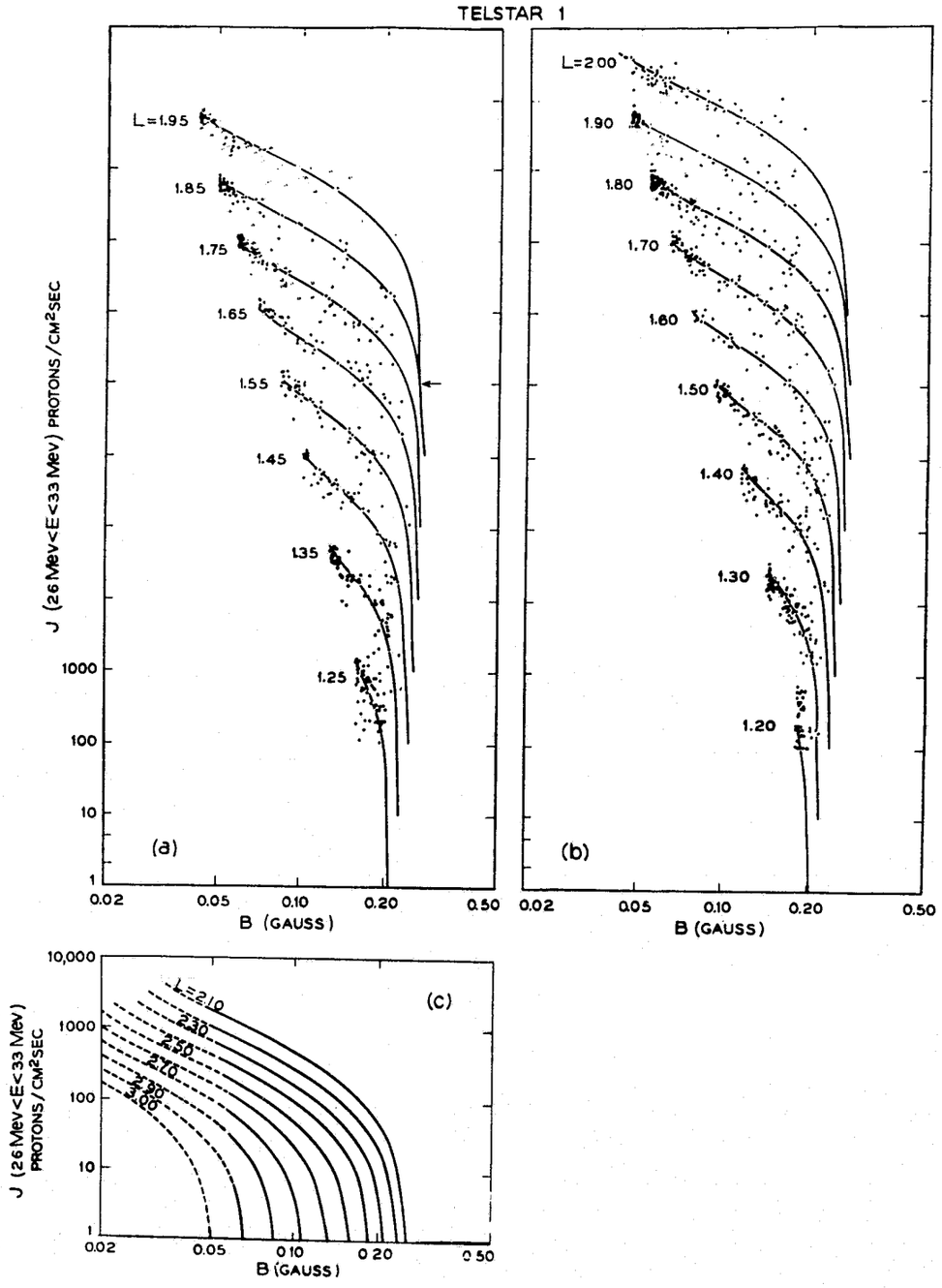

Fig. 3. Flux vs B contours for constant L for the 26–33 MeV protons measured on Telstar 1. The lines were generated with the model described in Table III. The remaining conditions in the caption of Figure 2 apply.

TABLE III

The functional fit to the 26–33 MeV proton data from Telstar 1

These expressions are valid only for $1.15 < L < 3.00$, $R < 1.95\ R_e$*, $J > 100$ protons/cm^2 sec.

$$C'(B, L) \begin{cases} = D^2 \left[1 - \left(\frac{x}{G}\right)^{5/4}\right]^{2N}, & x \leq G \\ = 0, & x > G \end{cases} \qquad \text{(a)}$$

where C' = omnidirectional counting rate, counts/sec, of protons with energies between 26 and 33 MeV

B = magnetic induction, Gauss

L = magnetic shell parameter

$x = \sqrt{1 - B_0/B}$

$B_0 = 0.311653/L^3$

$$D = \frac{D_1(L - L_1)}{D_2 + (L - L_1)^{D_3}}, \quad L \geq L_1 \qquad D = 0, \quad L < L_1$$

$$G = \sqrt{1 - \left(\frac{P}{L}\right)^3 \left[4 - 3\frac{P}{L}\right]^{-1/2}}$$

and $P = L_1 + P_1(L - L_1) + P_2(L - L_1)^2 + P_3(L - L_1)^3$.

$$J'(B, L) \approx 1700\ C'(B, L), \quad J' > 100 \qquad \text{(b)}$$

where J' = omnidirectional flux, protons/cm^2 sec, of protons with energies between 26 and 33 MeV.

$L_1 =$ 1.1667423
$D_1 =$ 1.695
$D_2 =$ 0.14926
$D_3 =$ 2.5859
$P_1 =$ 0.0923283
$P_2 =$ −0.278932
$P_3 =$ 0.2655505
$N =$ 0.62703

* $1\ R_e = 6371.2$ km

6. Equatorial Fluxes

Figure 7 summarizes the behavior of the omnidirectional flux J, as a function of L on the magnetic equator. Equatorial values of J have been taken from Figures 2 through 6. To these have been added the equatorial values of J for the later (Winter 1964) measurements of 49–145 MeV protons and the 18–27 MeV protons made with Telstar 2. The Telstar 1 50–135 MeV proton curve has been omitted from Figure 7 because it is virtually coincident with the Telstar 2 49–145 MeV proton curve for the summer of 1963 below $L = 1.95$. The dashes indicate extrapolation into regions where equatorial data are not available.

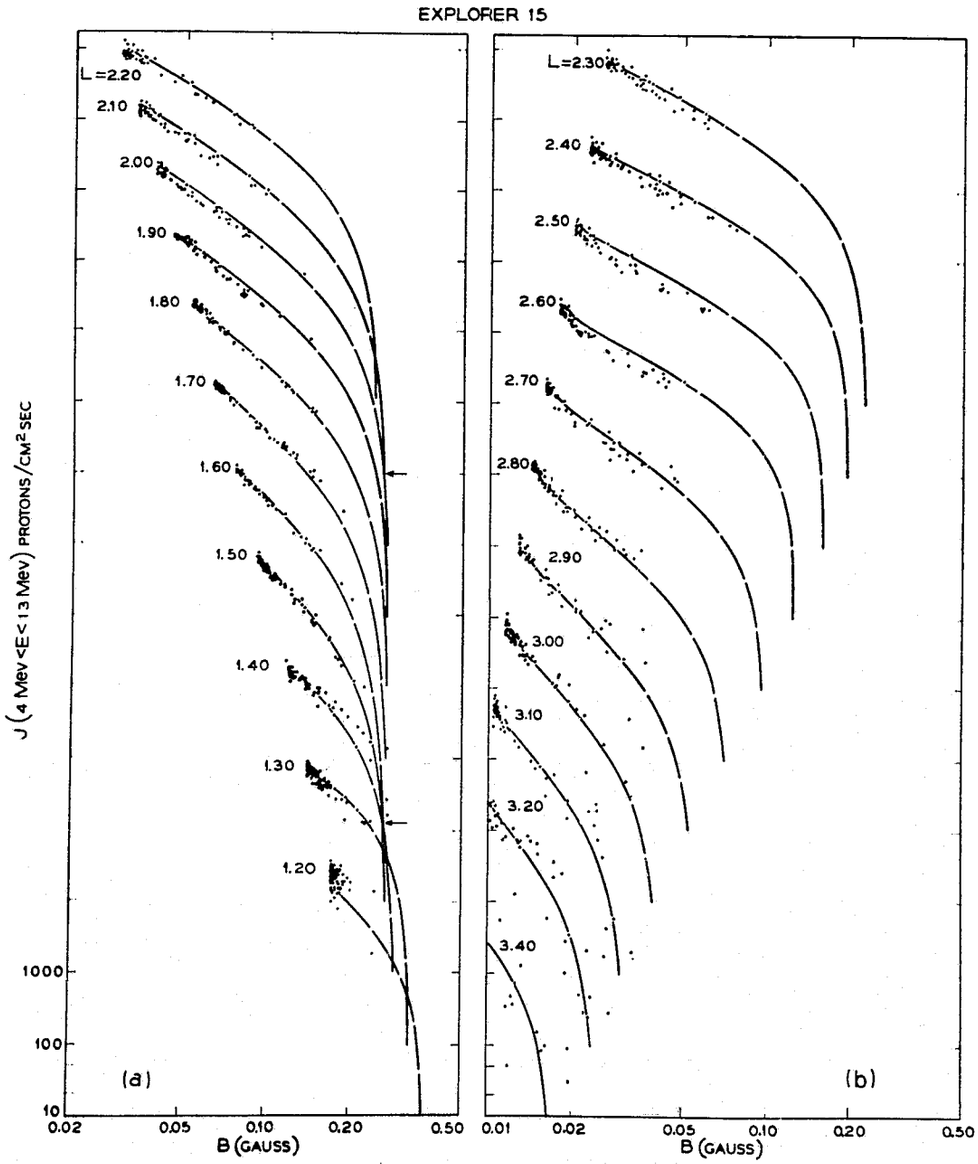

Fig. 4. Flux vs B contours for constant L for the 4–13 MeV protons measured on Explorer XV (November 1962 to January 1963). Each contour rises from $J = 10$. Only a representative sample of the interpolated data points are plotted. The lines come from a least squares fit to the data, and are extrapolated at the high-B end.

The substantial increase in equatorial flux as the energy of the protons decreases, and the movement of the maximum in the equatorial flux to lower values of L for the higher energy particles is observed in these results as in the

results of previous experiments (DAVIS and WILLIAMSON, 1962; and FILLIUS and MCILWAIN, 1964). The effect of this behavior on the energy spectrum is treated later.

MCILWAIN (1963) observed a secondary maximum at the equator at $L \sim 2.2$ in the 40–110 MeV proton distribution measured by him with Explorer XV in late 1962. This secondary maximum was not observed by Telstar 1, whose *equatorial* coverage reached only to $L=1.95$. The Telstar 2 measurements of 49–145 MeV protons (made subsequent to May 1963) show no secondary maximum, although the Summer 1963 and Winter 1964 curves in Figure 7 display a well defined plateau near $L=2.2$. Apparently, the secondary maximum

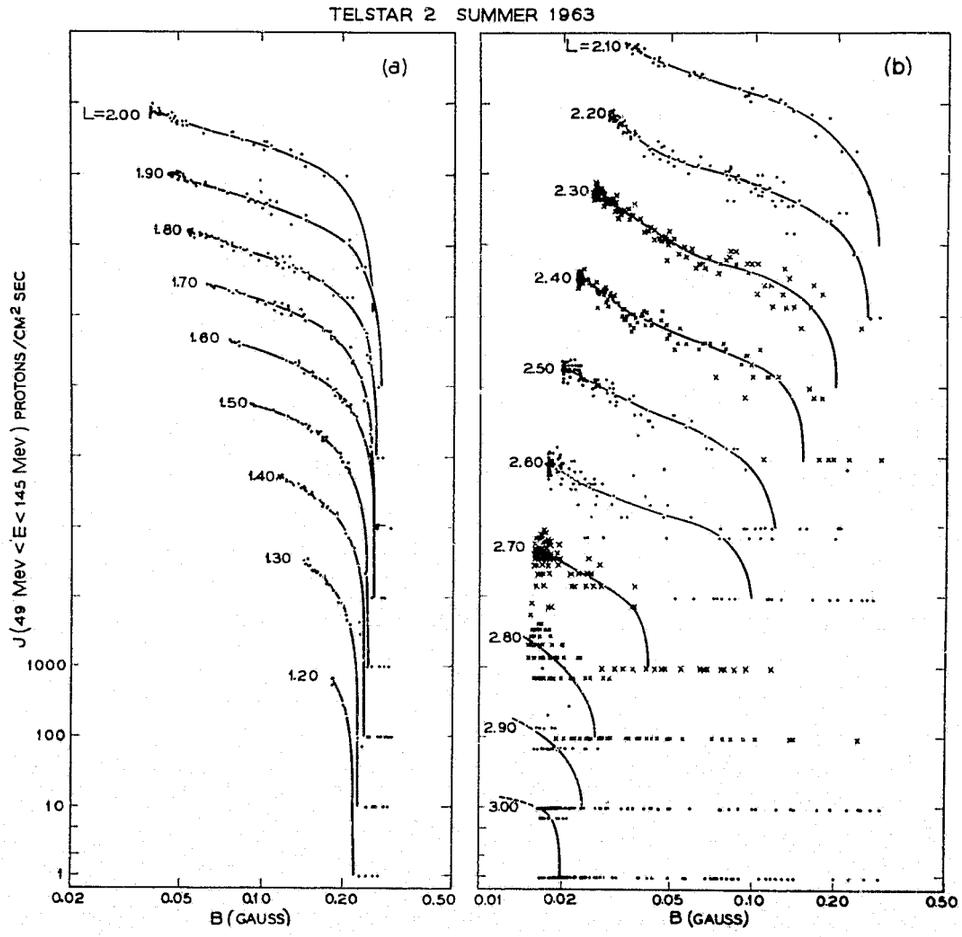

Fig. 5. Flux vs B contours for constant L for the 49–145 MeV protons measured on Telstar 2 from May to September 1963. The representation is as in Figure 2. The lines were hand drawn through the points.

has decreased with time relative to the main part of the proton distribution.

Temporal effects are also apparent in Figure 7. The equatorial flux of both the 49–145 MeV and 18–27 MeV protons is higher for the Winter 1964 curves than for the Summer 1963 curves for L less than about 2.2, while the inverse is true for higher values of L. These curves, however, are averages over several months of measurement, and the data will be considered in more detail below to see what underlies these changes.

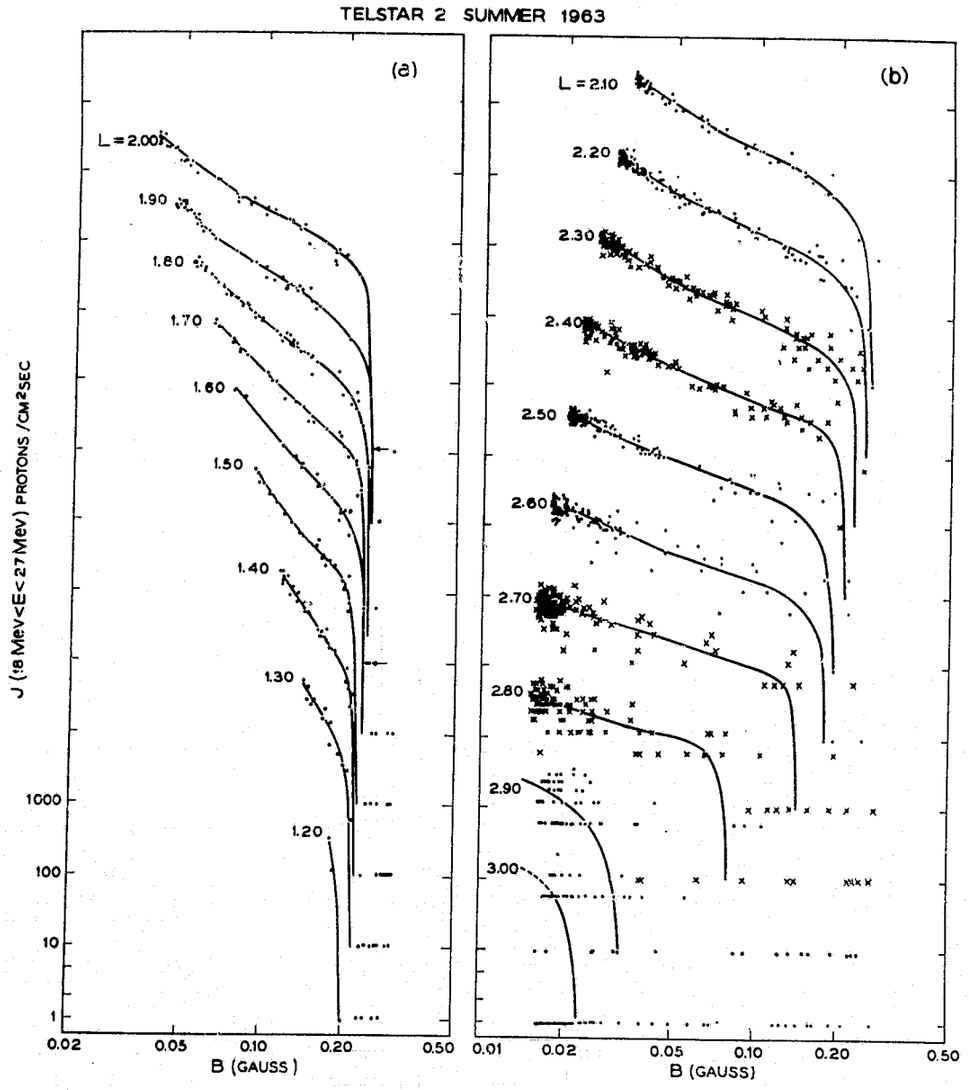

Fig. 6. Flux vs B contours for constant L for the 18–27 MeV protons measured on Telstar 2 from May to September 1963. The representation is as in Figure 2. The lines were hand drawn through the points.

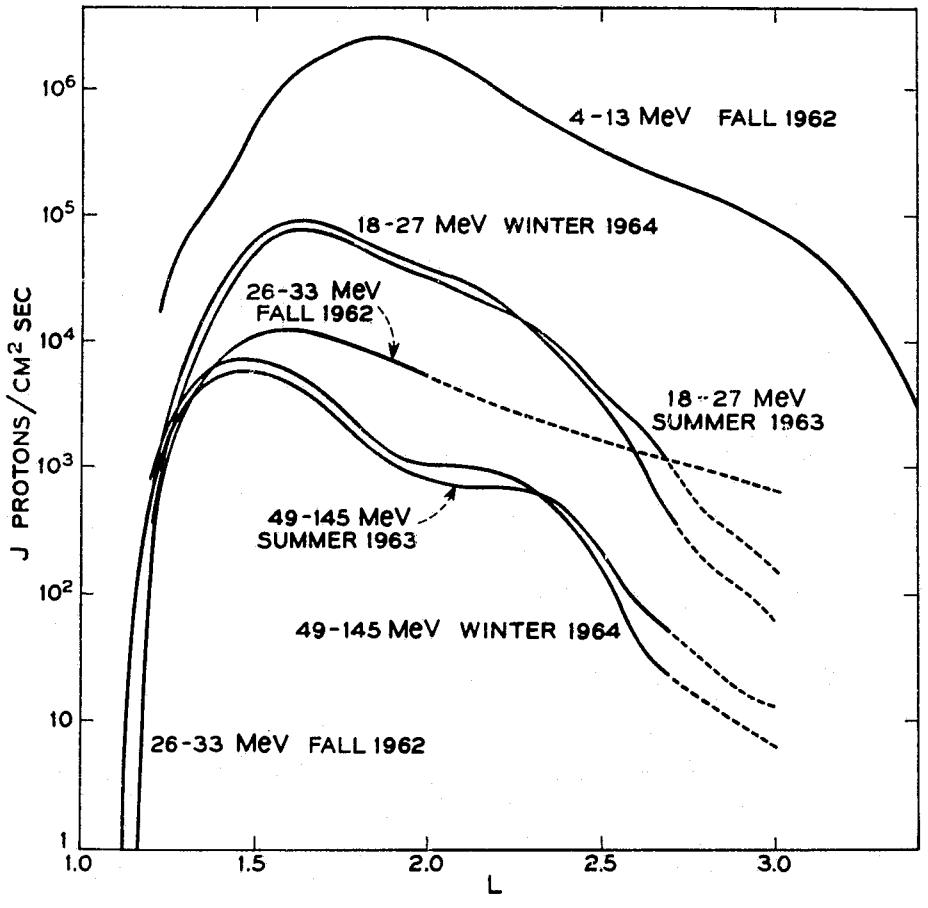

Fig. 7. Flux vs L contours at the magnetic equator. Seasons are the approximate midpoints of the time intervals during which the measurements were made. Dashes are extrapolations.

7. Temporal Effects

The character of the temporal effects in the 49–145 MeV protons on Telstar 2 is displayed in Figure 8, which is a plot of J vs time in days in the various B-L cells indicated in the legend.

Figure 8a, for $1.85 \leqslant L \leqslant 1.90$, is typical of the temporal behavior of the Telstar 2 protons in both (18–27 MeV and 49–145 MeV) energy ranges for $L \lesssim 2.2$. The flux increases steadily with time, and the rate of increase appears independent of B. A careful analysis of the Telstar 1 protons in the energy ranges 26–33 MeV and 50–135 MeV shows no corresponding secular increase between July 1962 and February 1963. The secular temporal effects observed by Telstar 2 are surprisingly large and include at least some long term changes in instrumental sensitivity. A more detailed examination of these effects, based

TELSTAR 2

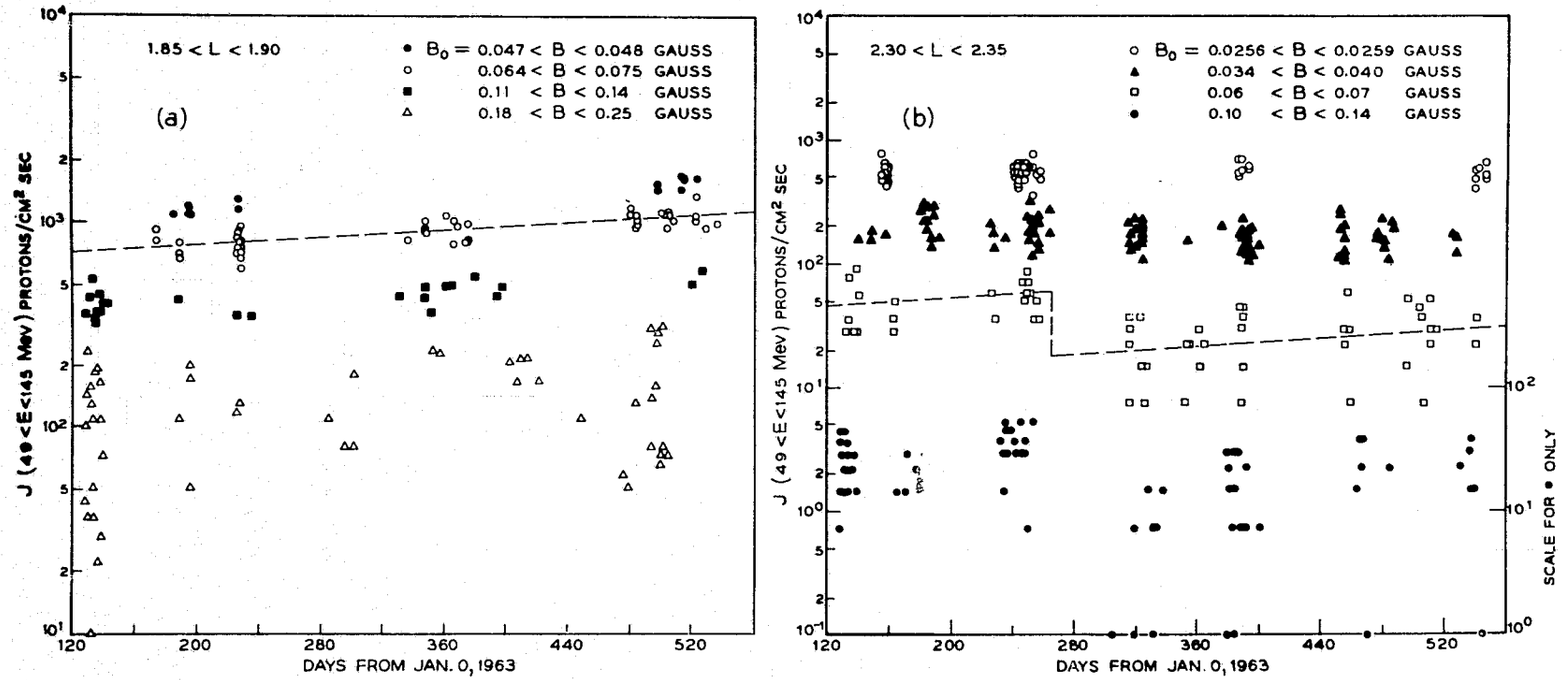

Fig. 8. Flux vs time in days for the 49–145 MeV protons measured on Telstar 2. The points are data taken when the satellite was in the *B*-*L* cells specified in the legend. In (a) note that the flux increases with time and the increase is approximately independent of *B*. In (b) note the decrease in the flux caused by the magnetic storm of day 265, 1963. The fractional decrease is greater in cells for which *B* is larger.

on residuals from computer fits is planned in an attempt to separate out the instrumental component.

In the more sophisticated analysis of the Telstar 2 data presently in progress, a parametric expression of the form

$$y(x) = A[1 + K(t - 265)]\left[\frac{x_e^2 - x^2}{x_e^2(1 - x^2)}\right]^{1/4}\left[1 - \left(\frac{x}{x_c}\right)^2\right]^S \qquad (2)$$

where y=least-square prediction of $\sqrt{\text{counts/sec}}$, $x=\sqrt{1-B_0/B}$; $B_0=(0.311653/L^3)$; t=time in days in 1963; and A, K, x_c, and S are fitted parameters, is fitted to the square root of the counting rate of data in narrow

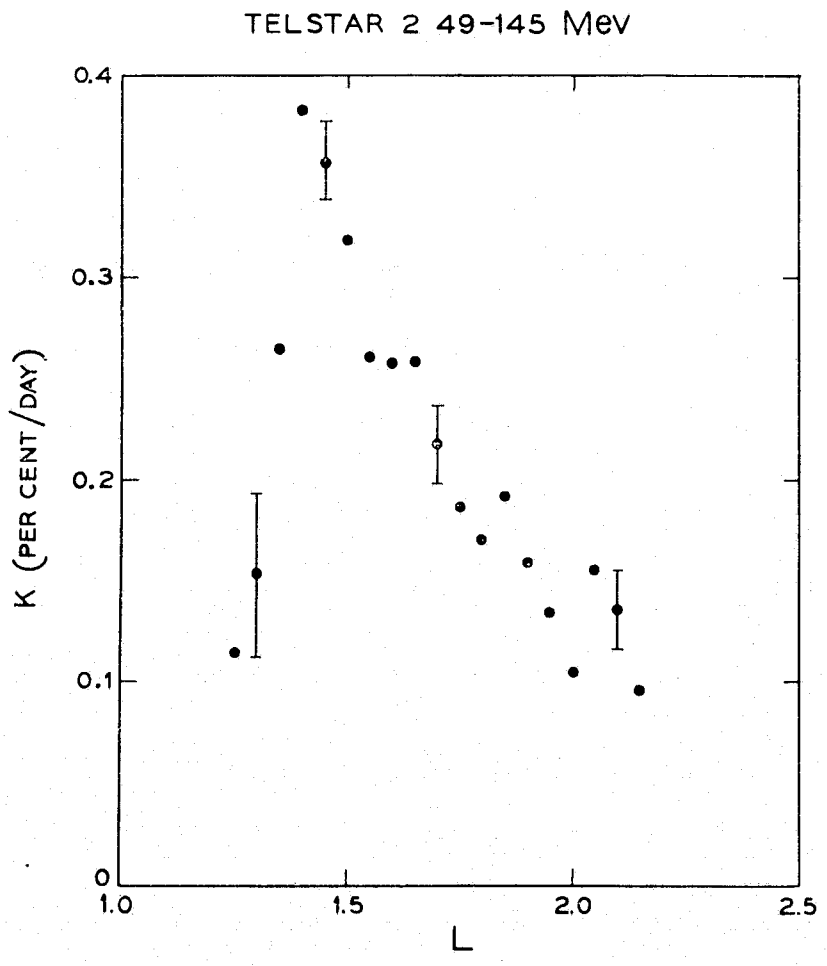

Fig. 9. The values of K, Equation (2), plotted against L. K is the time rate of change of the *square root* of the flux of 49–145 MeV protons from May 1963 to June 1964. The bars are two standard deviations. The per cent change in flux is $\sim 2K$.

L-slices. The parameter K gives the time dependence of the data in the L-slice. The time variation of the data shows no statistically significant dependence on x (or thus B) within L-slices. The values of K from a few preliminary fits to the 49–145 MeV data are plotted against L in Figure 9. The per cent increase in

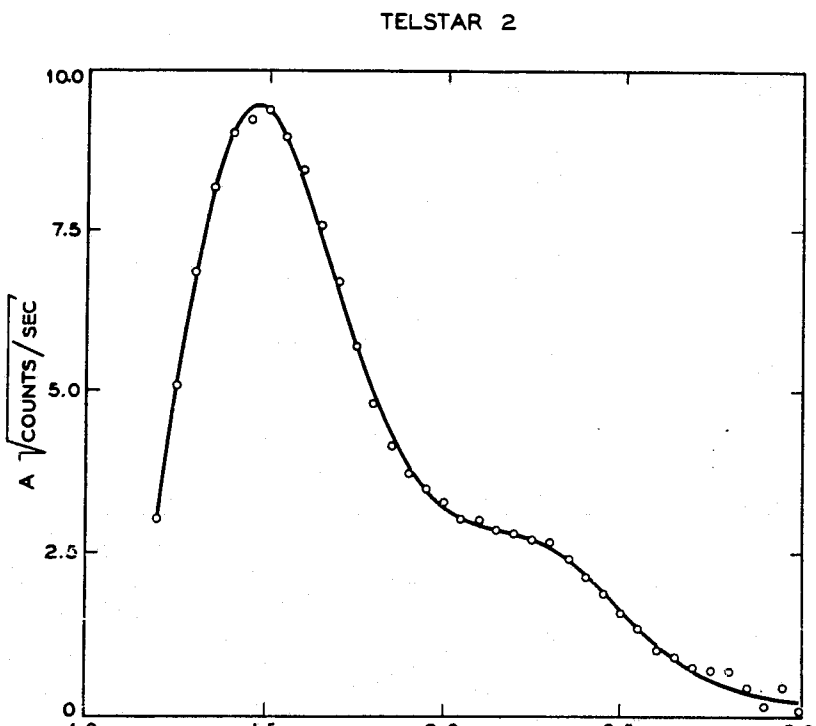

Fig. 10. The value of the equatorial flux for 45–149 MeV protons on day 265, 1963 is given by 76 A^2. See Equations (2) and (3).

flux (flux$\sim(\sqrt{\text{counting rate}})^2$) is$\approx 2K$, and is seen to be 0.7 per cent/day near $L=1.35$, but to drop to 0.2 per cent/day near $L=1.2$ and $L=2.2$. The secular behavior of the 18–27 MeV protons follows the same pattern. These changes are quite large and are presently unexplained.

The values of A in Equation (2) which represent the square roots of the prestorm equatorial counting rates corrected to day 265, 1963 are plotted against L in Figure 10. The line in Figure 10 is given by the expression

$$A(L) = \frac{7.07(L-1.124)}{0.168+(L-0.838)^{5.26}} + 1.49\exp\left[-\left(\frac{L-2.30}{0.313}\right)^2\right] \qquad (3)$$

in which the values of the coefficients are the result of a least-squares fit to the points.

For values of $L \gtrsim 2.2$ the unusual effect of the magnetic storm of day 265, 1963 is superimposed on the secular effect. The Telstar observations of the storm effect extend to higher equatorial altitudes than those of Relay 1, but qualitative agreement between the Telstar 2 and Relay 1 measurements (McIlwain, 1964) is good where the data overlap in space. The storm decreased the number of trapped protons with energies between 49 and 145 MeV and between 18 and 27 MeV for $L \gtrsim 2.2$, and the depletion was completed in less than a day. The magnitude of the storm effect was heavily dependent on both B and L. Although the B-L cells in Figure 8b do not have data immediately subsequent to the storm, the B dependence of the depletion in the L range 2.30–2.35 for the 49–145 MeV protons is apparent. The equatorial fluxes were not noticeably affected, but there is a substantial decrease in flux at the higher B values. Some recovery of the fluxes is also evident. That the effect of the storm was more pronounced at higher values of L may be seen from Figure 7.

The reaction of the 18–27 MeV flux distribution to this storm was qualitatively very similar to that of the 49–145 MeV distribution, although somewhat less pronounced.

8. Energy Spectra

The equatorial flux values prior to the magnetic storm of day 265, 1963 have been corrected to integral flux above the minimum energy of the detector. In the higher energy detectors this has been done by making self-consistent determinations of M in an integral power law spectrum of the form

$$J(>E) \sim E^{-M} \tag{4}$$

in the 18 to 145 MeV region. The 4–13 MeV points have been corrected to integral flux above 4 MeV by extrapolating the power law spectrum for the higher energy detectors down to 13 MeV and adding this contribution to the 4–13 MeV flux. The equatorial results for various values of L are plotted as $J(>E)$ vs E on a log-log scale in Figure 11. To prevent overlap, each set of points is slipped one decade to the right. The values of $M(\pm \approx 0.3)$ are given on their respective curves. The equatorial spectrum in the energy range above 18 MeV is softest near $L=1.9$, hardens slightly with increasing L up to $L=2.8$, and hardens notably with decreasing L between $L=1.9$ and 1.3.

The character of the spectral dependence on B for fixed L may be seen in Figure 12. The points in Figure 12 were derived from the flux maps in the same manner as those in Figure 11. On a given L shell the spectrum hardens with increasing B.

It is clear from the plots that a simple power law is *not* in general sufficient to describe the spectrum down to 4 MeV, although it does reasonably represent the higher energy data. These trends as well as the values of the slopes defining

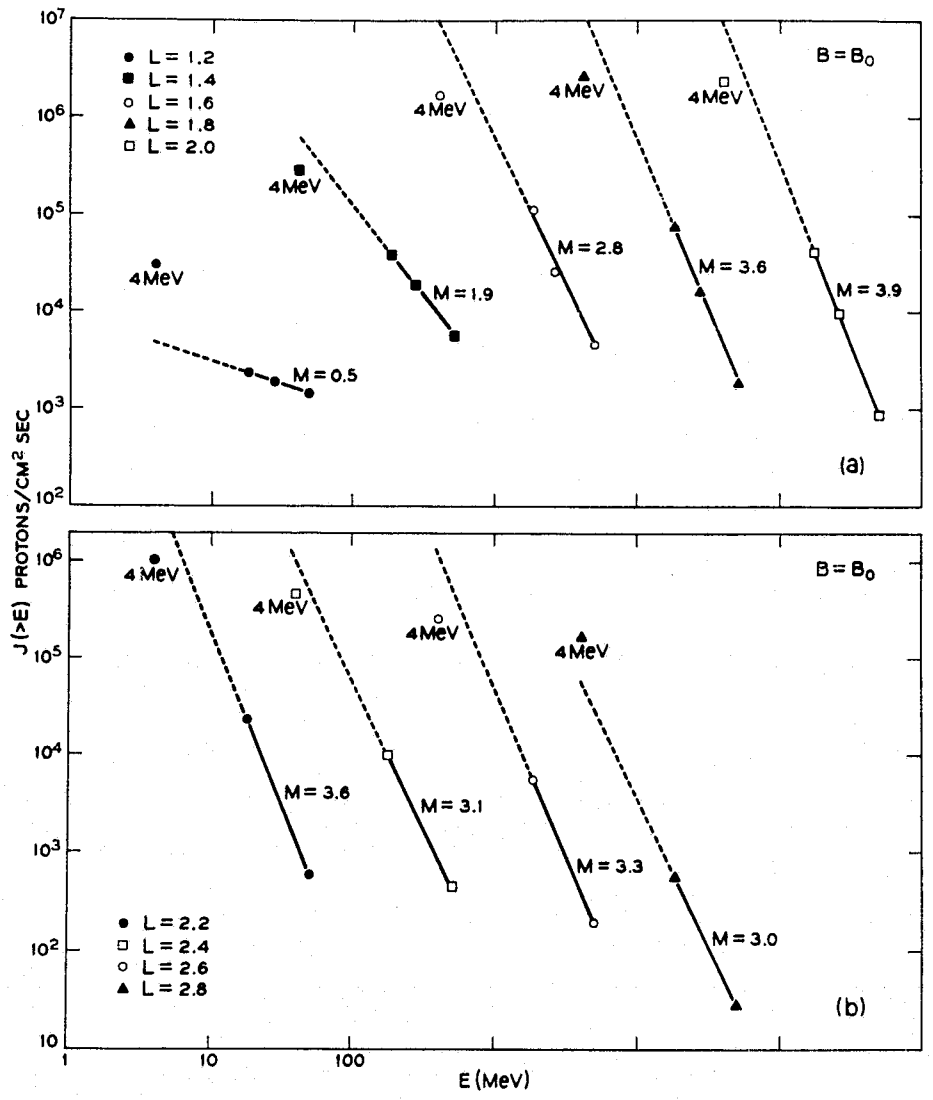

Fig. 11. Integral energy spectra on the magnetic equator.

the spectra are in very good agreement with the published results of other investigators (FILLIUS and MCILWAIN, 1964; and FREDEN *et al.*, 1965) where the data overlap. The present results, however, extend to higher altitudes than were accessible in the earlier experiments.

Various processes for introducing and removing protons from the radiation belt and for influencing the spacial and energy distributions of those present are

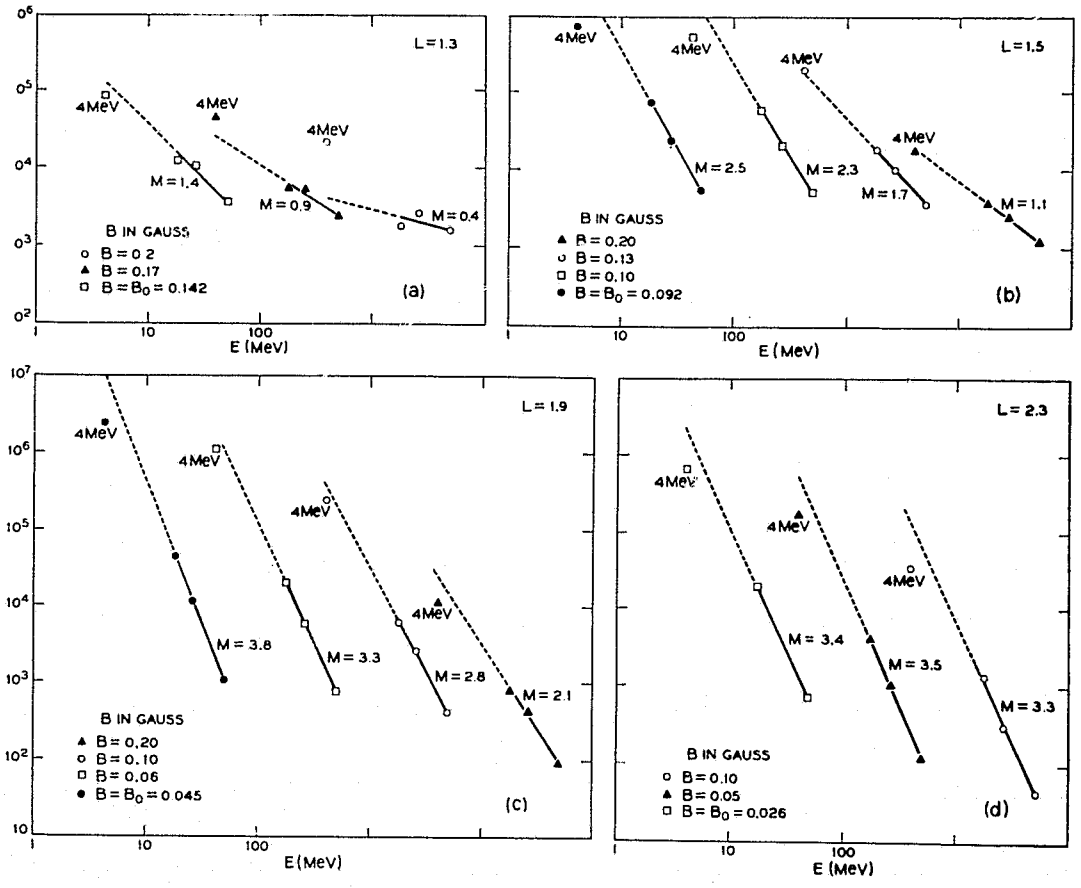

Fig. 12. Integral energy spectra on four L shells.

discussed at length in other papers in this symposium. However, the underlying mechanisms are not yet sufficiently well understood to serve as a basis for a quantitative explanation of the observed flux distributions and energy spectra presented here.

9. Acknowledgement

The authors are indebted to a large number of people for their contributions to this work. In particular, the nonlinear, multidimensional fitting procedures used were developed by Dr. M. B. Wilk. Major contributions to the data analysis were also made by Mrs. M. Becker, Miss E. A. Blake, Mrs. N. L. Graham, Mrs. W. Mammel, Mr. S. Polk, and Mrs. E. E. Yamin.

References

BROWN, W. L.: 1965, *Symposium Proceedings of the Plasma Space Science* (ed. by C. C. CHANG and S. S. HUANG), Dordrecht, D. Reidel Publ. Comp., 1965, p. 189.

BROWN, W. L., BUCK, T. M., MEDFORD, L. V., THOMAS, E. W., GUMMEL, H. K., MILLER, G. L., and SMITH, F. M.: 1963, *Bell System Tech. J.* **42**, 899.
BROWN, W. L. and GABBE, J. D., *Project Telstar Report on Communications and Radiation Experiments with Telstar II* (Bell Telephone Laboratories, Inc., Murray Hill, N. J., 1964), Section 5.
BROWN, W. L., GABBE, J. D., and ROSENZWEIG, W. : 1963, *Bell System Tech. J.* **42**, 1505.
BUCK, T. M., WHEATLEY, H. G., and RODGERS, J. W.: 1964, *IEEE Transactions Nuclear Science* **11**, 294.
DAVIS, L. R. and WILLIAMSON, J. M.: 1963. *Space Res.* **3**, 365.
FILLIUS, R. W. and MCILWAIN, C. E.: 1964, *Phys. Rev. Letters* **12**, 609.
FREDEN, S. C., BLAKE, J. B., and PAULIKAS, G. A.: 1965, *J. Geophys. Res.* **70**, 3113.
GABBE, J. D., WILK, M. B., and BROWN, W. L.: 1966, to be published.
JENSEN, D. C. and CAIN, J. C.: 1963, *J. Geophys. Res.* **67**, 3568.
MCILWAIN, C. E.: 1961, *J. Geophys. Res.* **66**, 3681.
MCILWAIN, C. E.: 1962, private communications.
MCILWAIN, C. E.: 1963, *Science* **142**, 355
MCILWAIN, C. E.: 1964, 'Redistribution of Trapped Protons During a Magnetic Storm' (Department of Physics, University of California at San Diego, April, 1964).
ROBERTS, C. S.: 1965, *J. Geophys. Res.* **70**, 2517.

CHAPTER 3

OBSERVATIONS OF THE TRANSIENT BEHAVIOR OF ELECTRONS IN THE ARTIFICIAL RADIATION BELTS

W. L. BROWN
Bell Telephone Laboratories, Inc.,
Murray Hill, New Jersey

1. Introduction

The sudden artificial alteration of the electron distribution in space by high altitude nuclear tests has provided a unique opportunity to study the relaxation processes or loss mechanisms that are effective in controlling the natural particle distribution. Observations of the artificial belts of energetic electrons and their transient decay following the U.S. and U.S.S.R. nuclear tests of 1962 have been made by instruments on the Telstar I and II, Relay I and II, and Explorer XV and XXVI satellites. The most dramatic results from these experiments have been obtained on Telstar I and Explorer XV which were advantageously in orbit at times of major activity during the testing period. Descriptions of their observations are contained in Sections 2 and 3 and comprise the primary part of this paper. Some observations made by Relay II long after the creation of the artificial radiation belts will be discussed in Section 4.

All the measurements described in this paper were made with the same type of particle detector, a silicon diffused p-n junction device (BUCK *et al.*, 1964) with a sensitive volume about 2 millimeters in diameter and 0.4 millimeters in thickness. The geometrical arrangement of the detector, its entrance aperture and absorber, varied among the different experiments as did also the electronics that processed the pulses produced in a proportional way by charged particles in the sensitive volume. Because of the relatively small size of this sensitive volume the measurement of high energy electrons required entrance absorbers to remove the lower energy portion of the electron flux distribution. In the Telstar I configuration with an open entrance aperture the detector had a principle sensitivity to electrons of less than 1 MeV and primarily measured electrons above about 0.5 MeV. In the Explorer XV experiments a series of detectors were used with different entrance absorbers. Results from three of these devices measuring electrons above 0.5 MeV, above 1.9 MeV, and above 2.9 MeV are described in Section 3.

2. Telstar I, Starfish and the U.S.S.R. Tests

2.1 *Electron distributions following the Starfish test*

Telstar I was launched on June 10, 1962 (day 191), one day after the U.S. high altitude nuclear test Starfish. The order of these events has clouded the evaluation of the effect of the nuclear explosion because of the meager information concerning the natural electron distribution present before the test in

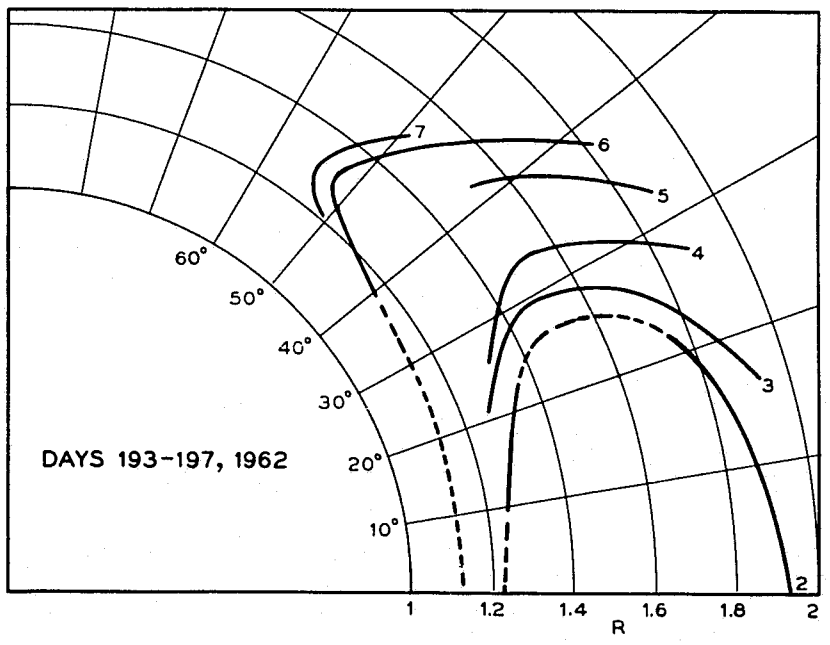

Fig. 1. Contours of equal omnidirectional counting rate for electrons from Telstar I in the time period from Day 193–197, 1962. The contours are two to a decade as follows: $2 - 6.6 \times 10^7$/cm^2 sec; $3 - 2.1 \times 10^7$; $4 - 6.6 \times 10^6$, etc. The omnidirectional counting rate is related to the omnidirectional flux of particles by the efficiency factor of the detector.

most of the region that Telstar I actively explored. The changes in the distribution observed by Telstar subsequent to July 10 lead to the conclusion that Starfish introduced a high flux of electrons over a very extensive region of space. These electrons may have originated from fission beta decay (CARTER *et al.*, 1959) or alternatively they may have been thermal electrons heated by a shock wave created by the explosion as discussed by COLGATE (1966).

The earliest electron distribution that could be well determined from Telstar I data (BROWN *et al.*, 1963a; BROWN and GABBE, 1963) is shown in Figure 1. The plot is in R-λ space where the coordinates are derived from the McIlwain parameter L (MCILWAIN, 1961) and from the magnetic field strength B as given by the 48 term

Jensen and Cain expansion for the earth's field (McIlwain, 1962). The figure spans a five-day time period starting on July 12 (day 193) three days after Starfish. A period of five days was required to gather enough data to construct a satisfactory contour plot. The distribution is changing radically in time as will be seen in subsequent figures, and thus the contours of Figure 1 are averages over the indicated time period. The contours are of equal omnidirectional counting rate and were hand drawn through sets of measured points corresponding to a given

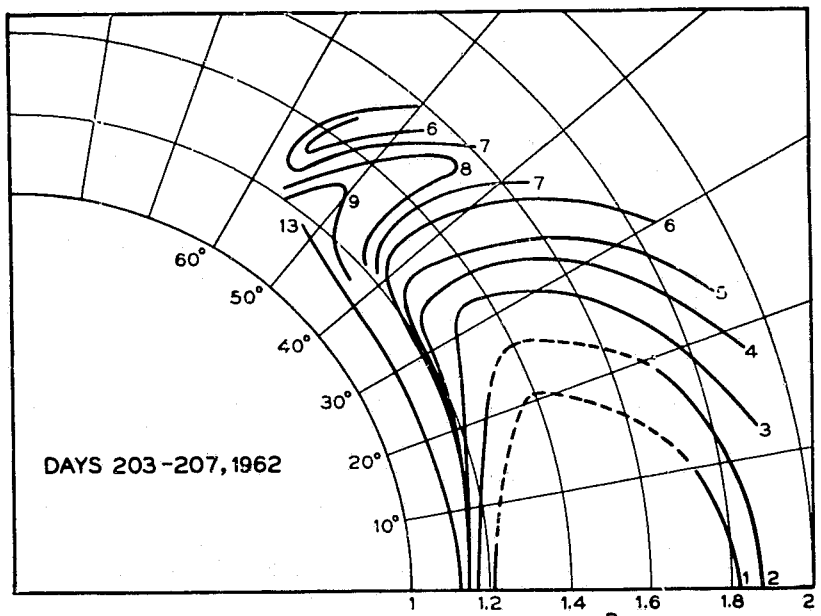

Fig. 2. Contours of equal omnidirectional counting rates for Days 203–207, 1962. The contour labelling is the same as in Figure 7 except that Contour 1 with an omnidirectional counting rate of 1.5×10^8 is now in evidence. This contour is slightly out of the normal two-to-a-decade order.

range of values of the omnidirectional counting rate (Brown *et al.*, 1963a). The contours are two to a decade and are dashed where data is missing. Contour 1, for the highest electron flux density measured, does not show in the distribution of Figure 1 because of the satellite orbit. The contour number has been saved for use on later figures. Contour 2, the highest in Figure 1, corresponds to an omnidirectional counting rate of about $7 \times 10^7/\text{cm}^2$ sec. Notice that the contours of Figure 1 show only a single maximum in electron flux even up to latitudes above 50 degrees where the outer electron belt would be expected to be seen.

Figure 2 illustrates the electron distribution about two weeks after Starfish and 10 days later than Figure 1. Contour 1 is now observed at low latitudes,

near the equator at both high and low altitudes. The satellite orbit has not yet precessed sufficiently to complete the contour as indicated by the dashed portion of the curve. Contour 1 has an omnidirectional counting rate of about 1.5×10^8 counts/cm^2 sec. Because of the detector sensitivity as a function of electron energy, the overall efficiency of the detector in the presence of an electron spectrum produced by fission fragment beta decay is approximately 0.2 (BROWN *et al.*, 1963a). The highest flux contour thus represents a total electron flux for

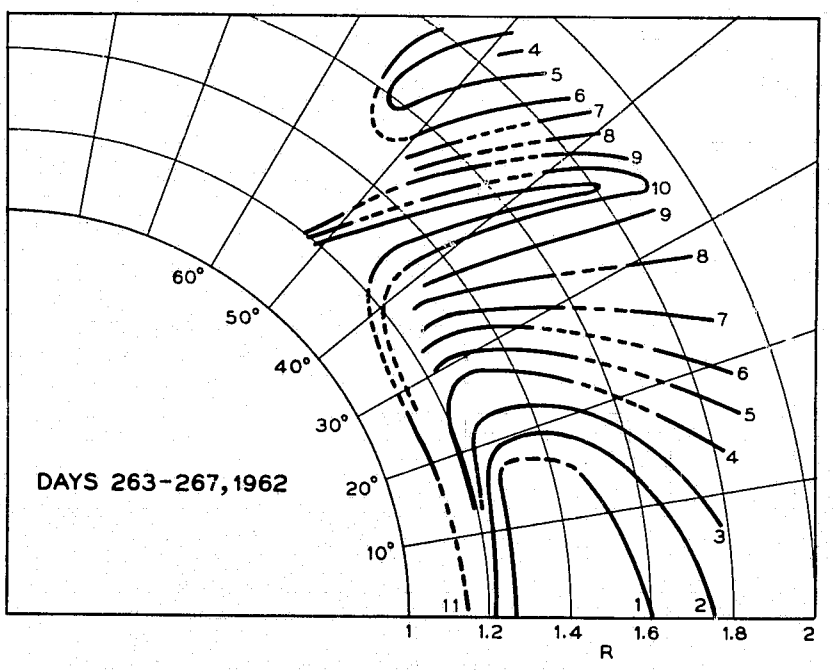

Fig. 3. Contours of equal omnidirectional counting rates for Days 263–267, 1962. The contour designations are the same as in Figures 1 and 2.

that assumed spectrum of approximately 8×10^8/cm^2 sec. If the spectrum is substantially softer than a fission beta decay spectrum, as it probably is in much of the figure, the total electron flux corresponding to Contour 1 might decrease by as much as a factor of 1.5. The contours in Figure 2 have changed very substantially in comparison with those in Figure 1. A second maximum in the distribution now appears as a result of a decrease in the electron flux that is particularly pronounced in the region between 35 and 50 degrees latitude. This second maximum is the tip of the outer belt which was indistinguishable from the inner belt because of the anomalous population of electrons that had earlier filled in "the slot" between the two. Notice also that where Contour 2 had

crossed the $R=1.8$ earth radii line at about $\lambda=18$ degrees in Figure 1, Contour 3 occupies a similar position in Figure 2. There has been a general decay in the electron population.

Decreases in the electron flux distribution over the whole region of Telstar I's orbit continued throughout the summer. The situation in mid-September is shown in Figure 3. Contour 5 now crosses $R=1.8$ at 18 degrees, a decrease by a factor of 30 compared with Figure 1. The slot between the inner and outer belt has become very deep. The omnidirectional counting rate at $R=1.6$ and $\lambda=40$ degrees is given by Contour 11, $2\times10^3/\text{cm}^2$ sec., a thousand times less than the intensity at the same position in Figure 1.

2.2 *Decay times for the Starfish electrons*

Figure 4 shows the omnidirectional counting rate on several L lines as a function of time between the launch of Telstar I and the day before the first of the U.S.S.R. high altitude nuclear tests on October 22 (day 295). The figure shows in a more continuous way the electron flux decay discussed in connection with

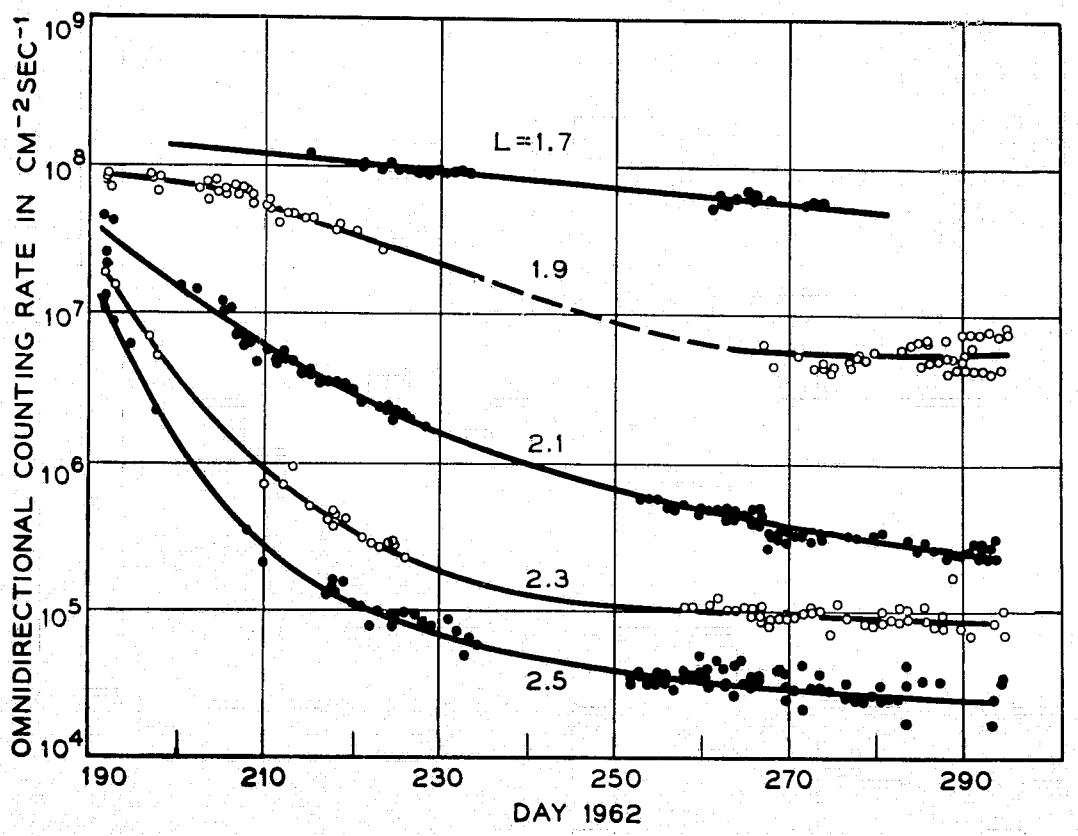

Fig. 4. The time dependence of the counting rate in narrow lamda ranges on several L lines.

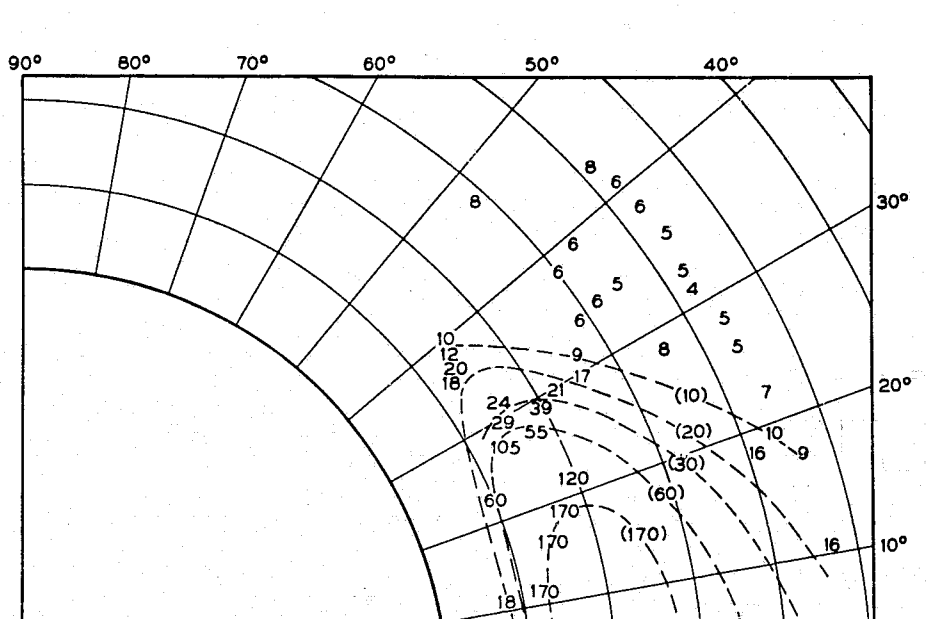

Fig. 5. The initial time constants from data such as in Figure 4 displayed in R, λ space. The decay times are in days. The dashed lines connect regions of equal decay times as indicated by the numbers in parentheses.

Figures 1 through 3. The points are taken in each case in a narrow range of λ on an individual L line. The λ intervals are taken near the equator for $L=1.7$ and 1.9 and at increasingly large λ values for larger values of L. The data points occur in clusters because of the precession of the satellite orbit. On $L=2.5$ the decay is observed to be fast and, overall, very large. This region is in the heart of the slot where the contour plots show the decay of a factor of about 1000. On $L=1.7$ the decay is slow and only amounts to about a factor of two over the three month period. There are indications that in the last month of the time interval the electron flux on the higher L lines tends toward a steady-state. This may quite possibly be at values determined by natural source and loss processes.

The decay curves of Figure 4 are not exponential. If they were, the curves would be straight lines on the semilogarithmic plot and would approach a steady-state value with a rather sharp corner. However, assuming the initial decay is approximately exponential, a time constant has been associated with the initial slope of these curves and others like them throughout the space in which Telstar I collected data. The time constants are themselves plotted in R-λ space in Figure 5. At the lowest altitudes the decay times are short as noted by VAN ALLEN (1964). At intermediate altitudes near the equator the decay

time is relatively long and at the highest altitudes and in the slot the time is once again short. The lightly dashed lines in the figure attempt to connect regions of approximately equal decay time. The shape of these lines is very roughly equivalent to the shape of the inner belt itself as seen in Figure 3. Clearly the rates of decay of the particles are closely related to the number of particles to be found in different regions. This is to be expected in a steady-state case and in a case of a still decaying transient following a broad injection of new particles. The decay times over the slot region are the order of a week and vary very little with L. Decay times of this same order are observed in the outer belt region after natural increases in the normally unstable outer belt flux (BOSTROM and WILLIAMS, 1965).

The question of the loss mechanisms responsible for the results of Figure 5 is of evident importance. At low altitudes (on L lines below about 1.3 earth radii) there seems to be no question but that loss is produced by interaction of the electrons with the earth's atmosphere. This correspondence is very beautifully displayed in the results of VAN ALLEN (1964) from the Injun satellite and the calculations that WALT (1964) has made of atmospheric scattering processes. The Telstar results are entirely consistent with this work but are much less extensive because of differences in the orbital properties of the Telstar and Injun satellites. The lifetime for atmospheric scattering increases very rapidly with increasing altitude and is incapable of explaining lifetimes the order of a year between $L=1.3$ and 1.6, much less lifetimes the order of a week on still higher L lines that fall in slot. It has been proposed by DUNGEY (1963) and by CORNWALL (1964) that resonant interaction of circularly polarized electromagnetic whistlers with the high energy trapped electrons might provide the new loss mechanism needed. Figure 6 shows lifetimes from Figure 5 replotted against L and compared with Dungey's initial calculations. Decay times measured by Explorer XV for electrons with energy >1.9 MeV have been added to the >0.5 MeV results of Telstar I in the region between $L=2.0$ and 2.6. The higher energy particles also have decay times in this region which are of the order of one to two weeks. Figure 6 shows an extremely appealing correspondence with the observed L dependence of τ on the high altitude side of the inner belt. However, ROBERTS (1966) has shown in a more complete calculation of the whistler model that there are very substantial failures of this model when an attempt is made to explain the observations of the L, λ, and energy dependence of the electron decay times.

2.3 *New particles from the U.S.S.R. tests*

A series of three high altitude nuclear tests on October 22 (day 295), October 28 and November 1 again grossly disturbed the electron population in the region of the slot and the high altitude side of the still slowly decaying Starfish belt.

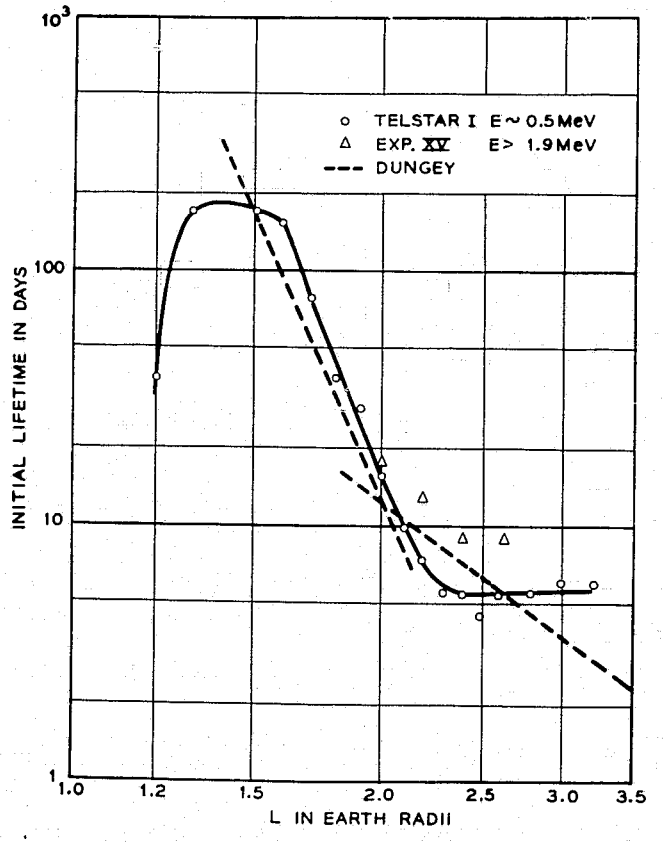

Fig. 6. The L dependence of the initial decay time for electrons compared with Whistler mode electron loss according to DUNGEY (1963).

No new electrons were detected on L lines below 1.7 in any of these three tests. Because of the character of the new particle distributions and the more extensive satellite instrumentation which was in space to observe them (MCILWAIN, 1963, 1966; KATZ, 1966; IMHOF and SMITH, 1965 and WEST, 1966) these events added significantly in support and extension of information gained from the Starfish test. Telstar observations are shown in Figure 7 for three L lines in the slot region. The figure shows the long period of decay following Starfish and the sudden increase in flux on day 295, almost a factor of 100 on $L=2.2$. A rapid decay (decay time of the order of three days on $L=2.2$) is observed immediately afterward. It is followed by another upsurge in electron flux on day 301. The decay following the second U.S.S.R. test is not quite so rapid as that following the first, but still the characteristic time constants are the order of a week or less. A third U.S.S.R. test on November 1 added no electrons to any of the L lines shown in Figure 7. As will be seen in the results of Explorer XV, the third test created a very narrow band of electrons on an L shell of approximately 1.76.

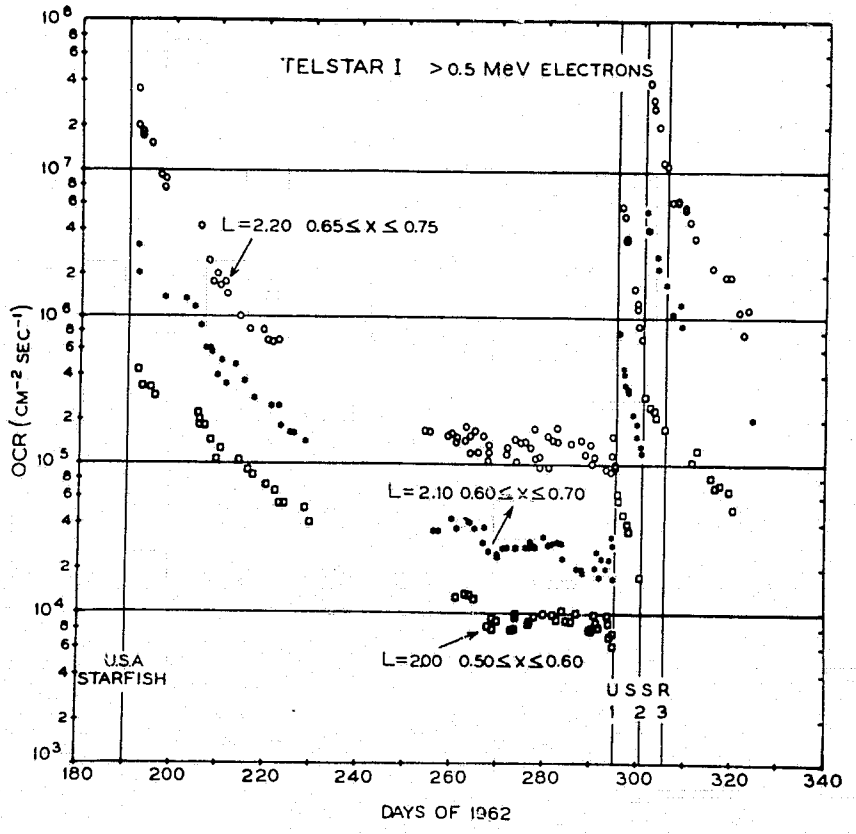

Fig. 7. Telstar observations of the U.S.S.R. tests on October 22, October 28, and November 1 following long term decay of electrons from Starfish. In the figure $x=\sqrt{1-B_0/B}$.

3. Explorer XV, the U.S.S.R. Tests

3.1 *New particles from the second and third U.S.S.R. tests*

Explorer XV was launched into a low inclination orbit about five hours before the second U.S.S.R. test on October 28. Fortuitously it was thus able to obtain data on one complete orbit before new electrons were added to the distribution. The data for the early orbits on October 28 are shown in Figure 8 for an electron detector measuring electrons >0.5 MeV. Orbit 1′ is the nearly equatorial returning half of the first orbit and shows the inner edge of the outer belt, the slot and the rise toward the inner belt maximum. The slot is not as empty of electrons as it was a week earlier because of particles added in the first U.S.S.R. test (see Figure 7). At 0407 hours on October 28 the satellite crossed $L=2.0$. When it crossed outward bound about an hour later (0518) new particles had been added above $L=1.8$. The initial transient of particles in their longitudinal distribution around the earth is not yet complete at this time as evidenced by

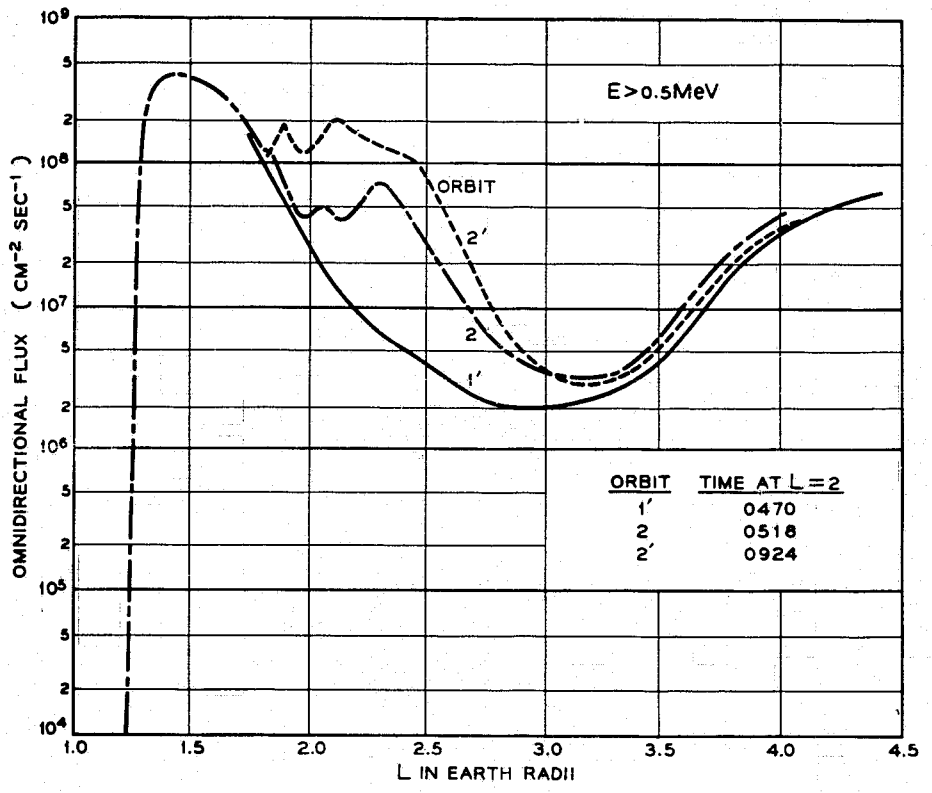

Fig. 8. The omnidirectional flux of electrons of >0.5 MeV for Explorer XV for the early passes on October 28, 1962. The satellite is nearly equatorial and the figure thus gives a nearly equatorial trace through the particle distribution.

the further increases in flux seen on the returning half of the second orbit some four hours later, curve 2′. By this time electrons with energies >0.5 MeV will have drifted at least five times around the earth and the distribution in various L shells should be longitudinally reasonably uniform. The observation of the transient in longitude permits a rough determination of the initial time of injection of new particles at 0440 ± 10 minutes (BROWN, 1965).

Figure 9 shows the early results of a second detector on Explorer XV which measures electrons above 1.9 MeV. The two small spikes on orbit 1′ at $L=1.85$ and 2.0 are probably remnants from the first U.S.S.R. test as is most of the flux in the slot region. In this higher energy detector a higher flux of electrons is observed in orbit 2 at $L\approx 1.8$ then in orbit 2′. This might indicate electron decay, but it is more likely to be due to a clump of newly injected high energy electrons not yet dispersed in longitude on orbit 2. By orbit 2′ the clump will have disappeared. The structure of the added electrons is quite complex as observed in both the low and high energy electron detectors. It is related in a complicated

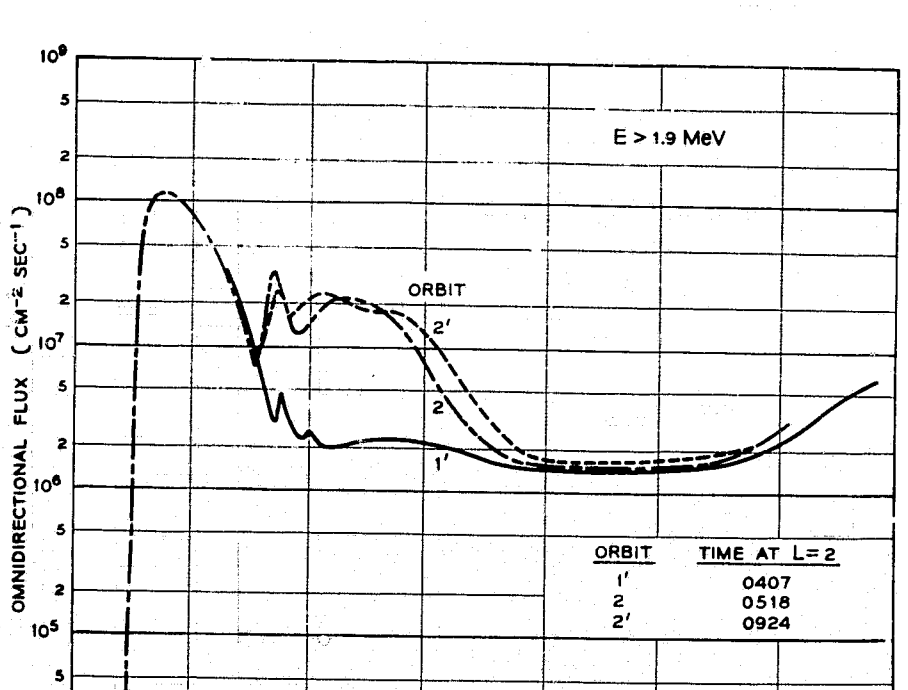

Fig. 9. The omnidirectional flux of electrons of > 1.9 MeV from Explorer XV for the same period as that in Figure 8.

way to the motion of the radioactive fragments carried in the expanding plasma of the nuclear explosion and to the geometry of shock waves created by the explosion.

A qualitative picture of the spectral distribution of the electrons can be obtained by combining the results from the 0.5 MeV and 1.9 MeV detectors with results from a third detector measuring electrons with energies greater than 2.9 MeV. Figure 10 shows these three curves for orbit 1′, just before the second U.S.S.R. test. The vertical spacings between these curves on the semilogarithmic plot give the relative spectral hardness of the electron distribution. If the spectrum is that of equilibrium fission beta decay the ratios between the curves should be 1:0.3:0.09. Such ratios are very nearly observed in the peak of the inner belt (not shown in the figure) at an L value of about 1.4. It is clear from Figure 10 that in the center of the slot the spectrum is much harder than a fission beta spectrum; it is much softer in the outer belt, and it is substantially softer on the high-L side of the inner belt. There is no particular reason why the spectrum of particles should be appropriate to fission beta decay in any of these

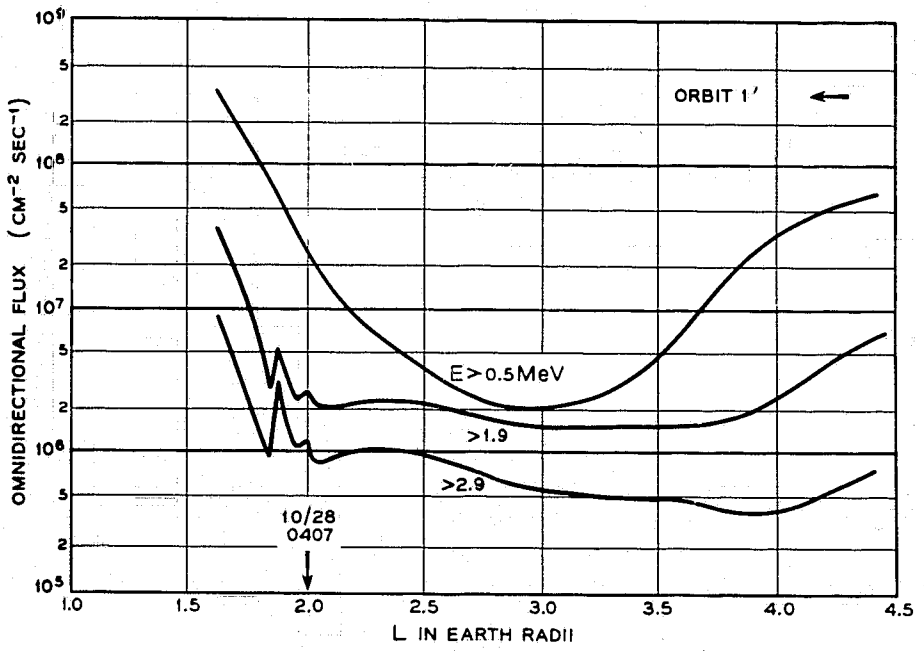

Fig. 10. The omnidirectional flux from three electron detectors on Explorer XV for the first returning pass from apogee on October 28. The variation in the vertical spacing of the curves in the semilogarithmic plot indicates the change in the spectral distribution of the electrons.

regions. The outer belt is composed primarily of natural electrons. The slot contains a residue of electrons from the first U.S.S.R. explosion degraded by loss mechanisms over a period of six days. The high-L side of the inner belt contains a substantial residue of electrons from the Starfish test as well as electrons from the first U.S.S.R. test. The curve spacings of Figure 10 may now be compared with those of Figure 11 which show the results for the same three detectors for orbit 2′, after the added electrons have had time to disperse longitudinally. The spectrum in the slot is substantially softer than it was before at $L=3.0$. A greater number of 0.5 MeV electrons have been added to the population in comparison to the higher energy electrons than would be the case if the added electrons had a fission spectrum. A similar thing is true to varying degrees throughout the region affected by the second U.S.S.R. test. These spectral characteristics are not understood. They either represent degradation of an initial fission beta spectrum or they represent particles that are associated with the explosion but do not originate from the fission beta process at all. Spectral differences of this kind and the difference in the detector response characteristics of the Telstar I and Injun I detectors are doubtless responsible for the apparent discrepancy between the Telstar I and Injun I pictures of the Starfish electron distribution in space (BROWN *et al.*, 1963b).

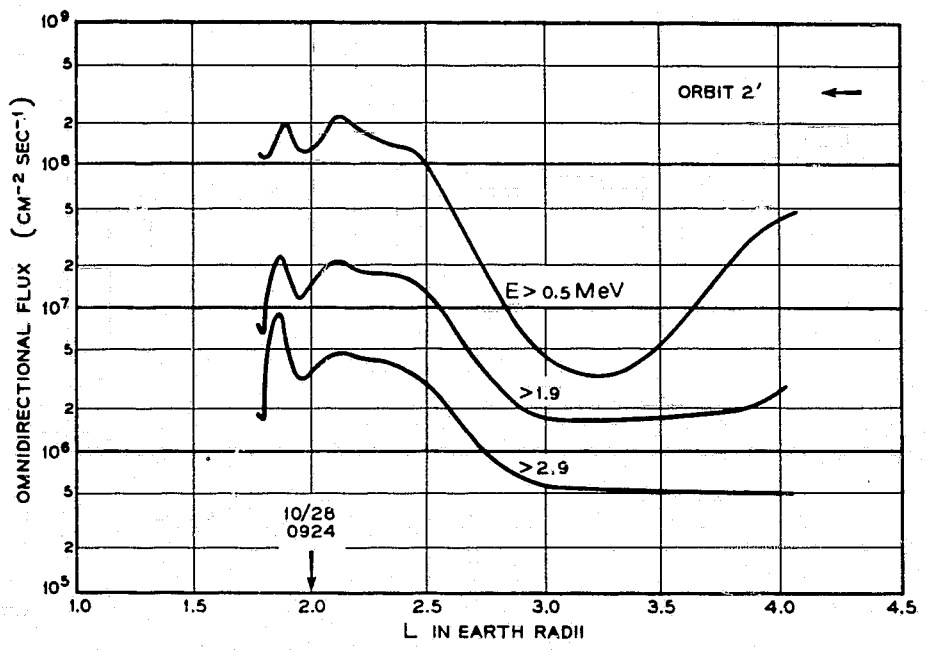

Fig. 11. The omnidirectional flux from the electron detectors of Figure 10 for the second returning pass of Explorer XV. The newly injected electrons have now had time to disperse uniformly in longitude.

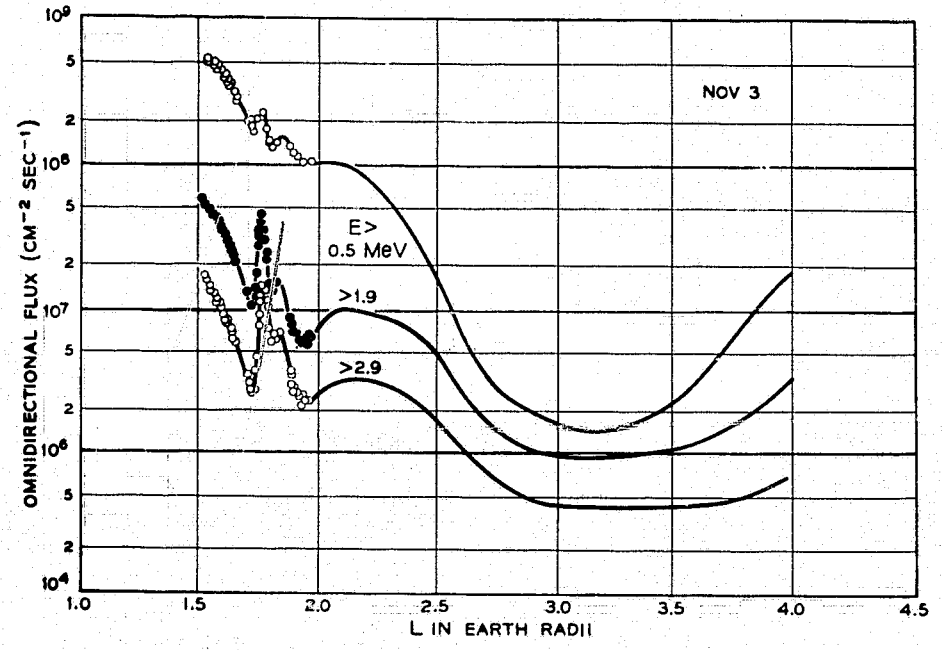

Fig. 12. The omnidirectional flux of electrons from the electron detectors of Figures 10 and 11 on Explorer XV following the third Soviet test on November 1, 1962. The spike of newly added electrons at $L = 1.75$ is extremely narrow.

Figure 12 shows the influence of the third U.S.S.R. test of November 1 as observed on November 3. The only electrons added by this test are contained in a narrow spike at an L value of about 1.76. The second peak at about 1.83 is one of the peaks created by the second U.S.S.R. test. The actual data points are shown on the curves in the low L region to indicate the resolution of the measurements which is important to determination of possible cross-L diffusion of electrons from the new spike. (See Section 3.3.) The spectrum of added particles in this new spike is very nearly that appropriate to fission beta decay.

3.2 *The transient flux distribution along field lines*

The changes in the flux distribution along particular field lines during the general decay of the particle flux following a nuclear test has not been considered explicitly in earlier sections of this paper. Three cases of this kind have been selected from the >1.9 MeV data of Explorer XV, and are shown in Figures 13, 14, and 15. Figure 13 is for $L=1.75$. Each plotted value is obtained by interpolation between actual data points measured along an individual satellite pass.

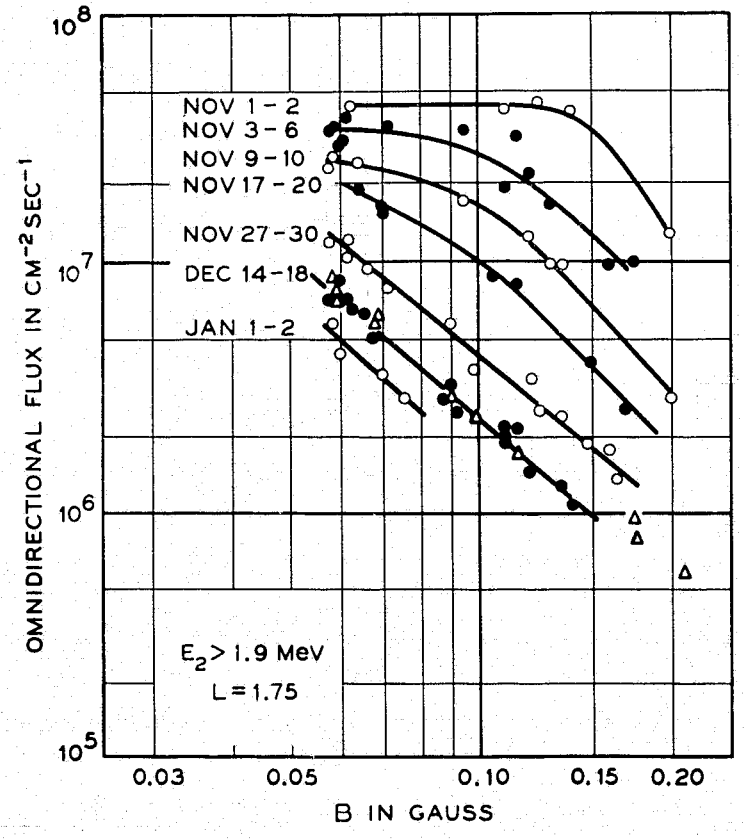

Fig. 13. The B-variation of the electron distribution along the $L=1.75$ line as it changes with time. The triangles are points obtained before the third U.S.S.R. test on November 1.

The triangles in the figure are points obtained prior to the third U.S.S.R. test. There were no particles added at an L value as low as $L=1.75$ by the first or second tests. The triangles define a reasonably straight line in this log flux-log B plot. That is, the distribution is essentially an inverse power law in B, in this

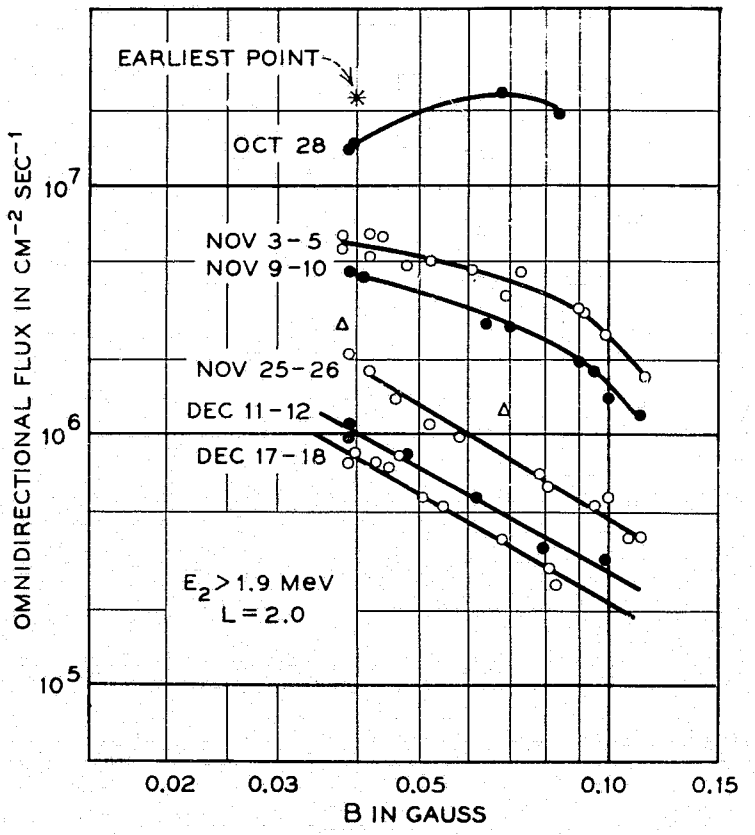

Fig. 14. The B-variation of the electron distribution along the $L=2.0$ as it changes with time. The triangles are the two points obtained before the second U.S.S.R. test obtained on October 28. The star is the earliest point following the shot as in Figure 9.

case with a power of approximately two. The lowest values of B in the figure correspond to the equator on $L=1.75$, and the region of data coverage extends out to approximately $B/B_0 \approx 3$, or $\lambda \approx 30$ degrees.

On November 1 the flux jumps up suddenly by a factor of about five at the equator and a factor of about 20 at $B \approx 0.2$ gauss. The distribution is altered drastically and is no longer nearly a simple power law in B. Over the next few weeks the anomalous new shape of the distribution gradually disappears. By the end of November the distribution is again nearly an inverse power law in

B and at later times the shape is maintained while the distribution as a whole decreases in intensity. More rapid disappearance of particles at large values of B in an abnormal distribution along the field line, and the decay of the distribution as a whole at long times are to be expected in processes controlled by

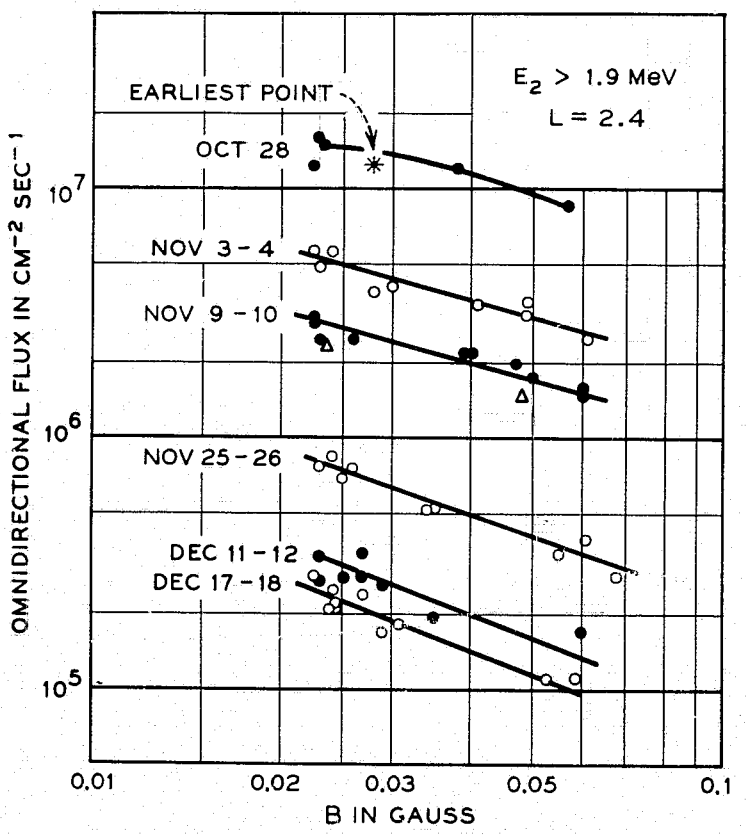

Fig. 15. The B-variation of the electron distribution along the $L = 2.4$ line as it changes with time. The triangles and the star are the same as in Figure 14.

diffusion of particle mirror points along field lines with ultimate particle loss in the atmosphere. This is a situation found by WELCH *et al.* (1963) and by WALT (1964) for lower L values where the atmosphere controls the whole process. It is also the situation discussed by ROBERTS (1966) for a general case of pitch angle diffusion. The fact that the flux in January in Figure 13 has dropped below the data of the triangles for late October is presumably due to a continuing high energy decay of electrons from the Starfish test.

Figure 14 is anologous to Figure 13 but for $L = 2.0$. There are now only two data points (triangles) before the second U.S.S.R. test on October 28. One of

these corresponds to the outgoing, the other to the incoming pass of the first orbit of Explorer XV. The equatorial point is that for orbit 1′ of Figure 9. The star marked "earliest point" in Figure 14 is for orbit 2, at which time the high energy electrons had not yet dispersed in longitude. At $L=2.0$ the flux-B variation shows a maximum off the equator, an even more anomalous distribution than that seen on $L=1.75$. Such a new distribution results from injection of new particles far off the equator (WEST, 1966). This grossly distorted shape rapidly disappears and the decay process carries past the triangles of October 28 because of continuing decay of electrons from the first U.S.S.R. test. The slope of the power law distribution which characterizes the steady-state shape during the later stages of decay has a value on $L=2.0$ of only approximately 1.35.

Results for a third field line $L=2.4$, are shown in Figure 15. On this field line the shape of the electron distribution following injection is much less anomalous and a steady-state power law dependence is rapidly reassumed. The slope of this line is approximately 1.05.

The form of the decay illustrated in Figures 13, 14, and 15 is characteristic of all the field lines examined. The decay is in essence by normal modes. Higher modes, corresponding to more extreme deviations from the steady-state shape, decay rapidly. However, there are systematic L dependent trends in the parameters of the system. First, the decay is more rapid going to higher L values from

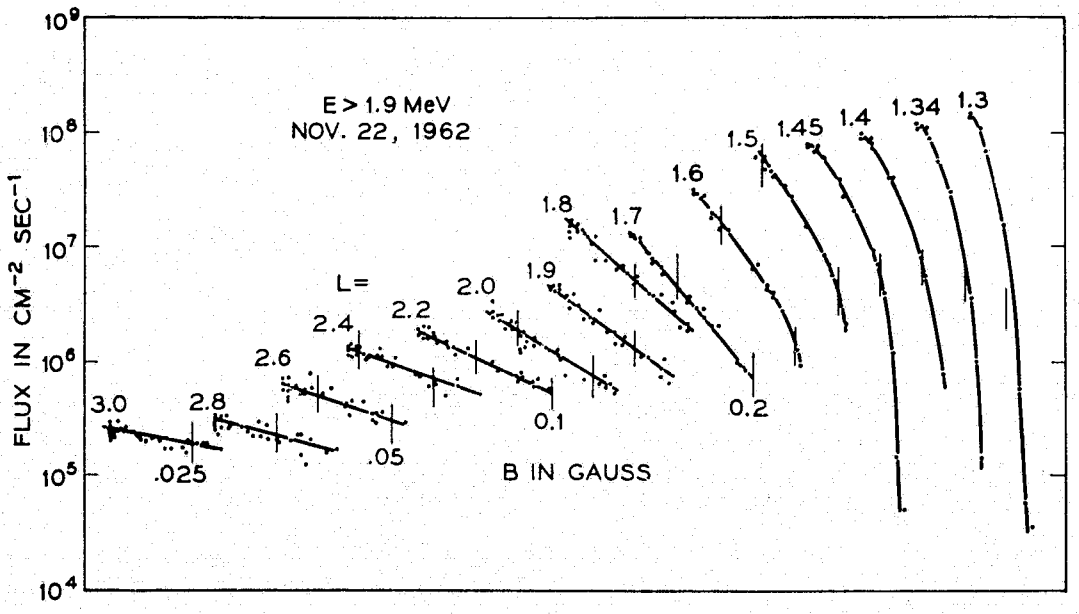

Fig. 16. The B-variation of the electron flux along a number of different L lines as observed by Explorer XV on November 22. Note the decrease in the slope of the log flux vs log B lines as L increases.

$L=1.7$. This is in reasonable quantitative agreement with the lower energy electron results of Telstar I following the Starfish test as shown in Figure 6. Second, the steady-state shape of the log flux-log B distribution is progressively more shallow on higher L shells. This feature is illustrated more completely in Figure 16 which shows the distributions on November 22 over a wide range of L values. The curves in the figure have been shifted horizontally with respect to one another to avoid overlapping. Since the observed particle loss rate increases in going to L values greater than 1.7, and since the gradient of the distribution at the same time decreases, then a pitch angle diffusion mechanism which may be stirring up the particles on a given field line and bringing them at random into the atmospheric loss cone, must operate with increasing effectiveness on higher L lines. That is, the pitch angle diffusion coefficient must increase with L.

3.3 *The width of the electron distribution from the third U.S.S.R. test – Cross-L diffusion*

As was observed in Figure 12, the U.S.S.R. test on November 1 introduced a very narrow band of high energy electrons at $L \approx 1.76$, below the electron distributions added by the two earlier tests. The width of this band as a function of time provides a sensitive measure of cross-L diffusion in this region of space. Figure 17 shows snapshots of the >1.9 MeV electrons in this band observed in four passes of Explorer XV during the three weeks following the creation of this new perturbation in the trapped particle distribution. A total of 18 such passes have been examined in comparable detail. Each peak in Figure 17 is marked with the L value of the center of the peak and with it the corresponding time and value of B. In each case examined the center falls at $L=1.765\pm0.010$. This variability is due to limitations in the calculated value of the L parameter arising from uncertainties in the magnetic field. The flux observed in the peak is a function of both B and time as noted in Figure 13. During November the distribution is decaying toward the steady-state shape that characterizes its lowest normal mode. In each part of Figure 17 the data shown include a portion of the high-L side of the inner belt at L values below the new peak. The >1.9 MeV electrons in this region are those left from the Starfish test of July. They are continuing to decay slowly. The passes also show fragments of the data at L values above the new peak. These electrons were those created in the first and second U.S.S.R. tests. They are decaying more rapidly than the Starfish electrons at $L=1.7$ and below but not much more rapidly than the new peak itself. There are breaks in the data which occur because of the time sharing mode in which this part of the experiment in the satellite is being operated.

The full width at half maximum of each peak in Figure 17 is indicated. It has been deduced assuming a Gaussian shape and is obtained by subtraction of an extrapolated background of the Starfish electrons. The fit has made use

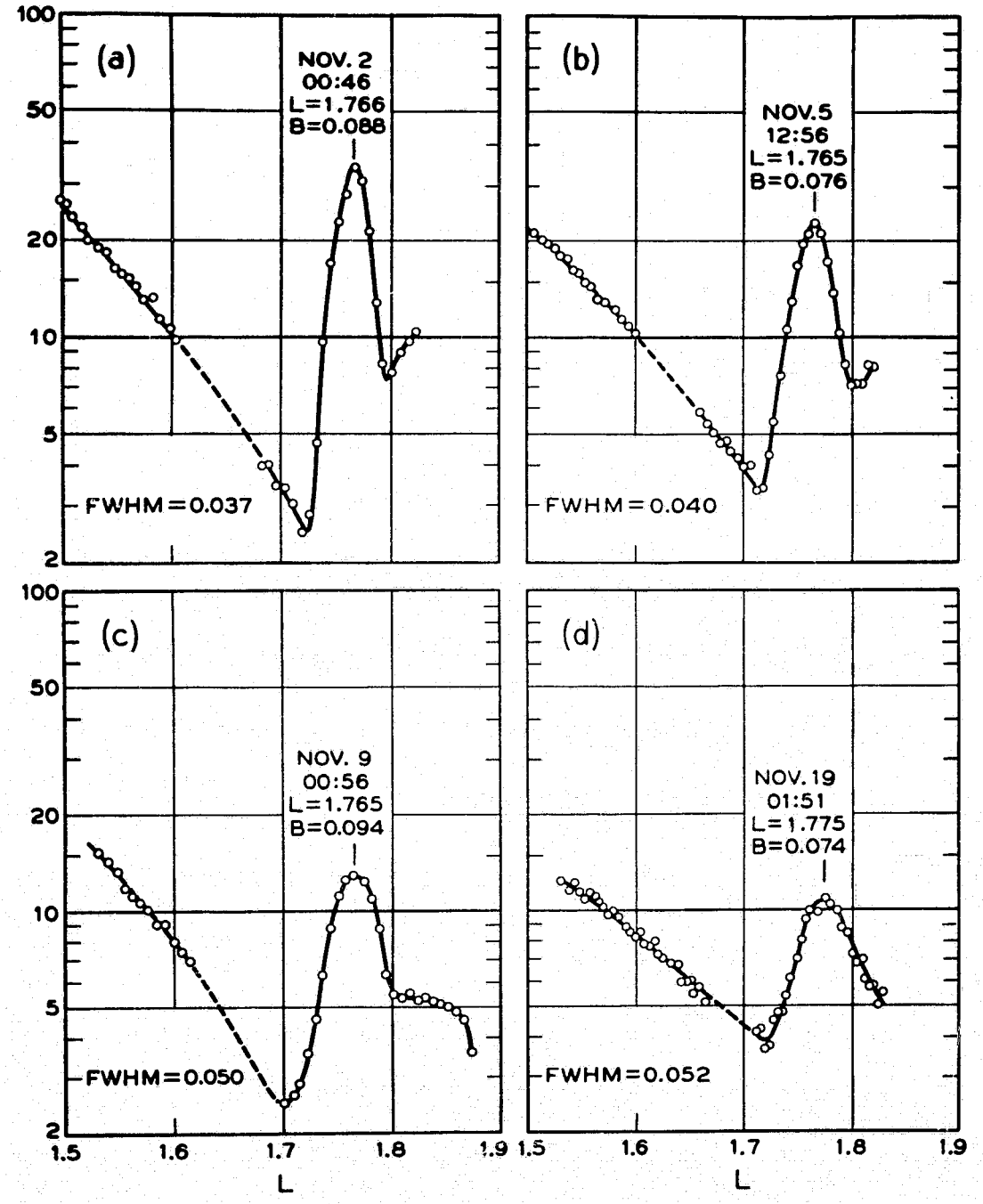

Fig. 17. Details of the narrow peak produced by the third U.S.S.R. test as observed on four passes in November. The date, time and B value of each peak center are noted as is also the full width at half maximum of a Gaussian fitted to the peak.

of the high-L side of the peak only for determination of the peak's center location. The width has been determined from the low-L side where the background subtraction is more easily carried out. The widths observed are all quite narrow, varying from 0.037 earth radii for part (a) to 0.052 for part (d) of the figure. The electrons are thus located in a shell about 250 kilometers thick, a dimension still large compared with the approximately one kilometer radius of the electron spiral in the magnetic field.

Figure 18 is a compilation of the line widths measured on 18 different satellite passes. The square of the full width at half maximum is plotted against time.

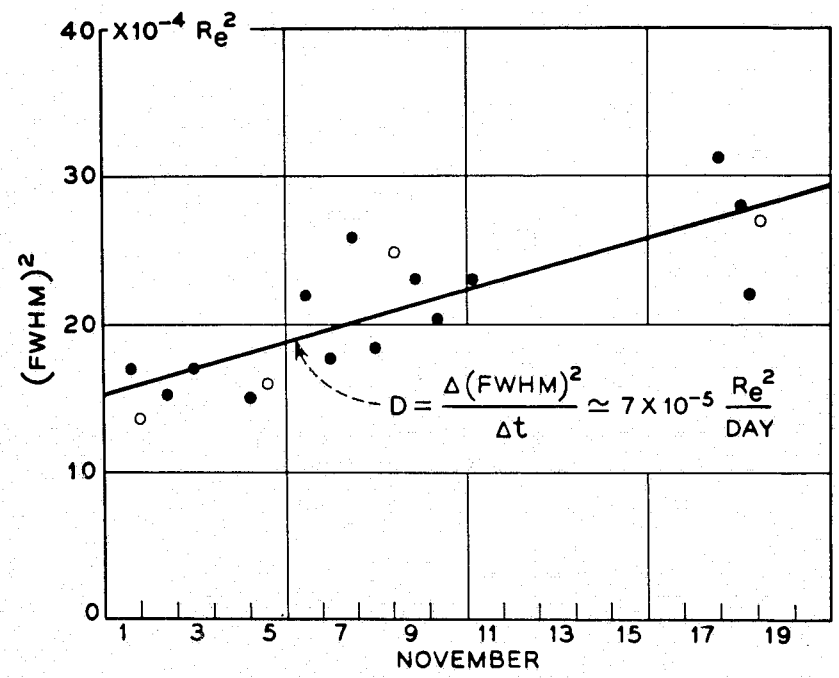

Fig. 18. Composite results of the peak width from 18 different passes of the satellite. The four passes included in Figure 17 are shown as open circles.

The scatter of the determinations is rather large, due primarily to the difficulties of peak fitting. The peak width nevertheless clearly increases with time. The square of the width is satisfactorily represented as a linear function of time as would be expected if the initially created width were broadening by diffusion. The diffusion coefficient corresponding to the line drawn in the figure is $7 \times 10^{-5} R_e^2$/day, a very small diffusion coefficient. There does not seem to be any systematic shift in the peak position over the time of measurement. Certainly any such linear diffusion (FRANK, 1966) is less than $2 \times 10^{-4} R_e$/day.

The broadening of the peak contributes very little to the decrease in the electron flux trapped in it. In the B and time range of the measurements in Figure 17 the peak flux decreased by a factor of about four, much more than the 30 percent decrease that would be expected if the same electrons were simply confined in a broader region of trapping.

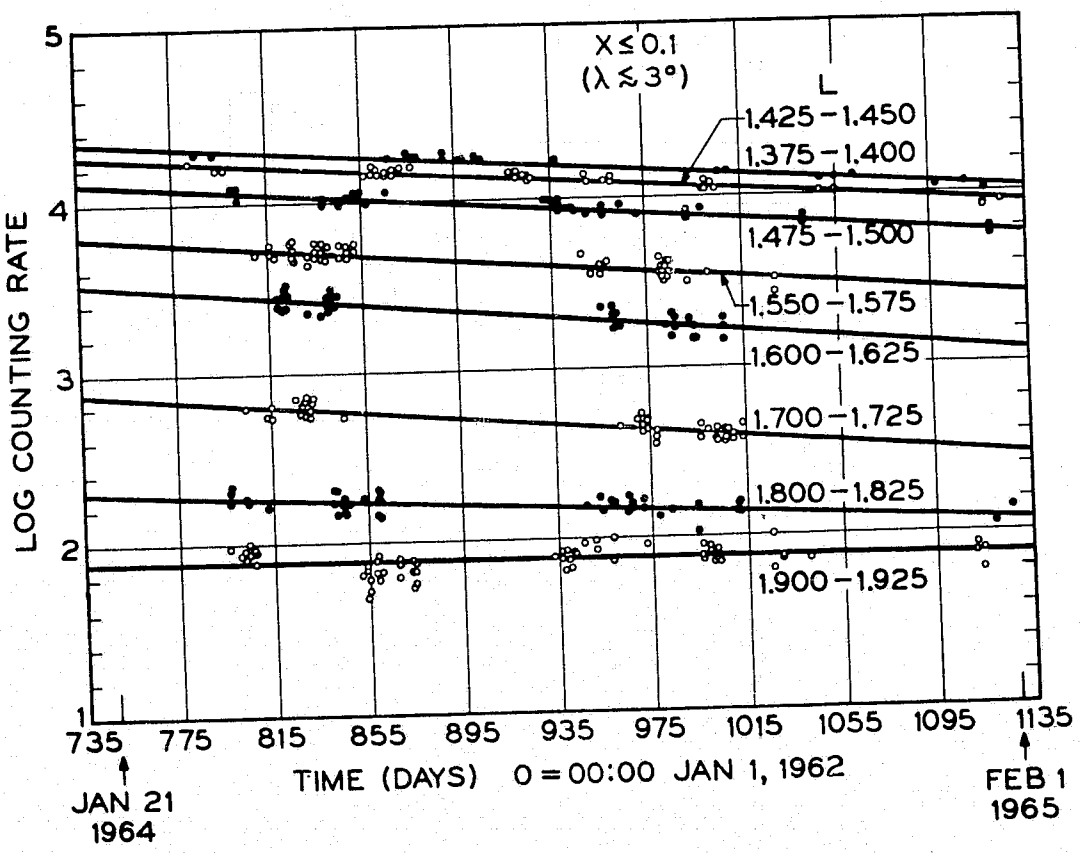

Fig. 19. The decay of electrons >0.75 MeV as observed by Relay II during 1964. The lines are exponentials, least square fit to the points.

4. Relay II, the Artificial Radiation Belt at Long Times

Relay II has provided a measure of the continuing decay of the electron flux in the higher altitude portions of the artificial belt during 1964 and 1965. The detector in this case is counting electrons >0.75 MeV in the directional flux perpendicular to the magnetic field. The results for near the magnetic equator ($x=\sqrt{1-B_0/B}<0.1$ or $\lambda<3$ degrees) for a number of narrow L slices are shown in Figure 19. The figure starts about a year and a half after the Starfish test. The measured points are in clusters because of the precession of the satellite

orbit. The lines are least square fits of exponentials to the data. They show gradual particle decays over the year of measurement.

The values of the decay constants determined from fits of the kind shown in Figure 19 have been plotted against L in Figure 20, not only for the near equatorial measurements, but also for three other regions in x further along the field lines. The near equatorial values have vertical bars which indicate the confidence limits of the fits. There seems to be a tendancy for decay constants at higher values of x to be greater than the near equatorial values, but the tendency is not far outside the accuracy of the determinations. The results also suggest decay constants slightly higher between $L=1.55$ and 1.7 than between $L=1.35$ and 1.55, but this L variation of K is quite small. The decay constant definitely decreases as one goes above $L=1.7$ and actually passes through zero at an L of about 1.9. For still higher L values the negative values of K imply small net increases in the electron flux over the one year period.

The results of Figure 20 are quite different from those determined from measurements soon after the nuclear tests, for example as shown in Figure 6. In Figure 6 the decay time is a maximum of about half a year between $L=1.3$ and 1.6 and decreases on higher L lines into the slot. However, in Figure 20 the decay constants, which are reciprocals of decay times, imply minimum decay times of the order of a year between $L=1.35$ and 1.7 and longer decay times at higher values of L. The two sets of results do not, however, seem to be in essential conflict. It is only in those regions where the number of residual excess electrons is large compared with the steady-state distribution of natural particles that the fitted decay constants will be a simple measure of the decay properties of the excess particles. In the region of $L=1.7$ or 1.8, if the measured initial decay times, the order of 40 to 60 days, had persisted, a flux decrease of between 10^4 and 10^6 would have been expected over the intervening two years. Such a decrease would almost certainly have brought the >0.75 MeV electrons to their steady-state distribution and a measurement of the decay constant would yield a value of zero. In the region where substantial numbers of excess particles still exist between $L=1.35$ and 1.7, decay processes with time constants the order of one or two years are operating. For decay times this long, particle loss might be proceeding by cross-L diffusion to regions where loss processes are normally more active.

Such diffusion could also account for the non-zero values of decay constant observed on L-lines above $L=1.7$, since the central maximum in the particle distribution could be feeding electrons onto these higher lines. However, if the cross-L diffusion coefficient discussed in Section 3.3 for $L=1.76$ is applicable over the $L=1.35$ to $L=1.7$ region and at the different electron energy of the two sets of measurements, it is too small to account for the Relay II observations. This whole question deserves more detailed consideration.

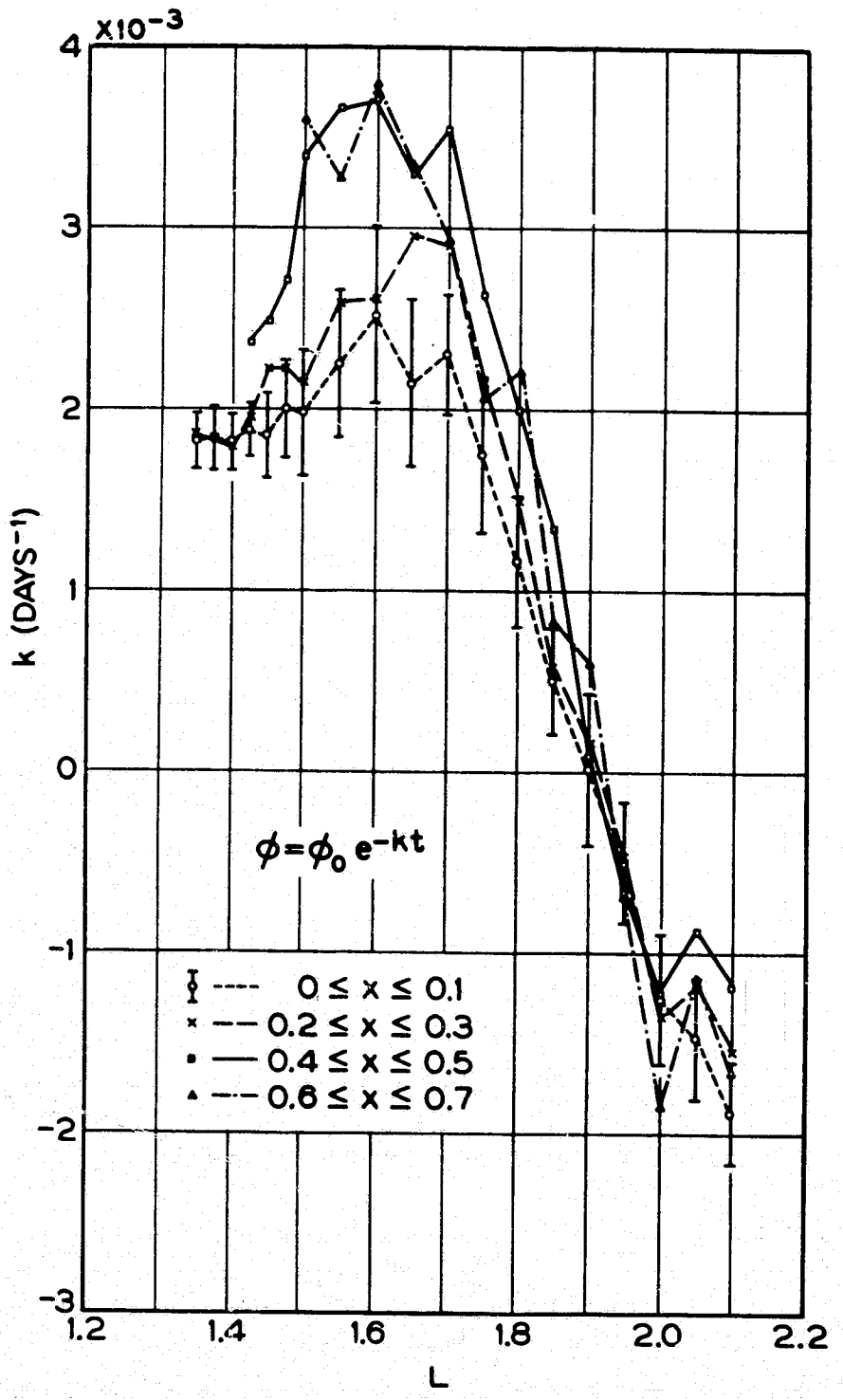

Fig. 20. The decay constant K corresponding to the exponential fits of electron decay curves such as those of Figure 19.

5. Acknowledgements

The results described in this paper have been obtained with the indispensable collaboration of a number of colleagues: J. D. Gabbe who carried out the analysis of the Telstar I data, Mrs. W. L. Mammel who managed the data reduction on Explorer XV, Miss L. W. Davidson who had a similar role for the Relay results, and C. S. Roberts who has given detailed consideration to the transient decay of electrons by pitch angle scattering. Their contributions to this work are gratefully acknowledged.

REFERENCES

Bostrom, C. O. and Williams, D. J.: 1965, J. Geophys. Res. 70, 240.

Brown, W. L.: 1965, Proc. Plasma Space Sci. Symp., D. Reidel Publ. Comp., Dordrecht, p. 189.

Brown, W. L., and Gabbe, J. D.: 1963, J. Geophys. Res. 68, 607.

Brown, W. L., Gabbe, J. D., and Rosenzweig, W.: 1963a, Bell System Tech. J. 62, 1505.

Brown, W. L., Ness, W. N., and Van Allen, J. A.: 1963b, J. Geophys. Res. 68, 605.

Buck, T. M., Wheatley, G. H., and Rogers, J. W.: 1964, IEEE Trans. Nucl. Sci. 11, 294.

Carter, R. E., Reines, F., Wagner, J. J., and Wyman, M. E.: 1959, Phys. Rev. 113, 280.

Colgate, S. A.: 1966, Radiation Trapped in the Earth's Magnetic Field., D. Reidel Publ. Comp., Dordrecht, p. 693.

Cornwall, J. M.: 1964, J. Geophys. Res. 62, 1251.

Dungey, J. W.: 1963, Planet. Space Sci. 11, 591.

Frank, L. A.: 1966, Radiation Trapped in the Earth's Magnetic Field., D. Reidel Publ. Comp., Dordrecht, p. 422.

Imhof, W. L. and Smith, R. V.: 1965, J. Geophys Res. 70, 569.

Katz, L.: 1966, Radiation Trapped in the Earth's Magnetic Field., D. Reidel Publ. Comp., Dordrecht, p. 129.

McIlwain, C. E.: 1961, J. Geophys. Res. 66, 3681.

McIlwain, C. E.: 1962, private communication.

McIlwain, C. E.: 1963, Science 142, 335.

McIlwain, C. E.: 1966, Radiation Trapped in the Earth's Magnetic Field., D. Reidel Publ. Comp., Dordrecht.

Roberts, C. S.: 1966, Radiation Trapped in the Earth's Magnetic Field., D. Reidel Publ. Comp., Dordrecht, p. 403.

Van Allen, J. A.: 1964, Nature 203, 1006.

Walt, M.: 1964, J. Geophys. Res. 69, 3947.

Welch, Jr., J. A., Kaufman, R. L., and Hess, W. N.: J. Geophys. Res. 68, 685.

West, H. I.: 1966, Radiation Trapped in the Earth's Magnetic Field., D. Reidel Publ. Comp., Dordrecht, pp. 634, 663.

CHAPTER 4

ELECTRON LOSS FROM THE VAN ALLEN ZONES DUE TO PITCH ANGLE SCATTERING BY ELECTROMAGNETIC DISTURBANCES

CHARLES S. ROBERTS

Bell Telephone Laboratories, Inc., Murray Hill, New Jersey

Abstract. Experimental observations indicate that relativistic electrons in the Van Allen zones are perturbed by physical processes that violate one or more adiabatic invariants of the electron's motion. This paper discusses one such possible process, that of pitch angle or mirror point diffusion. A qualitative explanation of pitch angle diffusion and how this process can lead to loss of trapped particles is presented, and then a Fokker-Planck type diffusion equation is introduced to describe the process mathematically. This diffusion equation is used to treat the loss of electrons from trapped orbits due to pitch angle diffusion that results from cyclotron resonant scattering of electrons by whistlers. Predictions are compared with satellite data on the loss from the Van Allen zones of electrons artificially injected by a nuclear explosion. It is found that the data indicate that pitch angle diffusion does indeed play an important role in the loss process, but the dominant mechanism producing the pitch angle scattering must be something other than cyclotron resonant scattering by whistlers since this mechanism leads to several predictions that are in disagreement with the data. These include prediction of the electron pitch angle distribution, the variation of the pitch angle distribution with L-shell and energy, the variation of the loss rate with energy, and the magnitude of the loss rate. Further investigation reveals that a process that, unlike whistlers, scatters electrons more or less uniformly along their spiral path would produce a pitch angle diffusion mechanism in much better accord with observation. Interaction with some type of wide band electromagnetic noise is suggested as such a process which might be of importance.

1. Introduction

The simplest picture of charged particles trapped in the earth's magnetic field is provided by the adiabatic theory of charged particle motion (NORTHROP and TELLER, 1960; NORTHROP, 1963). In this picture a particle once trapped in the geomagnetic field would remain so forever, since its motion is such as to conserve the three adiabatic invariants. Since the time of the initial discovery of the trapped radiation zones (VAN ALLEN *et al.*, 1958) a wealth of experimental evidence has been accumulated which indicates that such a picture is inadequate to describe the behavior of the electrons trapped in the Van Allen zones (BROWN *et al.*, 1963; BROWN, 1965; FRANK *et al.*, 1964; FRANK, 1965; MCILWAIN, 1963; O'BRIEN, 1962, 1964; VAN ALLEN *et al.*, 1959; VAN ALLEN, 1964; WILLIAMS and SMITH, 1965; also many of the papers in this *Proceedings* volume). These measurements all indicate that instead of being conserved one or more of a trapped electron's adiabatic invariants changes, even during

periods of low magnetic activity, by a significant amount in times of the order of a few hours to a few years, depending upon the energy of the electron and its location in the trapping region. One result of this is that electrons do not remain trapped in the earth's field forever, but instead are eventually lost due to these nonadiabatic processes. This paper is concerned with such loss of electrons from the Van Allen zones as a result of one particular type of nonadiabatic process, that of pitch angle diffusion.

WALT and MAC DONALD (1964) have shown that for L-shells (MCILWAIN, 1961) below 1.25 small angle coulomb scattering of electrons by the atmospheric constituents is the dominant loss mechanism. Above $L=1.25$ the atmospheric scattering mechanism becomes too weak to be responsible for the observed rates of electron loss. We are thus led to the hypothesis that above $L=1.25$ the loss rate of electrons must be governed by electromagnetic disturbances in the temperate, tenuous plasma which permeates this region. This hypothesis must still be regarded as just an educated guess, however, since experiments have yet to support its validity or to shed much light upon the characteristics of electromagnetic disturbances which may actually exist. DUNGEY (1964) has reviewed some possible effects of such disturbances upon trapped particles and has concluded that cross L-shell diffusion, energy diffusion, and pitch angle diffusion can all result. Thus a model of electron loss based upon pitch angle diffusion alone cannot be expected to describe the actual state of affairs in the Van Allen zones unless it is known beforehand that cross L-shell diffusion and energy diffusion are negligible.

There is experimental evidence that in the region below about $L=2.5$ cross L-shell diffusion is negligible compared with other processes, at least for electrons above about 0.5 MeV in energy. In this region the observed rate of cross L-shell diffusion (FRANK, 1965) is too low to be of much importance in times as short as the typical lifetimes for these electrons. Verification of this fact was provided by electrons artificially injected into narrow L-ranges of the trapping zone by nuclear detonations. These narrow shells of electrons created by the Argus tests (VAN ALLEN *et al.*, 1959) and the Russian test of November 1, 1962 (BROWN, 1965) were all lost with only a very minor amount of cross L-shell movement or spreading. Thus if interest is confined to relativistic electrons trapped below about $L=2.5$, the neglect of cross L-shell diffusion processes seems justified.

The case for the neglect of processes which change electron energy is not so clear cut however. Fluctuating electric fields produce changes in both energy and pitch angle. Pure pitch angle diffusion with no energy diffusion can be produced by perturbing electron orbits with magnetic fields, since a magnetic field alone can never change the energy of a charged particle. But since Maxwell's equations require that any disturbance containing a fluctuating magnetic field

must also contain a fluctuating electric field, it is clear that this electric field will always cause some energy diffusion to accompany pitch angle diffusion. The relative importance of the energy diffusion will depend upon E/B, the ratio of the magnitude of the fluctuating electric field in the disturbance to that of the fluctuating magnetic field, and also upon v/c, the ratio of the velocity of the particles being diffused to that of light. The case of relativistic particles being perturbed by a disturbance with E/B small is the one in which energy diffusion would be expected to be negligible compared to pitch angle diffusion. This is the case for the scattering of greater than 0.5 MeV electrons by disturbances propagating in the natural whistler mode, where $E/B \approx 0.1$, a case which we shall want to consider in detail later in this paper. The relative importance of energy diffusion for the processes which actually affect electrons in the Van Allen zones is, unfortunately, still unknown.

2. Qualitative Description of Pitch Angle Diffusion

A charged particle trapped in the earth's magnetic field moves in a spiral path around a line of force between two conjugate mirror points. The location of a mirror point on a line of force may be specified by any of several coordinates such as B, the local magnetic field strength, or λ, the magnetic latitude. However, for the considerations of this paper it is simpler to use the x coordinate described by ROBERTS (1965), which equals zero at the minimum B point or magnetic equator of the line of force and increases monotonically towards unity as one moves along the line towards the earth. As an adiabatically trapped particle travels between mirror points the value of its local pitch angle α, which is the angle between the local magnetic field vector and the particle velocity vector, oscillates between a minimum value α_0 and a maximum value $\pi - \alpha_0$, the extremum values α_0 and $\pi - \alpha_0$ being obtained as the particle crosses the magnetic equator and the value $\pi/2$ being obtained at the mirror points. The value of a particle's pitch angle at some point along its orbit is directly related to the position of its mirror points by the so called mirror equation

$$\mu^2(x) = (x_m^2 - x^2)/(1 - x^2) \tag{1}$$

where $\mu = \cos \alpha$, x is the instantaneous position of the particle, and x_m is the position of the mirror point. Thus specifying a pitch angle for a particle at a given point is equivalent to specifying its mirror position and *vice versa*. In particular, the particle's pitch angle as it crosses the magnetic equator is related to its mirror position by the simple relationship $x_m = \mu_0$, where $\mu_0 = \cos \alpha_0$. Thus descriptions of a particle's orbit in terms of the mirror point position or the equatorial pitch angle are equivalent.

Suppose now that instead of travelling adiabatically between mirror points, the trapped particle interacts with some electromagnetic disturbance along its orbit, which changes the direction of its velocity vector by a small amount. Another way of describing this is to say that the pitch angle of the particle has undergone a scattering by the disturbance. Since such a change in local pitch angle must according to (1) result in a corresponding change in mirror point position, we see that a pitch angle scattering is equivalent to a mirror point scattering, and *vice versa*. Similarly, since $x_m = \mu_0$ a scattering of the mirror point must be related to a corresponding scattering of the particle's equatorial pitch angle. Relating all scatterings occurring anywhere along a particle's orbit to the corresponding change in the equatorial pitch angle is a very convenient way to keep track of the effects of many small scatterings and is the technique which will be used in this paper.

If a population of many trapped particles is subjected to a series of small pitch angle scatterings that are random in both direction and size, the individual particles of the population will undergo a sort of random walk in their equatorial pitch angle, and a diffusion process in equatorial pitch angle space results. Such a diffusion process will result in loss of trapped particles because of the exponentially increasing atmospheric density near the earth and the fact that diffusion of pitch angles also means diffusion of mirror positions. The presence of the atmosphere creates a "loss cone" for particle pitch angles since particles having pitch angles smaller than some critical value will have mirror positions close enough to the earth so that it becomes overwhelmingly probable that loss by interaction with the atmospheric constituents will occur. Thus particles whose pitch angles diffuse into the loss cone will be removed from the trapped particle population. It is interesting that even for pitch angle scattering, a so called nonatmospheric loss mechanism, it is the atmosphere which is responsible for the actual loss of the particles.

3. Fokker-Planck Equation for Pitch Angle Diffusion

MAC DONALD and WALT (1961) used a Fokker-Planck equation to treat the simultaneous pitch angle and energy diffusion of a population of trapped particles caused by interactions with the atmospheric constituents. The Fokker-Planck equation for pure pitch angle diffusion can be obtained from their equation by setting the energy diffusion coefficients equal to zero. Doing this, we obtain

$$\frac{\partial f(\mu_0, t)}{\partial t} = -\frac{\partial}{\partial \mu_0} f \langle (\Delta \mu_0) \rangle + \frac{1}{2} \frac{\partial^2}{\partial \mu_0^2} f \langle (\Delta \mu_0)^2 \rangle + Q(\mu_0) \qquad (2)$$

Here t is the time, $\mu_0 = \cos \alpha_0$ is the cosine of the particle's equatorial pitch

angle, and $f(\mu_0, t)$ is the MAC DONALD and WALT (1961) distribution function for the particles under consideration, which will be of a specified kinetic energy and type. If, for example, we are considering electrons with energies lying in a small energy interval centered around 0.5 MeV, $f(\mu_0,t)\,\mathrm{d}\mu_0\,\mathrm{d}A_0$ would represent the number of these particles which would cross the equator with pitch angle cosine between μ_0 and $\mu_0+\mathrm{d}\mu_0$ trapped at time t in a tube of force of equatorial cross sectional area $\mathrm{d}A_0$. The distribution function f is related to the equatorial unidirectional flux by the expression

$$j(\mu_0,t) = f(\mu_0,t)/4\pi\mu_0 t_b \tag{3}$$

where t_b is the time for the trapped particle to travel from one mirror point to the other. In (2) the term $Q(\mu_0)$ is a source term, and $Q(\mu_0)\,\mathrm{d}\mu_0\,\mathrm{d}A_0$ equals the number of particles per unit time injected into a tube of force of equatorial cross sectional area $\mathrm{d}A_0$ with equatorial pitch angle cosines between μ_0 and $\mu_0+\mathrm{d}\mu_0$. The diffusion coefficients $\langle(\Delta\mu_0)\rangle$ and $\langle(\Delta\mu_0)^2\rangle$ in (2) depend on the nature of the process producing the pitch angle diffusion and represent the average, over all scatterings, of $(\Delta\mu_0)$ and $(\Delta\mu_0)^2$ multiplied by the scattering frequency. The quantity $(\Delta\mu_0)$ represents the change in one scattering of μ_0. It should be noted that for scatterings which occur off the magnetic equator the change $(\Delta\mu_0)$ in equatorial pitch angle cosine must be computed from the change in local pitch angle cosine with the formula

$$(\Delta\mu_0) = (\Delta\mu)\left(\frac{\partial\mu_0}{\partial\mu}\right) + \tfrac{1}{2}(\Delta\mu)^2\left(\frac{\partial^2\mu_0}{\partial\mu^2}\right) \tag{4}$$

The second term on the right hand side of (4) is necessary since the Fokker-Planck formalism is one in which all second order terms are retained. The derivatives in (4) are computed by differentiating the mirror equation,

$$\mu_0^2 = \mu^2(1-x^2) + x^2 \tag{5}$$

holding the value of x constant. It is apparent from (4) that even if the average of $(\Delta\mu)$ taken over all scatterings is zero, the average of $(\Delta\mu_0)$ can be nonzero.

Before working with (2) it is convenient to make a few mathematical substitutions. We let

$$D(\mu_0) = \tfrac{1}{2}\langle(\Delta\mu_0)^2\rangle, \qquad D'(\mu_0) = \tfrac{1}{2}\langle(\Delta\mu_0)^2\rangle - \mu_0\langle(\Delta\mu_0)\rangle,$$
$$r(\mu_0) = D'/D \tag{6}$$

$$w(\mu_0,t) = D(\mu_0)f(\mu_0,t)/8\pi\mu_0 L r_c \tag{7}$$

where L is McIlwain's (1961) parameter for the shell of interest and r_e is the average radius of the earth $\approx$6371 km. Using (6) and (7), Equation (2) now becomes

$$\frac{1}{D(\mu_0)}\frac{\partial w}{\partial t} = \frac{1}{\mu_0}\frac{\partial}{\partial \mu_0}\left[r(\mu_0)w + \mu_0\frac{\partial w}{\partial \mu_0}\right] + s(\mu_0)\bar{q}(\mu_0) \tag{8}$$

where $\bar{q}(\mu_0)$ is the average over the particle's spiral path of the source strength in particles/cm^3 sec ster, and $2Lr_e s(\mu_0)$ is the distance along the spiral path between mirror points. Evaluation of integrals over a particle's spiral path, such as $\bar{q}(\mu_0)$ and $s(\mu_0)$, have been previously discussed by LENCHEK *et al.* (1961) and LENCHEK and SINGER (1963) as well as by several other authors. For a dipole magnetic field LENCHEK *et al.* (1961) give the approximation for $s(\mu_0)$

$$s(\mu_0) = 1.38 - 0.32\left[(1-\mu_0^2)^{1/2} + (1-\mu_0^2)^{1/4}\right] \tag{9}$$

In terms of $w(\mu_0, t)$, the equatorial unidirectional flux is

$$j(\mu_0, t) = vw(\mu_0, t)/D(\mu_0)s(\mu_0) \tag{10}$$

4. Normal Mode Solution of the Fokker-Planck Equation

Equation (8) is a partial differential equation in two variables, the solutions of which give the behavior of a population of particles undergoing pitch angle diffusion. As discussed in Section 2, the presence of the earth's atmosphere produces a loss cone for particle pitch angles, and therefore to account for this (8) must be solved subject to the boundary condition $w(\mu_{c0}, t)=0$, where μ_{c0} is the cosine of the equatorial loss cone angle. Equation (8) is a separable partial differential equation, and its general solution may be written

$$w(\mu_0, t) = w_e(\mu_0) + \sum_{l=1}^{\infty} w_l(\mu_0)\exp(-k_l t) \tag{11}$$

where $w_e(\mu_0)$ satisfies the equation

$$\frac{1}{\mu_0}\frac{\mathrm{d}}{\mathrm{d}\mu_0}\left[rw_e + \mu_0\frac{\mathrm{d}w_e}{\mathrm{d}\mu_0}\right] = -s\bar{q} \tag{12}$$

The $w_l(\mu_0)$ are the eigenfunctions and k_l the eigenvalues of the equation

$$\frac{1}{\mu_0}\frac{\mathrm{d}}{\mathrm{d}\mu_0}\left[rw_l + \mu_0\frac{\mathrm{d}w_l}{\mathrm{d}\mu_0}\right] = -\frac{k_l}{D}w_l \tag{13}$$

subject to the boundary condition $w_l(\mu_{c0})=0$. Equation (11) is called the normal mode solution and the $w_l(\mu_0)$ the normal modes of the diffusion equation in analogy to the similar type of general solution that occurs in the theory of vibrating strings.

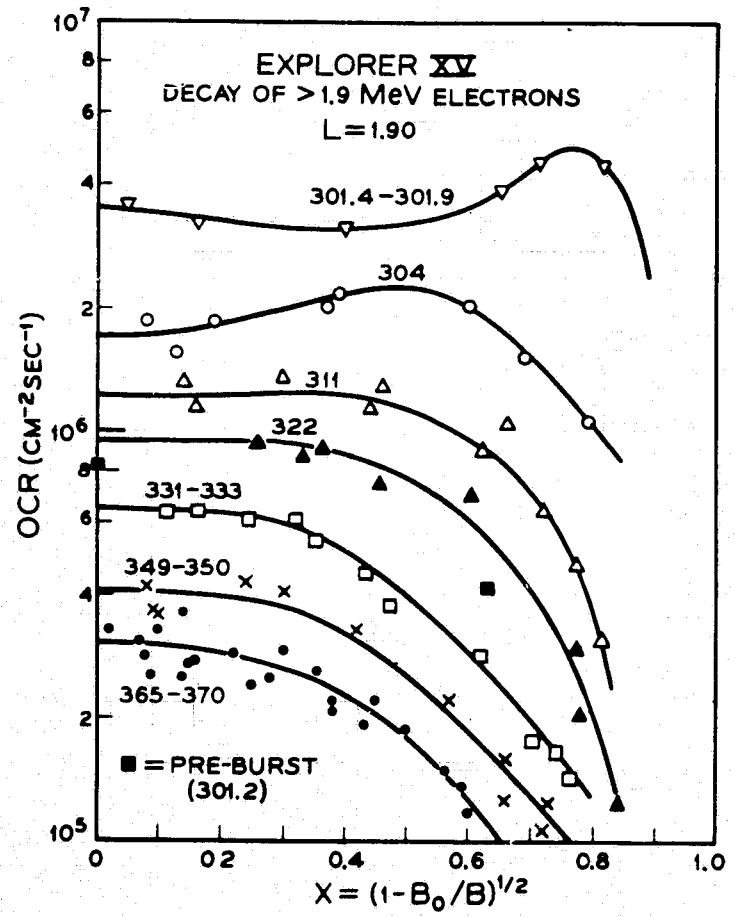

Fig. 1. Counting rate of the Bell Telephone Laboratories >1.9 MeV electron detector aboard Explorer XV after the U.S.S.R. nuclear detonation of October 28 (day 301), 1962. The data points and associated curves show the omnidirectional counting rate on $L=1.9$ plotted as a function of position on the L-shell measured with the x-coordinate. The various curves and data point symbols are for the different time periods indicated (in days of 1962). The sequence of curves shows how a severely perturbed particle distribution decays back to the "normal shape", as represented by the data after about day 330.

Several interesting properties of a population of particles undergoing pitch angle diffusion can be understood from the normal mode solution. First, there will be a smallest eigenvalue, k_1, for Equation (13), which in practice usually

turns out to be about a factor of 3–6 smaller than k_2. This means that after a sufficiently long time the $l \geqslant 2$ terms in the summation of (11) will become negligible compared to the $l=1$ term, and the time dependence will thereafter be a simple exponential decay. Thus the decay of an artificially injected population of particles via pitch angle diffusion can be divided into an initial stage, where the time dependence of the flux is not exponential and the pitch angle distribution changes with time, and a later stage, where $(w-w_e) \approx w_1(\mu_0) \exp(-k_1 t)$. Second, Equations (12) and (13) differ only in the term on the right hand side of the equal sign, and it turns out that the solutions for $w_e(\mu_0)$ and $w_1(\mu_0)$ are rather insensitive to the μ_0 dependence of this term. This results in the following interesting features. The μ_0 dependence of $w_e(\mu_0)$ is insensitive to the μ_0 dependence of $\bar{q}(\mu_0)$, and thus one can tell almost nothing about the pitch angle dependence of the source by looking at the equilibrium pitch angle distribution. Also, both $w_e(\mu_0)$ and $w_1(\mu_0)$ will have very nearly the same μ_0 dependence so that in the later stage of the decay, where $l \geqslant 2$ terms in (11) can be neglected, $w(\mu_0, t) \approx w_e(\mu_0)[1 + C \exp(-k_1 t)]$, where C is some constant, and the pitch angle dependence remains approximately constant with time. Thus if one plots flux of particles on a logarithmic scale versus μ_0 at various times during this later stage of decay, the shape of the curves will remain approximately constant.

Data showing the decay of electrons artificially injected into the trapping region by the U.S. high altitude nuclear test, Starfish, of July 9, 1962 and the U.S.S.R. tests of October 22, October 28, and November 1, 1962 seem to be in accord with the idea that pitch angle diffusion plays an important part in the loss mechanism for these electrons. An illustration of this is shown in Figure 1, which shows the decay of >1.9 MeV electrons following the second U.S.S.R. test. The data points were obtained by the Bell Telephone Laboratories' experiment aboard the Explorer XV satellite, and the omnidirectional counting rate of the electron detector is plotted versus the x coordinate at various times after the nuclear burst. The omnidirectional counting rate of the detector is proportional to J, the omnidirectional flux of electrons >1.9 MeV, and the function $J(x,t)$ is in turn related to $j(\mu_0, t)$ and $w(\mu_0, t)$ by an integral transformation (ROBERTS, 1965). The curves show that up until around day 320–330, the dependence of the counting rate upon x changes with time, while after that the main change is a downward displacement of the same shape curve. The rate of this downward displacement can be seen in Figure 2 where the equatorial counting rate of the Explorer XV electron detectors is plotted versus time. The points for the >1.9 MeV electrons show nearly exponential decay between about day 320 and day 360. It thus appears that the period before day 320–330 can be identified with the initial stage of the decay, discussed in connection with the normal mode solution (11), while the period from day

330–360 can be identified as the later stage of the decay where only the $l=1$ term in (11) need be considered. The deviations of the data from this simple picture may be attributable to several things. First, the solution (11) gives the flux of electrons at one particular kinetic energy, while the electron detector counts electrons greater than 1.9 MeV. Since k_1 may be a strong function of

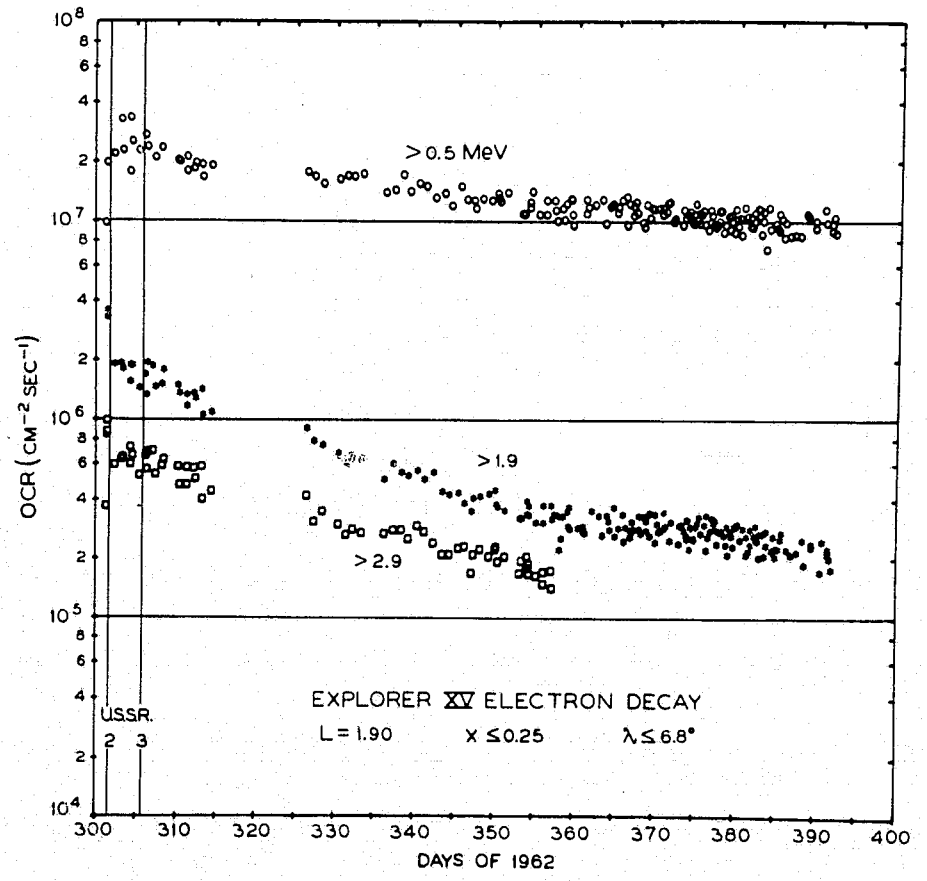

Fig. 2. Counting rate of the Bell Telephone Laboratories' electron detectors aboard Explorer XV for the near equatorial region, $x \leqslant 0.25$, on $L=1.9$. The omnidirectional counting rate is plotted versus time, and the times of the second and third U.S.S.R. nuclear tests on October 28 (day 301) and November 1 (day 305) are marked with vertical lines.

electron energy one would really like to compare with the counting rate of a detector measuring electrons in a narrow energy range. Secondly, energy diffusion may be of some importance, and therefore a treatment based upon pure pitch angle diffusion would be incomplete. Finally, the diffusion coefficients $D(\mu_0)$ and $D'(\mu_0)$, which depend upon the number of electromagnetic

disturbances present, are probably not really independent of time. Instead their value is probably correlated with magnetic activity (McIlwain, 1963). Despite these complications, the overall behavior of the data obtained after artificial injection of electrons is in general accord with the idea that pitch angle diffusion plays at least an important role in the subsequent loss of these electrons. The paper by West in this *Proceedings* volume contains further experimental verification of this.

5. Loss of Electrons Due to Interaction with Whistlers

Dungey (1963a) and Cornwall (1964) have suggested that pitch angle scattering due to cyclotron resonant interactions with whistlers might be responsible for the loss of electrons from the Van Allen zones above $L \approx 1.7$. Equation (8) will now be used to compute the properties of such a process, and these will then be compared with existing experimental knowledge concerning electrons in this region.

In order to apply (8) to the scattering of electrons by whistlers the diffusion coefficients $D(\mu_0)$ and $D'(\mu_0)$, defined in (6), must be evaluated on the basis of the dynamics of the electron-whistler interaction. Although specific formulas and details will be left for another paper (Roberts, 1969), a sketch of the important ideas involved will be given here. This should suffice to enable the reader to understand physically the qualitative results which ensue.

Computation of the diffusion coefficients involves determining the points at which cyclotron resonance occurs between a whistler and an electron. A whistler is a type of disturbance that has its origin in the electromagnetic energy released in a lightning bolt discharge below the ionosphere (Helliwell, 1965), and for our purposes here it may be thought of as an electromagnetic wave whose frequency at a given point in space decreases with time. For simplicity, we take the direction of the whistler propagation vector **k** to be parallel to the earth's magnetic field. The condition for cyclotron resonance is

$$(\omega + kv_{\|} - \Omega) = 0 \tag{14}$$

where $\omega/2\pi$ is the frequency of the whistler, $v_{\|}$ the electron's velocity component parallel to the earth's field, $2\pi/k$ the wavelength of the whistler, and $\Omega/2\pi$ the electron cyclotron frequency. Equation (14) simply states that resonance occurs when the instantaneous frequency of the whistler doppler shifted by the electron's motion is equal to the local electron cyclotron frequency. Since the quantities in (14) all change with time as the electron travels along its orbit, it is clear that cyclotron resonance can only be achieved instantaneously, unless very fortuitous conditions are obtained. Using the fact that the

cyclotron frequency of a relativistic electron varies inversely as the total energy of the electron, (14) can be rewritten

$$\omega = \Omega_r \frac{T_r}{(T_r + T)(1 + n\mu\beta)} \tag{15}$$

where $\Omega_r/2\pi$ is the cyclotron frequency for a nonrelativistic electron, T_r is the rest energy of an electron $=0.51$ MeV, T is the kinetic energy of the electron, $n=ck/\omega$ is the index of refraction for whistler mode propagation at frequency ω, $\mu=\cos\alpha=v_{\|}/v$, and $\beta=v/c$. Equation (15) shows how the whistler frequency necessary to resonate with an electron varies with local magnetic field intensity,

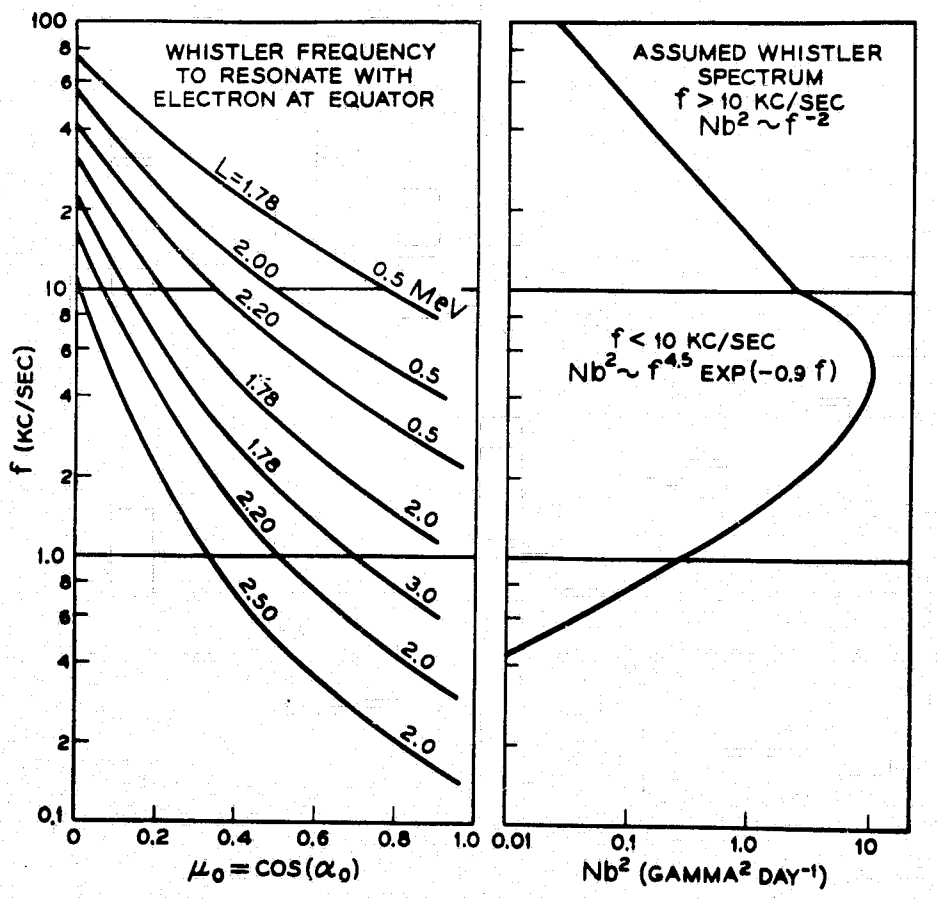

Fig. 3. Whistler frequency needed to produce cyclotron resonance with an electron crossing the magnetic equator plotted versus μ_0 for various L-shells and electron energies. The right graph shows the whistler power spectrum that was assumed in computing the diffusion coefficients for pitch angle scattering by whistlers. Comparison of the left and right graphs gives an estimate of the relative amount of pitch angle scattering that will occur at various energies, L-shells, and equatorial pitch angles.

electron energy, and electron pitch angle, and this is displayed graphically on the left side of Figure 3, which shows the whistler frequency necessary to resonate with an electron passing through the magnetic equator plotted as a function of the cosine of its equatorial pitch angle. Curves are drawn for several L values and electron energies so that one may also see the dependence upon these factors. Resonance, is of course, possible off the magnetic equator, and similar curves could be drawn for those cases. Such curves would necessarily lie above the corresponding equatorial curves since as (15) will verify an electron resonates with the lowest possible frequency when it crosses the equator.

For each resonant whistler-electron interaction it is necessary to compute the perturbation produced in the electron's local pitch angle by the fields of the whistler wave. The motion of an electron in resonance with a circularly polarized wave has been solved exactly (ROBERTS and BUCHSBAUM, 1964), but the perturbation technique of integrating over the zero order helix of the electron (DUNGEY, 1963b) is sufficient to yield $(\Delta\mu)$, the change in local pitch angle cosine as a result of the interaction. The value of $(\Delta\mu)$ is of course dependent upon the strength of the whistler at the frequency necessary to produce cyclotron resonance, and thus the diffusion coefficients $D(\mu_0)$ and $D'(\mu_0)$ turn out to be dependent upon the whistler frequency spectrum. It is most convenient to express this spectrum in terms of $Nb^2(\omega)$, which is the average sum at the frequency ω over all whistlers per day of b^2, the square of the whistler magnetic field intensity.

Unfortunately, few if any experimental measurements are yet available on the spectrum of whistlers above the ionosphere above about 10 kc/sec. However measurements have been made of the spectrum of lightning discharges which produce whistlers (HELLIWELL, 1965; HORNER, 1961). These indicate that b^2 peaks around a frequency of 5 kc/sec and drops about a factor of 4 at 2 kc/sec and 10 kc/sec, and that above 10 kc/sec, b^2 decreases approximately as the inverse square of the frequency. Since the spectrum of whistlers should resemble the spectrum of the lightning which produces them, a hypothetical whistler spectrum based upon the preceding facts was constructed and used to compute the diffusion coefficients. This spectrum is shown in the right hand graph of Figure 3. The value at the peak of 10 gamma^2/day seems to be a reasonable guess based upon satellite measurements below 10 kc/sec (CAIN *et al.*, 1961; GURNETT and O'BRIEN, 1964).

Simultaneous examination of the two graphs of Figure 3, shows that the rate of pitch angle diffusion should be highly dependent upon L, energy, and pitch angle. Scattering will be greatest when the resonance can occur with a whistler frequency of about 5 kc/sec, the frequency at which the whistler spectrum peaks. Scattering of electrons which mirror near the equator, $\mu_0 \approx 0$,

will be small since whistlers have only a small amount of energy at the high frequencies necessary to resonant with these electrons. Typical results of these effects can be seen in Figure 4 which shows the diffusion coefficient $D(\mu_0)$ as computed for diffusion by whistlers on $L=1.9$. The curves are for electron

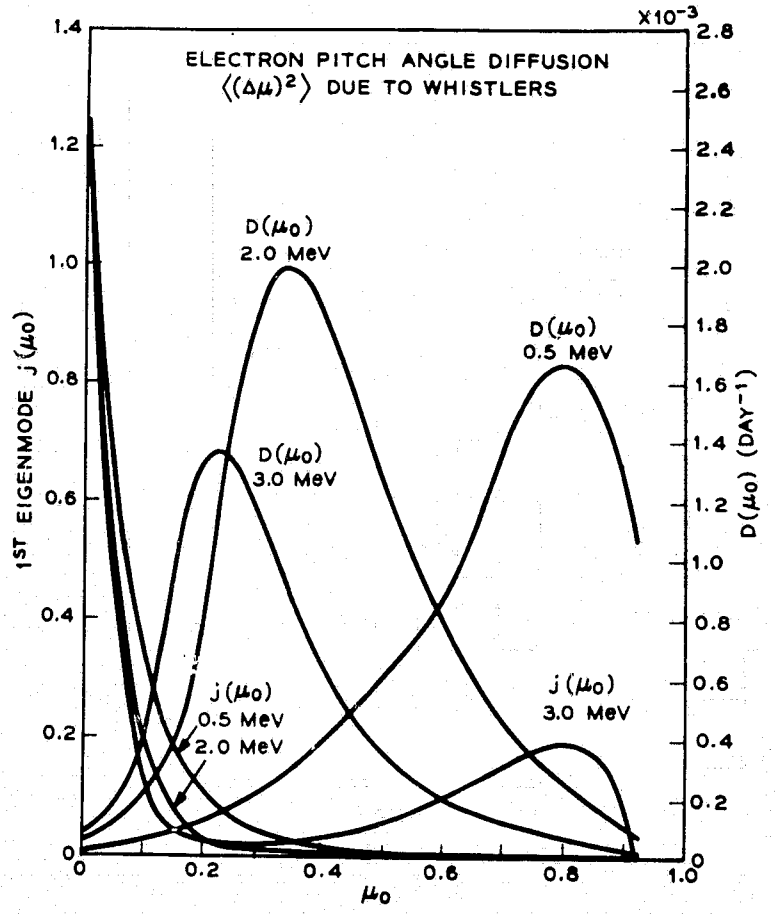

Fig. 4. Some results of the calculation of electron pitch angle diffusion on $L=1.9$ produced by cyclotron resonant scattering of the electrons by whistlers. The diffusion coefficient $D(\mu_0)$, defined by Equation (6), and the equatorial unidirectional flux given by the $l=1$ solution of Equation (13) are plotted as a function of $\mu_0=\cos\alpha_0$ for 0.5, 2.0, and 3.0 MeV electrons.

energies 0.5, 2.0, and 3.0 MeV, and the $l=1$ eigenmode unidirectional flux $j(\mu_0)$ as calculated with (13) and (10) is also shown. The large peaks in $D(\mu_0)$are typical of the whistler mechanism, and result from the peak in the whistler spectrum.

When the results of this pitch angle diffusion calculation are compared with

experiment, severe discrepancies are found to exist. The $l=1$ eigenmode solution of (13) and equilibrium solution of (12) with any reasonable source $\bar{q}(\mu_0)$ both have about the same μ_0 dependence, as previously pointed out in

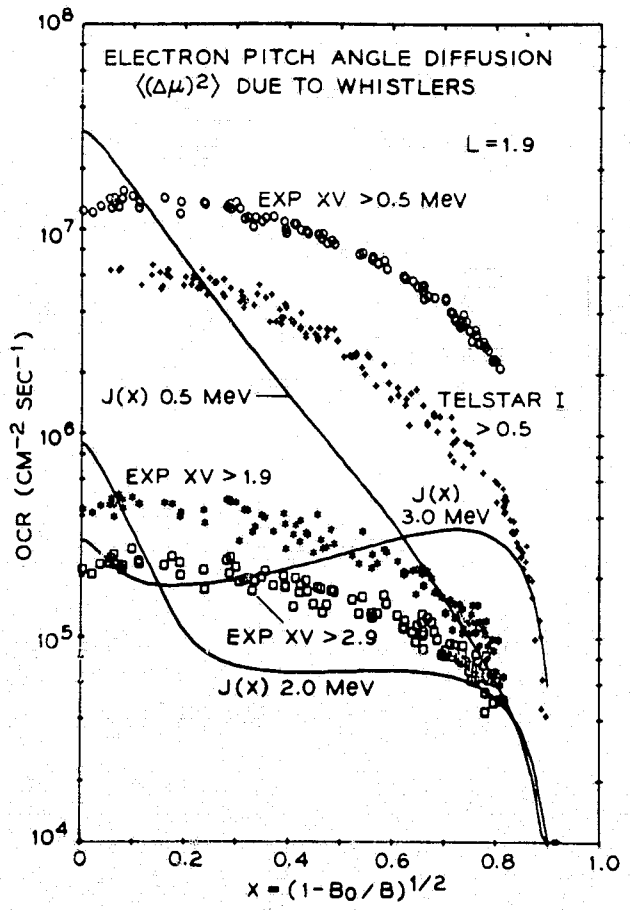

Fig. 5. Omnidirectional flux J of electrons on $L=1.9$, as predicted by the whistler pitch angle diffusion mechanism, plotted versus the x-coordinate. The theoretical $J(x)$ curves for the 0.5, 2.0 and 3.0 MeV electrons were computed from the corresponding equatorial unidirectional fluxes $j(\mu_0)$ shown in Figure 4, and all the $J(x)$ curves may be displaced vertically on the log scale by an arbitrary amount. The shapes of the theoretical curves are in severe disagreement with the shapes of the sets of data shown, thus indicating that something other than whistlers is responsible for the pitch angle diffusion of these electrons.

Section 4, and they both predict a unidirectional flux $j(\mu_0)$ that disagrees violently with that observed experimentally. An example of this is given in Figure 5, which shows the dependence of the omnidirectional counting rate upon the x coordinate for >0.5, >1.9, and >2.9 MeV electrons on $L=1.9$.

The data were obtained by the Bell Telephone Laboratories' experiments aboard the Explorer XV and Telstar I satellites, as marked, and the x dependence of the data points shown is typical for periods when the x dependence does not vary with time. The solid curves in Figure 5 show the omnidirectional flux $J(x)$ as computed from the theoretical $l=1$ eigenmode $j(\mu_0)$ shown in Figure 4. These $J(x)$ curves may be displaced vertically by any desired amount, since an eigenmode may always be multiplied by an arbitrary constant. The point however is that the x dependence of the computed curves is in violent disagreement with the x dependence of the data, i.e. the shapes are different. This failure of the whistler mechanism to predict correct x or μ_0 dependences applies also to other L values and energies. The computed pitch angle distributions typically have a large peak at $\mu_0=0$, due to the relatively small amount of whistler energy present at the high frequencies necessary to resonate with electrons mirroring near the equator, and also display bumps and dips whose position varies with energy and L. None of these features are in agreement with observation since time independent pitch angle distributions for electrons of any energy above a few hundred keV are generally qualitatively similar to those represented by the data points in Figure 5.

The failure of the whistler mechanism to predict correct pitch angle distributions does not depend critically upon the details of the whistler spectrum that was assumed. Rather it depends only on the fact that the spectrum falls rapidly above 10 kc/sec and that a maximum exists at some frequency below 10 kc/sec. On the basis of the information already presented about the spectrum of lightning that causes whistlers, it is difficult to see how the actual whistler spectrum could fail to possess these features. The true whistler spectrum should actually fall even more rapidly above 10 kc/sec than the lightning spectrum in Figure 3, since higher frequencies are attenuated more in passing through the ionosphere.

Another prediction of the whistler mechanism that disagrees with observation is the dependence of the loss rate on electron energy. For instance on $L=1.9$, the decay constant k_1 associated with the $l=1$ eigenmodes shown in Figure 4 are 0.65×10^{-3}, 2.6×10^{-3}, and 3.0×10^{-3} day^{-1} respectively for 0.5, 2.0, and 3.0 MeV electrons. Thus the whistler mechanism predicts that 3 MeV electrons should decay more rapidly than 2 MeV electrons. Experimentally, the Bell Telephone Laboratories' experiment aboard Explorer XV measured decay rates for 1.9 MeV electrons which were higher than those for 2.9 MeV electrons, as is evident in Figure 2, in disagreement with the whistler predictions. Similar disagreements exist at other energies and L values, and are particularly serious if one considers electrons of about 0.25 MeV. Since the frequencies necessary to resonate with these electrons on $L=1.9$ would lie in the very weak portion of the whistler spectrum, their loss rate would be expected to be very low.

Instead, Telstar I observed loss rates for such electrons comparable to those for 0.5 MeV electrons. Finally, one should note that the absolute value of the decay rates as predicted by whistlers are generally too low. For instance on $L=1.9$, the decay constants given above for 0.5, 2.0, and 3.0 MeV electrons

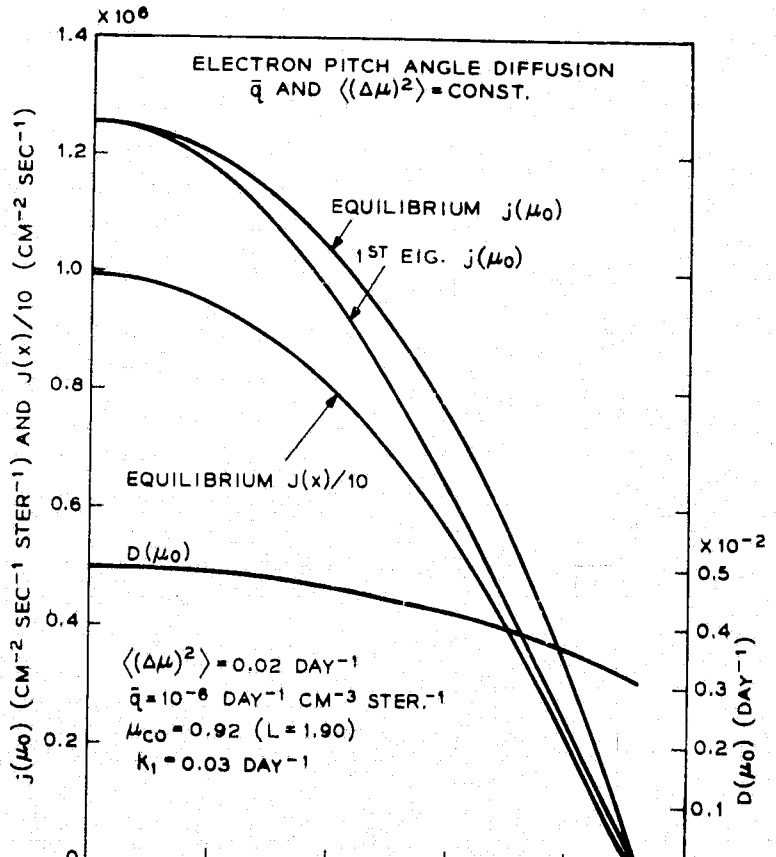

Fig. 6. Results on $L = 1.9$ for a pitch angle diffusion process that has $\langle \Delta\mu \rangle = 0$, $\langle (\Delta\mu)^2 \rangle$ = constant, where μ is the cosine of the *local* pitch angle. The equilibrium curves come from the solution of Equation (12) with a constant source term $\bar{q}$. The first Eig. $j(\mu_0)$ comes from the $l = 1$ solution of Equation (13).

are a factor of 30, 10, and 5 lower respectively than the decay constants measured by Explorer XV. This disagreement in absolute value is, however, directly dependent upon the value of 10 gamma^2/day taken as the peak of whistler frequency spectrum in Figure 3. Since this number is apt to be in error, either high or low, one should attach minimum significance to absolute values of

predicted decay rates. However, on the basis of the qualitative disagreements one must conclude that resonant pitch angle scattering of electrons by whistlers is not the dominant mechanism responsible for loss of electrons in the Van Allen zones.

6. Pitch Angle Diffusion with Constant $\langle(\Delta\mu)^2\rangle$

In order to get a feel for what type of a pitch angle scattering process would predict unidirectional flux functions $j(\mu_0)$ that agree with experiment, a scattering process for which $\langle(\Delta\mu)\rangle = 0$ and $\langle(\Delta\mu)^2\rangle =$ constant was investigated. The quantity $\langle(\Delta\mu)\rangle$ is the average of the change in *local* pitch angle cosine,

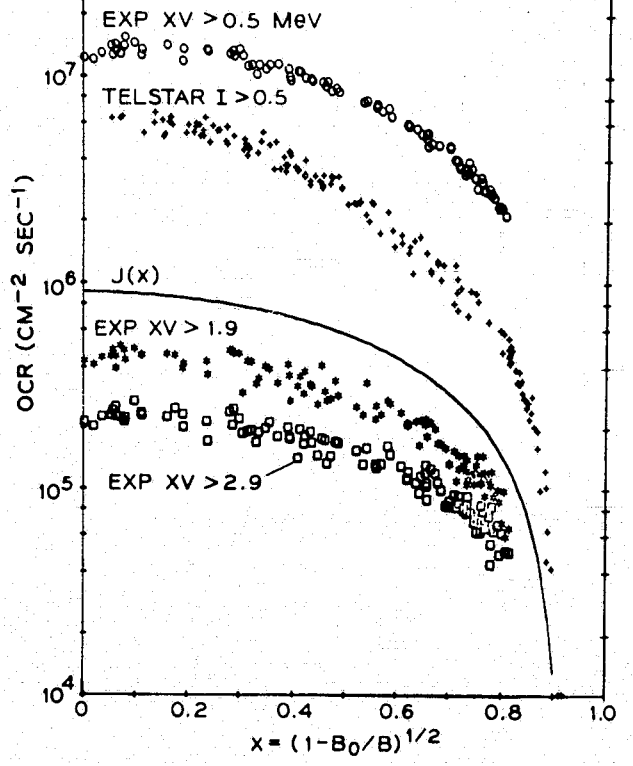

Fig. 7. The omnidirectional flux function $J(x)$ corresponding to the first Eig. $j(\mu_0)$ shown in Figure 6. The curve may be displaced vertically on the log scale by an arbitrary amount. The data shown is the same data shown in Figure 5 with the $J(x)$ results based on the whistler mechanism. The shape of the $J(x)$ curve in Figure 7 clearly resembles the shapes of the sets of data better than do the $J(x)$ curves in Figure 5, indicating that the pitch angle diffusion mechanism represented by Figures 6 and 7 must be closer to the truth than the whistler mechanism.

and $\langle(\Delta\mu)^2\rangle$ is the average of the square of this quantity. Physically, this would correspond to a scattering process which produces perturbations in local pitch angle cosine that are random in direction and independent of where along the particle's spiral path the scattering occurs. Figures 6 and 7 show the results of the diffusion calculation for such a process operating on $L=1.9$. In Figure 7 the predicted omnidirectional flux for the $l=1$ eigenmode is plotted along with the data previously shown in Figure 5. The curve in Figure 7 can be displaced vertically by any desired amount, corresponding again to the multiplication of an eigenmode by an arbitrary constant. However, unlike the whistler case shown in Figure 5, there is general agreement between the shape of the predicted curve in Figure 7 and the shape of the data. Thus pitch angle scattering by a process which operates more or less uniformly along the electron's spiral path yields a physical model which is in much better agreement with observation than pitch angle scattering by whistlers. Scattering by whistlers does not of course operate uniformly along the spiral path since the whistler frequency necessary to produce resonance changes along the spiral path, and the spectrum of whistlers varies with frequency. Instead, one would guess that pitch angle scattering produced by interaction with some sort of wide band noise would yield a mechanism that operates more or less uniformly along the electron's spiral path. The wide band noise need not be whistler mode noise; it could be noise propagating in any of the other possible plasma modes including the longitudinal modes. It appears that electromagnetic noise sources and their possible effects on trapped electrons is a subject worthy of future investigation, both experimental and theoretical.

7. Conclusion

It seems likely that pitch angle diffusion is at least an important part of the loss mechanism for relativistic electrons in the Van Allen zones in the region $L\approx1.7$ to 2.5 and possibly also elsewhere. On the basis of pitch angle diffusion one can explain several of the features of the loss of electrons artificially injected into the trapping region by nuclear explosion. Among these are the fact that the electrons move only a very small amount in L during their lifetime, that the rate of loss is faster when the shape of the electron pitch angle distribution is perturbed severely from its normal or equilibrium shape, that a "shape independent" stage exists in the decay when the shape of the pitch angle distribution on a log scale no longer changes much with time and the flux at all pitch angles decreases with time approximately as $\sim \exp(-kt)$, and that the pitch angle distribution seems finally to settle down after a severe perturbation to a shape which is very similar to that during the shape independent stage of the decay. What remains unanswered, however, is the key question: what physical process

is responsible for producing the electron pitch angle diffusion? Pitch angle diffusion produced by cyclotron resonant interactions between electrons and whistlers leads to several predictions that disagree with observations, and so this mechanism is ruled out as the dominant one. Some other physical process that scatters the local pitch angle more or less uniformly all along the electron's spiral path would lead to better agreement with the data. It is not yet clear, however, just what the nature of such a process might be. Interaction between electrons and some kind of wide band electromagnetic noise seems at present to be a likely possibility.

REFERENCES

Brown, W. L., Hess, W. N., and Van Allen, J. A.: 1963a J. Geophys. Res. 68, 605.

Brown, W. L., Gabbe, J. D., and Rosenzweig, W.: 1963b, Bell System Tech. J. 42, 1505.

Brown, W. L.: 1965, Proceedings of the Plasma Space Science Symposium, D. Reidel Publishing Co., p. 189.

Cain, J. C., Shapiro, I. R., Stolarik, J. D., and Heppner, J. P.: 1961, J. Geophys. Res. 66, 2677.

Cornwall, J. M.: 1964, J. Geophys. Res. 69, 1251.

Dungey, J. W.: 1963a, Planet. Space Sci. 11, 591.

Dungey, J. W.: 1963b, J. Fluid Mech. 15, 74.

Dungey, J. W.: 1964, Space Sci. Rev. 4, 199.

Frank, L. A., Van Allen, J. A., and Hills, H. K.: 1964, J. Geophys. Res. 69, 2171.

Frank, L. A.: 1965, J. Geophys. Res. 70, 3533.

Gurnett, D. A. and O'Brien, B. J.: 1964, J. Geophys. Res. 69, 65.

Helliwell, R. A.: 1965, Whistlers and Related Ionospheric Phenomena, Stanford University Press, p. 121.

Horner, F.: 1961, J. Atmos. Terr. Phys. 21, 13.

Lenchek, A. M., Singer, S. F., and Wentworth, R. C.: 1961, J. Geophys. Res. 66, 4027.

Lenchek, A. M. and Singer, S. F.: 1963, Planet. Space Sci. 11, 1151.

MacDonald, W. M. and Walt, M.: 1961, Ann. Phys. (N. Y.) 15, 44.

McIlwain, C. E.: 1961, J. Geophys. Res. 66, 3681.

McIlwain, C. E.: 1963, Science 142, 355.

Northrop, T. G. and Teller, E.: 1960, Phys. Rev. 117, 215.

Northrop, T. G.: 1963, The Adiabatic Motion of Charged Particles, Interscience Publishers.

O'Brien, B. J.: 1962a, J. Geophys. Res. 67, 1227.

O'Brien, B. J.: 1962b, J. Geophys. Res. 67, 3687.

O'Brien, B. J.: 1964, J. Geophys. Res. 69, 13.

Roberts, C. S. and Buchsbaum, S. J.: 1964, Phys. Rev. 135, A381.

Roberts, C. S.: 1965, J. Geophys. Res. 70, 2517.

Roberts, C. S.: 1969, Rev. of Geophysics, 7, Nos. 1 and 2, p. 305.

Van Allen, J. A., Ludwig, G. H., Ray, E. C., and McIlwain, C. E.: 1958, Jet Propulsion 28, 588.

Van Allen, J. A., McIlwain, C. E., and Ludwig, G. H.: 1959, J. Geophys. Res. 64, 877.

Van Allen, J. A.: 1964, Nature 203, 1006.

Walt, M., and MacDonald, W. M.: 1964, Rev. Geophys. 2, 543.

Williams, D. J., and Smith, A. M.: 1965, J. Geophys. Res. 70, 541.

CHAPTER 5

CYCLOTRON- AND BOUNCE-RESONANCE SCATTERING OF ELECTRONS TRAPPED IN THE EARTH'S MAGNETIC FIELD

CHARLES S. ROBERTS
Bell Telephone Laboratories, Inc.,
Murray Hill, N.J., U.S.A.

Abstract. Pitch-angle diffusion into the loss cone is an important loss mechanism for radiation-zone electrons trapped in the magnetosphere. This paper examines two wave-particle interactions which are likely to be important for producing pitch-angle scattering. These are cyclotron-resonance scattering by whistler-mode disturbances and bounce-resonance scattering by disturbances having electric- or magnetic-field components parallel to the earth's magnetic field. Both mechanisms can operate effectively not only with sinusoidally varying disturbance fields but also with irregular, noise-like field fluctuations. The latter have rather wide-band power-spectral-density functions, and the strength of the scattering is proportional to the power present at the frequency appropriate to produce either cyclotron or bounce resonance. Irregular whistler-mode disturbances with r.m.s. magnetic-field fluctuations of order $10^{-3}\gamma$ or higher are significant in producing rates of pitch-angle diffusion in agreement with observed electron lifetimes in the slot and outer electron zone. If the whistler-mode power-spectral-density function decreases rapidly with increasing frequency, then this mechanism may have difficulty in explaining the pitch-angle scattering of nearly equatorially mirroring electrons. Contributions from bounce-resonance scattering can also be significant for the pitch-angle diffusion of relativistic electrons. This requires irregular parallel electric-field fluctuations of order 0.01–0.1 V/km r.m.s. or magnetic-intensity fluctuations of order 10^{-5}–10^{-4} r.m.s. of the earth's magnetic intensity at the equator of the line of force of interest. The experimentally observed loss of radiation-zone electrons may actually be due to a combination of the two mechanisms, bounce resonance being more important for electrons mirroring near the magnetic equator and cyclotron resonance being dominant for electrons mirroring sufficiently far off the magnetic equator.

1. Introduction

Particles trapped in the earth's radiation zones are subject to many physical processes which violate one or more of the three adiabatic invariants of the motion. McIlwain (1967) has reviewed the physical processes which act upon trapped electrons and has attempted to categorize them phenomenologically. One type of process which operates he terms 'persistent decay', which basically means that a group of trapped electrons will not remain trapped forever, but instead will gradually be lost from the trapping region or suffer energy degradation until their energy is below some threshold of interest. The effect of this process upon electrons has now been observed experimentally many times, both after natural and artificial injection of electrons into the radiation belts. Studies of such data during periods when the time decay of the trapped electron flux is approximately exponential and when contributions from natural electron sources can be neglected have yielded valuable information on the decay time, or lifetime, which characterizes this loss process (see, e.g., Brown (1966), McIlwain (1966, 1968), Van Allen (1966), and the references cited therein). These studies show that this decay time is a strong function of the line of force or L-shell on which the electrons are trapped. Figure 1 shows some typical decay time vs. L results for some

measurements made on >0.5 MeV electrons with several different satellite experiments. While WALT and MACDONALD (1964) have shown that Coulomb scattering off the residual atmosphere can account for the observed decay time below $L=1.25$, a complete and satisfactory explanation of the portion of the curve in Figure 1 above $L=1.25$ has not yet been presented.

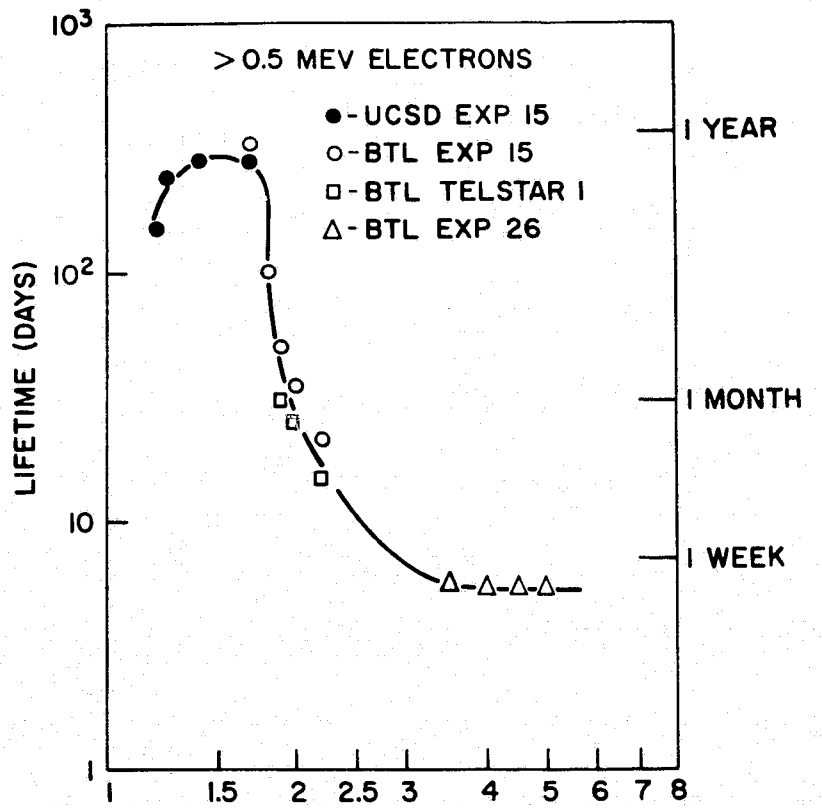

Fig. 1. Lifetime vs. L for radiation-zone electrons.

Several features of the mechanism responsible for electron loss in the region above $L=1.25$ now seem clear, however. By process of elimination, the loss mechanism must involve interaction of the electrons with fluctuating electric or magnetic fields (turbulence) present in the magnetospheric plasma. Such an interaction, or scattering, must lead to a violation of M (the magnetic moment or first adiabatic invariant), of J (the second adiabatic invariant), or of both in order to account for the observed loss. Strong experimental evidence supports the idea that pitch-angle diffusion into the loss cone plays a very important role in the electron loss process (see among others: BROWN, 1966; ROBERTS, 1966; WEST, 1966). The extent to which energy change is involved is not yet so clear.

In this paper we shall explore two of the many wave-particle interactions which may be important for electrons in the magnetosphere and which can produce pitch-angle diffusion. The first of these, cyclotron resonance with fluctuations in the whistler mode, causes a breakdown of both M and J. Various aspects of this loss mechanism have been discussed previously by other authors (DUNGEY, 1963, 1964; CORNWALL,

1964; KENNEL and PETSCHEK, 1966; ROBERTS, 1966). This paper will emphasize interaction of electrons with whistler-mode fluctuations having a rather broad-band power spectral density. In other words, one will consider interaction with whistler-mode noise rather than with discrete whistler-mode emissions or signals. The second interaction to be considered will be bounce-frequency resonance of electrons with fluctuations in the compressional-Alfvén and ion-acoustic modes. Some aspects of the effects of bounce resonance on electrons has been considered by DUNGEY (1964) and CORNWALL (1966). This mechanism is one in which M is conserved and J is violated. Again, the emphasis will be upon interactions with broad-band disturbances rather than with regularly oscillating signals.

Throughout this paper the author has chosen to adopt a particular philosophy with regard to the relationship between the trapped particles and the waves or turbulence in the plasma acting upon them to produce scattering and, ultimately, loss. The view will be taken that the turbulence is present *a priori* in the magnetospheric plasma, and no attempt will be made to explain or understand the origin of the turbulence. Thus, all results to be derived for the scattering of trapped particles by field fluctuations will contain the power-spectral-density function of the field fluctuations as an unknown. Before any computations can be made to compare with trapped particle experiments, an independent determination of the power spectral density must be made. This may be done from actual data on field fluctuations in the magnetosphere, or possibly from theoretical arguments in cases where the applicable theory is well enough known.

In one respect this viewpoint of treating the origin of plasma turbulence and the effect of plasma turbulence upon particles as two separate problems is unrealistic. It is ultimately found that particles themselves must be the source of the waves which comprise the plasma turbulence. The influence of these waves on the particles alters, in turn, the source of the turbulence, and so the complete problem is inherently nonlinear. Treatment of the complete problem therefore involves considering not only the scattering of the particles by the waves but also the production of waves by the particles and the coupling between the two processes. Although the difficulty of this problem is such that it taxes the capabilities of present day plasma theory, progress has been made by several authors in understanding some different aspects of the problem (CHAMBERLAIN, 1963; CHANG and PEARLSTEIN, 1965; KENNEL and PETSCHEK, 1966; CORNWALL, 1966; EVIATAR, 1966). It is felt by this author, however, that where the physics of the problem permits, as in the case of weak diffusion of electrons into the loss cone, there is a real advantage in separating the problem into two parts with the power-spectral-density function providing the interface. In this way determinations of the power spectral density by experiments designed to measure electric and magnetic fields will allow one to evaluate particle-scattering mechanisms and turbulence-generating mechanisms independently. Hopefully, one can then better determine which parts of the theory are good and which parts are poor approximations to the actual situation in the magnetosphere. Such a determination seems absolutely necessary in view of the many complications and approximations involved in present-day plasma-turbulence theory.

2. Cyclotron-Resonance Scattering

A. FREQUENCY TO RESONATE WITH AN ELECTRON

Signals propagating in the whistler mode are in the correct frequency range to produce cyclotron resonance with trapped electrons. The exact whistler frequency needed to resonate with a given electron depends upon several parameters. If we consider a plane whistler wave with angular frequency ω and propagation vector $\mathbf{k}$ then the condition for cyclotron resonance with an electron is

$$\omega \pm k_{\parallel} v_{\parallel} = \Omega . \tag{1}$$

Here $v_{\parallel}$ and $k_{\parallel}$ are the components parallel to the earth's magnetic field of the electron velocity vector and wave propagation vector respectively. The quantity Ω is the *relativistic* electron cyclotron frequency. If ω_c is the non-relativistic electron cyclotron frequency and if the electron energy is determined by $\gamma = m/m_0 = (1-\beta^2)^{-1/2}$, where $\beta = v/c$, then one obtains

$$\Omega = \omega_c (1 - \beta^2)^{1/2} = \omega_c / \gamma . \tag{2}$$

The relativistic electron cyclotron frequency is always less than the non-relativistic. The phase velocity of the whistler wave is $\omega/k = c/n$ where n, the index of refraction for whistler-mode propagation, depends on the frequency ω. In Equation (1) the plus sign is the physically important choice since the whistler frequency of interest is usually lower than Ω, and therefore it requires an upward Doppler shift. If the angle between $\mathbf{k}$ and the earth's magnetic field is denoted by θ, then $\cos\theta = k_{\parallel}/k$ and Equation (1) can be rewritten

$$\omega (1 + k v_{\parallel} \cos\theta / \omega) = \omega_c / \gamma . \tag{3}$$

Since $v_{\parallel} = \beta c \mu$, where $\mu = v_{\parallel}/v = \cos\alpha$ is the cosine of the electron's local pitch angle, Equation (3) can be rearranged to read

$$\omega = \frac{\omega_c}{\gamma (1 + n \beta \mu \cos\theta)} . \tag{4}$$

Equation (4) gives the frequency necessary to produce cyclotron resonance with a given electron, and this frequency is a function of several important parameters. It is a strong function of position in the magnetosphere, since ω_c and n vary with position. It is a function of electron energy through γ and β; for relativistic electrons the main dependence is through γ. For example, one has $\gamma \approx 2$ for a 0.5 MeV electron and $\gamma \approx 5$ for a 2 MeV electron. And finally the resonant frequency is a function of μ, the electron's pitch-angle cosine, since this determines the fraction of the electron's velocity which can be used to produce Doppler shift. Since n is generally between 5 and 100 for the whistler mode in the magnetosphere, the Doppler-shift term is very important and the dependence upon μ is strong.

We shall show in this paper that the scattering of a given electron by a whistler-mode disturbance is proportional to the power in the disturbance at the resonant

frequency given by Equation (4). If electrons are scattered by disturbances which are not rather wide band disturbances, i.e., if the power-spectral-density function of the disturbance is a strong function of frequency, then the varying amount of power present at different frequencies will cause the strength of the scattering to be a function of the parameters which affect the resonance frequency. Thus, rapidly decreasing or peaked power-spectral-density functions will produce electron scattering which is a strong function of electron pitch angle and kinetic energy if scattering by whistler-mode disturbances is the only scattering mechanism operative. Experimental evidence indicates, however, that for relativistic electrons pitch-angle diffusion is not a very strong function of either electron pitch angle or energy. This fact has been previously pointed out by ROBERTS (1966) in arguing against the idea that lightning-bolt-produced whistlers are the dominant scatterers of radiation-zone electrons. For the lightning-bolt whistler case the power spectral density is strongly peaked between 2 and 10 kHz, and 0.5 MeV electrons mirroring near the magnetic equator on L-shells below approximately 3.5 are unable to resonate with this frequency range. This leads to serious disagreements between the observed and the theoretically predicted electron pitch-angle distribution for such a scattering process. Clearly, analogous arguments will also apply to other types of whistler-mode disturbances having power spectral density functions strongly dependent upon frequency.

B. PITCH-ANGLE DIFFUSION COEFFICIENT

The approximate effect upon trapped electrons of interactions with whistler-mode disturbances can be calculated in an elementary way. The whistler mode is basically a circularly polarized mode, the waves having exact circular polarization when their direction of propagation is parallel to the earth's magnetic field. Calculation of the effects of whistlers is simplified if one assumes only parallel propagation, and we shall make that approximation in this paper. An exact solution to the motion of an electron in a whistler wave propagating parallel to the earth's field has been given (ROBERTS and BUCHSBAUM, 1964), but one can also compute the effects on the electron in an approximate way which is sufficient for our purposes. We consider the interaction of an electron with a single-frequency whistler-mode wave whose frequency is given by Equation (4), so that we have the case of exact cyclotron resonance. Let the angle between $\mathbf{v}_\perp$, the component of the electron's velocity perpendicular to the earth's field, and $\mathbf{b}$, the rotating magnetic field vector of the whistler wave, be given by ϕ. We wish to consider relativistic electrons, and since n is rather large ($n \sim 10$) for the whistler mode in the magnetosphere, we neglect the force on the electron due to the electric field of the whistler and retain only the force resulting from $\mathbf{b}$. In this approximation, the energy of the electron remains unchanged, and the only effect of the whistler is to change the direction of the electron's velocity vector, i.e., its pitch angle. The main effect of $\mathbf{b}$ is to exert an additional force on the electron parallel to the earth's field, and by application of the Lorentz force formula one obtains

$$\mathrm{d}p_\parallel/\mathrm{d}t = ebv_\perp \sin\varphi/c\,, \tag{5}$$

where p is the electron's momentum and e its charge. We have assumed exact cyclotron resonance, and we consider only sufficiently small values of b so that the angle ϕ does not change significantly over many cyclotron periods. Integrating Equation (5), we find that the change in $p_\parallel$ produced by the wave after time t is given by

$$\Delta p_\parallel = ebv_\perp t \sin\varphi/c\,. \tag{6}$$

Since $\mu = p_\parallel/p$, the corresponding change in the electron's local pitch-angle cosine is

$$\Delta\mu = \Delta p_\parallel/p = (e/mc)\,(1-\mu^2)^{\frac{1}{2}}\, bt \sin\varphi\,. \tag{7}$$

To treat the effect of pitch-angle diffusion on a population of electrons trapped in the magnetosphere the Fokker-Planck equation may be used (WENTWORTH, 1963; MACDONALD and WALT, 1961). Using the electron equatorial pitch-angle cosine, μ_0, as the variable in which to describe the diffusion, the two Fokker-Planck diffusion coefficients are related to $\langle(\Delta\mu)^2\rangle/t$, the mean square change in local pitch-angle cosine per unit time (ROBERTS, 1966). Since the phase ϕ is random for the electron-whistler wave interaction, one obtains from Equation (7) the relation:

$$\langle(\Delta\mu)^2\rangle/t = \tfrac{1}{2}(e/mc)^2\,(1-\mu^2)\,b^2 t\,. \tag{8}$$

Equation (8), derived for the case of resonance with a pure plane wave, may now be taken over to the case of interaction with a broad-band disturbance. The average over time of the square of one component of the wave magnetic field is $b^2/2$ in the plane-wave case, and in the broad-band case this quantity must be replaced by the product of a power-spectral-density function evaluated at the resonance frequency and an effective bandwidth for the resonance. In the Appendix, we show that after interaction for a time t, the effective bandwidth Δf of the whistler resonance is given by $t^{-1}\,[1+v_\parallel/v_g(\omega_0)]^{-1}$, where $v_g = \mathrm{d}\omega/\mathrm{d}k$ is the whistler-mode group velocity. Denoting the power-spectral-density function of one component of the fluctuating disturbance field as $\mathscr{B}_x(f)$, the replacement

$$\tfrac{1}{2}b^2 \to \mathscr{B}_x(f_0)\,t^{-1}\,[1+v_\parallel/v_g(\omega_0)]^{-1} \tag{9}$$

will make Equation (8) valid for interaction with broad-band disturbances. The final result is:

$$\langle(\Delta\mu)^2\rangle/t = (e/mc)^2\,(1-\mu^2)\,[1+v_\parallel/v_g(\omega_0)]^{-1}\,\mathscr{B}_x(f_0)\,. \tag{10}$$

Equation (10) can be used to obtain some order-of-magnitude values for whistler-mode diffusion. The lifetime for electrons is approximately the reciprocal of $D(\mu_0) = \langle(\Delta\mu_0)^2\rangle/t$, the Fokker-Planck diffusion coefficient. We approximate $D(\mu_0)$ as

$$D(\mu_0) \approx \tfrac{1}{3}(e/mc)^2\,\mathscr{B}_x(f_0)\,, \tag{11}$$

where the factor of $\frac{1}{3}$ has been put in as a guess for the discarded and neglected factors and effects that would enter into the correct expression for $D(\mu_0)$. If $\mathscr{B}_x(f_0) = 10^{-10}\,\gamma^2/\mathrm{Hz}$ ($1\gamma = 10^{-5}$ Gauss), Equation (11) gives $D(\mu_0) \approx 10^{-6}\ \mathrm{sec}^{-1}$, which corresponds to an electron lifetime of approximately 10 days. Thus, broad-band whistler-

mode disturbances with power spectral densities of approximately 10^{-10} γ^2/Hz are capable of accounting for the observed lifetime of radiation zone electrons. If the total bandwidth of the disturbance is taken to be $\approx 10^4$Hz, the r.m.s. field fluctuations in such disturbances would be of the order of one milligamma. GURNETT (1968) has observed that in the frequency range 0.2–7.0 kHz noise of at least this intensity is a very common occurrence in the 50° to 70° magnetic-invariant-latitude region at altitudes up to 2700 km. These measurements strongly suggest that scattering by whistler-mode noise plays an important role in determining the lifetime of radiation zone electrons. Measurements must be made in the equatorial region on the relevant lines of force and also to higher frequencies, however, before a more definitive statement can be made. For example, to scatter 0.5 MeV electrons mirroring near the magnetic equator on $L=2$ would require that the power spectral density at the magnetic equator be broad-band up to approximately 55 kHz and on $L=3$ up to 16 kHz. Diffusion of electrons mirroring near the magnetic equator on a line of force seems to be one of the most difficult features for the whistler-mode mechanism to explain.

3. Bounce-Resonance Scattering

A. PARALLEL EQUATION OF MOTION

A trapped particle in the magnetosphere has three basic periodicities associated with the three adiabatic invariants of its motion, and one would expect to find resonant wave-particle interactions associated with each of these periodicities. The previous section of this paper considered perturbations in an electron's orbit produced by interaction with signals at the electron's cyclotron frequency. Strong perturbations also occur due to electric and magnetic fluctuations having power at the particle's drift frequency (FÄLTHAMMAR, 1965, 1966). In this section we show that, as expected, a resonant interaction also occurs when a particle is subjected to field fluctuations having power at the particle's bounce frequency. Such a process violates J, the adiabatic invariant associated with the bounce frequency, but conserves M, the particle's magnetic moment. This is because the bounce frequency is so much lower than the cyclotron frequency for particles trapped in the magnetosphere. Like cyclotron resonance, bounce-resonance interaction can change a particle's pitch angle and thus lead to trapped-particle loss through pitch-angle diffusion into the loss cone.

To treat bounce resonance quantitatively we use the parallel equation of motion for a particle trapped in a magnetic field (NORTHROP, 1963). We shall treat the motion non-relativistically, since it considerably simplifies the problem to do so. If s is the distance from the magnetic equator measured along the line of force of interest, the parallel equation of motion is

$$m \frac{\mathrm{d}^2 s}{\mathrm{d}t^2} = qE_{\parallel} - M \frac{\partial B}{\partial s} . \tag{12}$$

Here m and q are the mass and charge of the particle being considered, M its conserved magnetic moment, and $E_{\parallel}$ and B are the fields that act on the particle as it moves from

mirror point to mirror point. The total magnetic field B consists of two parts

$$B(s, t) = B_{\text{earth}}(s) + b_{\parallel}(s, t) \tag{13}$$

where $\mathbf{b}(s, t)$ is the fluctuating part of the magnetic field due to any disturbances which may be present. We consider only small disturbances such that $b/B_{\text{earth}} \ll 1$. Assuming the earth's field to be a dipole field, $B_{\text{earth}}(s)$ may be expanded around $s=0$ (the magnetic equator) as follows:

$$B_{\text{earth}}(s) = B_0(1 + 9s^2/2L^2R_E^2 + \cdots). \tag{14}$$

The next term in the expansion would be proportional to s^4. In Equation (14), R_E is the radius of the earth, L is the geocentric distance, measured in earth radii, to the equator on the line of force of interest, and B_0 is the field magnitude at the equator. The two terms of the expansion given in Equation (14) are a good approximation to the field magnitude for latitudes up to approximately 20°. The neglected terms, containing higher powers of s, will cause the bounce of particles mirroring at latitudes above approximately 20° to be anharmonic. This anharmonicity serves only to complicate the Equation of motion (12) since it is not really vital to the physical mechanism involved in bounce resonance. Using the two terms in Equation (14), the parallel equation of motion (12) can be written

$$\mathrm{d}^2s/\mathrm{d}t^2 + \omega_0^2 s = F(t)/m, \tag{15}$$

where $F(t)$ is the force parallel to the earth's field which acts on the particle due to fluctuating electric and magnetic fields.

$$F(t) = qE_{\parallel} - M(\partial b_{\parallel}/\partial s). \tag{16}$$

The constant ω_0 in Equation (15) is 2π times the bounce frequency of a particle that mirrors near the magnetic equator:

$$\omega_0 = 3(MB_0/m)^{1/2}/LR_E. \tag{17}$$

Remembering that $M = \frac{1}{2}mv_{\perp 0}^2/B_0 = \frac{1}{2}mc^2\beta^2 \sin^2\alpha_0/B_0$, where α_0 is the particle's equatorial pitch angle, Equation (17) can be written:

$$\omega_0/2\pi = \left(\frac{3c}{2\pi\sqrt{2}\,R_E}\right)\left(\frac{\beta \sin\alpha_0}{L}\right) \tag{18a}$$

$$= 15.9\left(\frac{\beta \sin\alpha_0}{L}\right) \text{sec}^{-1} \tag{18b}$$

Equation (15), which describes the motion of the trapped particle parallel to the earth's field, is the equation of a forced harmonic oscillator. The forcing term, $F(t)/m$, comes from any electric and magnetic disturbances present. If no disturbances are present, the right-hand side of Equation (15) is zero, and its general solution is $s(t) = -s_m \cos(\omega_0 t + \psi)$, $\dot{s}(t) = v_{\parallel 0} \sin(\omega_0 t + \psi)$, where s_m is the distance along the line of force to the particle's mirror point, ψ is an arbitrary phase constant, and $v_{\parallel 0} = \omega_0 s_m$.

Using this solution, we find that the particle's second invariant, J, is simply related to its parallel energy at the magnetic equator.

$$J = \oint p_{\parallel}\, \mathrm{d}s = \int_0^{2\pi/\omega_0} p_{\parallel} v_{\parallel} \mathrm{d}t = m v_{\parallel 0}^2 \int_0^{2\pi/\omega_0} \sin^2(\omega_0 t + \psi)\, \mathrm{d}t$$
$$J = \pi m v_{\parallel 0}^2/\omega_0 = W_{\parallel 0}\tau_b . \tag{19}$$

Here $\tau_b = 2\pi/\omega_0$ is the bounce period, and $W_{\parallel 0} = \frac{1}{2} m v_{\parallel 0}^2$ is the particle's equatorial parallel energy. When disturbances are present so that the right-hand side of Equation (15) is nonzero, then $W_{\parallel 0}$, and consequently J also, is no longer a constant of the motion.

B. FREQUENCIES AND PLASMA MODES OF INTEREST

Figure 2 shows the approximate value at the magnetic equator of some critical frequencies in the magnetosphere plotted vs. L. The bounce-frequency values shown

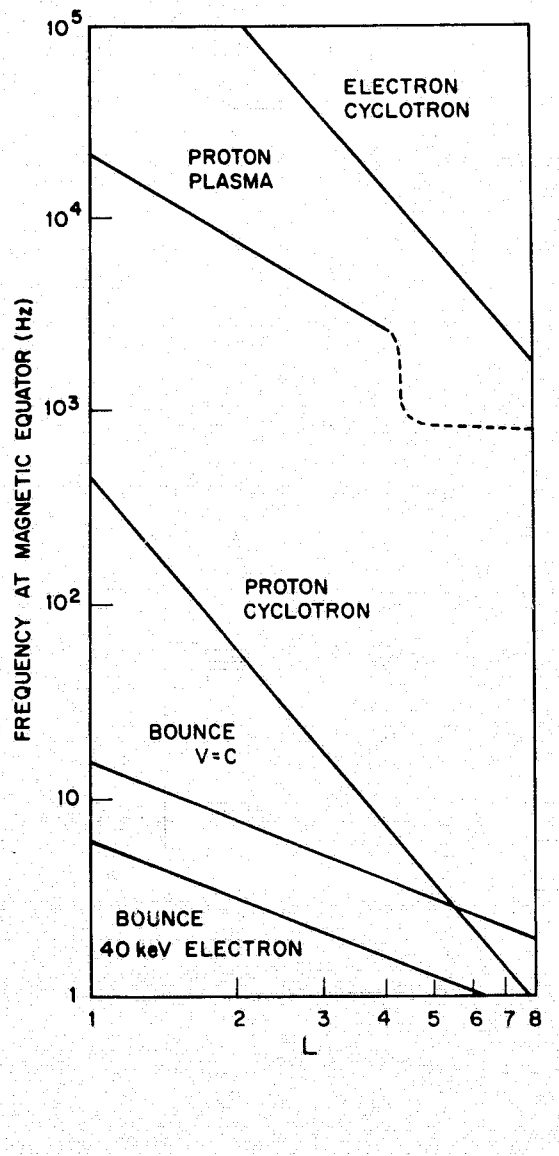

Fig. 2. Approximate values on the magnetic equator for some frequencies of interest to magnetospheric physics.

in Figure 2 were obtained from Equation (18b) with $\alpha_0 = \pi/2$. The bounce frequency of trapped particles is actually not a very strong function of mirror point position even when the anharmonic terms are included in Equation (14). This can be seen in Figure 3, which shows as a function of equatorial pitch angle the bounce frequency of a particle on any line of force in a dipole field. The bounce frequency is expressed

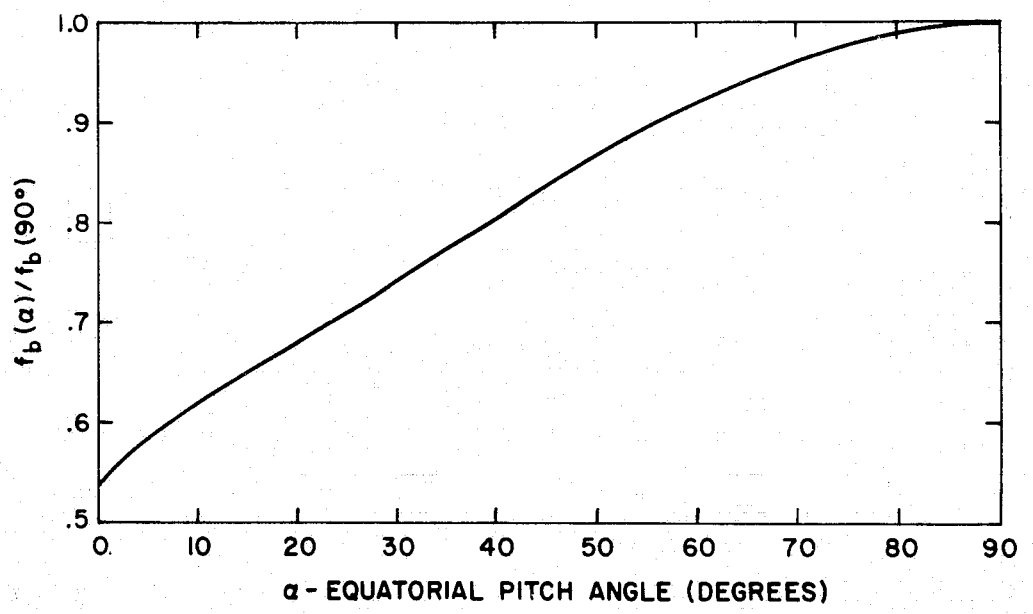

Fig. 3. Bounce frequency vs. pitch angle for a constant-energy particle trapped on a dipole line of force.

in units of the bounce frequency for a particle of the same energy having $\alpha_0 = \pi/2$. From Figure 3 we see that the variation in bounce frequency is less than a factor of 2, no matter where the location of the particle's mirror point.

We require field fluctuations having power at the bounce frequency to produce

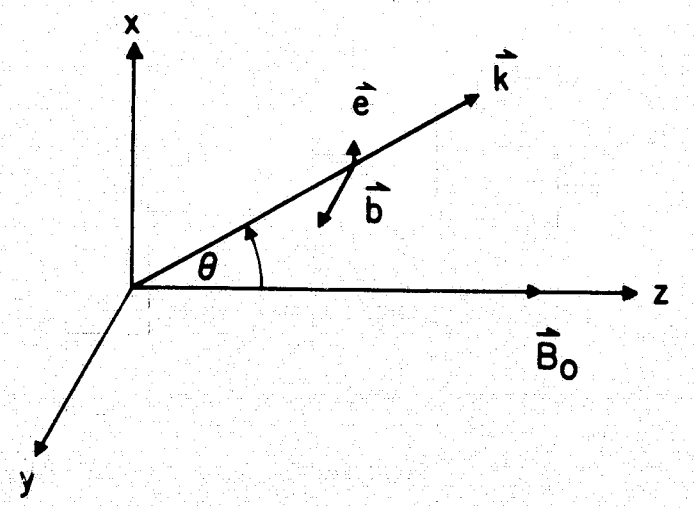

Fig. 4. Geometry of the fluctuating fields in a plane torsional Alfvén wave.

bounce-resonance scattering of particles, and from Figure 2 we see that this frequency is below the proton plasma and proton cyclotron frequencies almost everywhere in the magnetosphere. In this frequency range there are three plasma modes in which wave propagation is possible. These are the ion-acoustic, torsional Alfvén and compressional Alfvén modes, although other terminology for the three modes is in common use. The ion-acoustic mode is basically an electrostatic mode, and it will contribute to the scattering force $F(t)$ in Equation (16) through $E_{\|}$. The field geometry in the torsional Alfvén wave is shown in Figure 4, and since it has no field components parallel to $\mathbf{B}_0$ it does not contribute to $F(t)$. The compressional Alfvén wave, shown in Figure 5, has a fluctuating magnetic-field component parallel to $\mathbf{B}_0$ provided that $\mathbf{k}$ is not exactly parallel to $\mathbf{B}_0$. Thus ion-acoustic and compressional Alfvén-mode disturbances will be important for bounce-resonance scattering.

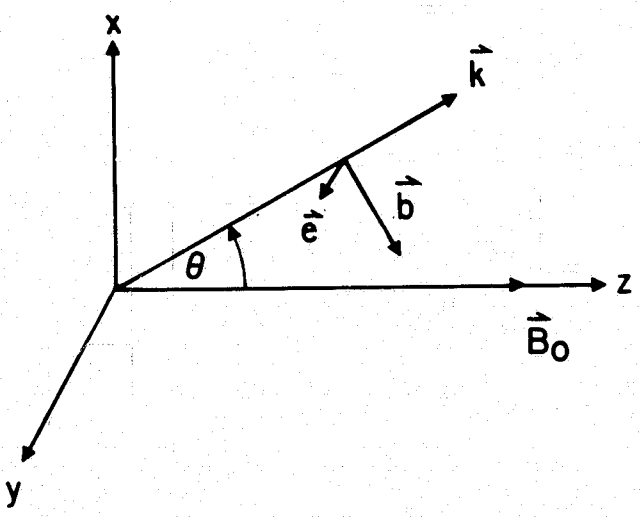

Fig. 5. Geometry of the fluctuating fields in a plane compressional Alfvén wave.

C. DIFFUSION COEFFICIENT FOR BOUNCE-RESONANCE SCATTERING BY NOISE

When $F(t)$ is non-zero, the general solution to Equation (15) can be written

$$s(t) = -s_m \cos(\omega_0 t + \psi) + \frac{1}{m\omega_0} \int_0^t \mathrm{d}t_2 F(t_2) \sin \omega_0 (t - t_2) \tag{20a}$$

$$\dot{s}(t) = \omega_0 s_m \sin(\omega_0 t + \psi) + \frac{1}{m} \int_0^t \mathrm{d}t_2 F(t_2) \cos \omega_0 (t - t_2). \tag{20b}$$

Multiplying Equation (15) by $m\dot{s}(t)$ gives the oscillator energy equation:

$$\frac{\mathrm{d}}{\mathrm{d}t} [\tfrac{1}{2} m\dot{s}^2 + \tfrac{1}{2} m\omega_0^2 s^2] = \dot{s}(t) F(t). \tag{21}$$

The quantity in the brackets in Equation (21) is just $W_{\|0}$, the particle's equatorial parallel energy. Integrating Equation (21) over a time interval t gives

$$\Delta W_{\|0} = \int_0^t \mathrm{d}t_1 \dot{s}(t_1)\, F(t_1). \tag{22}$$

Suppose now that the particle is subject to random electric- or magnetic-field fluctuations so that $F(t)$ is a rather irregular function of time. While we have no way of knowing exactly how the function $F(t)$ behaves with time, we can define an ensemble of possible functions $F(t)$. Figure 6 shows some possible members of the ensemble for the type of $F(t)$ we are considering. All physical effects produced by such an ensemble must depend on certain averages taken over all possible members of the ensemble.

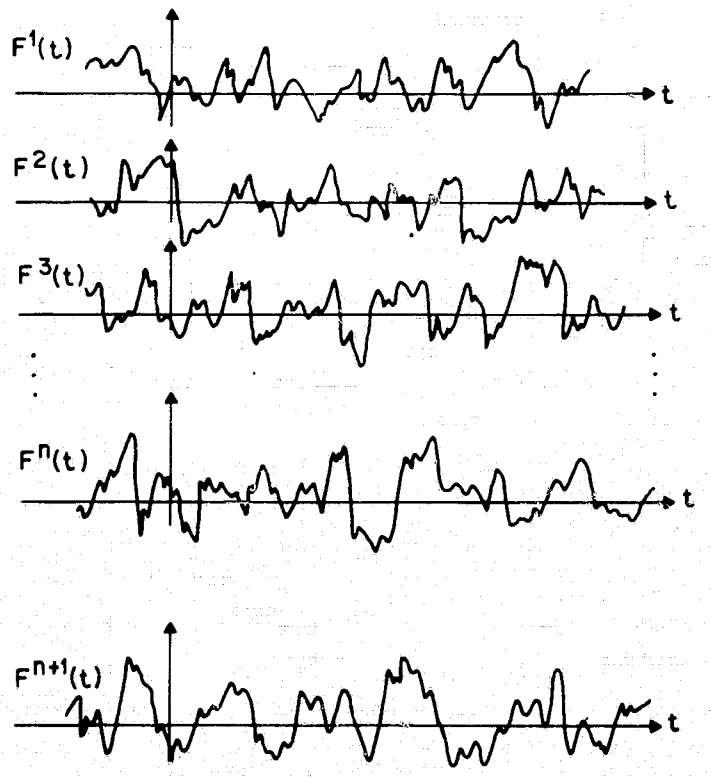

Fig. 6. Ensemble of random force vs. time functions.

Denoting ensemble average by $\langle\ \rangle$, we demand that $\langle F(t)\rangle = 0$, since the force should not be preferentially in one direction. The ensemble average $\langle F(t_1)\, F(t_2)\rangle$ is called the 'autocovariance function' of the force (MIDDLETON, 1960), which we denote by $K_F(t_1 - t_2)$. The autocovariance is a function only of the time difference $(t_1 - t_2)$ since we insist that the ensemble be stationary, i.e., the origin of time is unimportant.

Equation (22) can now be used to calculate the average change in parallel energy due to some $F(t)$ ensemble. Using Equation (20b) in Equation (22) and performing the ensemble average gives:

$$\langle \Delta W_{\parallel 0} \rangle = \frac{1}{m} \int_0^t \mathrm{d}t_1 \int_0^{t_1} \mathrm{d}t_2 \cos \omega_0 (t_1 - t_2) \langle F(t_1) F(t_2) \rangle . \tag{23}$$

The quantity $\langle F(t_1) F(t_2) \rangle$ is the autocovariance $K_F(t_1 - t_2)$. Transforming the double integral by letting $\lambda = t_1 - t_2$ and $\tau = t_1 + t_2$ allows Equation (23) to be written in the form

$$\langle \Delta W_{\parallel 0} \rangle = \frac{t}{m} \int_0^t \mathrm{d}\lambda (1 - \lambda/t) K_F(\lambda) \cos \omega_0 \lambda . \tag{24}$$

As $t \to \infty$, the contribution of the $-\lambda/t$ term to the integral in Equation (24) becomes vanishingly small. This occurs because $K_F(\lambda) \to 0$ very rapidly for large λ. Remembering that the power-spectral-density function is 4 times the Fourier cosine transform of the autocovariance (MIDDLETON, 1960), we find for the average change in parallel energy per unit time

$$\langle \Delta W_{\parallel 0} \rangle / t = \mathscr{F}(f_0)/4m , \tag{25}$$

where $\mathscr{F}(f)$ is the power-spectral-density function of the force, $F(t)$.

It is interesting to note that Equation (25) could have been derived in a more elementary manner by solving Equation (15) for a sinusoidal force and then passing over the broad-band case by replacing the average 'power' by the power-spectral-density function times a bandwidth. This was the technique used in Section 2 of this paper to derive the diffusion coefficient due to scattering by a broad-band whistler-mode disturbance. If we take $F(t) = \mathrm{d} \cos(\omega_0 t + \phi)$ in Equation (15) we find that after averaging over ϕ,

$$(\Delta W_{\parallel 0})/t = \mathrm{d}^2 t/8m . \tag{26}$$

The average 'power' in $\mathrm{d} \cos(\omega_0 t + \phi)$ is $\frac{1}{2}d^2$, and the bandwidth of the resonance after interaction for time t is just $1/t$. Thus, replacing $\frac{1}{2}d^2$ by $\mathscr{F}(f_0)/t$ in Equation (26) gives the same result as Equation (25), which was derived using the autocovariance.

We now relate the force power-spectral-density function $\mathscr{F}(f)$ to the power-spectral-density function of the fluctuating electric and magnetic fields producing the scattering. For the electric-field case, this is trivial since, according to Equation (16), $F(t) = qE_{\parallel}(t)$. Thus

$$\mathscr{F}(f) = q^2 \mathscr{E}_{\parallel}(f) \tag{27}$$

where $\mathscr{E}_{\parallel}(f)$ is the power-spectral-density of the parallel electric-field component. The compressional Alfvén-wave case is slightly more difficult. Referring again to Figure 5, we find $b_{\parallel} = b \sin\theta \sin(\omega t - ks \cos\theta + \phi)$ for a single wave component, and we assume out of ignorance that all directions of propagation are equally likely. Thus, averaging over solid angle and time gives

$$b_{\parallel}^2 = \frac{1}{8\pi} \int_0^{2\pi} \mathrm{d}\varphi \int_0^{\pi} \mathrm{d}\theta \, b^2 \sin^3 \theta = \tfrac{1}{3} b^2 . \tag{28}$$

According to Equation (16), the force due to this single wave is $Mbk\sin\theta\cos\theta\cos(\omega t - ks\cos\theta + \phi)$. Again averaging over all solid angle and time we obtain

$$\overline{F^2} = \tfrac{1}{15}M^2k^2b^2 = \tfrac{1}{5}M^2k^2\overline{b_\parallel^2}\,. \tag{29}$$

Since $\overline{F^2} = \int_0^\infty \mathrm{d}f\,\mathscr{F}(f)$ and $\overline{b_\parallel^2} = \int_0^\infty \mathrm{d}f\,\mathscr{B}_\parallel(f)$ we must have

$$\mathscr{F}(f) = \tfrac{1}{5}M^2k^2\,\mathscr{B}_\parallel(f), \tag{30}$$

where $\mathscr{B}_\parallel(f)$ is the power-spectral-density function of $b_\parallel(t)$. If v_A is the Alfvén speed, then in Equation (30)

$$k = 2\pi f/v_A\,. \tag{31}$$

D. APPROXIMATE LIFETIMES

In order to evaluate the importance of bounce-resonance scattering for particles in the magnetosphere we compute the time to move a particle's mirror point from the magnetic equator to a point L earth radii down the line of force, i.e., $s_m = LR_E$. We call this time the 'particle's lifetime', since the $1/e$ decay time of a population of particles trapped on the line of force should also be of this approximate magnitude. When $s_m = LR_E$, then we find $W_{\parallel 0} = \frac{1}{2}m\omega_0^2 s_m^2 = \frac{1}{2}m\omega_0^2 L^2 R_E^2$, and we take for the lifetime τ

$$\tau \approx \tfrac{1}{2}m\omega_0^2 L^2 R_E^2\,[\Delta W_{\parallel 0}\rangle/t]^{-1}\,. \tag{32}$$

Using Equation (25) for the quantity in brackets in Equation (32) and Equation (17) for ω_0 we get

$$\tau \approx 9m^2v_{\perp 0}^2/\mathscr{F}(f_0). \tag{33}$$

Considering first bounce-resonance scattering by parallel electric fields, we use Equation (27) in Equation (33) to obtain

$$\tau \approx 9m^2v_{\perp 0}^2/q^2\mathscr{E}_\parallel(f_0) \tag{34}$$

for the approximate lifetime due to parallel electric fields. For electrons, Equation (34) can be rewritten

$$\tau \approx 30\,\mathrm{sec}\,(v_{\perp 0}/c)^2/\mathscr{E}_\parallel(f_0) \tag{35}$$

where in Equation (35) $\mathscr{E}_\parallel$ is in units of $(\mathrm{V/km})^2/\mathrm{Hz}$. If $\mathscr{E}_\parallel(f_0) \approx 3\times 10^{-5}\,(\mathrm{V/km})^2/\mathrm{Hz}$, then Equation (35) gives a lifetime of approximately 10^6 sec $\approx$ 10 days for relativistic electrons. If the total bandwidth of the noise is approximately 30 Hz, then this corresponds to $(\Delta E_\parallel)_{\mathrm{r.m.s.}} \approx 0.03$ V/km electric-field fluctuations. Even smaller electric-field fluctuations would be significant for lower-energy electrons for which $(v_{\perp 0}/c)^2 \ll 1$.

For the bounce-resonance scattering by magnetic-field compressions, $b_\parallel$, we use Equation (30) for $\mathscr{F}(f_0)$ in Equation (33) to obtain

$$\tau \approx 45m^2v_{\perp 0}^2/M^2k^2\,\mathscr{B}_\parallel(f_0), \tag{36}$$

which can be written using Equation (31) as

$$\tau \approx \frac{180v_A^2}{v_{\perp 0}^2\omega_0^2\,[\mathscr{B}_\parallel(f_0)/B_0^2]}\,. \tag{37}$$

The Alfvén speed v_A at the magnetic equator is given approximately by $(v_A/c)^2 \approx 5\times10^{-4}L^{-3}$, and using Equation (18b) for ω_0, we get finally:

$$\tau \approx \frac{10^{-5}\,L^{-1}\ \text{sec}}{(v_{\perp 0}/c)^4\,[\mathscr{B}_{\parallel}(f_0)/B_0^2]}. \tag{38}$$

For relativistic electrons, $\mathscr{B}_{\parallel}(f_0)/B_0^2 \approx 10^{-11}$/Hz would give a 10-day lifetime. Assuming $\approx$10 Hz bandwidth for the noise, this corresponds approximately to $(\Delta b_{\parallel})_{\text{r.m.s.}}/B_0 \approx 10^{-5}$, i.e., small, irregular, 1 part in 10^5 compressions of the earth's magnetic field are significant for scattering relativistic electrons! The importance of this magnetic scattering drops off rapidly with decreasing electron energy, however, due to the $(v_{\perp 0}/c)^4$ term which enters the denominator of Equation (38).

E. EFFECT OF SPATIAL VARIATIONS OF THE FIELDS

In Equation (16) defining the force function $F(t)$, the fields are to be evaluated *at the particle's instantaneous position at time t*. For example, if the electric field is a function of both time t and position on the line of force s, we may denote the parallel component of the electric field as $E_{\parallel}(s, t)$. If this $E_{\parallel}$ is sufficiently small so that the particle's mirror position does not change significantly over many bounce periods, then the bounce motion of the particle may be represented by $s(t) = -s_m \cos(\omega_0 t + \psi)$. The function $F(t)$ due to this electric field would then be given approximately by

$$F(t) = qE_{\parallel}(s(t), t) = qE_{\parallel}(-s_m \cos(\omega_0 t + \psi), t). \tag{39}$$

Similarly, all the power spectral density functions used in this section refer to the power spectral density as seen in *the frame of reference of the bouncing particle*. This may be very different from the power-spectral-density-function observed at one particular point in space.

Let us define an approximate field correlation distance, s_c, to be the average distance over which $E_{\parallel}$ (or $\partial b_{\parallel}/\partial s$ if we are considering magnetic scattering) changes sign. If $s_m > s_c$ we might expect $\mathscr{E}_{\parallel}(f)$, the power-spectral density observed in the particle's frame of reference, to be very different from the power-spectral-density observed at one point in space. The wavelength in the magnetosphere of compressional Alfvén waves of frequency near the relativistic electron bounce frequency is approximately 0.1 R_E. The wavelength of ion-acoustic waves of this frequency is likely to be even smaller since the proton thermal speed is probably smaller than the Alfvén speed. Thus for disturbances composed of these waves, $s_m \gg s_c$ for all particles except those which mirror very near the magnetic equator. Since when $s_m \gg s_c$ the particle will experience a great number of sign reversals of the field during one bounce period, the power in these disturbances in the particle's frame of reference will appear at frequencies much higher than the bounce frequency. Such disturbances may therefore be orders of magnitude less effective in producing bounce resonance scattering than the formulas of this section would predict with $\mathscr{E}_{\parallel}(f)$ and $\mathscr{B}_{\parallel}(f)$ naively taken to be the power spectral density observed at one point in space.

If the situation described in the preceding paragraph is a good description of the

actual situation for trapped electrons in the magnetosphere, then the importance of bounce-resonance scattering will decrease with s_m, the distance of the electron's mirror point from the magnetic equator. On the other hand, whistler-mode scattering, described in Section 2 of this paper, will be effective for electrons mirroring off the magnetic equator. The true importance of bounce-resonance scattering may then be as a feeder mechanism for whistler mode scattering. Electron loss could then be accounted for by a combination of the two processes producing pitch-angle diffusion into the loss cone. Figure 7 shows how this would work. If an electron suffered only bounce-resonance scattering, then it would maintain a constant equatorial perpendicular energy, $W_{\perp 0}$, and it would diffuse along a line parallel to the dashed line in Figure 7 labeled 'Pure Bounce Diffusion'. If whistler-mode scattering were all that occurred, the electron's total energy would remain approximately constant, and diffusion would be along a line parallel to the dashed line labeled 'Constant Energy Line'. With bounce resonance dominating the scattering for near-equatorial mirroring electrons and whistler mode scattering dominating elsewhere, diffusion into the loss cone would be along a path similar to that labeled, 'Electron Diffusion Line' in Figure 7.

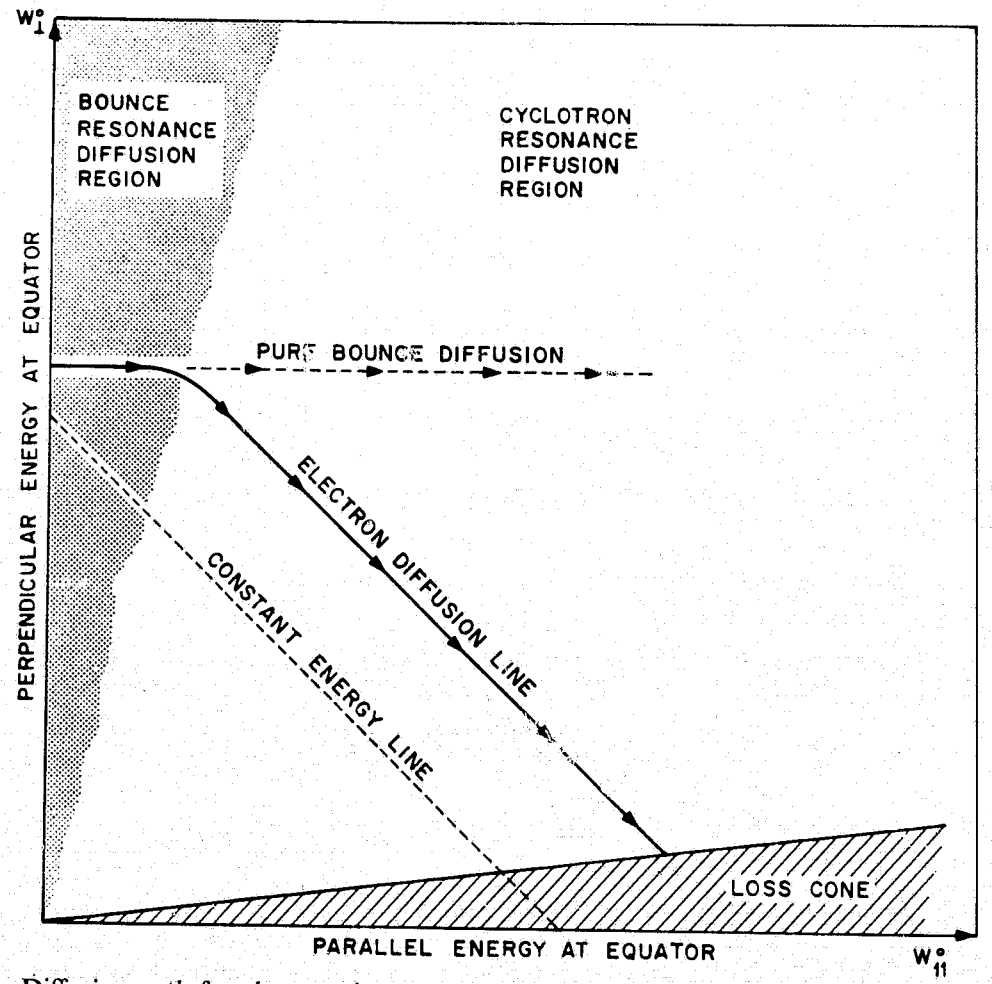

Fig. 7. Diffusion path for electrons into the loss cone due to a combination of bounce-resonance and cyclotron-resonance scattering. Bounce resonance is dominant when the electron mirrors near the magnetic equator; cyclotron resonance is dominant elsewhere.

4. Conclusions

Both cyclotron-resonance scattering due to whistler-mode disturbances and bounce-resonance scattering due to ion-acoustic or compressional Alfvén-mode disturbances are likely to be important in producing loss of radiation zone electrons through pitch-angle diffusion into the loss cone. The relative importance of the two mechanisms and the ability of either to account for the observed electron decay rates depends upon the power-spectral-density of the magnetic and electric fields in the scattering disturbances. Both mechanisms operate effectively with wide-band disturbances, the power at the applicable resonance frequency being selected out in either case.

In the whistler-mode mechanism, the exact frequency needed to resonate with an electron depends upon the electron's local pitch angle and energy and on the position in the magnetosphere where the interaction occurs. Therefore, to produce a rather uniform scattering of relativistic electrons having a wide range of energies and pitch angles requires whistler-mode disturbances with rather uniform power over a broad frequency range. The average power-spectral-density for the fluctuating magnetic field in the whistler-mode disturbances must be of the order of $10^{-10}\ \gamma^2/\text{Hz}$ to account for an observed electron lifetime of approximately 10 days. This corresponds to r.m.s. field fluctuations with magnitudes of the order of milligammas. If the average power-spectral-density function of the whistler-mode disturbances in the equatorial region is not broad-band up to approximately 0.5–0.6 of the equatorial electron gyrofrequency, then this mechanism will have difficulty in accounting for the scattering of relativistic electrons with nearly 90° equatorial pitch angles. Sufficient data have not yet been published on whistler-mode signals observed near the magnetic equator to allow a definitive statement to be made about the importance of cyclotron resonance scattering in accounting for electron pitch-angle scattering. Measurements made over a limited frequency range at high latitudes on the relevant lines of force (GURNETT, 1968) indicate that this mechanism is at least an important one for electrons with high-latitude mirror points.

In the bounce-resonance scattering mechanism, fluctuating electric or magnetic fields having components parallel to the earth's magnetic field alter the equatorial parallel energy and consequently the second adiabatic invariant J of the particle. The particle's equatorial perpendicular energy, and therefore its magnetic moment M, remain unchanged in this mechanism. A change in J with M constant means that the particle's equatorial pitch angle must change, and so this mechanism can contribute to particle loss via pitch-angle diffusion into the loss cone. The rate of scattering is proportional to the value at the particle's bounce frequency of the power-spectral-density of the fluctuating fields as seen in the frame of reference of the bouncing particle.

For radiation-zone electrons the bounce frequency is in the 1–10 Hz region. If parallel electric-field fluctuations in this frequency range are present, then power spectral densities of 10^{-4}–$10^{-5}\ (\text{V/km})^2/\text{Hz}$ are sufficient to make bounce-resonance scattering an important contributor to pitch-angle diffusion having approximately a

10-day lifetime. The r.m.s. parallel electric-field fluctuations for such disturbances would be of the order of 0.01–0.1 V/km. While no measurements of parallel electric-field fluctuations in the magnetosphere are presently available, several authors have given arguments for their existence (CHAMBERLAIN, 1963; BOSTRÖM, 1967). From knowledge of ionospheric current systems and also from direct measurements with plasma clouds (HAERENDEL *et al.*, 1967) it is known that perpendicular electric fields of the order of several V/km do exist in the magnetosphere.

Bounce-resonance scattering can also be important for relativistic electrons due to small fluctuations in the local magnetic-field intensity. Such fluctuations would be produced by small-amplitude compressional Alfvén waves propagating in directions other than exactly parallel to the earth's field. This interaction operates through what may be termed Fermi acceleration, and PARKER (1961) has considered a version of this mechanism which does not emphasize its resonant nature at the bounce frequency. If $\mathscr{B}_{\|}(f_0)$ is the power-spectral density at the bounce frequency of the magnetic-intensity fluctuations observed in the electron's frame of reference, then $\mathscr{B}_{\|}(f_0)/B_0^2 \approx 10^{-10}$–$10^{-11}$/Hz is sufficient to contribute to the pitch-angle diffusion of relativistic electrons having lifetimes of approximately 10 days. Here B_0 is the magnitude of the earth's field at the equator of the line of force of interest. Such disturbances need contain r.m.s. field fluctuations of the order of only 10^{-4}–10^{-5} of B_0. Preliminary studies (HOLZER *et al.*, 1966) of experimental data on magnetic-field fluctuations in the magnetosphere indicate that the power spectral density in the 1–10 Hz region is large enough to be important for bounce-resonance scattering of trapped relativistic electrons.

In bounce-resonance scattering by either parallel electric- or magnetic-field fluctuations, the strength of the mechanism is proportional to the value at the bounce frequency of the fluctuation power-spectral-density function in the frame of reference of the bouncing particle. If the disturbances producing the scattering have many spatial variations in the distance from the magnetic equator to the particle's mirror point, then the power spectral density in the particle's frame of reference may be very different from the power-spectral density at one point in space. This effect tends to make the importance of bounce-resonance scattering diminish rapidly as the particle's mirror point moves away from the magnetic equator. For relativistic electrons, this could mean that the main importance of bounce-resonance scattering is to move electron mirror points sufficiently far off the magnetic equator that cyclotron-resonance scattering by whistler-mode disturbances can operate effectively on them.

While this paper has examined two of the possible wave-particle interactions that may be important for trapped particles in the magnetosphere, there remains a multitude of other possible mechanisms which may or may not be important. Some of these have been considered elsewhere, e.g., the scattering of radiation zone electrons by electron plasma oscillations (EVIATAR, 1966). Others perhaps destined to emerge in the near future may be presently tucked away in the subconscious realm of assorted theorists. Better and more extensive experimental measurements of the electric- and magnetic-field fluctuations which actually occur in the magnetosphere are necessary in order to

permit definitive evaluations to be made on the importance of present-day and future mechanisms.

Appendix: Bandwidth for Resonant Interaction with Whistler-Mode Disturbances

If an electron interacts with a whistler-mode disturbance for only a finite length of time, then effective cyclotron resonance may be accomplished not only by the exact resonant frequency, ω_0, but by a band of frequencies of width $\Delta\omega$. To see how this comes about and to evaluate $\Delta\omega$ we remember that when an electron interacts with a single whistler component propagating parallel to the earth's field, the force on the electron at any time is proportional to $\cos\Phi(\omega)$ and/or $\sin\Phi(\omega)$, where

$$\Phi(\omega) = [\omega + v_{\|}k(\omega) - \Omega]t. \tag{40}$$

Since ω_0 is the exact resonance frequency, $\Phi(\omega_0)=0$ by the resonance condition, Equation (1). To evaluate $\Phi(\omega)$ for a frequency $\omega_0 \pm \frac{1}{2}\Delta\omega$ close to ω_0, we can expand $k(\omega)$

$$k(\omega_0 \pm \tfrac{1}{2}\Delta\omega) = k(\omega_0) \pm \tfrac{1}{2}\Delta\omega(\mathrm{d}k/\mathrm{d}\omega), \tag{41}$$

where the derivative $(\mathrm{d}k/\mathrm{d}\omega)$ is evaluated at ω_0. Since $\mathrm{d}\omega/\mathrm{d}k$ is the whistler-mode group velocity, $v_g(\omega)$, we may write

$$\Phi(\omega_0 \pm \tfrac{1}{2}\Delta\omega) = \pm\tfrac{1}{2}\Delta\omega[1 + v_{\|}/v_g(\omega_0)]t. \tag{42}$$

Until $|\Phi(\omega)|$ becomes larger than some critical value, the effects of the electron-wave interaction must be the same for a wave at the exact resonance frequency ω_0 as for a wave at some frequency very close to ω_0. A more sophisticated analysis reveals that this critical value is π, so that setting

$$\tfrac{1}{2}\Delta\omega[1 + v_{\|}/v_g(\omega_0)]\, t = \pi \tag{43}$$

gives us the bandwidth of the resonance after time t. Since $\omega = 2\pi f$, one finds

$$\Delta f = \Delta\omega/2\pi = \frac{1}{t(1 + v_{\|}/v_g)}. \tag{44}$$

Acknowledgments

The work in this paper on bounce-resonance scattering was done in collaboration with Dr. M. Schulz. The author would like to thank Dr. S. J. Buchsbaum for pointing out the importance of the term $-M(\partial b_{\|}/\partial s)$ in Equation (16).

REFERENCES

Boström, R.: 1967, Aurora and Airglow (ed. by B. M. McCormac), Reinhold Publishing Corp., New York, p. 293.

Brown, W. L.: 1966, in Radiation Trapped in the Earth's Magnetic Field (ed. by B. M. McCormac), D. Reidel Publishing Co., Dordrecht, Holland, p. 610.

Chamberlain, J. W.: 1963, "Plasma Instability as a Mechanism for Auroral Bombardment," J. Geophys. Res. 68, 5667.

Chang, D. B. and Pearlstein, L. D.: 1965, "On the Effect of Resonant Magnetic-Moment Violation on Trapped Particles," J. Geophys. Res.,70, 3075.

Cornwall, J. M.: 1964, "Scattering of Energetic Trapped Electrons by Very-Low-Frequency Waves," J. Geophys. Res.,69, 1251.

Cornwall, J. M.: 1966, "Micropulsations and the Outer Radiation Zone," J. Geophys. Res. 71, 2185.

Dungey, J. W.: 1963, "Loss of Van Allen Electrons Due to Whistlers," Planetary Space Sci. 11, 591.

Dungey, J. W.: 1964, "Effects of Electromagnetic Perturbations on Particles Trapped in the Radiation Belts," Space Sci. Rev. 4, 199.

Eviatar, A.: 1966, "The Role of Electrostatic Plasma Oscillations in Electron Scattering in the Earth's Outer Magnetosphere," J. Geophys. Res. 71, 2715.

Fälthammer, C. G.: 1965, "Effects of Time-Dependent Electric Fields on Geomagnetically Trapped Radiation," J. Geophys. Res. 70, 2503.

Fälthammer, C. G.: 1966, "On the Transport of Trapped Particles in the Outer Magnetosphere," J. Geophys. Res. 71, 1487.

Gurnett, D. A.: 1968, in Earth's Particles and Fields (ed. by B. M. McCormac), Reinhold Publishing Corp., New York, p. 337.

Haerendel, G., Lüst, R., and Rieger, E.: 1967, "Ionospheric Electric Fields at Midlatitudes during Twilight," Trans. AGU 48, 66.

Holzer, R. E., McLeod, M. G., and Smith, E. J.: 1966, "Preliminary Results from the Ogo 1 Search Coil Magnetometer: Boundary Positions and Magnetic Noise Spectra," J. Geophys. Res. 71, 1481.

Kennel, C. F. and Petschek, H. E.: 1966 "Limit on Stably Trapped Particle Fluxes," J. Geophys. Res. 71, 1.

MacDonald, W. M. and Walt, M.: 1961, "Distribution Functions of Magnetically Confined Electrons in a Scattering Atmosphere," Ann. Phys. (N. Y.) 15, 44.

McIlwain, C. E.: 1966, in Radiation Trapped in the Earth's Magnetic Field (ed. by B. M. McCormac), D. Reidel Publishing Co., Dordrecht, Holland, p. 593.

McIlwain, C. E.: "Processes acting upon outer zone electrons, 1, Adiabatic perturbations" (preprint), UCSD-SP-66-5, Physics Department, University of California, San Diego, 1966b.

Middleton, D.: 1960, Introduction to Statistical Communication Theory, McGraw-Hill Book Co., New York.

Northrop, T. G.: 1963, The Adiabatic Motion of Charged Particles, Interscience Publishers, New York, p. 9.

Parker, E. N.: 1961, "Effect of Hydromagnetic Waves in a Dipole Field on the Longitudinal Invariant," J. Geophys. Res. 66, 693.

Roberts, C. S. and Buchsbaum, S. J.: 1964, "Motion of a Charged Particle in a Constant Magnetic Field and a Transverse Electromagnetic Wave Propagating along the Field," Phys. Rev. 135, A381.

Roberts, C. S.: 1966, in Radiation Trapped in the Earth's Magnetic Field (ed. by B. M. McCormac), D. Reidel Publishing Co., Dordrecht, Holland, p. 403.

Van Allen, J. A.: 1966, in Radiation Trapped in the Earth's Magnetic Field (ed. by B. M. McCormac), D. Reidel Publishing Co., Dordrecht, Holland, p. 575.

Walt, M. and MacDonald, W. M.: 1964, "The Influence of the Earth's Atmosphere on Geometrically Trapped Particles," Rev. Geophys. 2, 543.

Wentworth, R. C.: 1963, "Pitch Angle Diffusion in a Magnetic Mirror Geometry," Phys. Fluids 6, 431.

West, H. I.: 1966, in Radiation Trapped in the Earth's Magnetic Field (ed. by B. M. McCormac), D. Reidel Publishing Co., Dordrecht, Holland, p. 634.

CHAPTER 6

Acceleration of Trapped Particles during a Magnetic Storm on April 18, 1965

W. L. BROWN,[1] L. J. CAHILL,[2] L. R. DAVIS,[3] C. E. MCILWAIN,[4] AND C. S. ROBERTS[1]

This paper describes a polar substorm-particle event observed with the magnetic field and trapped particle detectors on Explorer 26 during the worldwide magnetic storm of April 17–18, 1965. The event occurred between 0600 and 0830 UT on April 18 within the main phase of the magnetic storm. During this time the satellite was near apogee ($L \simeq 5$) and at a local time of ~1300 hours. Nearly coincident with the polar substorm, the satellite records show that the local magnetic field decreased by about 40 γ, while the proton flux (100–345 kev) increased by more than a factor of 10. About twenty minutes later the electron flux (10–1000 kev) started to increase. Both the field and particles show large fluctuations that are inveresly correlated. Some of the possible explanations of the event and the limitations imposed by the observations are discussed.

INTRODUCTION

The magnetosphere is a complex dynamic system. Energetic particles are trapped on the framework provided by the geomagnetic field. The field is subjected to compressional stresses by the solar wind pushing on its outer boundary as well as to internal stresses due to plasma within. Fluctuations in the solar wind, or in the interplanetary magnetic field it carries, cause magnetic fluctuations within the magnetosphere, changes in the fluxes of energetic trapped particles, and changes in the energy density of the lower energy particles of the plasma. The most spectacular changes occur during great magnetic storms when large, abrupt increases in energetic particle flux, auroral displays, and violent polar substorms give evidence of dynamic processes occurring in the outer or auroral regions of the magnetosphere. This is also the time when the inner magnetosphere is inflated by the lower energy 'ring current' particles. It is apparent that the polar substorms play a key role in the physics of magnetic storms and of particle acceleration. The present paper is an account of a polar substorm-particle acceleration event that took place in an interval of a few hours during the great magnetic storm of April 17–18, 1965.

Acceleration of energetic particles during magnetically disturbed periods has been noted earlier [*Frank,* 1965]. A preliminary account of this April 1965 event has been reported by *Davis and Williamson* [1966]. The effects of the magnetosphere inflation on high-energy protons in the inner belt during the April storm have been discussed by *McIlwain* [1966*b*], and a description of the inflation has been presented by *Cahill* [1966]. Recent reviews have outlined the general status of studies of the magnetosphere and of several theories that have been proposed to account for some of the magnetosphere phenomena [*Hess,* 1962; *Parker,* 1962; *Akasofu,* 1963; *Dungey,* 1965; *Cole,* 1966].

The Explorer 26 scientific payload and its orbit are well-suited to the studies of the inner magnetosphere. Listed in Table 1 is the complement of energetic particle detectors and magnetic field sensors that are considered in this paper. The orbit lies close to the equatorial plane, and the satellite is between 2 and 5 R_E for 80% of the time. Orbital parameters are listed in Table 2.

The interval to be discussed in this paper (0600–0830 UT, April 18) was within the main phase of a magnetic storm that commenced on April 17. A large polar substorm producing worldwide magnetic disturbance was in progress during this interval. Figure 1 summarizes geophysical parameters of interest during a 10-day

[1] Bell Telephone Laboratories, Murray Hill, New Jersey 07971.
[2] University of New Hampshire, Durham, New Hampshire 03824.
[3] Goddard Space Flight Center, Greenbelt, Maryland 20771.
[4] University of California at San Diego, La Jolla, California 90237.

TABLE 1. Explorer 26 Experiments

Organization	Instrument	Range of Operation
GSFC	Ion-electron detector	Protons of energies from 100 kev to 10 Mev, in eight levels and energy flux of 10–100 kev electrons.
UCSD	Directional electron detectors	Electrons of energies greater than 0.5 Mev and greater than 0.9 Mev.
BTL	Electron detectors	Electrons of energies greater than 0.3 Mev to greater than 3.7 Mev in six detectors. Two of these give both directional and spin-averaged flux.
UNH	Two-axis fluxgate magnetometer	Sensors parallel to and perpendicular to the satellite spin axis. ±2000 γ range for each sensor.

TABLE 2. Orbital Parameters

Apogee	5.11 R_E
Perigee	1.05 R_E
Inclination	20.1°
Period	7 hr. 36 min.
Local time of apogee, April 18	1400
Latitude of apogee, April 18	+17°

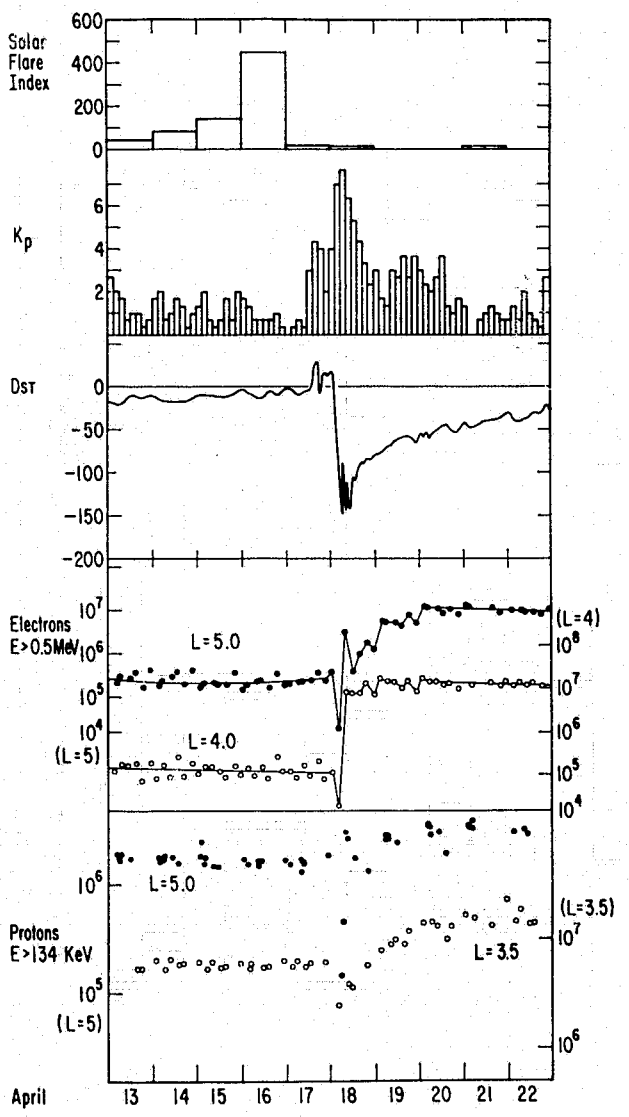

Fig. 1. Record of ground-level and satellite observations for ten days, including substorm on April 18, 1965. The solar flare index was obtained from the High Altitude Observatory, and Space Disturbance Forecast Center, Boulder, Colorado; the *Kp* index from *Lincoln* [1966]; *Dst* (in gammas) was computed using Honolulu and San Juan records provided by the U.S. Department of Commerce, Environmental Science Services Administration. The electron fluxes ($E > 0.5$ Mev at $L = 5$ and $L = 4$ in particles/cm² sec) were obtained from the UCSD detectors, and the proton fluxes ($E > 134$ kev at $L = 5$ and $L = 3.5$ in particles/cm² sec ster) were obtained from the GSFC detectors.

period that includes the event. Typical examples of particle flux observations near 5 R_E during the same 10-day period are also shown for comparison with the results to be presented in the next section.

Results

The principal features of the event are shown in Figure 2. First evidence of the storm, at 0612 UT, was an increase in the flux of protons (energy >134 kev and pitch angle, α, 27.5°). These particles were an order of magnitude lower in flux than the high pitch-angle particles, $\alpha = 87.5°$, before 0610 UT. By 0618 the two fluxes were equal, and an increase in the high pitch-angle particles became apparent. The high pitch-angle flux may have also increased before 0618, but an increase equal to that observed for the low pitch-angle particles would be obscured by the higher initial level of the particles at $\alpha = 87.5°$. By 0625 UT the proton flux at all pitch angles had leveled off. Fluxes

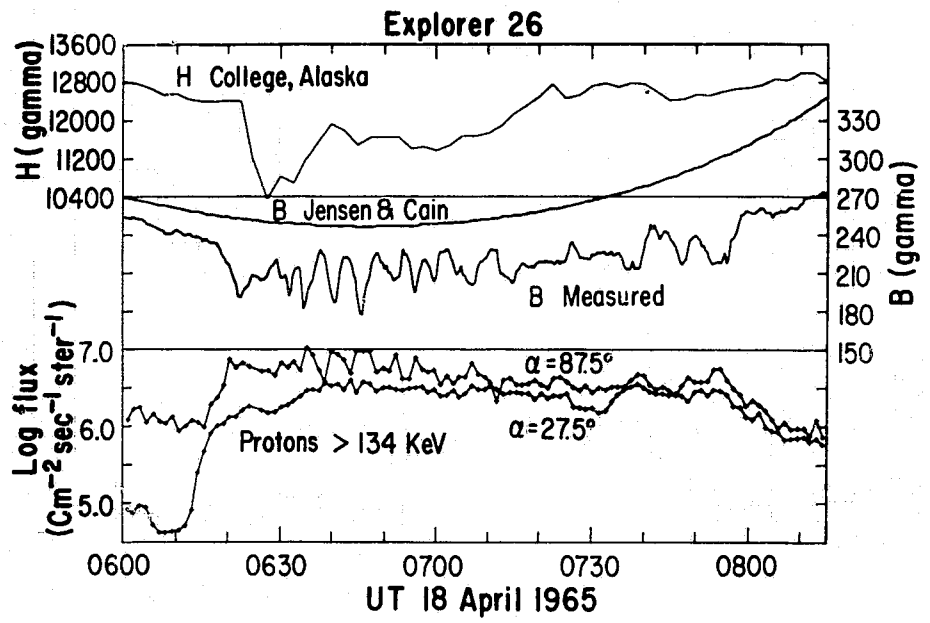

Fig. 2*a*. The College *H* magnetogram is plotted in gammas, and the predicted [*Jensen and Cain*, 1962] and measured field at the satellite are shown in gammas. The proton fluxes (protons/cm² sec ster) are plotted as the logarithm of flux at two pitch angles, 87.5° and 27.5°.

of protons with energies greater than 98 kev and those greater than 180 kev, not shown, also increased between 0612 and 0622 UT. No increase in protons of energies above 345 kev and above 513 kev was seen until 0625 UT [*Davis and Williamson*, 1966]. Coincident with the rise in proton flux ($E > 134$ kev, $\alpha = 87.5°$), the magnetic field magnitude at the satellite, already depressed 20 γ below the predicted value, began a further 40-γ decrease.

The College, Alaska, magnetogram, at the top of Figure 2, shows a large, 2200-γ, negative bay decrease in *H* beginning at 0622 UT. College was in the evening quadrant at this time, while

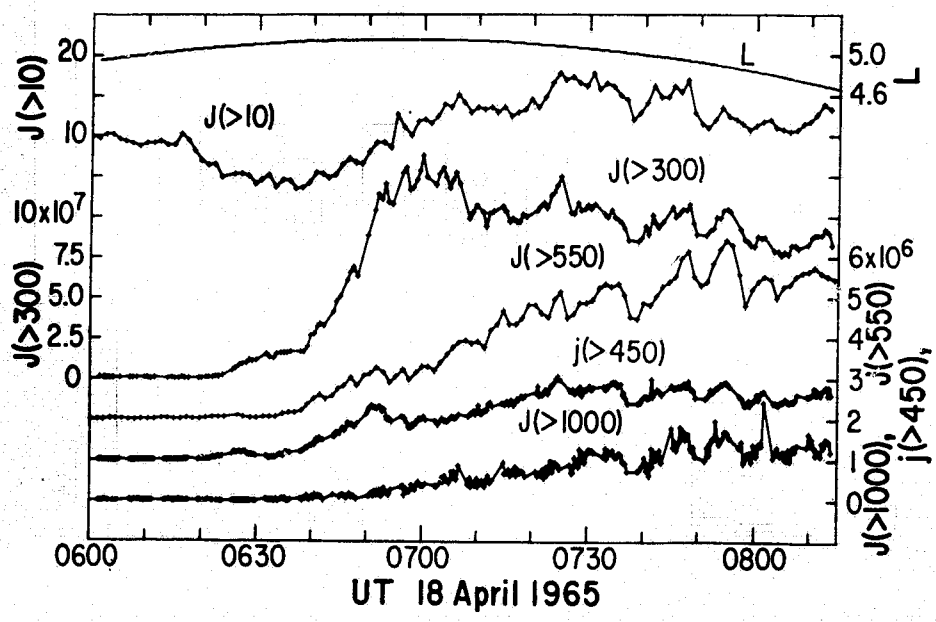

Fig. 2*b*. The *L* value of the satellite at the time of the measurements is shown at top (scale at right). Omnidirectional electron fluxes for energies > 550 kev and > 1000 kev are shown, with linear scale on right in particles/cm² sec. Directional flux for electrons of energy > 450 kev is shown in particles/cm² sec ster, using scale on right. Omnidirectional flux of electrons, energy > 300 kev, is shown in particles/cm² sec with scale at left, and the omnidirectional flux of electrons of energy > 10 kev is shown at top left with an arbitrary linear scale.

the satellite was near 1400 local time. The event was seen, in some form, at all auroral stations, but there was a wide spread, 0610–0630 UT, in onset times. The event was worldwide, and evidence of the disturbance was seen at magnetic observatories as close to the equator as Honolulu and Guam. The College record was unique only in the magnitude of the bay; apparently, College was close to an auroral electrojet at this time. Less intense magnetic activity in the auroral zone commenced as early as 0100 UT, April 18, as the magnetic storm main phase started to develop.

The high-energy electrons, $E > 300$ kev, rise above background after 0625 UT. Lower energy electrons, $E > 10$ kev, start to decrease as the proton fluxes increase. The low-energy electrons had displayed an increase in flux at 0440 UT, when the satellite was near $L = 3.7$. The low-energy electron fluxes are slowly rising by 0640 UT, however, and continue to rise until 0730 when the electron energy spectrum is much flatter than before the event [*Davis and Williamson,* 1966].

The fluctuations in particle flux and field magnitude are of interest. The most striking correlation is between the field magnitude and the low-energy ($E > 134$ kev, $\alpha = 87.5°$) protons. In general, whenever the proton flux rises, the field magnitude drops. A particularly clear example is seen from 0633 to 0650 UT, when there are three large positive pulses in proton flux and three corresponding decreases in field magnitude. The period of these fluctuations is approximately 300 seconds. Thereafter, the field magnitude usually goes down when the proton flux goes up, but the pulses are smaller and the time correlation less convincing. The largest fluctuations in the high-energy electron flux are between 0700 and 0800 UT. At the beginning of this interval the 300-kev fluctuations show correlation with the field magnitude changes, and between 0740 and 0800 there are several large pulsations in electron flux, for all energies shown, that correspond to decreases in field magnitude.

After 0800 UT the polar substorm subsides and the magnetic field observed at the satellite shows less fluctuation (but continues to drop further below the predicted field as the inbound satellite goes deeper into the magnetosphere). The low-energy proton flux decreases slowly, but the high-energy electrons continue to rise, reaching a peak at 0900 UT, when the satellite is near $L = 4$ (*McIlwain,* 1966*a*]. Their flux drops abruptly between $L = 3.5$ and $L = 2$.

Discussion

1. *Adiabatic changes.* The long-term changes in particle flux that are apparent in Figure 1 will be discussed first. The proton and electron fluxes shown there and those of particles of other energies, not shown, were steady in the region $L = 2$ to $L = 6$ until April 18. For most particles, a decrease by a factor of 3–10 was noted in the early hours of April 18, but the flux of 10- to 100-kev electrons showed an increase. During this time the magnetic storm main phase was developing; the surface field was depressed by 50–100 γ over much of the earth [*Cahill,* 1966]. *McIlwain* [1966*b*] has shown that an adiabatic (for all three invariants) decrease in flux occurred for 40- to 110-Mev protons at $L < 2.4$, as the main phase of the storm developed and the geomagnetic field decreased. This decrease was followed by a slow recovery to prestorm levels as the ring current decayed and the geomagnetic field returned to an unstressed condition. Some of the particles described here have much longer drift times (1.3 hours for 100-kev particles) than the 40- to 110-Mev protons. The main-phase field depression developed during a several-hour period, however, and an adiabatic decrease and recovery of particle flux is expected for all particles below $L = 5$ (except low-energy particles with drift period of several hours).

The initial adiabatic decrease expected is apparent in Figure 1. Also discernible is a slow recovery (except for the electrons at $L = 4$). The recovery proceeds *above* the prestorm flux to levels 50–100 times greater for the 0.5-Mev electrons and a factor of 2 higher for the 134-kev protons. High-energy protons ($E > 345$ kev) did not recover to prestorm values but remained depressed for at least ten days. Superimposed on the slow recovery, there is also a brief, temporary increase in protons and electrons at $L = 5$, one of the main topics of this paper.

2. *Nonadiabatic changes.* The recovery of most particles, at $L = 3$ to $L = 5$, to a higher flux level (not seen in the 40- to 110-Mev pro-

tons below $L = 2.4$) cannot be explained as due to adiabatic changes caused by the ring current. Also, the high-energy protons ($E > 345$ kev), although depressed, regain a lower than prestorm level as the ring decays. It appears that the event 0600–0800 UT, April 18, is an example of nonadiabatic acceleration processes with some particles enhanced and others depleted. It is also a period of a large polar substorm, widespread auroral displays, and rapid growth of asymmetric inflation of the inner magnetosphere. Thus attention is focused on this brief interval as being of vital importance in the dynamics of the magnetosphere.

Not all the available data are presented in Figure 2, but the significant features are adequately described. Although the satellite was in a very advantageous position between $L = 4.5$ and $L = 5$ during this event, only a small segment of the $L = 5$ shell came under direct observation as the satellite traveled in local time from 1300 to 1445. This magnetic storm, as apparent on both ground and satellite records, was decidedly asymmetrical with the greatest magnetosphere inflation somewhere between 1500 and 2400 local time in the early main phase of the storm. Although worldwide, the auroral event that started near 0620 UT produced the greatest magnetic effects at College, Alaska (near the 1900 local time meridian at the start of the event). The satellite observations, therefore, are not necessarily due to an axially symmetric trapped particle shell at $L = 5$. The primary injection or acceleration processes may have been occurring to the east with the resulting increased particle fluxes, after some delay, drifting past the satellite. College lies close to the ground-level trace of the $L = 5$ shell of the undisturbed field so that the satellite was close to, but probably somewhat below, the L shell of the greatest auroral effects. In the following paragraphs we shall explore some possible explanations of the particle event and mention the limitations imposed by the observations.

3. *Protons.* The protons dominate the event as observed at the satellite. They appear first, the lowest energy protons ($E = 100$–200 kev) rising by an order of magnitude several minutes before the onset of the negative bay at College. The magnetic field at the satellite, already lower than in the previous orbit, starts decreasing further as the 100-kev protons (pitch angle 87.5°) rise above 2×10^6 cm^{-2} sec^{-1} ster^{-1}. *Davis* [1966] has noted that the diamagnetic field (not including drift and other ring current contributions) produced by the protons [$\Delta B = -(4\pi/B)\rho E$] is -20 γ at 0622 UT, half of the observed change in $|B|$. Extrapolation of the observed proton spectrum to 10 kev (with the same exponential decay factor determined at energies in the vicinity of 100 kev) predicts sufficient proton flux to produce all of the observed change in $|B|$.

A. Local acceleration. The protons may have been introduced from higher or lower L shells, or they may have been lower energy particles, already at $L = 5$, that were rapidly accelerated.

If the process was local acceleration at $L = 5$, we must inquire if lower energy particles sufficient to produce the observed fluxes existed before the event. We have no direct knowledge of protons below 98 kev in energy, but comparisons of higher energy particles are possible. Considering particles with 90° pitch angle, it appears that almost enough protons, $E > 98$ kev, existed before 0615 UT to produce the observed flux of protons, $E > 180$ kev, at 0625. The enhancement of low pitch-angle particles is twice as great, however, and in this case there are not sufficient 98-kev protons. For the high pitch-angle protons an increase in energy by a factor of 2 within a 5-minute period is required if the particles were locally accelerated at $L = 5$.

B. Radial drift. If the particles are introduced from other regions, we can speculate as to how this might have occurred. One possibility is that the protons have moved up from lower L shells by electric fields associated with the main phase or with the substorm, or by outward motion of field lines as the storm inflation proceeds. This possibility appears unlikely on consideration of the proton velocity distribution. Starting with the proton mapping just before the storm and assuming conservation of the first two adiabatic invariants, the proton velocity distributions may be calculated [*Nakada et al.*, 1965]. It appears that outward drift would produce a decrease in proton intensity at $L = 5$. If the proton distribution below the satellite has changed by 0600 UT because of the storm, then outward drift is still a possible cause, but

inward drift, from a higher L shell, remains more promising. We will discuss this possibility later.

C. Longitudinal drift. The protons may have been introduced in the evening quadrant and then drifted west to the satellite. In this case a difference in arrival times for particles of various energies is expected. *Konradi* [1967] has observed, at higher L values, impulsive increases in low-energy protons, with the highest energy particles arriving first. In the present event acceleration or introduction close to the satellite in longitude appears to be required because of the nearly simultaneous observation (within 1 minute) of high pitch-angle protons with energies from 98 to 180 kev. (Small pitch-angle fluxes from 98 to 345 kev rose together.) The drift periods are 80 minutes for 100-kev protons and 40 minutes for 200-kev protons. Considering only $\nabla|B|$ drift, the particles must have been introduced or accelerated together within 10° east of the satellite. The presence of electric fields would change the drift rates and, if strong enough, they could dominate the $\nabla|B|$ drift so that particles of 100- to 200-kev energies would drift together. The electric field required is greater than 15 mv/m, pointing radially outward.

If they are due to drifting clumps of protons, an even more stringent limitation is associated with the pulsations in high pitch-angle protons that commence at 0633 UT. Protons from 100 to 500 kev arrive within 2 minutes. Either we are observing local injection or acceleration of these protons, or they have been introduced elsewhere, at $L = 5$, and moved to the satellite by means other than $\nabla|B|$ drift. A radially outward electric field seems plausible and is also consistent with the negative bay at College and Sitka (for electrojet current there controlled by Hall conductivity and by northward electric field).

D. Field fluctuations. The fluctuating decreases in field magnitude might be accounted for by diamagnetism of the observed clumps of protons moving past the satellite (with a reasonable extrapolation to lower energies). There are also fluctuations in field direction, as much as 10°, and before the initial drop in field at 0620 UT, there is an increase in declination of the field. An increase in declination in the northern hemisphere might indicate that the field lines are being pushed ahead of plasma advancing from the east. As the magnitude drops, the inclination increases, indicating that the field lines are being stretched outward, inflated by the intruding charged particles.

4. Electrons. The increases in electron flux are all delayed, and the 10-kev electrons initially decrease as the protons rise. Such delay is in disagreement with the movement of all particles from the east by strong electric fields. If electrons were accelerated with the protons, they would drift west under the influence of sufficiently strong electric fields and arrive with the protons. Electrons from 10–550 kev have started to rise by 0640 UT. The simultaneous arrival of 98- and 180-kev protons and the delay from 0620 to 0650 UT, between the first peak in arrival of 100-kev protons and the first peak in 300-kev electrons, could be explained by proton and electron acceleration less than 10° east of the satellite, rapid proton arrival, and delay in electron arrival because of a 30-minute $\nabla|B|$ drift time around the earth. Unfortunately, peaks in arrival of 450- and 550-kev electrons can be observed at about the same time; they should occur earlier, corresponding to a more rapid drift for these particles.

It may be that the acceleration of the 300-kev electrons took place with the protons, and the higher energy electrons followed somewhat later. The flux of higher energy electrons ($E > 450$ kev) continues to increase from 0700 to 0800 UT, suggesting a continuing electron acceleration mechanism. After the three strong pulsations in magnetic field and proton flux between 0630 and 0650 UT, the correlation between proton and field fluctuations is less impressive. The field pulsations continue, somewhat lower in amplitude and with shorter periods, from 0650 to 0710 UT. In this interval the electrons of energy greater than 300 kev exhibit pulsations of the same type as the protons in the preceding interval. When the electron flux increases, $|B|$ decreases. At this time the electron flux ($E > 300$ kev) has increased above 10^8 particles cm^{-2} sec^{-1}, but the observed electron energy density is still not sufficient to produce a significant portion of the field decrease. Again, between 0740 and 0800 UT, there are large field pulsations, and this time even the electrons J (>1000 kev) show related large fluctuations.

5. HM waves. We have attempted to explain the related particle and field fluctuations in terms of diamagnetic field depression by drifting clumps of protons or electrons. Waves propagating along the field lines in the acoustic mode also show this inverse relation between particle flux and field fluctuation [*MacDonald*, 1961; *Judge and Coleman*, 1962]. Both proton and electron increases would accompany field decreases. These pulsations might be evidence of a resonant oscillation, a standing P wave of the type described by MacDonald. Although he estimates the periods of such waves as many hours, it may be that, during such a violent substorm, physical properties of the magnetosphere are altered enough to shorten the period considerably.

Even if the fluctuations are not caused by hydromagnetic wave propagation past the satellite, they should be a source of HM waves with pulsations of field magnitude and direction propagating in various HM modes away from the source. A wave propagating along the field line, in the Alfvén or the acoustic mode, at $L = 5$ (approximately 1400 local time and 0700 UT) should reach the earth in northern Russia with little geometric or ionospheric attenuation. At Yakutsk, the closest observatory for which we have data, a 200-gamma positive bay in H starts abruptly at 0635 and recovers at 0710 UT. Within this bay there are three irregular pulsations of magnitude 30–40 γ, but they do not correspond in period or phase to those seen in the satellite record. The Yakutsk records and those of other high-latitude stations frequently register 10- to 20-γ pulsations with periods of 3–6 minutes.

6. Convection. We have discarded the possibility of particle movement from lower levels of the magnetosphere; movement of particles from higher levels must be considered. The convection models of *Dungey* [1961] and of *Axford and Hines* [1961] describe motion of low-energy plasma from the geomagnetic tail to the outer layers of the inner magnetosphere. As they move inward to regions of higher field intensity, the convected particles are energized, and, assuming a tail-field strength of 20 gammas, they could gain a factor of 10 in energy in moving to $L = 5$ where the field is 200 γ. The main convection pattern carries particles up the tail near the midnight meridian and around the earth on the dawn side. More energetic particles may escape the convective flow by $\nabla|B|$ drift as they move into regions of stronger field, protons drifting west and electrons east. The main-phase depression, developing since 0200 UT, could be due to this convection process, with protons and electrons of lower energy carried deeper into the magnetosphere. The observed particles might be the high-energy tail of the spectrum of convected, and energized, particles.

The sudden increase in protons and several other factors of the particle event appear not to fit this hypothesis. If the observed particles were part of the gradual inflation that began near 0200 UT, then a gradual increase in flux would be expected as the satellite moved to higher L values. However, increases in the polar-cap current system, as observed near 0620 UT, are often interpreted as evidence of enhancement of the magnetosphere convection pattern. A sudden increase in particle flux might be expected in this case. Proton drift west and electron drift east from the midnight meridian to the satellite would be indicated. Still present are many of the problems discussed previously: simultaneous arrival of protons with a range of energies, late arrival of high-energy electrons, simultaneous peaks in proton and electron flux. None of these features would result from $\nabla|B|$ drift of particles from the midnight meridian. It appears to us that a single, simple mechanism cannot explain all of the features of this complex event.

A final speculation is offered to resolve some of the conflicts mentioned above. Convection of particles into the inner magnetosphere is responsible for the main phase inflation. Beginning at 0200 UT low-energy particles ($E < 100$ kev) have been carried in to $L = 3$. The increase in low-energy (10–100 kev) electrons at 0440 UT ($L = 3.7$) is evidence of this convection and subsequent eastward electron drift. As Explorer 26 moved out to apogee, the low-energy protons were approaching from the east. These newly injected particles contained little or no measurable flux of energy greater than 100 kev at this time. At 0612 UT an instability (perhaps an interchange instability) developed in the drifting ring current particles [*Rosenbluth and Longmire*, 1957; *Sonnerup and Laird*, 1963]. The instability, or other effects related to it,

caused the substorm and also the acceleration of both protons and electrons, but since the satellite was on the western edge of the instability, the accelerated protons appeared at once, and the electrons ($E > 300$ kev) appeared after drifting eastward. Acceleration of higher energy electrons ($E > 450$ kev) is caused by a different mechanism and may be related to the pulsations that start after 0630 UT. Therefore, the fluxes of the higher energy electrons continue to grow from 0640 to 0750 UT. The fluctuations in particle flux and in magnetic field may have been due to oscillations in the instability. The event not only accelerated some of the newly injected protons but caused a loss of some that were present before the storm (the decrease of protons $E > 345$ kev suggests this).

Conclusions

Associated with the main and recovery phases of the magnetic storm of April 17–18, 1965, there is an adiabatic decrease and recovery of proton fluxes of energies 100–180 kev and of electrons of energies 300–500 kev in the region $L = 3$ to 5. Within this adiabatic event there is, in the interval 0600–0800 UT, a polar substorm, auroral event that coincides with a large, abrupt increase in fluxes of protons and electrons in most energy ranges observed. We identify this as an example of a nonadiabatic acceleration process that may be responsible for previously observed large increases in fluxes of outer-zone particles.

In any explanation of the event the following features must be considered:

1. Near simultaneous increase in protons of energies between 100 and 300 kev.
2. Delay before increase in 300-kev electrons.
3. Relation between increases in particle flux and decreases in field magnitude.
4. Close time relation between the magnetic bay at College, Alaska, and the particle and field event at the satellite.

The most plausible explanation, to us, is that the particles responsible for the main phase were convected into the magnetosphere and were energized in the process. The growth of the low-energy inflation caused adiabatic changes in particle flux ($E > 100$ kev). An instability due to the inflation was accompanied by a polar substorm and acceleration of particles, causing an increase in electrons and in protons of energies between 100 and 300 kev. Since the satellite was near the western edge of the event, the accelerated protons in the above energy range arrived together and almost immediately, while electrons near 300 kev in energy drifted east and arrived after a 30-minute delay. The higher energy electrons were accelerated, and the higher energy protons ($E > 345$ kev) were lost by other mechanisms. Early in the event the increased proton flux ($E > 100$ kev) contributed to a diamagnetic decrease in magnetic field strength. Later, related fluctuations in magnetic field and in both protons and electrons may be evidence of a hydromagnetic oscillation. The instability near the equator at $L = 5$ is reflected at the feet of the lines of force as a polar substorm.

Acknowledgments. This collaborative effort between Explorer 26 experimenters commenced with a meeting at the Space Science Laboratory, University of California at San Diego, and much of the assembly of data and writing of the report was done there.

The research was supported in part by NASA grant NsG-538 at UCSD, by NASA contract NAS 5-3058 at Bell Telephone Laboratories, and by NASA contract NASw-155 at UNH.

References

Akasofu, S. I., The main phase of magnetic storms and the ring current, *Space Sci. Rev., 2,* 91, 1963.

Axford, W. I., and C. O. Hines, A unifying theory of high latitude geophysical phenomena and geomagnetic storms, *Can. J. Phys., 39,* 1433, 1961.

Cahill, L. J., Inflation of the inner magnetosphere during a magnetic storm, *J. Geophys. Res., 71,* 4505, 1966.

Cole, K. D., Magnetic storms and associated phenomena, *Space Sci. Rev., 5,* 699, 1966.

Davis, L. R., Enhancement of trapped protons during the magnetic storm of April 18, 1965 (abstract), *Trans. Am. Geophys. Union, 47,* 426, 1966.

Davis, L. R., and J. M. Williamson, Outer zone protons, in *Proc. NATO Adv. Study Inst., Bergen, Norway, August, 1965, Radiation Trapped in the Earth's Magnetic Field,* edited by B. M. McCormac, D. Reidel Publishing Company, Dordrecht, Holland, 1966.

Dungey, J. W., Interplanetary magnetic field and the auroral zones, *Phys. Rev. Letters, 6,* 47, 1961.

Dungey, J. W., Effects of electromagnetic perturb-

ations on particles trapped in the radiation belts, *Space Sci. Rev., 4,* 199, 1965.

Frank, L. A., A survey of electrons $E > 40$ kev beyond 5 earth radii with Explorer 14, *J. Geophys. Res., 70,* 1593, 1965.

Hess, W. N., Energetic particles in the inner Van Allen belt, *Space Sci. Rev., 1,* 278, 1962.

Jensen, D. C., and J. C. Cain, An interim geomagnetic field (abstract), *J. Geophys. Res., 67,* 3568, 1962.

Judge, D. L., and P. J. Coleman, Observations of low-frequency hydromagnetic waves in the distant geomagnetic field: Explorer 6, *J. Geophys. Res., 67,* 5071, 1962.

Konradi, A., Proton events in the magnetosphere associated with magnetic bays, *J. Geophys. Res., 72,* 3829, 1967.

Lincoln, J. Virginia, Geomagnetic and solar data, *J. Geophys. Res., 71,* 2411, 1966.

MacDonald, G. J. F., Spectrum of hydromagnetic waves in the exosphere, *J. Geophys. Res., 66,* 3639, 1961.

McIlwain, C. E., Acceleration of outer-zone electrons (abstract), *Trans. Am. Geophys. Union, 47,* 131, 1966*a*.

McIlwain, C. E., Ring current effects on trapped particles, *J. Geophys. Res., 71,* 3623, 1966*b*.

Nakada, M. P., J. W. Dungey, and W. N. Hess, On the origin of outer-belt protons, 1, *J. Geophys. Res., 70,* 3529, 1965.

Parker, E. N., Dynamics of the geomagnetic storm, *Space Sci. Rev., 1,* 62, 1962.

Rosenbluth, M. N., and C. L. Longmire, Stability of plasmas confined by magnetic fields, *Ann. Phys., 1,* 120, 1957.

Sonnerup, B. U. O., and M. J. Laird, On the magnetospheric interchange instability, *J. Geophys. Res., 68,* 131, 1963.

CHAPTER 7

Comparison of the Electron Response in the Magnetosphere at $L = 5$ with the Solar Wind during the April 17–18, 1965, Magnetic Storm

L. J. LANZEROTTI

Bell Telephone Laboratories, Inc.
Murray Hill, New Jersey 07971

Recently published data by *Gosling et al.* [1967] show the temporal changes in the solar wind parameters during the large magnetic storm of April 17–18, 1965. Since the mechanism for the coupling of the solar wind energy to the particle population in the interior of the magnetosphere is of interest, we believe a qualitative comparison of the temporal behavior of the solar wind with the outer-belt electron response of the magnetosphere during this magnetic storm period is of value.

The Explorer 26 satellite was fortuitously located at its apogee of about 5 R_E during the initial period of large magnetospheric particle increases on April 18. The local time at apogee was 1340 hours. For the temporal comparisons of the magnetosphere before and during the storm, we will use the detector channel $E_5(E_e > 0.3$ Mev) in the Bell Laboratories experiment onboard Explorer 26. Data from this channel at the beginning of the storm have been discussed previously elsewhere [*Roberts and Brown,* 1966; *Vette and Lucero,* 1967].

The sun was very quiet before April 16 (day 106) on which day the solar flare index increased to a value of 450. The magnetic index K_p increased suddenly to 4 on April 17 (day 107) and further increased to 8^- during the early part of April 18. Figure 1 shows the 3-hour average magnetic index Kp for days 104–110, 1965. Also shown in the figure are the solar wind proton velocity and temperature for this period as reported by Gosling et al. from the Vela 2A Satellite. Shown at the top of the figure is the median counting rate in the BTL detector at $L = 5$ R_E.

From the figure it can be seen that after about 1200 hours on day 107, the Kp index increased suddenly with the onset of the sudden commencement of the magnetic storm (1312 UT, day 107). This increase in Kp is seen to correlate with the change in character of the solar wind velocity and temperature as observed on Vela 2A. The solar wind measurements indicate that the proton velocity and temperature reached a plateau around 2400 hours on day 107, at about the same time that Kp leveled off and dropped to 2.

Kp again increased on day 108 and reached its maximum value in the 3-hour interval between 0600 and 0900 hours. The solar wind proton parameters, however, were just beginning to show another increase in the 0900- to 1200-hour period. In both of these observed Kp increases, Kp reached its maximum value before the solar wind parameters reached their peak.

The outer-belt dayside Explorer 26 electrons ($E_e > 0.3$ Mev), as shown at the top of the figure, do not respond to either the changed solar wind conditions or the changed terrestrial magnetic field conditions as expressed by Kp until about 0630 on day 108. This is some 12 hours after the initial Kp increases and solar wind changes, during a calm solar wind period. The figure also shows that there was an order of magnitude depopulation of the $L = 5$ electrons observed at about 0600 hours on day 108 before the particle increase was seen. The satellite was at $L = 5$ at 0054 hours on day 108 on the previous orbit. The depopulation occurred between these two observation times during the morning hours.

The initial rapid particle increases at $L = 5$ were observed by Explorer 26. The counting rate of approximately 5×10^3 electrons/1.43 seconds at about 0630 on day 108 corresponds to the median initial increased electron flux as observed at $L = 5$ before the satellite began its transit into perigee.

The figure indicates that on the next orbit the $L = 5$ electron rate was observed to be only about 8×10^2 electrons/1.43 seconds. On successive passes the electron flux slowly increased

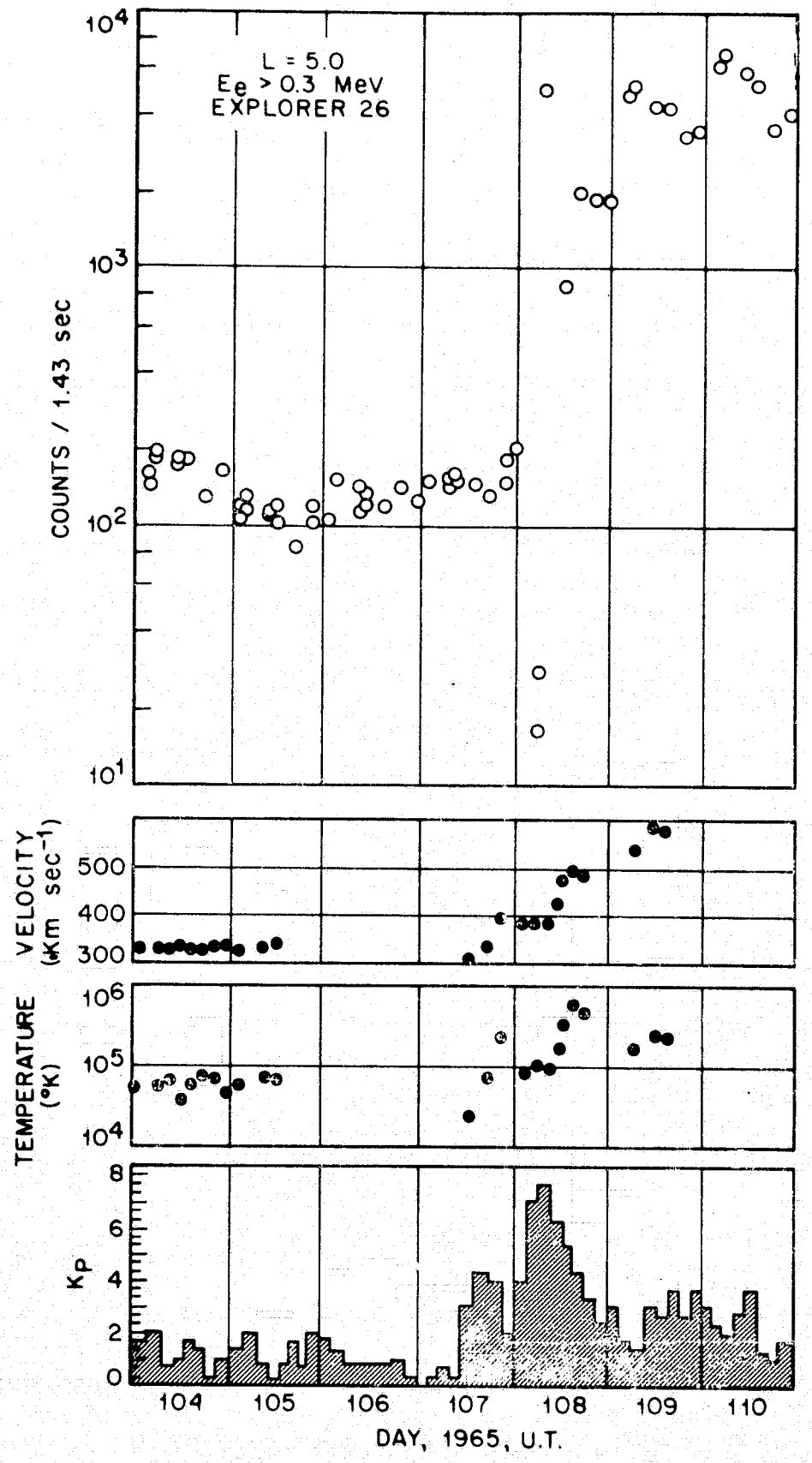

Fig. 1. Comparison of Explorer 26 electrons ($E_e > 0.3$ Mev) at $L = 5\ R_E$ with the solar wind temperature and velocity as observed by Vela 2A during the time interval from day 104 to day 110, 1965. The Vela 2A data is extracted from Figure 2 of *Gosling et al.* [1967].

to a maximum during day 109. The flux then began an approximate exponential decay lasting about one day. The flux again increased and began another decay during day 110.

The large electron flux changes that were observed during the April storm at $L = 5$ appear to have two separate features. First, the rapid electron increase observed at about 0630 occurred near the onset of an intense polar substorm. This particle increase and magnetospheric activity began some 12 hours after the initial solar wind changes and the magnetic storm's sudden commencement caused by the interaction of the solar wind with the magnetosphere. These electrons observed during the initial flux increase appear to have been lost within about 4 hours. Second, the slower flux increase during day 108 to the maximum on day 109 is typical of outer-belt electron increases during a magnetic storm. This type of flux increase has been termed a 'rapid nonadiabatic acceleration' by *McIlwain* [1966]. The 12-hour time delay between the solar-wind-induced sudden commencement and the magnetospheric electron response is strikingly different from the time response of the electron flux increases observed during the mangetic storm accompanying the solar proton event of February 5, 1965. The nonadiabatic acceleration of $L = 5$ electrons in that storm was observed to begin simultaneously with the sudden commencement [*Lanzerotti*, 1967].

Recent satellite measurements of the geomagnetic tail field have shown that there is a positive correlation of an increased tail field strength with *Kp* [*Behannon and Ness*, 1966]. The same work interprets positive correlations of the tail field strength with the worldwide horizontal component of the surface field as being due to a large-scale compression of the entire magnetosphere including the tail. Anticorrelation of the same two phenomena is interpreted as being due to an increased number of lines of force being carried into the tail by an enhanced plasma flow.

Low-latitude, earth-based magnetometers showed an increase in the H component of the field at the sudden commencement of the April 1965 storm [*Cahill*, 1966]. These observations correlate with the increase of *Kp* and suggest a compression of the magnetosphere by the solar wind plasma. During this initial compression stage no increase in the $L = 5$ electron flux was observed. The main phase decrease in field began during the early morning hours of day 108, the same time interval that the depopulation at $L = 5$ occurred. This depopulation could be interpreted as a loss of particles to the tail as they longitudinally drifted around the earth. *Williams* [1967] also observed this type of depopulation at $L = 5$ at high latitudes during this storm.

During the initial part of the main phase of the storm, the H component of the field indicates that more nightside field lines are drawn out to the tail region. The initial rapid increase in the $L = 5$ electron rate at 0630 could then occur while the nightside $L = 5$ field lines were drawn out to the tail. The rapid particle increase could then be due to a nonadiabatic particle injection process from the tail region. An injection process would be in contradistinction to the nonadiabatic acceleration process that acted upon the electron population for about a day during the storm main phase and the ring current development.

Axford et al. [1965] have discussed an interaction between the solar wind and the magnetotail, resulting in an energy storage in the magnetotail. The energy storage could take place during the compression of the magnetosphere. The $L = 5$ electron increases observed during this storm could then be due to a transfer of the energy from the tail to the interior of the magnetosphere, with a time constant of about 12 hours associated with the energy storage and transfer mechanism. Any theory for the coupling of the solar wind to the outer-belt magnetosphere particles must concern itself with the apparent 12-hour time delay between the solar wind changes and the $L = 5$ electron changes that were observed in this magnetic storm.

Acknowledgment. Many useful discussions with Dr. W. L. Brown are gratefully acknowledged.

References

Axford, W. I., H. E. Petschek, and G. L. Siscoe, Tail of the magnetosphere, *J. Geophys. Res., 70,* 1231, 1965.

Behannon, K. W., and N. F. Ness, Magnetic storms in the earth's magnetic tail, *J. Geophys. Res., 71,* 2327, 1966.

Cahill, L. J., Jr., Inflation of the magnetosphere during a magnetic storm, *J. Geophys. Res., 71,* 4505, 1966.

Gosling, J. T., J. R. Asbridge, S. J. Bame, A. J. Hundhausen, and I. B. Strong, Measurements of the interplanetary solar wind during the large geomagnetic storm of April 17–18, 1965, *J. Geophys. Res., 72,* 1813, 1967.

Lanzerotti, L. J., Outer zone electron fluxes during the February 5, 1965, solar proton event, *Ann. Geophys.,* to be published, 1968.

McIlwain, C. E., Processes acting upon outer zone electrons, 1, Adiabatic perturbations, paper presented at Interunion Symposium on Solar-Terrestrial Physics, Belgrade, Yugoslavia, September, 1966.

Roberts, C. S., and W. L. Brown, Observations of outer zone electrons on April 18, 1965, by the Explorer 26 satellite (abstract), *Trans. Am. Geophys. Union, 47,* 135, 1966.

Vette, J. I., and A. B. Lucero, Models of the trapped radiation environment, Vol. III: Electrons at synchronous altitude, *NASA SP-3024,* p. 78, 1967.

Williams, D. J., On the low-latitude trapped electron boundary collapse during magnetic storms, *J. Geophys. Res., 72,* 1644, 1967.

CHAPTER 8

Outer-Zone Electrons and the Interplanetary Magnetic Fields During Two Geomagnetic Storms

L. J. LANZEROTTI

Bell Telephone Laboratories, Inc., Murray Hill, New Jersey 07974

Many experimental correlation studies have been conducted in an attempt to understand the relationships between the interplanetary medium and geophysical disturbances. These correlations have been carried out in order to understand the mechanisms by which the solar wind plasma and magnetic fields couple with the earth's magnetosphere to produce the observed variations in various geophysical indices, both during quiet and storm times. The solar wind plasma is probably the primary source of energy that drives the processes producing the geophysical disturbances. Among the first to correlate the plasma particle properties with geophysical disturbances were *Snyder et al.* [1963], who found a correlation between the solar wind velocity and the daily sum of *Kp*. Recently, correlations between the interplanetary magnetic field and *Kp* have been discussed in studies examining the coupling mechanisms between the solar wind and the magnetosphere.

The strength of the measured interplanetary field has been found to correlate with *Kp* by *Wilcox et al.* [1967], and by *Schatten and Wilcox* [1967]. *Wilcox et al.* [1967] and *Rostoker and Fälthammar* [1967] have also shown that geomagnetic activity is stronger when there is a southward component to the interplanetary field. *Fairfield* [1967] has correlated IMP 2 magnetic field data with the auroral electrojet index *AE* and also concludes that a southward field is associated with disturbed geomagnetic conditions.

Ballif et al. [1967], in examining the magnetic field data from the first months of flight of Mariner 4, obtain a strong correlation between the fluctuations in the interplanetary field in the plane normal to the earth-sun line and variations in *Kp*. *Ballif and Jones* [1967] subsequently discuss these observations in detail for two sudden commencement (sc) storms on January 20 (day 20), and February 6 (day 37), 1965, and construct a qualitative model of the magnetic properties of solar streams. Their solar stream model consists of a core of high, uniform magnetic field surrounded by an asymmetric region of fluctuating fields. This solar stream model is used in discussing geomagnetic variability, in terms of *Kp*, as the earth passes through such a solar stream.

It is extremely useful to investigate these correlations between the interplanetary fields and *Kp*, as this gives some measure of the solar-wind-energy coupling necessary to drive the ionospheric currents that produce the relatively high latitude variations measured by *Kp*. However, another manisfestation of geomagnetic storm times is the sudden, nonadiabatic increases in the electron population of the outer radiation belt [*Freeman*, 1964; *Frank et al.*, 1964; *Williams and Smith*, 1965]. It is also, of course, the coupling of the solar wind to the magnetosphere during storm times that produces the sudden increases of these outer-zone electrons. A rough correlation between the solar-wind plasma and the $L = 5$ electron flux has been discussed by *Lanzerotti* [1968*a*] for the April 18, 1965, geomagnetic storm.

It is the purpose of this note to discuss the connection between the interplanetary magnetic field data of *Ballif et al.* [1967], and the outer-zone electron flux changes during the January 20 and February 6 sudden commencement storms. A correlation between the magnitude of the southward interplanetary field component and the observed time of the nonadiabatic electron increases after the sc is discussed. Also evidenced is an apparent correlation between the persistence of the large southward component after the electron increases and the strength of the geomagnetic storm. No consistent correlation is found between the outer-zone electron increases during the two storms

and the position of the earth in the solar stream model constructed by Ballif and Jones.

Interplanetary Magnetic Field and Outer-Zone Electron Data

The electron data used in the following discussion were obtained form the $E_e > 300$-kev electron channel on board the near-equatorial Explorer 26 satellite. The data that are presented during the storm times at $L = 4.5\ R_E$ and $L = 5.0\ R_E$ are the mean of the electron data measured by the experiment as the satellite passed through $L \pm 0.05\ R_E$. A further discussion of the experiment is contained in *Lanzerotti* [1968*b*].

The interplanetary magnetic field data are those contained in Figure 1 of *Ballif and Jones* [1967]. Here are plotted three components of the magnetic field: B_T being the interplanetary field component parallel to the earth's orbit; B_R being the component parallel to the sun-satellite line and positive outward; and B_N being the component in the direction of $R \times T$. The total field strength B is also included. During the two storms, the earth was between the sun and Mariner 4, and the earth-sun-satellite angle was less than 3°. The time lags between observations as seen at the earth and as seen at Mariner 4 have been discussed in *Ballif et al.* [1967], and their time lags are used here for both storms.

The January 20, 1965, geomagnetic storm sudden commencement occurred at 1612 UT and was observed as an sc by 49 stations [*Lincoln,* 1965]. The February 6, 1965, geomagnetic storm sudden commencement occurred at 1414 UT and was reported as an sc by 64 stations [*Lincoln,* 1965]. This latter storm was undoubtedly caused by the enhanced solar-wind plasma accompanying the solar proton event observed on February 5 from an importance 2 solar flare [*IQSY Notes,* 1965; *Krimigis and Van Allen,* 1967].

Figure 1 contains the time history of the $E_e > 300$-kev electron fluxes at $L = 4.5$ and 5.0 during the time of the January 20 sudden commencement storm. Plotted in the center of the figure are the Kp index and D_{st} (M. Sugiura and S. Hendricks, personal communication, 1967) for this time period. At the bottom of the figure is the interplanetary magnetic field data obtained from Figure 1 in Ballif and Jones. The dates at the bottom of

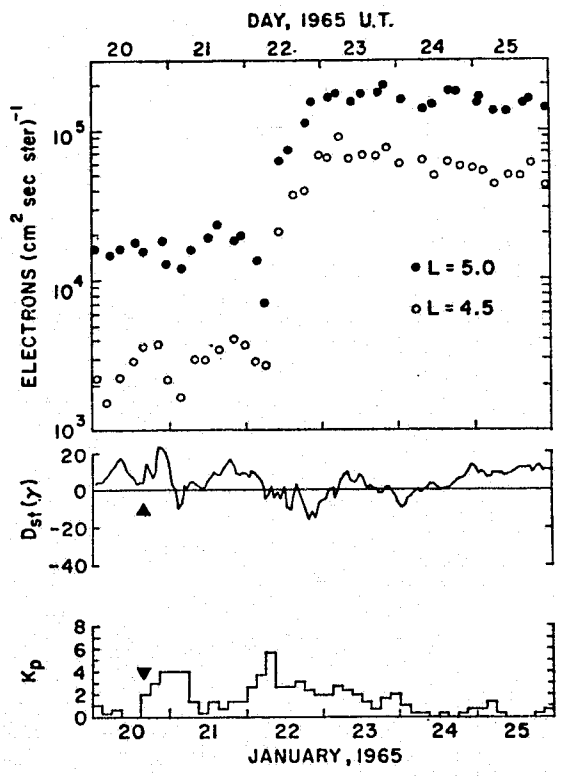

Fig. 1. Electron fluxes ($E_e > 300$ kev) at $L = 4.5$ and 5.0, D_{st}, and Kp for the time period around the January 20, 1965, sudden commencement geomagnetic storm. Plotted at the bottom of the figure is the interplanetary magnetic field data as extracted from Figure 1 of *Ballif and Jones* [1967]. The time delay between the earth-based data and the Mariner 4 data is discussed in *Ballif et al.* [1967].

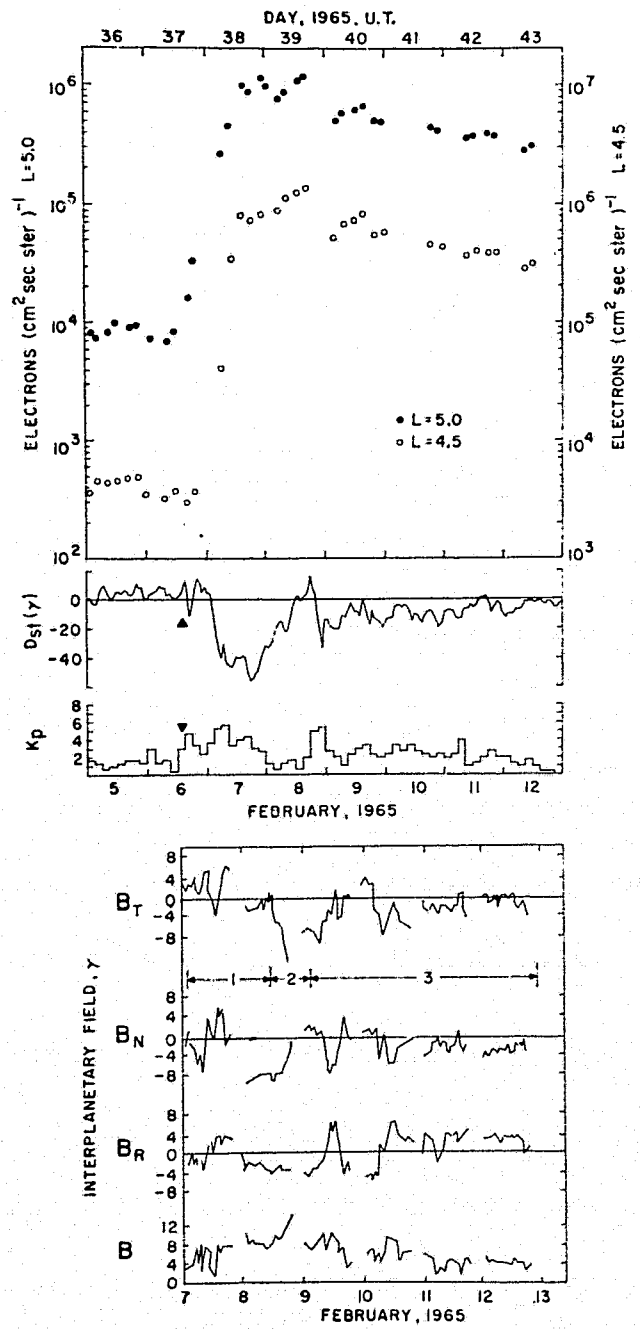

Fig. 2. Electron fluxes ($E_e > 300$ kev) at $L = 4.5$ and 5.0, D_{st}, and Kp for the time period around the February 6, 1967, sudden commencement geomagnetic storm. Plotted at the bottom of the figure is the interplanetary magnetic field data as extracted from Figure 1 of *Ballif and Jones* [1967]. The time delay between the earth-based data and the Mariner 4 data is discussed in *Ballif et al.* [1967].

the interplanetary field data are the dates the data were recorded at the satellite. The data are adjusted for the time delay, as discussed in *Ballif et al.* [1967], in the comparison in Figure 1 of this note. The intervals 1–3 on the magnetic field plot are those ascribed by Ballif and Jones to the passage of the earth through the increasing and fluctuating field (interval 1, sc and high Kp), passage through the high value but stable interplanetary field (interval 2, low Kp), and passage through the decreasing and large-amplitude fluctuating interplanetary field (interval 3, high and decreasing Kp).

From the Figure 1 plot of D_{st}, it can be seen that although there was a dip in D_{st} on about day 21.1, there was no long period of negative D_{st} until after about day 22.25. This period of negative, fluctuating D_{st} could perhaps be due to the development of a weak ring current. However, it is obvious that the storm, as measured by the equatorial D_{st}, was not very large and had almost no distinguishable main phase.

The nonadiabatic electron increases began at about day 22.35 for both L values. This was about 1.7 days after the sc and only about 0.1 day after the onset of the long period of slightly negative D_{st} values and the second Kp peak at about day 22.25. The electron fluxes at both L values reached half their peak values on day 22.6, about 0.35 days after the beginning of the negative D_{st} values. The nonadiabatic increases in the electron fluxes and the weak 'main phase' occurred near the beginning of solar stream period 3 as denoted by Ballif and Jones.

The electron data for the same L values for the time period around the February 6 geomagnetic storm are shown in Figure 2, along with D_{st}, Kp, and the interplanetary magnetic field data. The breaks in the magnetic field curves correspond to missing data. It is seen that the main phase of the storm began about 0.5 days after the sc. Although the $L = 5$ electron data began to increase first, immediately after the sc, the electron fluxes at both L values reached half their peak values at the same time, about day 38.4 or 0.3 days after the beginning of the main phase. The beginning of the main phase and the particle increases both occurred in solar stream interval 1 as denoted by Ballif and Jones.

The summary of the above electron time observations for both of these storms is contained in Table 1. During the larger (February 6) storm, the nonadiabatic electron increases occurred sooner. However, as stated above, electron increases during the February 6 storm occurred during Ballif-Jones interval 1

TABLE 1. Electron Response Times during the Two Geomagnetic Storms

Storm	Max. D_{st}, γ	Time after sc for Electrons to Reach Half-Peak Values, days
January 20, 1965	15	1.7 ± 0.1
February 6, 1965	55	0.8 ± 0.05

and during the January 20 storm during interval 3.

Discussion

Close inspection of the data presented in Figures 1 and 2 shows that a correlation may be observed between the particle data and B_N. The most intense southward B_N value observed during each storm was about 10 γ and was measured at approximately the time when the electron fluxes in each storm reached about half their ultimate peak values (Figures 1 and 2). This value of B_N in each storm was 3–4 γ larger than any other value of B_N measured during the storms.

A further interesting observation can be made between the storm magnitude, as measured by D_{st}, and the persistence of the large southward field component. If a temporal point of reference is taken as the time of half-maximum of the electron increases (corresponding to about the time of maximum southward B_N), then Table 2 indicates that for a larger storm there is a longer period of large southward interplanetary field component B_N. A large southward interplanetary field B_N was defined arbitrarily as a field $B_N \geq 8$ γ from Figures 1 and 2. Perhaps this observation explains why almost no main phase developed during the January storm: B_N never became large enough to initiate any substantial (as measured by the particle fluxes and D_{st}) 'reconnection' to the magnetospheric field until long after the sudden commencement. Furthermore, any reconnection at the time of the electron increases was apparently short-lived. Both of the above observations must be tempered by the fact that there are gaps in the February interplanetary field data.

As was discussed in the introduction, other authors have investigated the correlation of a southward component of the interplanetary field with Kp. It appears from the observations noted above that it is necessary to have a southward interplanetary field of sufficient magnitude (apparently ≥ 8 γ in these two cases) to initiate the solar-wind coupling necessary to produce the nonadiabatic outer-zone electron increases. The strength of the storm is then dependent upon the persistence of this large southward value of B_N. This critical magnitude of B_N would probably be seasonally dependent upon the tilt of the magnetic dipole of the earth and would be an interesting quantity to investigate in further field and electron data.

A recent theoretical study of the effects of the interplanetary field on the energy of geomagnetic disturbances has been carried out by *Maguire and Carovillano* [1968]. These authors have concluded independently from their theoretical arguments that magnetosphere particle energization is potentially the greatest when the interplanetary field is southward-directed.

Figures 1 and 2 show that the electron increases during each storm took place in a time interval of fluctuating interplanetary B_T, rather than in the central interval of quiet but intense interplanetary field. Other than this observation, there are no additional obvious time correlations between the time intervals of the Ballif-Jones solar stream model, based upon fluctuations of B_T, and the times or magnitudes of the observed storm main phases and nonadiabatic increases of the outer-zone electrons.

The solar stream model is based upon the observed correlation of Kp with the fluctuations in B_T. In these two storms the correlation of Kp with the outer-zone electron population and with D_{st} is not very good. Hence, it would be expected that the electron and D_{st} observations

TABLE 2. Magnetic Storm Size as a Function of the Large Southward Interplanetary Field Component

Storm	Max. D_{st}, γ	Days after Electron Increases $B_N \geq 8\gamma$
January 20, 1965	15	0.1 ± 0.05
February 6, 1965	55	0.4 ± 0.1

would not be related easily to the position of the earth in the proposed solar stream model.

In conclusion, the relationship between the nonadiabatic increases of the outer-zone electrons and the coupling of the interplanetary magnetic field with the magnetosphere is certainly very complex. The electron increases observed during the January 20 and February 6 storms had quite different time characteristics and did not correlate with a fixed temporal position of the earth in the solar stream model proposed by Ballif and Jones. While no correlations of the electron increases or the size of the storm main phase were observed with B_T, approximate correlations of the time of the maximum southward B_N with the time of the electron increases were observed. During these two storms, the southward B_N field apparently had to have a critical magnitude to produce the coupling necessary to initiate the large nonadiabatic storm-time electron increases. Also, it was seen that the strength of the storm, measured by maximum D_{st}, was dependent on the length of time that the southward B_N was large after the electron increases and the main phase began.

Acknowledgment. The author wishes to thank Dr. W. L. Brown for a stimulating discussion concerning the reconnection field model.

References

Ballif, J. R., and D. E. Jones, The magnetic morphology of solar streams and its relation to geomagnetic storms, *J. Geophys. Res., 72,* 5173, 1967.

Ballif, J. R., D. E. Jones, P. J. Coleman, Jr., L. Davis, Jr., and E. J. Smith, Transverse fluctuations in the interplanetary magnetic field: A requisite for geomagnetic variability, *J. Geophys. Res., 72,* 4357, 1967.

Fairfield, D. H., Polar magnetic disturbances and the interplanetary magnetic field, *Goddard Space Flight Center Document X-612-67-338,* July 1967.

Frank, L. A., J. A. Van Allen, and H. K. Hills, A study of charged particles in the earth's outer radiation zone with Explorer 14, *J. Geophys. Res., 69,* 2171, 1964.

Freeman, J. W., Jr., The morphology of the electron distribution in the outer radiation zone and near the magnetospheric boundary as observed by Explorer 12, *J. Geophys. Res., 69,* 1691, 1964.

IQSY Notes, No. 18, 103, IQSY Committee of ISCU, July 1965.

Krimigis, S. M., and J. A. Van Allen, Observation of the February 5–12, 1965, solar particle event with Mariner 4 and Injun 4, *J. Geophys. Res., 72,* 4471, 1967.

Lanzerotti, L. J., Comparison of the electron response in the magnetosphere at L = 5 with the solar wind during the April 17–18, 1965, magnetic storm, *J. Geophys. Res., 73,* 438, 1968*a*.

Lanzerotti, L. J., Outer-zone electron fluxes during the February 5, 1965, solar proton event, *Ann. Geophys.,* to be published, 1968*b*.

Lincoln, J. V., Geomagnetic and solar data, *J. Geophys. Res., 70,* 5953, 1965.

Maguire, John J., and Robert L. Carovillano, The effect of the interplanetary field on the energy of geomagnetic disturbances, *J. Geophys. Res., 73*(11), 1968.

Rostoker, G., and C.-G. Fälthammar, Relationship between changes in the interplanetary magnetic field and variation in the magnetic field at the earth's surface, *J. Geophys. Res., 72,* 5853, 1967.

Schatten, Kenneth H., and John M. Wilcox, Response of the geomagnetic activity index K_p to the interplanetary magnetic field, *J. Geophys. Res., 72,* 5185, 1967.

Snyder, Conway W., Marcia Neugebauer, and U. R. Rao, The solar wind velocity and its correlation with cosmic-ray variations and with solar and geomagnetic activity, *J. Geophys. Res., 68,* 6361, 1963.

Wilcox, John M., Kenneth H. Schatten, and Norman F. Ness, Influence of interplanetary magnetic fields and plasma on geomagnetic activity during quiet sun conditions, *J. Geophys. Res., 72,* 19, 1967.

Williams, D. J., and A. M. Smith, Daytime trapped electron intensities at high latitudes at 1100 kilometers, *J. Geophys. Res., 70,* 541, 1965.

CHAPTER 9

Outer zone electron fluxes during the February 5, 1965, solar proton event

by L. J. LANZEROTTI,

Bell Telephone Laboratories, Incorporated,
Murray Hill, New Jersey.

ABSTRACT. — *The solar wind plasma accompanying the solar proton event on Day 36, 1965, produced a sudden commencement magnetic storm observed on earth on Day 37, 1965. The effects of the magnetic storm on the low latitude outer belt electrons ($E_e > 0.3$, > 0.45 and > 1.0 MeV) as observed by the Explorer 26 satellite are studied at $L = 4.0, 4,5$ and $5.0\ R_E$. The time delay between the sudden commencement and the effects of the storm on the magnetosphere electrons is observed to be a function of both the electron L value and the electron energy. The storm is observed essentially simultaneously with the S.C. at $L = 5.0\ R_E$ for $E_e > 0.3$ MeV, while there is about a 30 hours time lag between the S.C. and the enhanced fluxes of electrons of $E_e > 1.0$ MeV at $L = 4.0\ R_E$. The time behaviour of the electron fluxes is correlated with the magnetic field index K_p, with the equatorial D_{st}, and with the auroral electrojet index A_E. The electron acceleration mechanism and the electron time correlations with other storm-induced effects are discussed in relationship to possible energy transfer mechanisms coupling the enhanced solar wind to the interior of the magnetosphere.*

Introduction

Many theories have been discussed and published [e.g., Axford and Hines, 1961 ; Parker, 1962 ; Piddington, 1966 ; Dessler and Walters, 1964 ; Dessler and Michel, 1966 ; Axford, *et al.*, 1965 ; Cole, 1966] which attempt to understand and explain terrestrial geomagnetic storms and their effects on the particle populations in the earth's radiation belts. The direct cause of geomagnetic storms is generally accepted to be the interaction of an enhanced solar wind plasma cloud with the magnetosphere. The process by which the energy in the solar wind is transferred to the magnetosphere plasma and particle population is still incompletely understood.

The electron population in the outer radiation belt often undergoes large flux changes on both a long-term and short-term time scale. Some more recent discussions of the outer belt electron population have been presented by Arens, *et al.*, 1967; Lanzerotti, *et al.*, 1967; Williams, 1966; Frank, 1965 *a*, *b*; McIlwain, 1966; Craven, 1966. The experimental observations show that during large geomagnetic storms the electron fluxes undergo large, sudden increases. The terrestrial geomagnetic storm produced by the enhanced solar wind resulting from the February 5, 1965, importance 2 solar flare was not unusual in most respects. However, it appears that the outer belt electron time response was qualitatively different in some aspects than the electron response during a storm in April, 1965. In order to obtain a better understanding of the processes which are operative on outer belt electrons during a magnetic storm, detailed studies of individual storms are necessary. This paper attempts to correlate various terrestrial geophysical phenomena arising from the solar flare with the changes observed by the Explorer 26 satellite in the magnetosphere outer-belt near-equatorial electron population.

Experiment

The Explorer 26 satellite was launched on December 21, 1964, with an inclination of 20°, an orbital period of about 7-1/2 hours, an apogee of 26,000 km and a perigee of 300 km. The satellite spin rate during the period discussed in this paper was about 24 rpm.

The experiment that was flown on Explorer 26 was designed to investigate the electron and proton particle populations in the trapped radiation belts. The experiment consisted of six solid state partially depleted *p-n* junction detectors [Buck, *et al.*, 1964]. By making use of the electron and proton energy loss characteristics and by changing the thickness of the detector active region by a change in detector bias, it was possible to distinguish between electrons and protons. The detectors were encapsulated in a nitrogen-oxygen environment at atmospheric pressure and were covered by a 0.3 mil Kovar diaphragm. Additional absorbers were used on individual detectors to allow the detection of a wide range of particle energies.

The three detectors whose electron flux observations are considered in this paper were designated E5, E6 and E1 and had electron threshold energies of 0.3 MeV, 0.45 MeV, and 1.0 MeV, respectively. The E5 and E6 detectors were directional, were perpendicular to the satellite spin axis, and were operated in the high bias, or electron mode. The E1 detector was omnidirectional, perpendicular to the satellite spin axis, and was also operated in the high bias mode. The contamination from protons, except for a small pre-storm admixture in E5 at $L = 4.0$, was negligible. The geometrical factors for E5, E6 and E1 were $1.5.10^{-3}$ cm^2 ster, $4.0.10^{-3}$ cm^2 ster, and $3.0.10^{-3}$ cm^2 ster, respectively.

The digital accumulation time for one of the detectors in its electron mode was 1.43 seconds. Due to the spin rate of the satellite, the data from E5 and E6 that is presented in the next section is thus the spin-averaged electron flux from a directional detector. Since most of the E5 and E6 data points correspond to data taken with the satellite spin axis at an angle greater than 60° to the local magnetic field, the spin averaged directional data is equivalent to the omnidirectional flux to within a factor of approximately 1.5.

Time History of the Geomagnetic Storm

An importance 2 solar flare was observed in H_α to begin at 1750 U.T. and end about 2010 U.T. on February 5, 1965. Polar cap absorption events of small intensity were observed at some ground stations beginning at various times after 1900 [IQSY Notes, 1965]. The proton onset time for $E_P > 30$ MeV observed at Mariner IV ($\sim$3700 R_E from earth and $\sim$9° from the antisolar direction) by Krimigis and Van Allen [1967] was approximately 1840 U.T. The three near-earth high latitude satellites 1963-38C [Bostrom, *et al.*, 1967; Williams and Bostrom, 1967], 1964-45A [Paulikas, *et al.*, 1966] and Injun 4 [Krimigis and Van Allen, 1967] were unable to establish a precise onset time for protons in the polar region. The first observation of protons ($E_p \sim 25$ MeV) by 1963-38C was during a pass beginning at 1914 U.T. February 5 [Bostrom, *et al.*, 1967]. A sudden commencement geomagnetic storm occurred some 20 hours after the flare, causing large increases in the electron population observed by the Explorer 26 satellite beyond $L = 4.0$ R_E.

The spin-averaged electron fluxes ($E_e > 0.3$ MeV) at $L = 4.0$, 4.5, and 5.0 R_E for the time period from February 5, 1965 (Day 36), through February 11, 1965 (Day 42), are shown in Figure 1. Each data

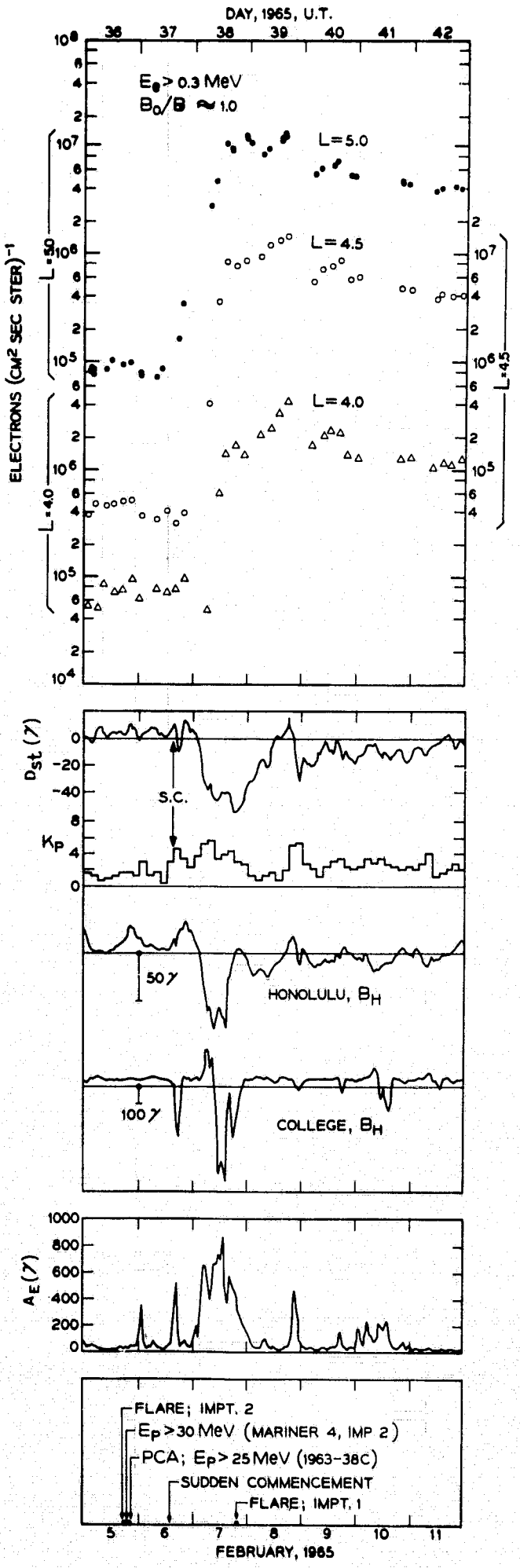

point corresponds to the median counting rate observed by the E5 electron detector on Explorer 26 as the satellite made one pass through the region of space defined by $L \pm 0.05\ R_E$. Multiple median data points at one time indicate that the data at that time was broken down into smaller averaging intervals. The data points correspond to B_O/B values ranging from about 0.3 to 1.0. Except for the $L = 4.0$ pre-storm data, plots of the counting rate versus B_O/B indicate a rate almost independent of B_O/B. (The significance of this observation for the post-storm electron loss mechanism will be discussed elsewhere.) The pre-storm data for $L = 4.0$, $E_e > 0.3$ MeV indicates that $j(0.3\ \text{MeV}, B_O/B) \sim (B_O/B)^2$. All of the pre-storm $L = 4.0$ data has been normalized to the equatorial $L = 4.0$ rates ($B_O/B = 1$).

Plotted below the electron data in Figure 1 are the hourly averaged D_{st} values, the three hour averaged magnetic index K_P, and the hourly averaged horizontal component magnetic field measured at ground stations at College (64.87° N, 147.83° W) and Honolulu (21.32° N, 158° W). The hourly averaged auroral electrojet index A_E is also shown for this time period [DAVIS and SUGIURA, 1966; FAIRFIELD, 1967] together with a gross time history of some of the solar flare induced phenomena.

The sudden commencement magnetic storm occurred at 1414 U.T., approximately 20 hours after the solar flare was first observed. This time delay, together with the sun-earth distance, indicates a solar wind velocity of about 2,000 km/sec. K_P showed an initial increase at the sudden commencement to 5^-, a decrease to 2^+ and a further increase beginning after midnight, Day 38, U.T., to 6^-. The immediate effect of the sudden commencement at College was a magnetic bay during the local morning hours of Day 37. A large increase in the A_E index also occurred following the sudden commencement and slightly before the College negative bay maximum.

The main phase of the magnetic storm observed at Honolulu began on Day 38, about the same time that College was observing a positive bay. A large negative bay at College began near 0700, while the Honolulu horizontal field was already near its minimum value. The initial time history of D_{st} approximately followed the Honolulu B_H trace. This was a moderate magnetic storm with a ring current D_{st} maximum value of less than —60γ. The A_E index

FIG. 1

Time history of the February 5, 1965, solar flare and associated terrestrial geomagnetic phenomena. The electron data ($E_e > 0.3$ MeV) is from the BTL Explorer 26 satellite experiment.

began increasing about 0300 and reached its peak value of 900γ about 1300 U.T. on Day 38.

Plots of the data from the high latitude satellites Injun IV and 1963-38C [WILLIAMS and BOSTROM, 1967] show that after the initial peak in the low energy solar flare proton rates, there were two broad maxima. These maxima occurred temporally near the sudden commencement increase in K_P and near the second K_P increase on Day 38.

An importance 1 solar flare occurred at 1819 U.T. on Day 38. No detectable increases in the solar proton counting rates have been reported from this flare. About 25 hours after the flare, K_P increased sharply from 2° to 5° and D_{st} showed an approximately 20γ negative excursion. Coincident with the D_{st} decrease was an increase in the A_E index.

The $E_e>0.3$ MeV electron data in Figure 1 indicates that an increase in the $L = 5.0$ electron flux was first observed on Day 37.7. This increase in the flux was during the first pass of Explorer 26 through $L = 5.0$ after the sudden commencement. A process to increase the electron flux had begun to act upon the $L = 5.0$ electrons within about 2.5 hours after the geomagnetic storm sudden commencement and the initial increase in A_E. The $E_e>0.3$ MeV electron fluxes at $L = 4.5$ and 4.0 did not begin to increase until after Days 37.8 and 38.2, respectively. Two satellite passes of data are not available near the beginning of Day 38, so a more precise onset time cannot be placed on the increase of the $L = 4.5$ flux. It is noted from Figure 1 that the $L = 4$ electron flux underwent a small decrease on Day 38.2 before it began increasing and while the fluxes at the other two L values were increasing.

The electron fluxes at the three L values reached a temporary maxima at about Day 38.6. The fluxes began to increase again on Day 39, but it will be seen below that this increase was of a different nature than that which occurred immediately after the sudden commencement.

Median electron flux data for $E_e>0.45$ MeV and $E_e>1.0$ MeV are shown in Figure 2. Only the $E_e>0.45$ MeV, $L = 4.0$ pre-storm data warrented normalization to $B_o/B = 1$. Again it can be seen that the fluxes at $L = 5.0$ began to increase before the $L = 4.5$ or $L = 4.0$ fluxes. There was also a large (factor of 5) decrease in the $L = 4.5$, $E_e>1.0$ MeV electron data before the flux increases. As seen above for the $E_e>0.3$ MeV data, the $E_e>0.45$ MeV data also show temporary maxima in the elec-

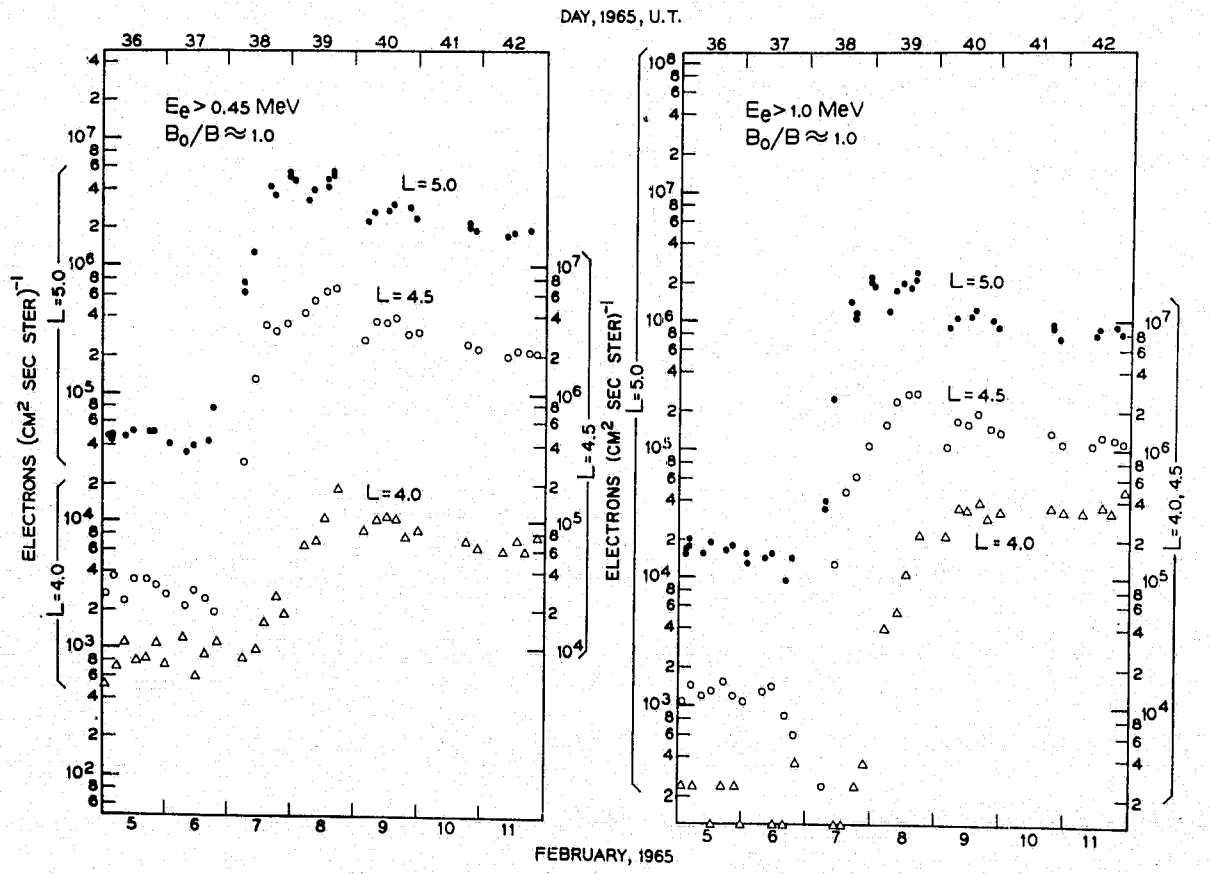

FIG. 2

Electron fluxes for $E_e>0.45$ MeV and $E_e>1.0$ MeV during the period of February 5-11, 1965.

tron rates for all L values at about Day 38.6. The data for $E_e > 1.0$ MeV do not show this temporary maximum as clearly for $L = 4.0$ and 4.5.

A pass-by-pass plot of the median data for $E_e > 0.3$ MeV during the time of the initial large flux increases is shown in Figure 3. Also indicated in the figure

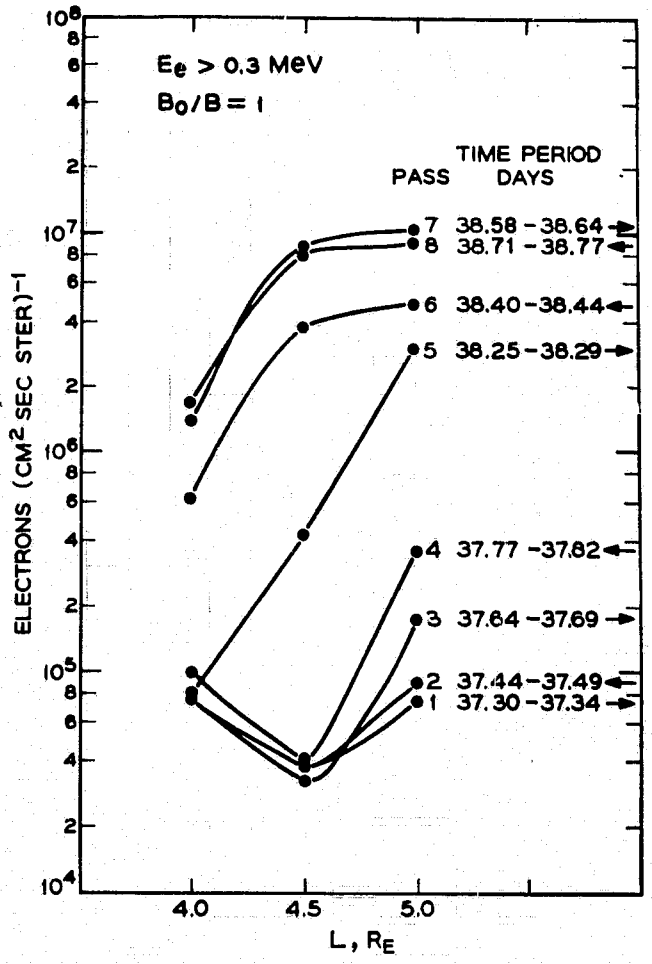

FIG. 3

Pass-by-pass electron data ($E_e > 0.3$ MeV) during the period of the large nonadiabatic flux increases. The arrows indicate inbound and outbound passes of the satellite. The time periods, in fractions of a day, indicate the time interval taken to travel from $L = 4$ to $L = 5$ (outbound) or $L = 5$ to $L = 4$ (inbound).

is the time period encompassed by the individual passes. This Figure also confirms that the storm effect was first observed at $L = 5$ and observed only later at the lower L values.

In order to obtain a better determination of the outer belt electron response to the geomagnetic storm conditions, the response time delays after the sudden commencement were plotted as functions of L and E_e in Figures 4 and 5, respectively. The time delay in the figures is the time from the S.C. to the time midway between the satellite pass that

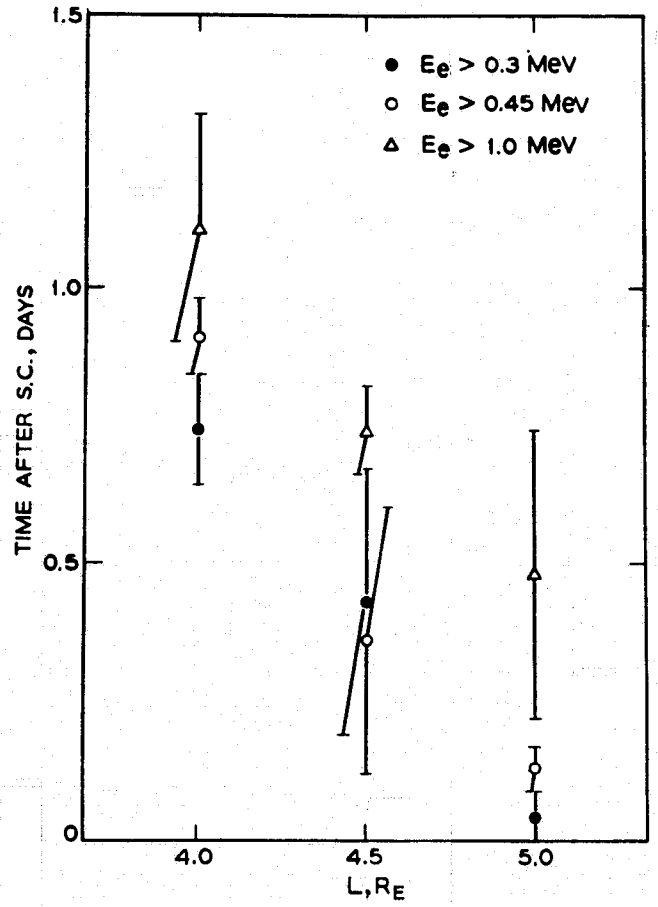

FIG. 4

Magnetosphere electron time response after the sudden commencement magnetic storm as a function of L.

first saw a flux increase and the immediately preceding pass. The error bars correspond to one-half the time interval between these two passes. From Figure 4, the relationship

$$\left.\frac{dL}{dt}\right|_{E_e} \sim -1.5\, R_E/\text{day}$$

holds to a good approximation for the period after the sudden commencement for all three energy channels. Figure 5 indicates that the response time after the sudden commencement versus electron energy was observed to be

$$\left.\frac{dE_e}{dt}\right|_{L} \sim 2\,\text{MeV/day}$$

Hence, although the higher L values responded to the storm first, the rate of acceleration of the different energy electrons at each L appears to be the same.

ADIABATIC EFFECTS

MCILWAIN [1966], following a suggestion by DESSLER and KARPLUS [1961], has shown with data from Explorer 15 ($L \lesssim 4$) that adiabatic acceleration

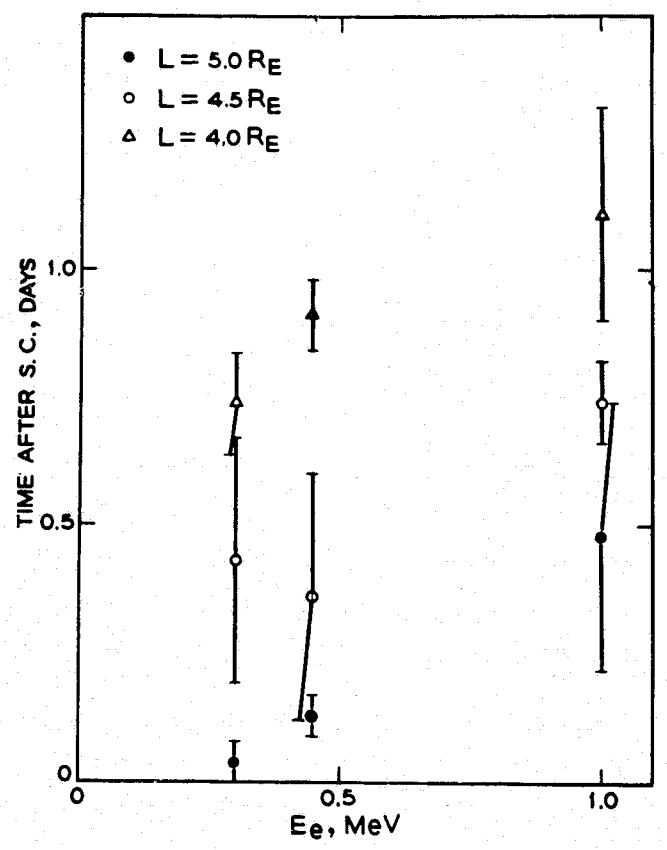

FIG. 5

Magnetosphere electron time response after the sudden commencement magnetic storm as a function of electron energy.

of electrons occurs via the betatron effect. The electron flux changes observed following the February 6 magnetic storm were investigated following McIlwain's treatment of his lower L value data. Figure 6 shows the $E_e>0.3$ MeV electron data for $L = 4.0$, 4.5 and 5.0. This is the same electron data plotted in Figure 1, except that the exponential electron flux decay following the storm induced flux increases has been removed. Superimposed upon the particle data is the D_{st} data of Figure 1, suitably normalized to the electron rates before and after the large flux changes during Days 37 and 38.

The exponential decay of the electron fluxes after Day 39 was removed from the data in Figure 1 by visually fitting a straight line to a semilog plot of the data versus time from about Day 39 to Day 54. The time for these $E_e>0.3$ MeV rates to decay by $1/e$ was determined to be 4.8 days, 5.2 days, and 6.1 days for $L = 5.0$, 4.5 and 4.0, respectively. These measured lifetimes are comparable to the outerzone decay rates measured at 1100 km ($E_e>0.280$ MeV) by WILLIAMS and SMITH [1965] during a magnetically quiet period in October, 1964.

The changes that should be observed in the particle intensities by the E5 detector due to „quiet-day" ring currents (i.e., preceeding and following the February 6 magnetic storm) were calculated following MCILWAIN [1966], with the exception that the B_o/B dependence of the electron rates was taken as a power law rather than an exponential. However, as pointed out above, the rates are approximately independent of B_o/B with the exception of the $L = 4$ pre-storm data. Figure 6 indicates, as McIlwain has shown with his data, that the temporal fluctuations in the non-storm period electron rates correlate closely with the changes in D_{st}, even on this more expanded time scale. Note also that D_{st} is plotted on a linear scale while the electron fluxes are logarithmic.

Figure 6 shows that the increases observed in electron fluxes beginning with the Explorer 26 pass on Day 39.2 are apparently caused by the recovery of D_{st} due to the decay of the storm-induced ring current. However, the solar wind from the Impt. 1 flare on Day 38 apparently induced another, smaller

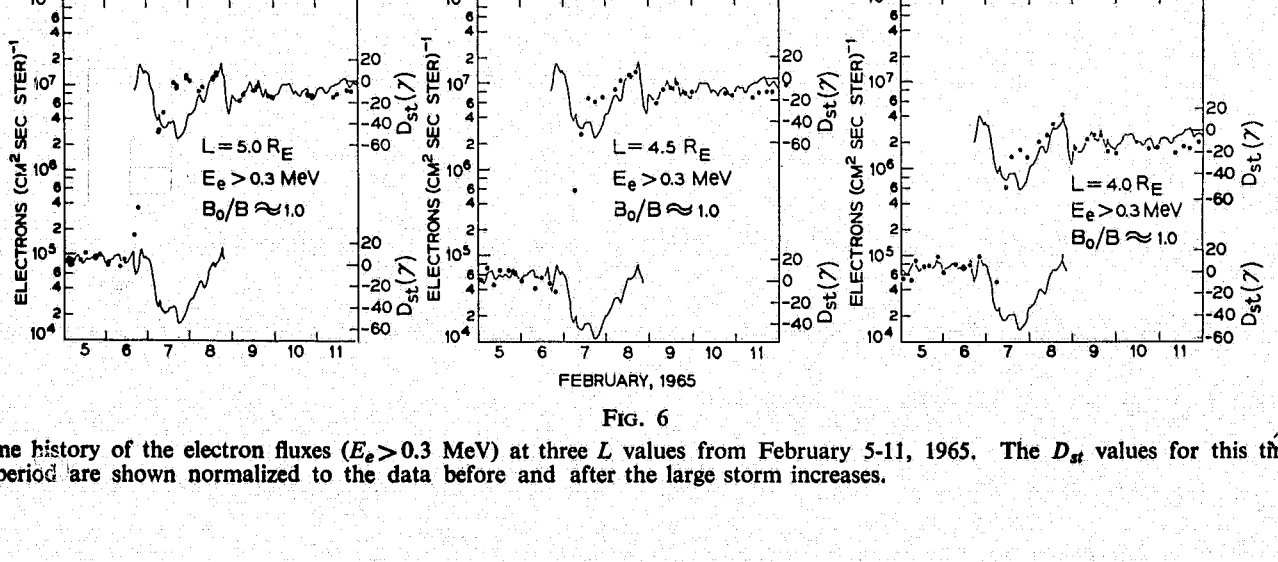

FIG. 6

Time history of the electron fluxes ($E_e>0.3$ MeV) at three L values from February 5-11, 1965. The D_{st} values for this time period are shown normalized to the data before and after the large storm increases.

ring current (perhaps located beyond $\sim 7Re$) during the end of Day 39. Unfortunately, no particle observations are available during the onset of this smaller ring current. However, the fluxes observed during the pass on Day 40.2 and the following passes follows the D_{st} recovery and subsequent fluctuations. An examination of the other two electron energy channels for these betatron acceleration effects shows the same type of flux changes with D_{st} as for the $E \geq 0.3$ MeV electrons.

Discussion

The outer belt electron data from Explorer 26 show that the effect of the solar flare induced geomagnetic storm was first observed at $L = 5$, and only later at lower L values. The large flux changes caused by the storm are perhaps what McIlwain [1966] has termed „rapid nonadiabatic accelerations".

After removing the adiabatic effects and the persistent decay from the data, as was done for the data in Figure 6, it is seen that the nonadiabatic process induced by the geomagnetic storm was observed to end during the satellite pass on approximately

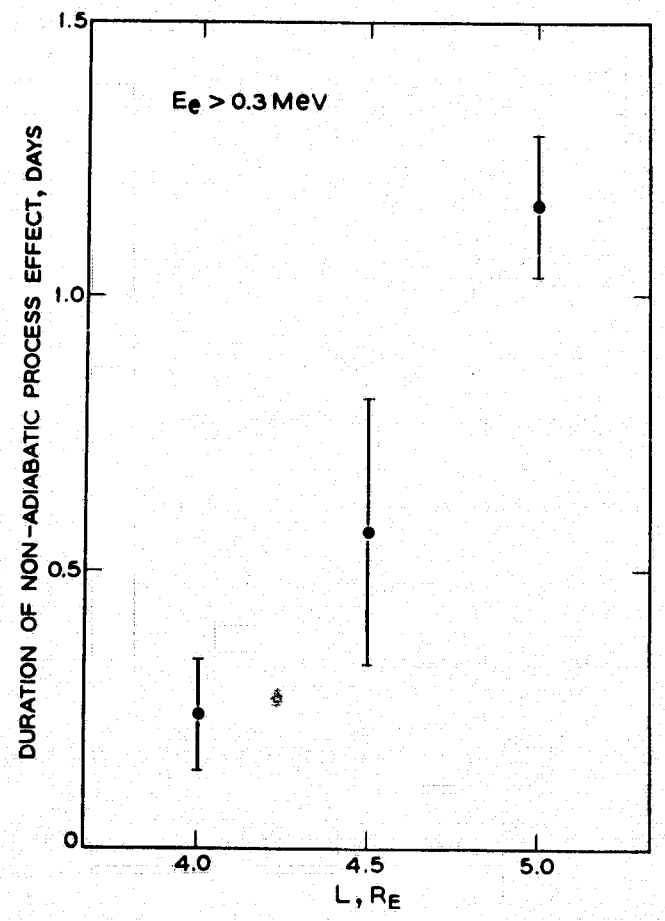

Fig. 7

Duration of the nonadiabatic process as seen by $E_e > 0.3$ MeV electrons, plotted as a function of L.

Day 38.6 for all three L values. The end of the process as determined from the particle observations corresponds very closely in time with the occurrence of the second peak observed in the College and Honolulu magnetic field measurements and the A_E index as observed on Day 38. The length of time that the nonadiabatic process acted at each L value for the $E_e > 0.3$ MeV electrons is shown in Figure 7. The error bars are essentially a measure of the uncertainty in the onset time of the storm at the given L value as discussed in connection with Figures 4 and 5. It should be noted that this nonadiabatic process ended about 1.5 hour before the storm ring current, as measured by D_{st}, attained its maximum value.

The nonadiabatic process was thus seen to begin essentially at, or close to, $L = 5$ by the observed increase in the $E_e > 0.3$ MeV electron fluxes. The onset time for the process was approximately coincident with the sudden commencement magnetic storm and large (500γ) A_E increase and slightly less than 1/2 day before the onset of the 60γ decrease in D_{st}. The process lasted for approximately 1.2 days and its effect was delayed by approximately 0.4 days and 0.7 days at $L = 4.5$ and 4.0, respectively. A possible explanation of the observations is that the nonadiabatic process was initiated by the sudden commencement storm and was confined locally to near $L = 5$ for about 1.2 days. The $L = 5$ electrons then underwent an inward diffusion of about 1.5 R_E/day. Frank [1965 *b*] has reported observations of inward diffusion of electrons ($E_e > 1.6$ MeV) mainly for $L \lesssim 4.0$. He found a diffusion rate of ~ 0.12 R_E/day for $L = 4.0$ and the rate $\sim L^8$. Craven [1966] discusses inward radial diffusion of electrons ($E_e > 1.6$ MeV) for low altitudes in the outer radiation zone during the first half of 1963. He finds a diffusion rate of ~ 0.2 R_E/day for $L \sim 5R_E$ and ~ 0.02 R_E/day for $L \sim 4$ R_E.

The rapidity, compared to Craven's and Frank's diffusion rates, with which the storm was observed at lower $L's$ after its first observation at $L = 5$ appears to rule out the possibility that the electrons were accelerated at $L = 5$ and radially diffused to the lower L values. In addition, if diffusion were the predominate mechanism for the enhancement of the lower L electron fluxes during the storm it would be expected that the peak flux at lower $L's$ would occur at later times, rather than approximately simultaneously as they apparently did.

A more probable explanation of the process observed during the magnetic storm is that a nonadiabatic mechanism was initiated by the geomagnetic storm near $L = 5$. The mechanism was apparently an acceleration process which „diffused" to lower L values at a rate of ~ 1.5 R_E/day. The acceleration appears to have been turned off simultaneously at all L values. Figure 7 appears to confirm this in that an extrapolation of the data to lower L values

would indicate that no disturbance should be observed near $L = 3.5$. Indeed, an examination of the Explorer 26 data at $L = 3.5$ shows no electron enhancement above a temporally constant proton population in the "slot" region.

This nonadiabatic mechanism may also "diffuse" to higher L values, although the Explorer 26 orbit did not allow higher L observations during this time interval. However, a magnetic storm that occurred on Day 63, 1965, was observed by Explorer 26 apparently to increase primarily the $L = 4.0$ electron flux, and was not seen as strongly at $L = 5$. This observation, if correct, would tend to indicate a process „diffusing" to higher L values, also. The time delays associated with the $E_e > 0.45$ MeV and $E_e > 1.0$ MeV electrons (Fig. 5) is probably due to the process requiring more time in order to accelerate electrons to the higher energies, rather than an inward diffusion of the higher energy electrons in a fraction of a day.

The cause of the initiation of the nonadiabatic flux increasing process is unknown. The process was observed to begin almost simultaneously with the sudden commencement geomagnetic storm. This is in contrast to the magnetic storm of April 18, 1965, where it was observed that the first particle increases were not seen until about 12 hours after the sudden commencement [LANZEROTTI, 1967]. The speculation was made in connection with the April storm that a time delay was needed between the interaction of the solar wind with the magnetosphere and geomagnetic tail before energy stored in the tail could be transferred to the interior of the magnetosphere [AXFORD, *et al.*, 1965]. There was almost no time delay in the magnetosphere response to the magnetic storm associated with the February 5 solar proton event. Perhaps the almost immediate access of the higher energy solar protons to the magnetosphere at the time of the sudden commencement [as pointed out above from the report of WILLIAMS and BOSTROM, 1967] somehow initiated the immediate energy release from the magnetotail to the interior of the magnetosphere. KRIMIGIS, *et al.*, [1967] have recently shown conclusively that solar protons have full and essentially immediate access from interplanetary space to the polar cap.

The increase in A_E that occurred with the sudden commencement on February 6 was about 2.3 times larger than the sudden commencement A_E increase observed on April 17, 1965, at the start of that magnetic storm. It is possible that the lower energy solar protons, incident directly on the polar cap, significantly contributed to increasing the intensity of the polar currents. These intensified currents could then cause or contribute to the almost immediate energy release from the magnetotail region to the interior of the magnetosphere.

As is clear from the above discussion, much more study is needed on individual magnetic storms in order to further illuminate the nonadiabatic mechanisms that enhance the electron fluxes in the outer radiation belt.

ACKNOWLEDGMENTS

I would like to thank Miss C. G. Maclennan for help in the Explorer 26 data reduction, Dr. C. S. Roberts for helpful discussions, and Dr. D. Fairfield of NASA/Goddard Space Flight Center for providing the A_E index data. I would also like to thank Dr. W. L. Brown for many valuable comments and useful discussions.

REFERENCES

ARENS J. F., WILLIAMS D. J., ROBERTS C. S. and LANZEROTTI L. J., "Comparison of Outer Zone Trapped Electron Behaviour at 1100 km and at 3-5R_E during the April 18, 1965, Magnetic Storm," *Trans. Am. Geophys. Union*, 1967, **48**, 169.

AXFORD W.I., PETSCHEK H. E. and SISCOE G. L., "Tail of the Magnetosphere," *J. Geophys. Res.*, 1965, **70**, 1231-1236.

BOSTROM C. O., KOHL J. W. and WILLIAMS D. J., "The February 5, 1965, Solar Proton Event: 1. Time History and Spectra Observed at 1100 km," *J. Geophys Res.*, 1967, **72**, 4487.

BUCK T. M., WHEATLEY G. H. and RODGERS J. W., "Semi-conductor Detector for the Telstar Satellite," *IEEE Trans. Nuc. Sci, NS*-11, 1964, 294-301.

COLE K. D., "Magnetic Storms and Associated Phenomena," *Space Science Reviews*, 1966, **5**, 699-770.

CRAVEN J. D., "Temporal Variations of Electron Intensities," *J. Geophys. Res.*, 1966, **71**, 5643-5664.

DAVIS T. N. and SUGIURA M., "Auroral Electrojet Activity Index A_E and Its Universal Time Variations," *J. Geophys. Res.*, 1966, **71**, 785-801.

DESSLER A.J. and KARPLUS R., "Some Effects of Diamagnetic Ring Currents on Van Allen Radiation," *J. Geophys. Res.*, 1961, **66**, 2289-2295.

DESSLER A. J. and MICHEL F. C., "Plasma in the Geomagnetic Tail," *J. Geophys. Res.*, 1966, **71**, 1421-1426.

DESSLER A. J. and WALTER G. K., "Hydromagnetic Coupling Between the Solar Wind and Magnetosphere," *Plant. and Space Science*, 1964, **12**, 227-234.

FAIRFIELD D., private communication.

FRANK L. A., "A survey of electrons $E > 40$ KeV beyond 5 earth radii with Explorer 14," *J. Geophys. Res.*, 1965*a*, 70, 1593-1626.

FRANK L. A., "Inward Radial Diffusion of Electrons Greater than 1.6 million Electron Volts in the Outer Radiation Zone," *J. Geophys. Res.*, 1965*b*, **70**, 3533-3540.

IQSY Notes, No. 13, IQSY Committee of ICSU, 103-104' July 1965.

KRIMIGIS S. M. and VAN ALLEN J. A., "Observations of the Solar Proton event of 5-12 February, 1965, with Mariner 4 and Injun 4," *J. Geophys. Res.*, 1967, **72**, 4471.

KRIMIGIS S. M., VAN ALLEN J. A. and ARMSTRONG T. P., "Simultaneous Observations of Solar Protons Inside and Outside the Magnetosphere," *Phys. Rev. Letters*, 1967, **18**, 1204-1207.

LANZEROTTI L. J., ROBERTS C. S. and BROWN W. L., "Temporal Variations in the Electron Flux at Synchronous Altitudes," *J. Geophys. Res.*, to be published, 1967, **72**, 5893-5902.

LANZEROTTI L. J., "Comparison of the Electron Response in the Magnetosphere at $L = 5$ with the Solar Wind During the April 17-18, 1965, Magnetic Storm," *J. Geophys. Res.*, 1968, **73**, 438-441.

MCILWAIN C. E., "Processes Acting Upon Outer Zone Electrons, I. Adiabatic Perturbations," Inter-union Symposium on Solar-Terrestrial Physics, Belgrade, Sept. 1966.

PARKER E. N., "Dynamics of the Geomagnetic Storm," *Space Science Revs.*, 1962, **1**, 62-99.

PAULIKUS G. A., FREDEN S. C. and BLAKE J. B., "Solar Proton Event of February 5, 1965," *J. Geophys. Res.*, 1966, **71**, 1795-1798.

WILLIAMS D. J. and SMITH A. M., "Daytime Trapped Electron Intensities at High Latitudes at 1100 Kilometers," *J. Geophys. Res.*, 1965, **70**, 541-556.

WILLIAMS D. J., "A 27-day Periodicity in Outer Zone Trapped Electron Intensities," *J. Geophys. Res.*, 1966, **71**, 1815-1826.

WILLIAMS D. J. and BOSTROM C. O., "The February 5, 1965, Solar Proton Event: 2. Low Energy Proton Observations and Their Relationship to the Magnetosphere," *J. Geophys. Res.*, 1967, **72**, 4497.

CHAPTER 10

Observations of Trapped Electrons at Low and High Altitudes

D. J. WILLIAMS, J. F. ARENS[1]

Goddard Space Flight Center, Greenbelt, Maryland 20771

L. J. LANZEROTTI

Bell Telephone Laboratories, Incorporated
Murray Hill, New Jersey 07904

Energetic ($\gtrsim$280 kev, $\gtrsim$ 1 Mev) trapped electron intensities have been simultaneously obtained at low and high altitudes for a 6-month period in 1965 by the satellites 1963 38C and Explorer 26. The data show that the $\gtrsim$280-kev electron population attains equilibrium within a flux tube after a magnetic storm significantly faster than do the $\gtrsim$1-Mev electrons. Mechanisms leading to the equilibrium state are therefore less effective at the higher energies. An example of this is given in terms of pitch-angle scattering by whistler mode noise. The comparison of particle response characteristics at low and high altitudes during a main phase storm also is used to obtain a rough measure of field expansion in the storm. In addition energetic electrons associated with main phase magnetic storms are observed to appear initially at L values well within the trapping regions and subsequently diffuse to lower and higher altitudes. The region of appearance of these electrons is strongly correlated with D_{st} magnitude. Preliminary results indicate that the acceleration mechanisms responsible for the appearance of these energetic electrons act on the high-altitude side of the whistler knee. The appearance of energetic electrons in the trapping regions from the equator to low altitudes during the April 17, 1965, storm also correlates very well spatially with an observed depletion of maximum ionospheric electron density $Nm\ F_2$ [*Bauer and Krishnamurthy*, 1968*b*].

INTRODUCTION

There have been a number of experimental studies reported concerning the behavior of energetic outer zone electrons at high altitudes (see, for example, *Freeman* [1964] and *Frank* [1965*a*]) and at low altitudes (see, for example, *Forbush et al.* [1962]; *O'Brien* [1963, 1964]; *Rose* [1966]; *Williams* [1966]). Such studies have contributed to our understanding of the electron spatial distributions and their relation to the distorted geomagnetic field, to the time behavior of these particles, and the relation of this time behavior to magnetic activity.

As these results emerged, efforts have turned toward studying possible source, loss, and transport mechanisms responsible for the observed trapped particle behavior [*Nakada and Mead*, 1965; *Roberts*, 1966; *Kennel and Petchek*, 1966; *Tverskoy*, 1964; *Fälthammar*, 1965]. In general, simultaneous observations from several locations within the magnetosphere are required to determine the problems and obtain possible solutions.

Therefore, in an effort to obtain further information concerning these mechanisms, we present herein a comparison of the time behavior of electrons mirroring near the magnetic equator and those mirroring at low altitudes. Energies $\gtrsim$280 kev and $\gtrsim$1 Mev are considered over the L range $3 < L < 5.5$. The data were obtained from the low inclination, high-altitude satellite Explorer 26 and the low-altitude polar-orbiting satellite 1963 38C over the time period January 1, 1965, through June 29, 1965. Preliminary results, covering only the April 17, 1965, magnetic storm were reported by *Arens et al.* [1967].

While such an approach is far from ideal, it does offer the opportunity of obtaining a further insight into these various mechanisms by observing the simultaneous behavior of particles trapped near the equator and at the end of the field line.

[1] NASA-NAS Postdoctoral Resident Research Associate.

Satellites, Instrumentation, and Orbits

The Explorer 26 satellite was launched on December 21, 1964, into an orbit having an inclination of 20.1°, an orbital period of ~7.5 hours, an apogee of 26,000 km, and a perigee of 200 km. The satellite was spin-oriented with the angle between the spin vector and the local magnetic field ranging from about 30° to 90°. The satellite spin rate gradually and uniformly slowed from about 32 rpm to about 9 rpm during the period discussed in this paper.

The experiment flown by Bell Telephone Laboratories on Explorer 26 was designed to investigate the electron and proton particle populations in the trapped radiation belts. The experiment consisted of six solid-state partially depleted p-n junction detectors [*Buck et al.*, 1964]. By making use of the electron and proton energy loss characteristics and by changing the thickness of the detector active region by a change in detector bias, it was possible to distinguish between proton and electron responses in the data. The detectors were encapsulated in a nitrogen-oxygen mixture at atmospheric pressure and covered by a 0.3 mil Kovar diaphragm. Additional absorbers were used in individual detectors to allow the detection of a wide range of particle energies.

The three Explorer 26 detectors whose electron flux observations are discussed in this paper were designated E5, E6, and E1 and had electron threshold energies of 0.3, 0.45, and 1.0 Mev, respectively. The E5 and E6 detectors were directional, had look angles oriented normal to the satellite spin axis, and were operated in the high bias, or electron mode. The E1 detector was omnidirectional, its symmetry axis oriented perpendicular to the satellite spin axis, and was also operated in the high bias mode. The efficiency-geometrical factors for E5, E6, and E1 were 1.5×10^{-3} cm^2 ster, 4.0×10^{-3} cm^2 ster, and 3.0×10^{-3} cm^2 ster, respectively.

A comparison of the high bias mode with the low bias mode of the experiment showed that at $L = 4.5$, 5.0, and 5.5, there was essentially no contamination of the electron data from protons. At $L = 3.0$, 3.5, and 4.0 the high bias data consisted of an admixture of electrons and protons except for the times when the fluxes were increased by magnetic storms. At this time, the high bias-low bias comparison indicated that the increased fluxes were essentially all electrons.

Satellite 1963 38C was launched on September 28, 1963, into a nearly circular polar orbit having a 1147-km apogee, a 1067-km perigee, a 89.9° inclination and a 107.4-minute period. The detectors of interest on 1963 38C are two 1000-micron surface barrier solid-state detectors measuring integral electron intensities at $E_e \geq 280$ kev and ≥ 1.2 Mev. As the satellite is magnetically aligned and the detectors are oriented to look out normal to the alignment axis, trapped electron intensities are obtained for those electrons mirroring at or very near the point of observation. Further details concerning the satellite and instrumentation have been reported by *Williams and Smith* [1965].

During the time period being considered here, January 1, 1965, through June 29, 1965, the apogee of Explorer 26 precessed through the local-time interval of 1730 hours to 1117 hours. Similarly, the orientation of the orbital plane of 1963 38C with respect to the earth-sun line swept through all local times. This is illustrated in Figure 1 where the projection of the two orbits onto the ecliptic plane is shown as viewed looking down from above the north pole.

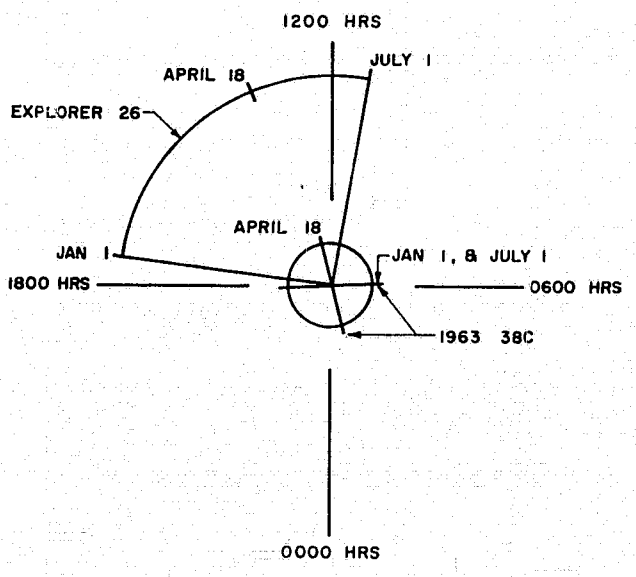

Fig. 1. Projection onto ecliptic plane of Explorer 26 and 1963 38C orbits showing local times sampled by these satellites during the 6-month period of January–June 1965.

Data

The trapped electron intensities to be presented were monitored simultaneously by the satellites Explorer 26 and 1963 38C throughout the period January 1, 1965, through June 29, 1965. The electron energies sampled were $E_e \geq 280$ kev and ≥ 1.2 Mev aboard 1963 38C and $E_e \geq 300$ kev, ≥ 450 kev, and ≥ 1.0 Mev aboard Explorer 26.

Electron intensities through the outer zone were obtained from the 1963 38C data by constructing five point averages at all desired L shells. This process yielded an L spread of ± 0.04 at $L = 3$ and ± 0.1 at $L = 5.5$. The response of an on-board proton spectrometer has shown that proton contamination in these low-altitude high-latitude regions is negligible [*Williams and Smith*, 1965; *Williams*, 1966].

In the following data presentation, each data point from the Explorer 26 satellite corresponds to the median counting rate observed by one of the electron detectors as the satellite made one pass through the region of space defined by $L \pm 0.05\ R_E$. The data points correspond to B_0/B values ranging from about 0.3 to 1.0. Plots of the counting rate versus B_0/B for $L = 4.5$, 5.0, and 5.5 indicate that the electron rates generally are essentially independent of B_0/B within the observed range. Where this is not true, $L = 3.0$, 3.5, and 4.0, the electron data have all been normalized to the rates of $B_0/B = 1$.

The digital accumulation time for one of the Explorer 26 detectors in its electron mode was 1.43 seconds. Owing to the spin rate of the satellite, the data from E5 and E6 that are presented in the next section are thus the spin-averaged electron flux from a directional detector. Most of the E5 and E6 data points correspond to data taken with the satellite spin axis at an angle greater than 60° to the local magnetic field. Thus the spin-averaged directional flux from day 1 to about day 120, 1965, is equivalent to the omnidirectional flux to within a factor of 1.5. After approximately day 120, 1965, the spin rate of the satellite had slowed sufficiently so that the experiment sampled less than 180° in the 1.43-second counting interval. An examination of the individual data points at each L value revealed that the effect of the slowing spin was observed mainly in the proton background at $L = 3.0$ and 3.5. The broad electron pitch-angle distributions obscured any noticeable spin modulation in the electron fluxes. No corrections to the data were necessary for this spin effect.

All the data for the period of interest from the ≥ 300-kev channel aboard Explorer 26 and the ≥ 280-kev channel aboard 1963 38C are shown in Figure 2 for the shells $L = 3.0$, 3.5, 4.0, 4.5, 5.0, and 5.5. Included in the figure are plots of D_{st} (M. Sugiura and S. Hendricks, personal communication) and Kp along with a measure of the orientation of the orbital plane of 1963 38C as viewed from above the north pole. Figure 3 is a similar plot for the data from the Explorer 26 ≥ 1.0-Mev channel and the 1963 38C ≥ 1.2-Mev channel.

Table 1 lists the conversion factors required to convert the relative counts shown in Figures 2 and 3 to absolute flux values (particles/cm^2 ster sec). The errors shown are mainly due to spectral uncertainties.

The proton sensitivity of the Explorer 26 ≥ 300-kev channel can be seen in Figure 2 to extend out to $L = 4.0$. However, the general features of the trapped electron storm-time behavior can be observed and compared with the low-altitude data.

Figures 2 and 3 show that at $L = 3$, only large, well-defined perturbations in the magnetic activity indices are associated with intensity changes in the trapped electron population. With increasing L, more and more intensity fluctuations appear that can be associated with a variety of magnetic perturbations. Finally, at $L = 5.5$ shown in Figures 2 and 3, intensity fluctuations appear that have no obvious association with a D_{st} variation. This lack of association is not surprising since the high L shells are well removed from the near-equatorial stations used to determine the D_{st} values. However, it does emphasize the trend that the trapped electron sensitivity to magnetic activity increases significantly with increasing L, in agreement with previous 1963 38C results [*Williams and Smith*, 1965; *Arens and Williams*, 1967].

Figures 2 and 3 also show that the behavior of ~300-kev electrons mirroring near the equator and at low altitudes is very similar. These ≥ 300-kev electron intensities at a given L value are observed generally to come quickly

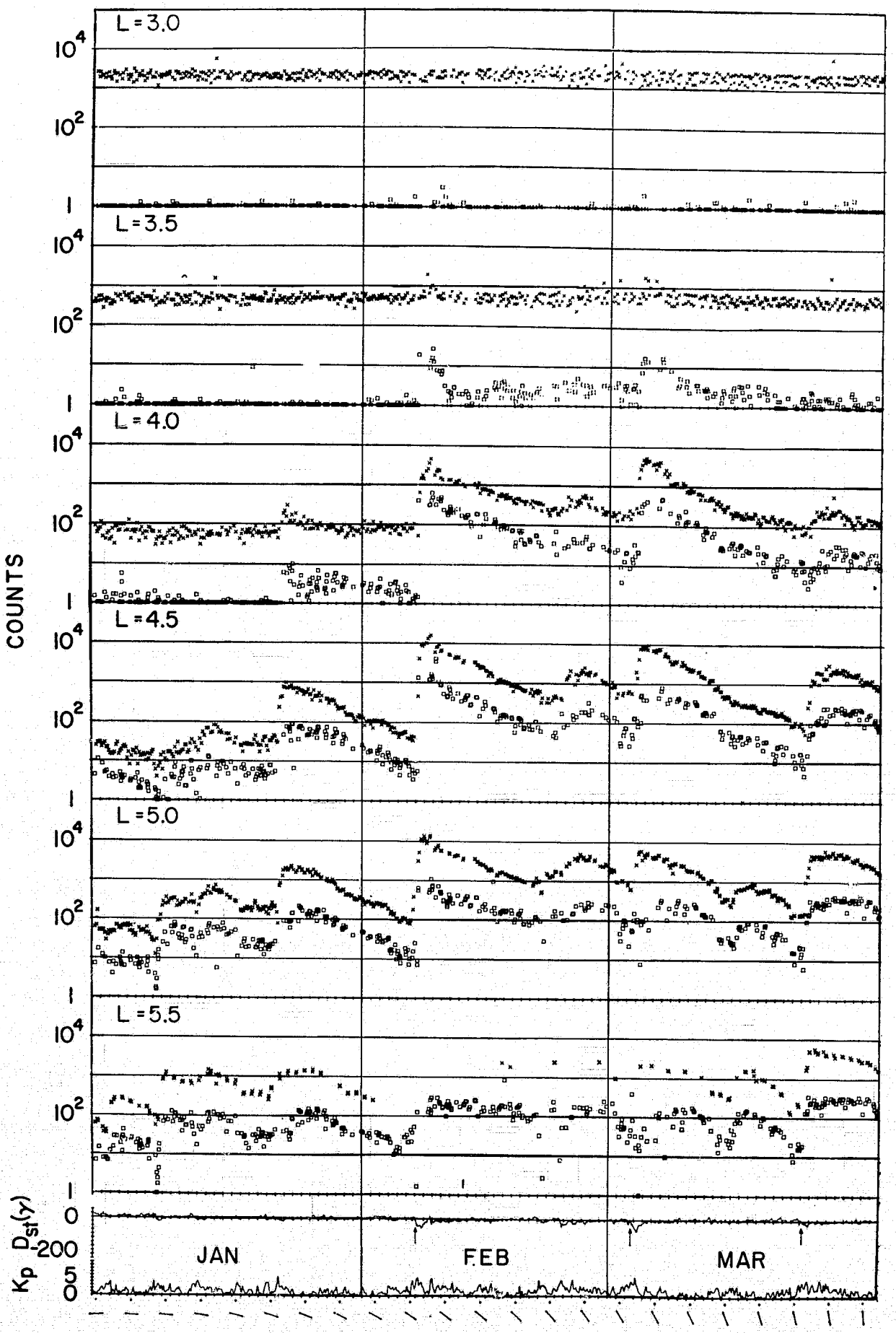
L = 3.0
L = 3.5
L = 4.0
L = 4.5
L = 5.0
L = 5.5
COUNTS
10^4
10^2
1
K_p
$D_{st}(\gamma)$
0
-200
5
0
JAN
FEB
MAR

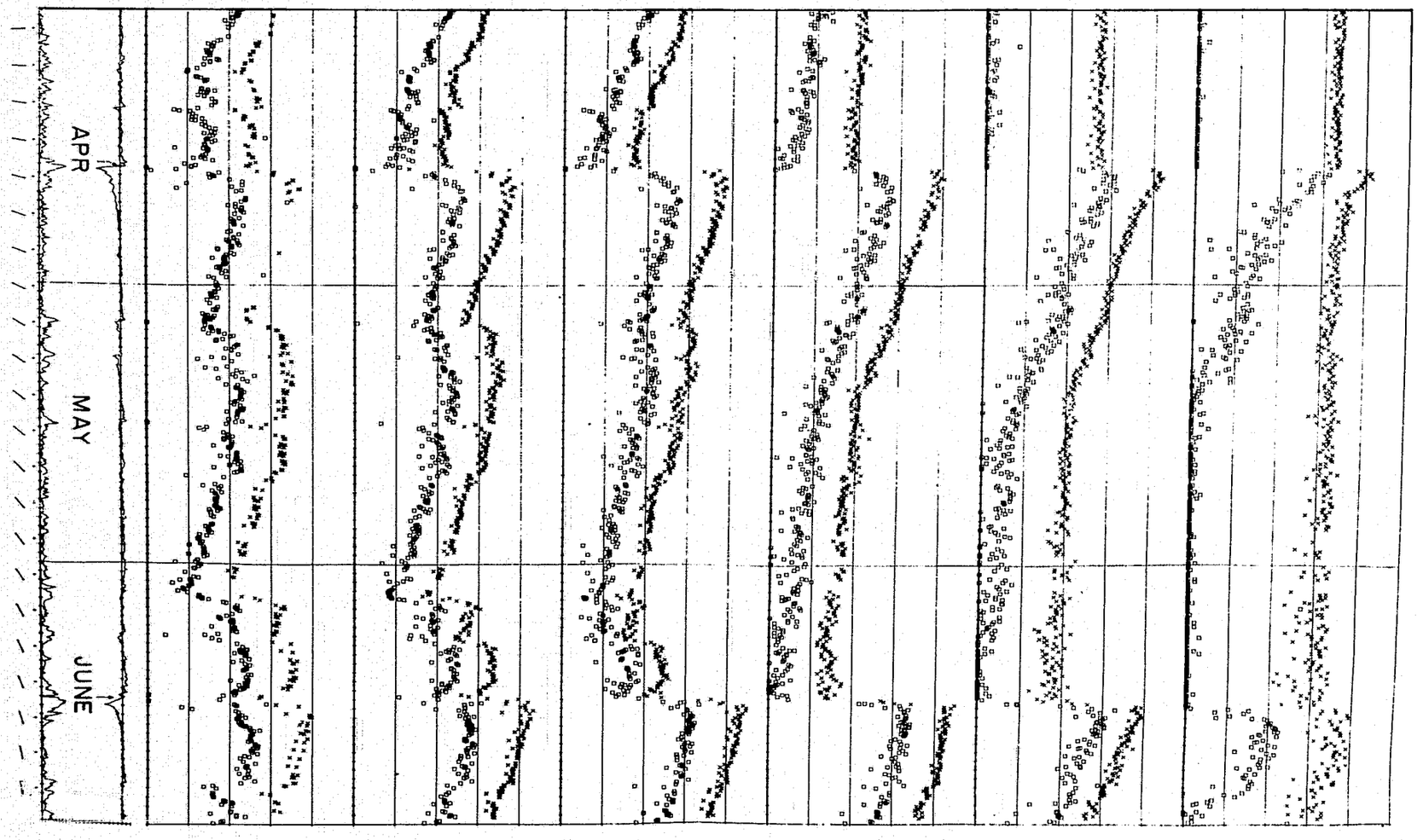

Fig. 2. Simultaneous electron data from the polar-orbiting satellite 1963 38C ($E > 280$ kev), denoted by □, and the near-equatorial satellite Explorer 26 ($E > 300$ kev), denoted by ×, for the period January 1, 1965, through June 29, 1965. The electron data at L = 3.0, 3.5, 4.0, 4.5, 5.0, and 5.5 are shown in terms of counts for each of the experiments counting intervals. See Table 1 for the conversion factors to convert the data to fluxes. Below the electron data are plotted the hourly average D_{st} and the 3-hour average Kp index for the 6-month period.

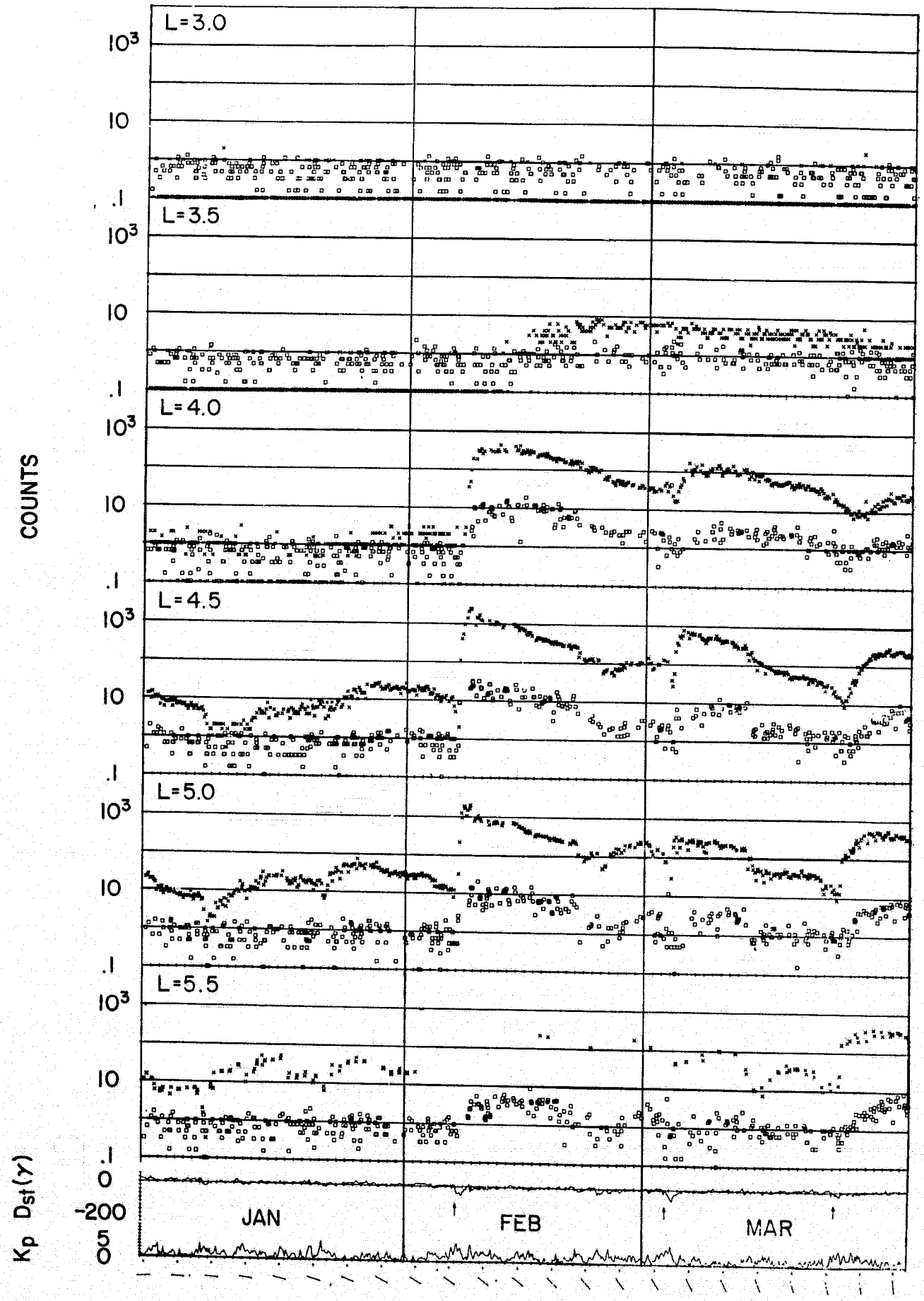
L=3.0
L=3.5
L=4.0
L=4.5
L=5.0
L=5.5
COUNTS
10^3
10
.1
0
-200
K_p D_{st} (γ)
5
0
JAN
FEB
MAR

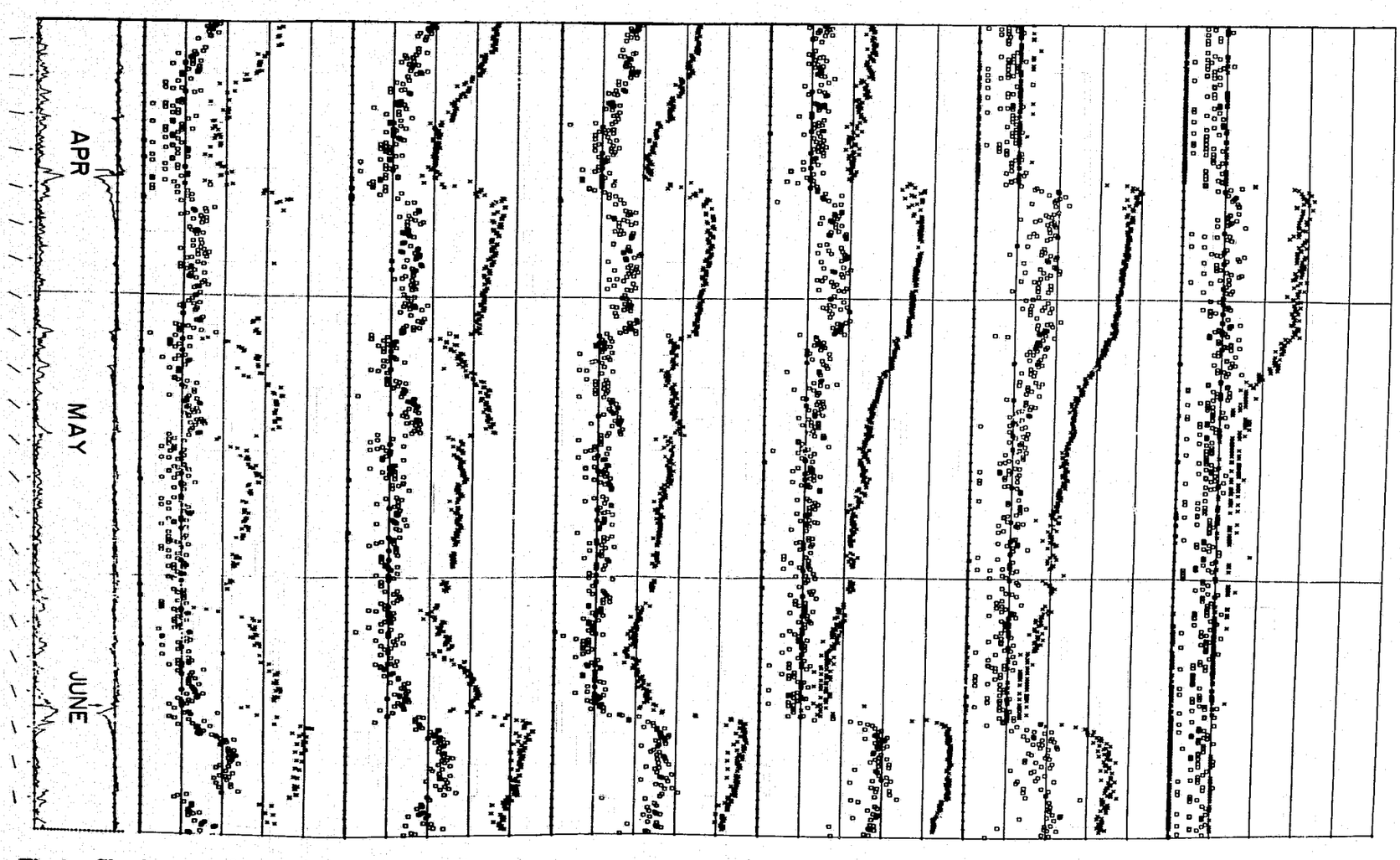

Fig. 3. Simultaneous electron data from the polar-orbiting satellite 1963 38C ($E > 1.2$ Mev), denoted by □, and the near-equatorial satellite Explorer 26 ($E > 1.0$ Mev), denoted by ×, for the period January 1, 1965, through June 29, 1965. The electron data at $L = 3.0$, 3.5, 4.0, 4.5, 5.0, and 5.5 are shown in terms of counts for each of the experiments counting intervals. See Table 1 for the conversion factors to convert the data to fluxes. Below the electron data are plotted the hourly average D_{st} and the 3-hour average Kp index for the 6-month period.

TABLE 1. Conversion Factors for Flux Values

Channel	Multiply Counts by (cm^{-2} $ster^{-1}$ sec^{-1})	Error
1963 38C $\geq$280 kev	600	±100
1963 38C $\geq$1.2 Mev	1200	±400
Explorer 26 $\geq$300 kev	900	±300
Explorer 26 $\geq$1.0 Mev	1200	±400

to equilibrium. The important distinction between identical low-and high-altitude L values (Figures 2 and 3) and a flux tube (line of force) is discussed in later sections of this paper.

Exceptions to the above uniform behavior occur near the beginning of magnetic storms with the appearance of electrons new to these regions of observation. The relative behavior of equatorially mirroring and low-altitude mirroring $\gtrsim$1-Mev electrons differs from the behavior at ~300 kev in that the $\gtrsim$1-Mev electrons do not come quickly to equilibrium after a magnetic storm.

To illustrate these differences, Figures 4 and 5 show an expanded time scale of several days of data taken around the geomagnetic storms of March 2, 1965, and June 15, 1965. Included in the plots are AE indices (D. H. Fairfield, personal communication) along with the D_{st} values.

First, it is noted that all along the field line the $\gtrsim$300-kev electrons rise to their maximum values much faster than do the $\gtrsim$1-Mev electrons. This was observed to hold for all the major storms in the period under consideration in agreement with earlier results [*Freeman*, 1964; *Williams and Smith*, 1965].

Second, it appears that the $\gtrsim$300-kev electrons reach equilibrium within a given flux tube faster than do the $\gtrsim$1-Mev electrons. In Figures 4 and 5 it can be seen that the low-altitude trapped electron intensities at $\geq$280 kev reach their peak value soon after the equatorial intensities and then essentially follow the behavior of the equatorial electron population. In fact, increases in the equatorial to low-altitude intensity ratio are observed to occur only during the 1–3 day period associated with the storm main phase depression for the $\gtrsim$280-kev population. At these times field expansion effects invalidate the concept of both low- and high-altitude L values characterizing the same line of force.

It can further be seen in Figures 4 and 5 that a similar relative behavior between equatorially mirroring and low-altitude mirroring electrons is not observed at $\gtrsim$1 Mev. Not only do the low-altitude $\gtrsim$1-Mev trapped electron intensities generally reach peak values well after the equatorial intensities, but in several instances they continue to increase in intensity long after the equatorial intensities have begun their decay (e.g., $L = 4.5$, Figure 4; $L = 5.0$, Figure 5). In addition, variations in the equatorial to low-altitude intensity ratio are observed to last generally for several days beyond the main phase depression. Thus, the time to attain equilibrium along a given L shell appears significantly longer at $\gtrsim$1 Mev than at $\gtrsim$300 kev.

A detailed study of the data in Figures 2 and 3 reveals a wide variety of electron intensity fluctuations that may be associated with various geomagnetic perturbations. In this paper we have chosen to study events characterized by large intensity increases occurring throughout the region of observation that could be associated with a well-defined magnetic storm. This study will thus emphasize the nonadiabatic appearance of new particles in the region of observation and the subsequent behavior of these particles.

The storms studied are indicated by the arrows in Figures 1 and 2 and are listed in Table 2. The D_{st} zero crossing time is the time at which the D_{st} values cross and remain below the zero level as the initial phase of the storm begins.

An important parameter in characterizing the outer-zone electron response to major magnetic perturbations is the arrival time of the bulk of new particles within a flux tube. The accurate determination of the start of the particle increase associated with the initial phase of the storm is complicated by several factors: (1) adiabatic effects due to sudden commencement compressions and ring current decompressions of the magnetosphere before and during the development of the storm, (2) the appearance

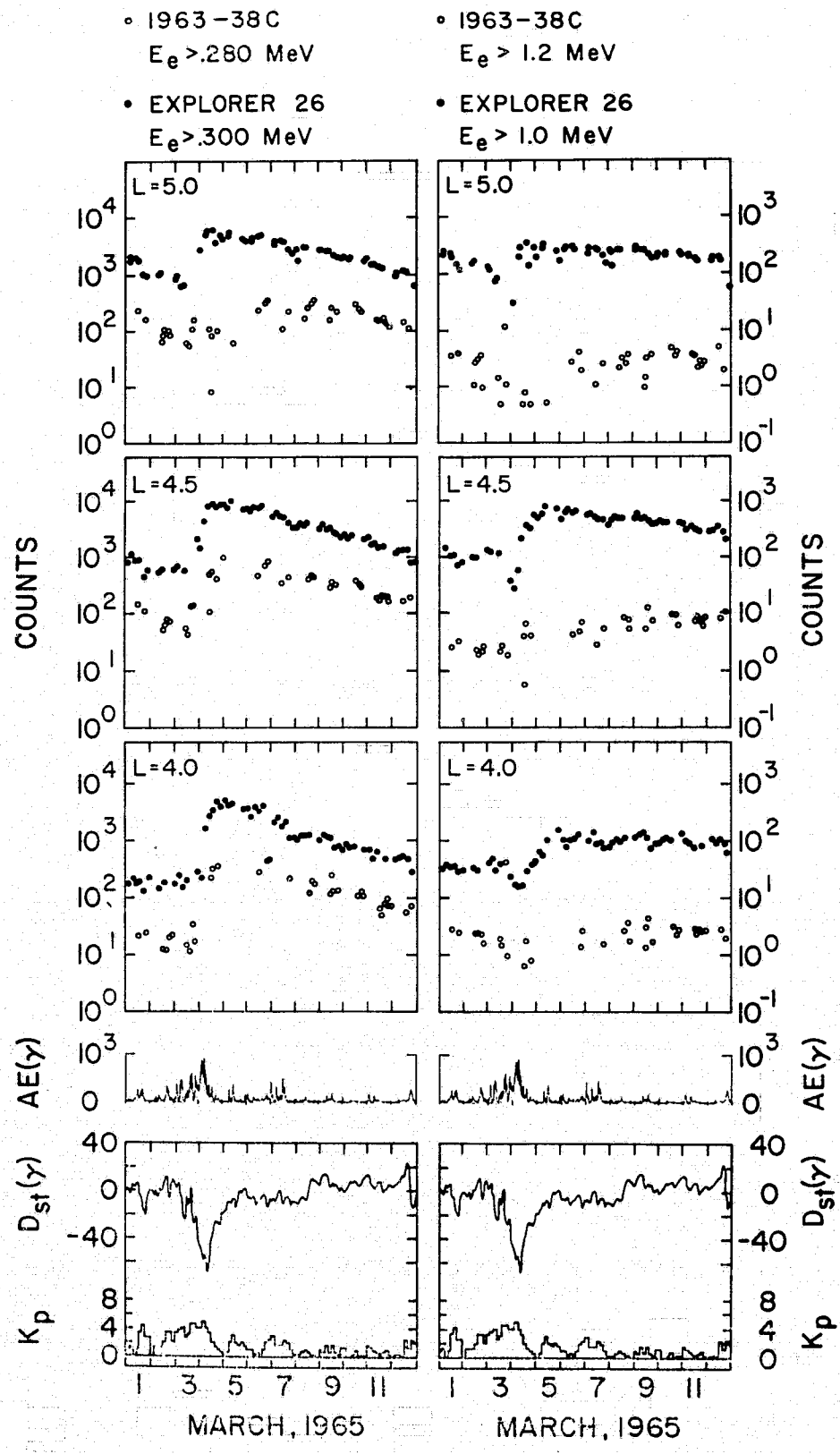

Fig. 4. Simultaneous electron data from the polar-orbiting satellite 1963 38C ($E > 280$ kev and $E > 1.2$ Mev) and the near-equatorial satellite Explorer 26 ($E > 300$ kev and $E > 1.0$ Mev) for March 1 through March 12, 1965. Electron data at $L = 4.0$, 4.5, and 5.0 are shown during the period of the March 3 geomagnetic storm. Below the electron data are plotted the *AE* index, D_{st}, and the *Kp* index.

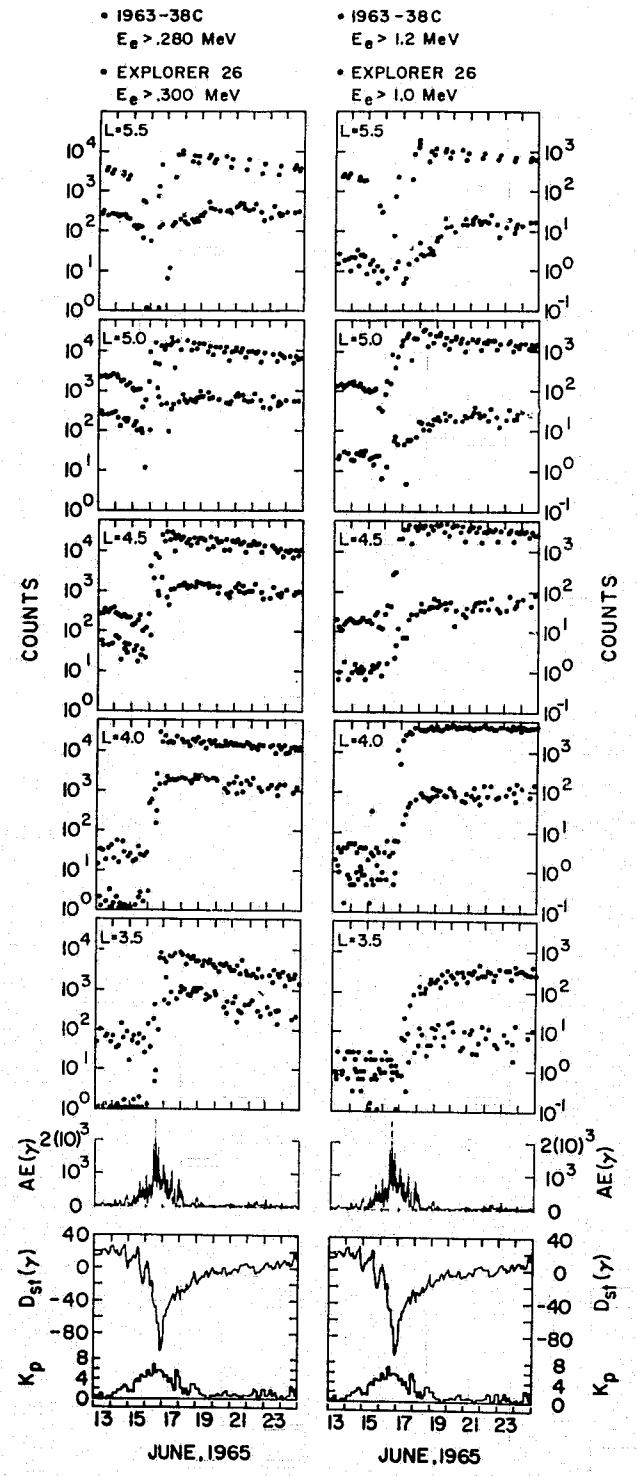

Fig. 5. Simultaneous electron data from the polar-orbiting satellite 1963 38C ($E > 280$ kev and $E > 1.2$ Mev) and the near-equatorial satellite Explorer 26 ($E > 300$ kev and $E > 1.0$ Mev) for June 13 through June 25, 1965. Electron data at $L = 3.5$, 4.0, 4.5, 5.0, and 5.5 are shown during the period of the June 15 geomagnetic storm. Below the electron data are plotted the *AE* index, D_{st}, and the *Kp* index.

TABLE 2. Major Storms Studied in Period January 1 to June 29, 1965

Date	sc	Maximum D_{st}, γ	D_{st} Zero Crossing Time
Feb. 6	1414 hours	−55	0130 hours, Feb. 7
March 2	1349–1458 hours <10 stations reported sc	−68	1700 hours, March 3
March 22	None	−31	0330 hours, March 23
April 17	1313 hours	−137	0330 hours, April 18
June 15	1100 hours	−102	0400 hours, June 16

of particles associated with polar substorm events that may not be associated with the large bulk increases of electron intensities during the storm main phase, (3) the measurement by an individual satellite of relative arrival times of particles on various L shells has a resolution governed by the satellite's orbital motion and, (4) the fact that all of the preceding effects have strong spatial variations.

In an attempt to minimize these difficulties, we have used the time for the electron intensity increases to reach one-half of their maximum value, $t_{m/2}$, as a measure of the arrival time on a given L shell of energetic electrons associated with a main phase geomagnetic storm. Generally, (see Figure 1) the larger intensity increases are rapid enough so that $t_{m/2}$ is quite insensitive to the above effects. The time for the observed intensity increases to attain full peak values on a given L shell was not used as a characteristic arrival time because it is very sensitive to diffusion effects and is therefore significantly less accurate than $t_{m/2}$. However, as the time of maximum intensity increase may frequently be very difficult to obtain, the intensity at maximum can be measured quite accurately, thus allowing a determination of $t_{m/2}$ to an accuracy not realized in finding the time of maximum.

Some of these various problems are illustrated by the data in Figures 6 and 7. Figure 6 shows a sequence of low-altitude outer-zone profiles along with D_{st} and *AE* plots just before and during the initial phase of the February 5, 1965, magnetic storm. Pass 1, occurring close to the

sudden commencement, displays no noticeable effects, and is shown for orientation purposes. Pass 2 is closely associated with the occurrence of a polar substorm as indicated by the spike in the *AE* indices and shows an intensity enhancement at high latitudes. Simultaneous data obtained from the 1963 38C proton spectrometer show that this enhancement was due to electrons only [*Bostrom et al.*, 1967]. Passes 3 and 4, obtained at the start of the initial phase, show the subsequent loss of these high-latitude electrons. Such a loss may be explained by a combination of adiabatic effects and loss from the trapping regions. Pass 5 shows the appearance of large numbers of trapped $\geq$280 kev electrons on the lower L shells. Pass 6 obtained at the recovery of D_{st} to approximately prestorm values shows the additional appearance of electrons at $5 \leq L \leq 9$. This may be the combined result of electrons injected at low L shells diffusing outward and electrons injected near the equator diffusing down the field line to these low altitudes.

It is seen from Figure 6 that the bulk of the electrons associated with this main phase storm appear between passes 4 and 5. The appearance of particles on high L shells during pass 2, which are associated with a polar substorm, would yield a false start time for the bulk of the particles associated with the main phase D_{st} decrease. The use of $t_{m/2}$ avoids the above difficulty.

Figure 7 again shows the February 5, 1965, storm but from the perspective of a time history of the comparison between the high-altitude and low-altitude data. Explorer 26 and 1963 38C data are shown for $E_e \gtrsim 300$ kev for $L = 4.0$ and 5.0. D_{st} and AE values are also included. The Explorer 26 data show the appearance of electrons at $L = 5.0$ occurring significantly before $L = 4.0$ [*Lanzerotti*, 1968]. However, the above arguments indicate that the two Explorer 26 points after the sudden commencement at $L = 5.0$ may be associated with the polar substorm occurring at that time and before the start of the storm main phase. The 1963 38C data shown at $L = 5.0$ also display an increase at this time but the following data point at the beginning of the storm initial phase shows the decrease discussed in Figure 6 above. It is possible that the Explorer 26 observations at $L = 5.0$ simply missed this decrease due to sampling resolution. The rapid rise and the

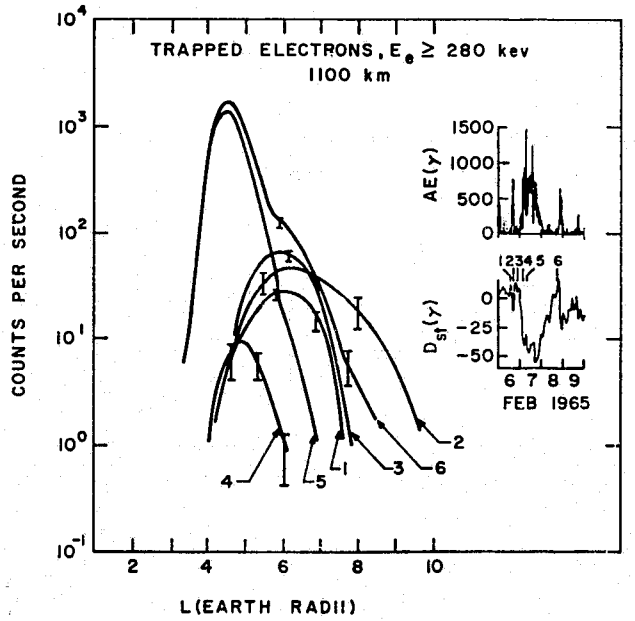

Fig. 6. Sequence of low-altitude trapped electron outer-zone profiles obtained by satellite 1963 38C during the February 6, 1965, magnetic storm. Numbered arrows in plot of D_{st} and AE values indicate time sequence of respective numbered passes. Note initial high-latitude appearance of electrons associated with substorm during main field compression, their subsequent loss to these low-altitude regions, and the later arrival of the bulk of energetic electrons associated with the storm main phase.

magnitude of the main electron intensity increase indicates again that $t_{m/2}$ is not very sensitive to the above effects.

Thus, from the above arguments we feel that $t_{m/2}$ is a more accurate measure of the characteristic time of arrival of energetic particles associated with a main phase geomagnetic storm than either the start of an intensity increase or the time to the maximum increase.

Results

Figures 8–12 show plots of $t_{m/2}$ as a function of L value for low-altitude mirroring electrons ($E_e \geq 280$ kev and $\geq$1.2 Mev) and near equatorially mirroring electrons ($E_e \geq 300$ kev and $\geq$1.0 Mev) for the five magnetic storms being studied. Also shown in Figures 8–12 are the maximum intensities attained during the respective storms for the various energies and altitudes observed.

These data show that there tends to exist for both the low-altitude and high-altitude data, a range of L values, which is associated with both a minimum in $t_{m/2}$ and a maximum in the

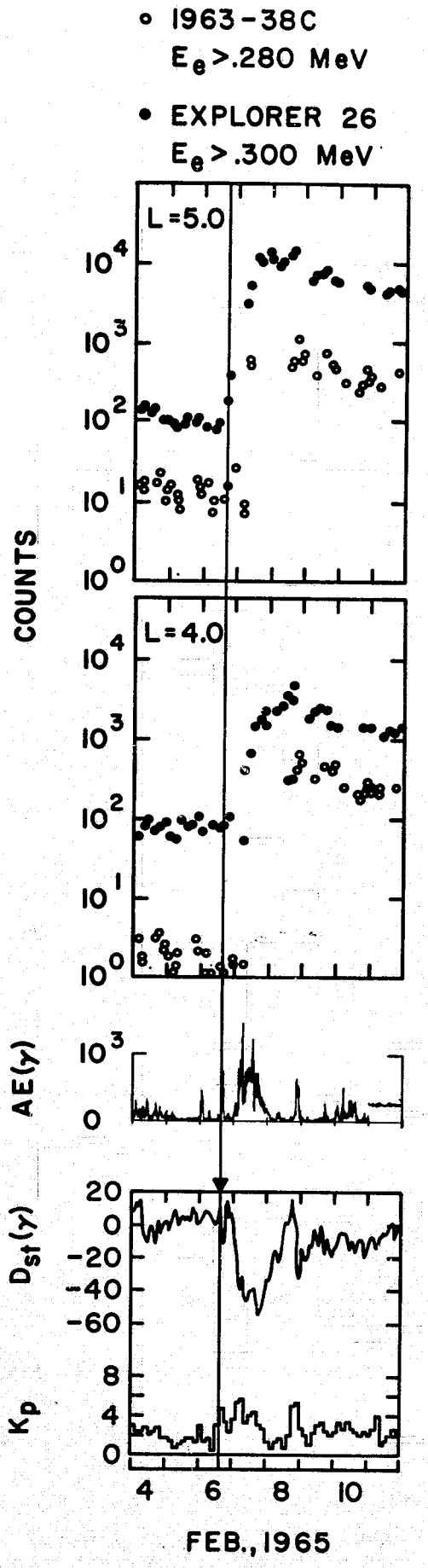

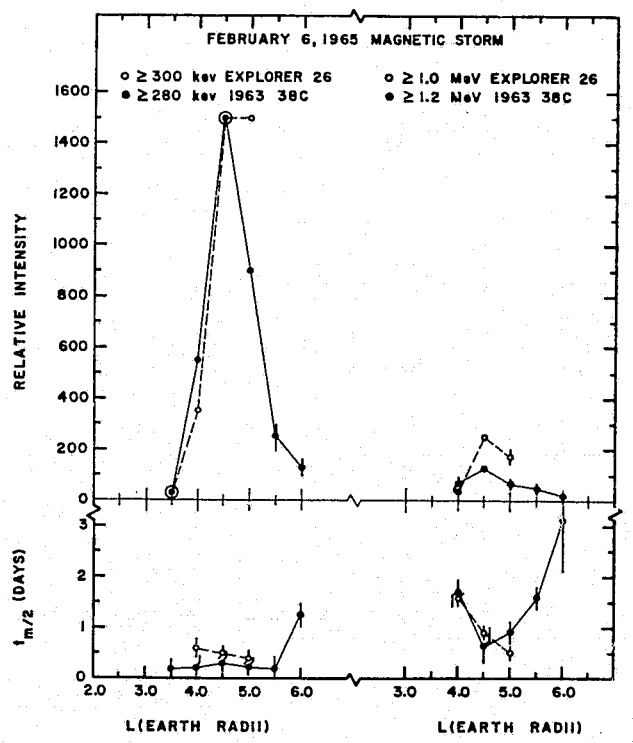

Fig. 8. February 6, 1965, geomagnetic storm. The maximum storm electron intensities and the time required for the intensities to reach half their peak values ($t_m/_2$) are plotted versus L for the high- and low-energy electrons observed on 1963 38C and Explorer 26. Explorer 26 $\geq$300 kev and $\geq$1.0 Mev data have been multiplied by 0.1, and 1963 38C $\geq$1.2 Mev data have been multiplied by 5. Using these factors, fluxes may be obtained from the conversion constants in Table 1.

number of newly observed electrons (see in particular Figures 11 and 12). This indicates that energetic electrons may appear during a main phase geomagnetic storm well within the stable trapping regions and subsequently diffuse both in toward lower L shells and out toward higher L shells. This observation is significant as it

Fig. 7. Simultaneous electron data from 1963 38C ($E > 280$ kev) and Explorer 26 ($E > 300$ kev) during the February 6, 1965, geomagnetic storm. Below the electron data are the AE and Kp indices and the equatorial D_{st}. The equatorial electron data show the first particle increases at $L = 5$, apparently correlated with the AE spike at the time of the sudden commencement. The low-altitude electron data also indicate an increase at this time. However, a decrease occurs after this substorm but before the storm main phase and major electron increase (see also Figure 6). Equatorial data are not available during this time interval.

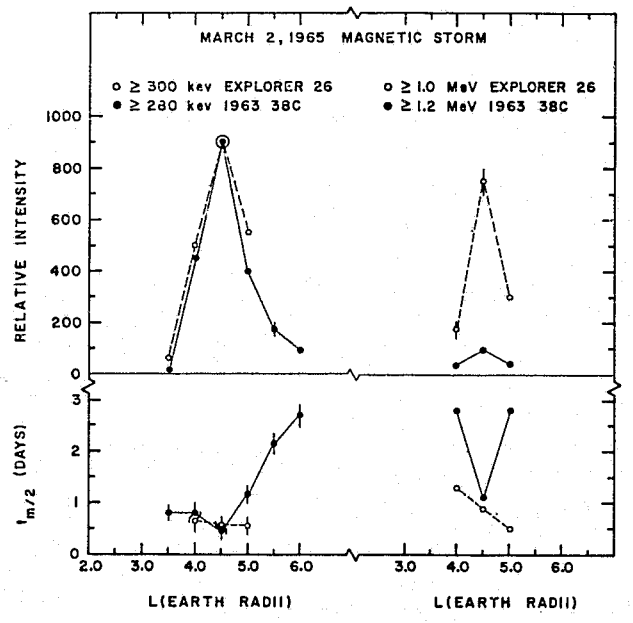

Fig. 9. March 2, 1965, geomagnetic storm. The maximum storm electron intensities and the time required for the intensities to reach half their peak values ($t_{m/2}$) are plotted versus L for the high- and low-energy electrons observed on 1963 38C and Explorer 26. Explorer 26 $\geq$300 kev data have been multiplied by 0.1, and 1963 38C $\geq$1.2 Mev data have been multiplied by 10. Using these factors, fluxes may be obtained from the conversion constants in Table 1.

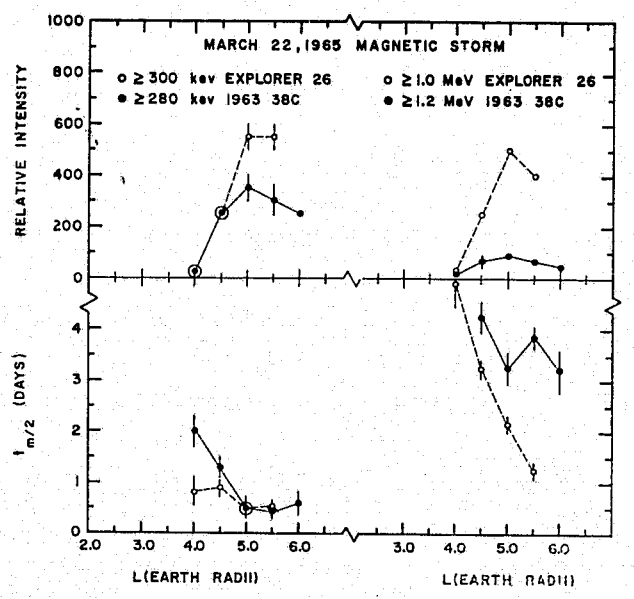

Fig. 10. March 22, 1965, geomagnetic storm. The maximum storm electron intensities and the time required for the intensities to reach half their peak values ($t_{m/2}$) are plotted versus L for the high- and low-energy electrons observed on 1963 38C and Explorer 26. Explorer 26 $\geq$300 kev data have been multiplied by 0.1, and 1963 38C $\geq$1.2 Mev data have been multiplied by 10. Using these factors, fluxes may be obtained from the conversion constants in Table 1.

shows that the source of these outer zone electrons is not necessarily the diffusion inward of a low-energy electron population located at the outer edge of the stable trapping region. In fact, a distant lower energy electron population will result from the outward diffusion of an energetic electron population appearing initially at low L shells. Before discussing our interpretation of the significance of these results, we shall discuss briefly the electron data for each of the storms under consideration.

February 6, 1965. The data from this storm are presented in Figure 8. The maximum intensities observed at 1100 km occurred at $L \simeq 4.5$ for both the $\geq$280 kev and $\geq$1.2 Mev electrons. The equatorial electrons show a maximum intensity at $L \simeq 4.5$ at $\geq$1.0 Mev and $L \simeq 4.5$–5.0 at $\geq$300 kev.

The data for $t_{m/2}$ are not as clear. The 1100-km data indicate a minimum at $L \simeq 4.5$ at

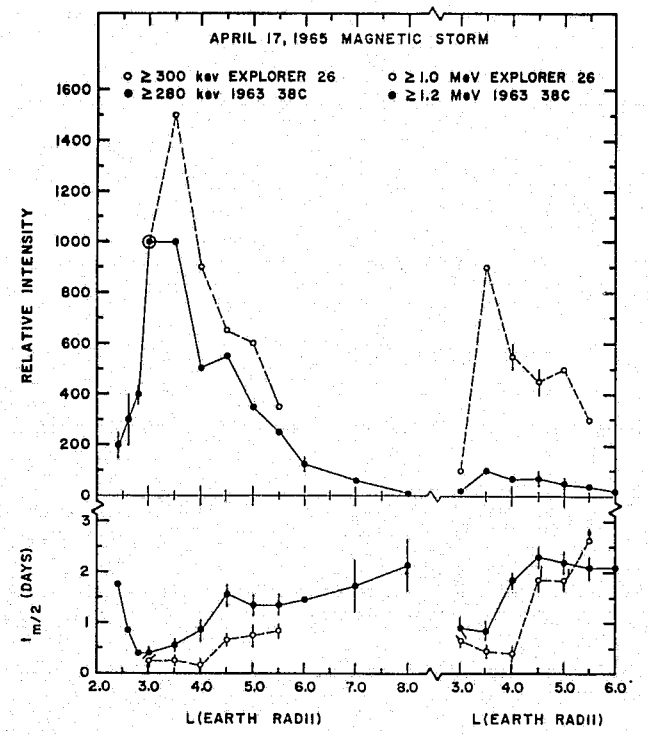

Fig. 11. April 17, 1965, geomagnetic storm. The maximum storm electron intensities and the time required for the intensities to reach half their peak values ($t_{m/2}$) are plotted versus L for the high- and low-energy electrons observed on 1963 38C and Explorer 26. Explorer 26 $\geq$300 kev data have been multiplied by 0.1, and 1963 38C $\geq$1.2 Mev data have been multiplied by 10. Using these factors, fluxes may be obtained from the conversion constants in Table 1. A possible second appearance of electrons was observed in the region $L = 4.5$–5.5.

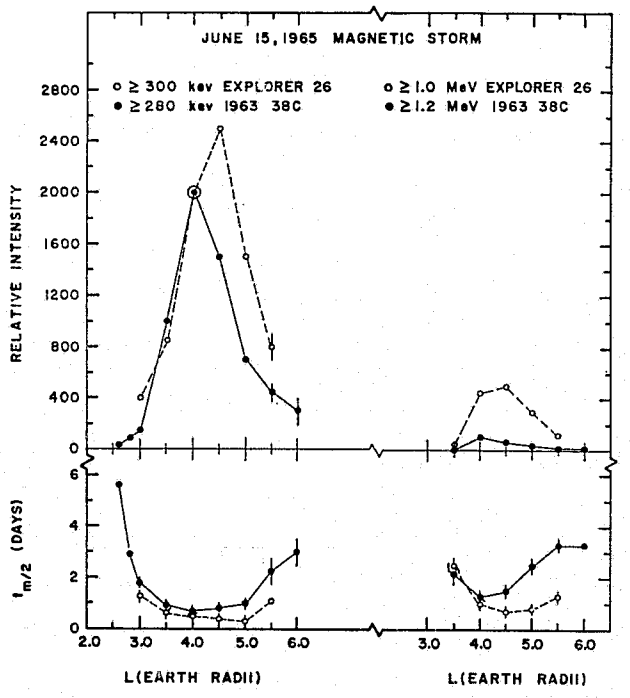

Fig. 12. June 15, 1965, geomagnetic storm. The maximum storm electron intensities and the time required for the intensities to reach half their peak values ($t_{m/2}$) plotted versus L for the high- and low-energy electrons observed on 1963 38C and Explorer 26. Explorer 26 $\geq$300 kev and $\geq$1.0 Mev data have been multiplied by 0.1. Using these factors, fluxes may be obtained from the conversion constants in Table 1. A very broad region (L = 3.5–5.0) of initial electron appearance was observed.

$\geq$1.2 Mev and a broad minimum from $L \simeq$ 3.5–5.5 for the $\geq$280-kev electrons. While the $\geq$280-kev data may be fit with a curve yielding a minimum $t_{m/2}$ consistent with the $\geq$1.2-Mev data, the difference in the width of the curves may be due to the source being sufficiently strong only at $L \simeq 4.5$ to produce a significant number of $\geq$1.2-Mev electrons.

The equatorial data points for $t_{m/2}$ indicate that both $\geq$300-kev and $\geq$1.0 Mev-electrons initially arrive beyond the region of observation, i.e., $L > 5.0$.

March 2, 1965. The data for this storm, given in Figure 9, show a maximum intensity for all observed electrons at $L \simeq 4.5$. This agrees with the observed minimum shown in $t_{m/2}$ for low-altitude mirroring electrons both at $\geq$280 kev and $\geq$1.2 Mev. The equatorial data are consistent with a minimum $t_{m/2}$, occurring over a relatively broad region at $L \gtrsim 4.5$ for the $\geq$300-kev electrons and beyond the observation region, $L > 5$, for the $\geq$1.0-Mev electrons.

The indication that the high-altitude minimum $t_{m/2}$ may be displaced toward higher L shells from the low-altitude minimum $t_{m/2}$ may be simply due to the geomagnetic field expansion during the storm main phase.

March 22, 1965. The data for this storm are shown in Figure 10. Maximum intensities are observed in the vicinity of $L \simeq 5$ for all electrons.

The minimum $t_{m/2}$ shown by the lower energy electrons matches the position of maximum intensities for these particles. The low-altitude $\geq$1.2-Mev data are not clear, and the equatorial $\geq$1.0-Mev data show that if a minimum $t_{m/2}$ exists it is at or beyond $L = 5.5$. The differing characteristics of the $\geq$300 kev and $\geq$1.0 Mev $t_{m/2}$ plots may be due to spatial variations in the source.

Figure 13 shows diffusion rates obtained from Figure 10, assuming that the apparent inward motion of the near-equatorial $\geq$1-Mev electrons is due solely to cross-L diffusion. The magnitude of the diffusion rates shown in Figure 13 are of

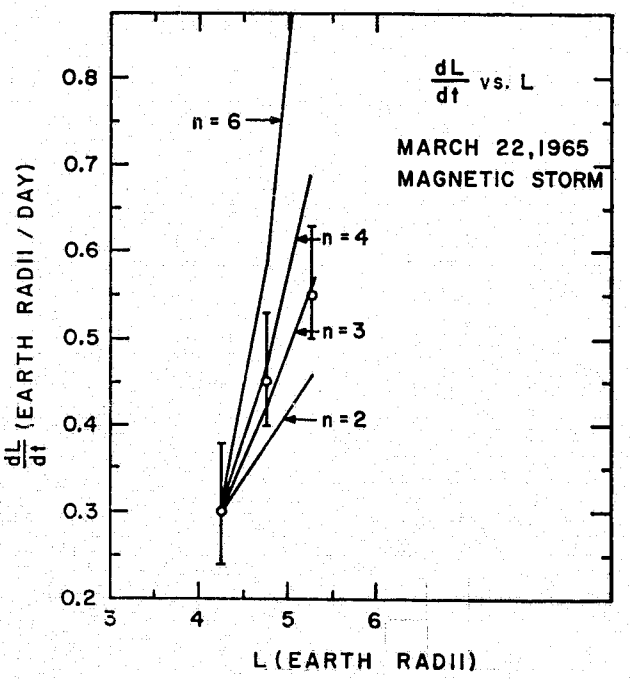

Fig. 13. Rate of apparent inward motion for the equatorial $E > 1.0$-Mev electrons plotted versus L from the March 22, 1965, geomagnetic storm (Figure 10). These data show the clearest example of possible inward electron diffusion for the storms examined. Plots of $dL/dt = L^n$ for several values of n are shown along with the data.

the same order as those reported by *Frank* [1965*b*] for the $L \sim 4.5$ region. However, the L^{-3} dependence shown in Figure 13 is in marked contrast to the L^{-8} diffusion rate dependence observed by *Frank* [1965*b*]. This may be due to the fact that the diffusion rates reported here were obtained shortly after a magnetic disturbance and may thus be related to transient activity associated with the storm. *Frank*'s [1965*b*] observations were obtained over a several-week period following an interval of enhanced magnetic activity and may thus represent more nearly quiescent magnetospheric conditions. The situation with the low-altitude $\geq$1.2-Mev electrons in Figure 10 is not clear since these regions are affected by diffusion down a flux tube as well as cross-L diffusion.

April 17, 1965. Figure 11 shows the electron data for this storm. Here the low-altitude $\geq$280-kev electrons displayed a maximum intensity at $L = 3.0$–3.5 and the equatorial $\geq$300-kev electrons peak at $L = 3.5$. Both the $\geq$1.2-Mev electrons mirroring at 1100 km and the $\geq$1.0-Mev electrons mirroring near the equator show a major peak at $L = 3.5$.

All observed electrons display a well-defined minimum $t_{m/2}$ at low L shells with the equatorial values being displayed toward higher L shells relative to the low-altitude values.

This storm shows a well-defined case of electrons initially appearing well within the trapping regions and subsequently diffusing in toward lower L shells and outward toward higher L shells (see also Figure 12). Note that the low-altitude $\geq$280 kev data show a much steeper $t_{m/2}$ curve toward lower L values than toward higher L values, in qualitative agreement with diffusion theory under conservation of the first two adiabatic invariants. A similar observation was reported for the October 24, 1963, magnetic storm where the time interval T_D between peak magnetic activity and attainment of peak $\geq$280-kev electron intensities was measured as a function of L [*Williams and Smith*, 1965]. It was found that $T_D \sim 0.3$ days at $L = 3$ increased to $\sim$4.3 days at $L = 2.5$ and also continuously increased to $\sim$4 days as L increased to $\sim 9\ R_E$.

Note also that all the data in Figure 11 show a definite change in character in the region of $L = 4.5$–5.5. The intensity plots either show a secondary maximum or a definite change of slope. The $t_{m/2}$ curves show either a secondary minimum or also a change of slope. We interpret this as evidence for a secondary appearance of electrons during this storm, occurring about 1.3 days after its start. Thus, Figure 11 shows a major arrival of energetic electrons occurring very shortly ($<$0.4 days) after the beginning of the storm in the region $L \simeq 3$–3.5 followed by an apparent secondary appearance of energetic electrons about one day later at $L \sim 4.5$–5.5.

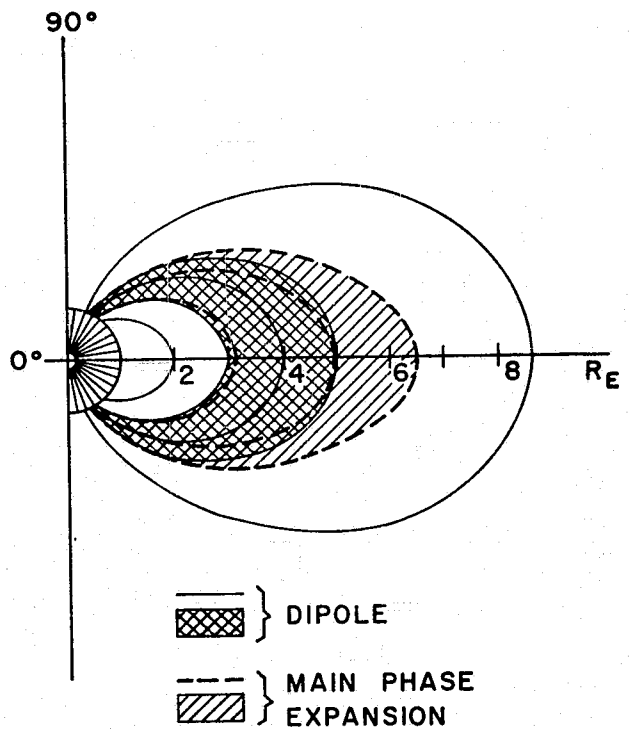

Fig. 14. Diagram, not to scale, qualitatively showing the projection of a wide source region in equatorial regions to a narrow latitude interval at low altitudes. Projection during a main phase field expansion shown as cross-hatched section. Dipole projection shown as shaded section for comparison.

The minimum $t_{m/2}$ values are not only displaced toward higher L shells at the equator but are also seen to have broader minima. This is in general agreement with the mapping of a flux tube from the equator to low altitudes during a period of enhanced field expansion. Figure 14 qualitatively illustrates this effect.

June 15, 1967. The data for this storm are shown in Figure 12. These data display broader maximum intensities and minimum $t_{m/2}$ curves than generally shown by the previous storms. In particular the $t_{m/2}$ plots indicate the arrival of energetic electrons at the equator and at low altitudes over a wide range of L values, but still

within the trapping regions. The equatorial values are again displaced toward higher L shells for both the maximum intensity and minimum $t_{m/2}$. Also, the L dependence of the slope of the $t_{m/2}$ plot is in qualitative agreement with cross-L diffusion theory, as in the April 18 storm (see Figure 11).

All storms. The energetic electron response to these main phase storms varies systematically with the size of the storm. To show this we have obtained, from Figures 8–12, the L shell at which the minimum $t_{m/2}$ and maximum intensity occur. These L values (or their lower limits) are shown in Figure 15 for all energies and altitudes observed as a function of maximum D_{st} occurring during the storm. These maximum D_{st} values are listed for each storm in Table 2.

It is seen that the L value associated with the maximum intensity and earliest arrival of new energetic particles decreases as the size of the storm increases, in agreement with previous low-altitude results [*Arens and Williams*, 1967]. In addition, the use of L as a parameter yields an apparent indication of the distortion present in the expanded field. The data associated with minimum $t_{m/2}$ in Figure 15 falls into two groups, the low-altitude and the near-equatorial trapped electrons. Assuming that the energetic electrons first observed at both low and high altitudes are within the same flux tube, the $t_{m/2}$ data indicate that, for a storm of $D_{st}^{max} \simeq -140$ γ, an expansion of $\sim$0.5 R_E occurs at an altitude of $\sim$3.2 R_E while for a D_{st}^{max} of $\simeq -30$ γ an expansion of $\simeq$0.2 R_E occurs at $\sim$5.2 R_E. That is, a field line crossing the equator at $\sim$3.2 R_E during quiescent conditions will cross the equator at $\sim$3.7 R_E during a main phase storm when $D_{st} \simeq -140$ γ.

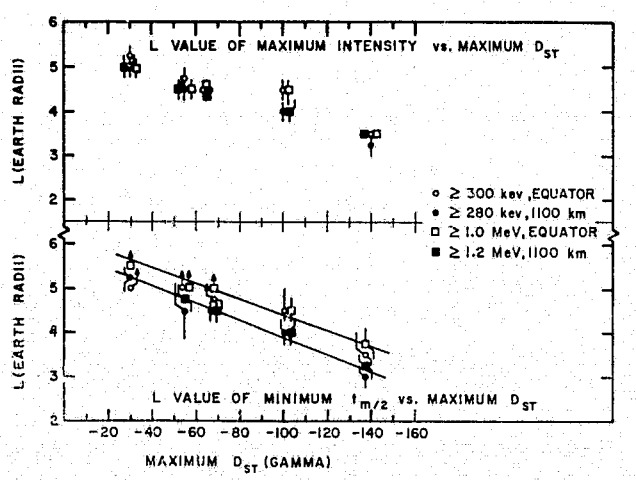

Fig. 15. (*a*) The L value of maximum electron intensity plotted versus the peak D_{st} value for the five geomagnetic storms examined in Figures 8–12. Both energies at both low and high altitudes are included. (*b*) The L value of the earliest $t_{m/2}$ plotted versus the peak D_{st} value for the same five geomagnetic storms. A separation, attributable to a measure of the magnetospheric expansion, is observed between the high- and low-altitude electron data.

The expansion shown in Figure 13 for the 140 γ storm of April 17, 1965, agrees well with the more accurate values of $\Delta R \sim 1$ R_E at R ~ 4 R_E and $\Delta R \sim$0.5 R_E at $R \sim 3$ R_E obtained by L. R. Davis (personal communication), utilizing field expansion data of *Cahill* [1966] obtained during this storm. The expansion noted at $\sim$5.2 R_E for a 30-γ storm is a lower limit since equatorial minimum $t_{m/2}$ were not observed within the region of observation.

The position of maximum intensity in Figure 15 does not display any readily discernable expansion effect. This is because the position of maximum intensity is strongly affected by diffusion down a flux tube and cross-L diffusion. The minimum $t_{m/2}$ values are not significantly affected by these effects since they occur within 0.5 day of the beginning of the storm initial phase and, thus, before significant diffusion takes place.

Decay times. Figures 2 and 3 show a variety of particle decreases including decay effects over an extended time period. Since the decay time measured by a threshold detector is affected in a complex way by energy loss mechanisms as well as particle transport processes, care has to be exerted in the interpretation of such decay times.

The lifetimes, τ, for both the low-altitude $\geq$280 kev electrons and the equatorial $\geq$300-kev electrons are shown in Figure 16 for two different time periods after the April 17, 1965, magnetic storm. The lifetime measured is the time for the electron intensities to reach e^{-1} of their initial value.

The upper portion of Figure 16 shows a plot of τ versus L for the immediate post-storm period, April 19–22.5, 1965. No points are shown for $L \geq 4.5$ since the intensities in these regions never decayed during the immediate post-storm period. The bottom of Figure 16 shows τ versus L for the long-term post-storm period of April 22.5 to May 3, 1965. The error bars on the data

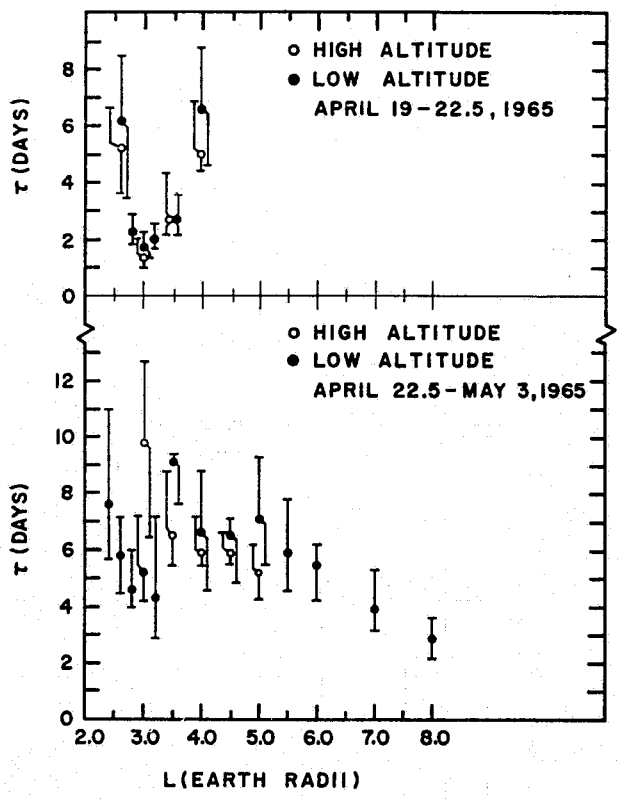

Fig. 16. Lifetimes (time to e^{-1} of initial value) for energetic electrons plotted versus L for two periods after the April 17, 1965, geomagnetic storm. (a) Lifetimes for the immediate post-storm period, April 19–April 22.5, 1965. Data beyond $L = 4.0$ were not available because outward electron diffusion was still operative during portions of this time period at the higher L values, and no decay was observed. (b) Lifetimes for the post-storm period April 22.5–May 3, 1965. The decay rates at the low L values have increased by a factor of about 2 over the rates in (a) at $L = 2.6$–3.5. At all L values, for both periods of time, the decay rates observed for these energetic electrons at high and low altitude are nearly identical.

points are not standard deviations but are upper and lower limits obtained by visually fitting the data points with a straight line on a logarithmic plot.

Not only do the low-altitude and high-altitude data display similar lifetimes for ~300-kev electrons, but their immediate post-storm and long-term post-storm behavior agree. It is seen that immediately after the storm the decay times out to $L = 3.5$ are significantly shorter than the long-term decay times. This effect is difficult to observe at $L = 4$, and no comparisions can be made for $L > 4$.

This effect may be simply due to the fact that energy loss and particle transport mechanisms may be enhanced during the time when the magnetosphere is perturbed by the storm, and, as the storm subsides, the loss mechanisms and subsequent decay approach a more normal mode. The fact that Figure 16 shows this effect in the region around $L = 3$ may be due to this being the region of initial appearance of energetic electrons during the storm and thus probably the region of greatest magnetoelectric perturbations.

Discussion

Losses. As pointed out earlier, Figures 2–5 show that generally the ~300-kev electrons on a given L shell rapidly ($\lesssim$1–2 days) come to equilibrium after a large geomagnetic storm.

The differences in response on a particular L shell of the low-altitude $\geq$280-kev electrons and the equatorial $\geq$300-kev electrons at the beginning of a storm may be due to (a) field expansions that invalidate a constant L label for an entire flux tube (Figure 15) and (b) the appearance of new particles having an anisotropic pitch-angle distribution.

A good example of pitch-angle effects during the appearance of new particles can be seen by examining the unidirectional electron data obtained by Explorer 26 at $L = 5\ R_E$ during the onset of the April 17 storm. Explorer 26 was at apogee during the onset of the storm and measured the first two hours of electron flux increases [*Brown and Roberts*, 1966]. In addition to the omnidirectional measurements, the $\geq$450-kev electron flux was also sampled rapidly during one satellite rotation to give a measure of the unidirectional counting rate. This measured unidirectional data was reduced to absolute unidirectional flux as a function of the cosine of the electron pitch angle for each complete set of measurements taken during a satellite rotation.

Each set of unidirectional electron data was then fit by least squares (using two independent variables) to the function, flux $= A[1 - (\mu_0^2/\mu_{0C}^2)]^S$, [*Roberts*, 1965] where $\mu_0 = \cos \alpha_0$, α_0 = equatorial pitch angle, and μ_{0C} is the loss cone. The variable A is for normalization purposes. Figure 17 contains a plot of the exponent S versus time during the April 17 storm. The behavior of S shows that the pitch-angle distribution was initially peaked toward $\cos \alpha_0 = 0$ and changed to a rather uniform distribution

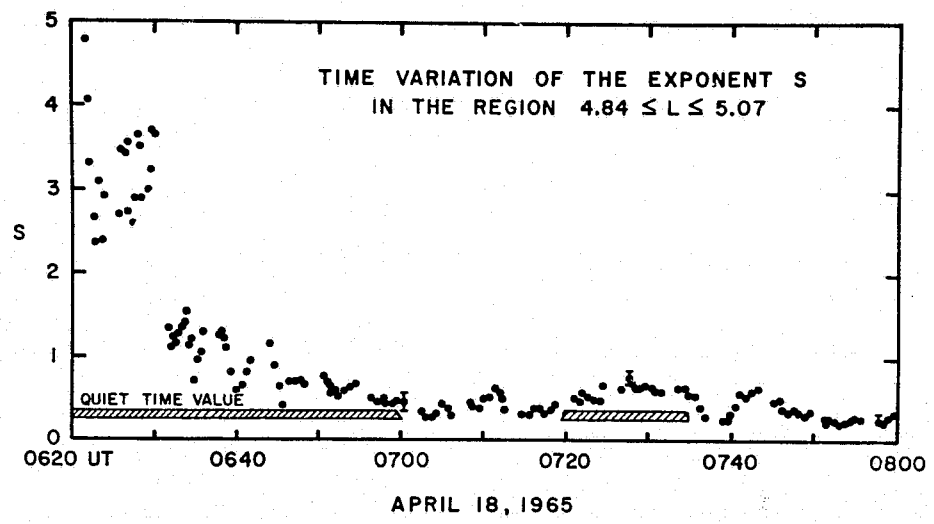

Fig. 17. Plot of the value of the exponent s in the fit to the pitch-angle electron data ($E > 0.45$ Mev) versus time during the onset of the April 18, 1965, geomagnetic storm near $L = 5\ R_E$. The exponent s very rapidly tends toward the quiet time value after the $L = 5$ storm onset at about 0620. This indicates that an initial electron population, peaked in pitch-angle distribution at the equator, rapidly changes to a rather uniform electron flux population over all pitch angles.

over all pitch angles in less than two hours certainly and possibly less than one hour.

We thus conclude that equilibrium within a given *flux tube* is attained rapidly for >300-kev electrons ($\lesssim$0.1 day) and that the longer periods (~1–2 days) of nonuniform behavior on a given *L shell* (Figure 2) for $\geq$300-kev electrons are due to field expansion during the storm (Figure 15).

The uniform behavior of the ~300-kev electron population throughout a given flux tube causes the long-term ($\gtrsim$0.5 day) diffusion and decay to appear to be independent of pitch-angle at these energies. It was seen above that the initial energization (injection) was pitch-angle dependent but rapidly ($\lesssim$2 hours) reached an equilibrium distribution. The simplest conclusion to be drawn from these facts appears to be that the rapidity of the pitch-angle diffusion mechanism causing electrons to diffuse down the line of force makes the slower processes (cross-L diffusion and decay) appear to be pitch-angle independent.

The ~1-Mev electron population does not display the same general appearance of pitch-angle independence for diffusion and decay as does the ~300-kev population. This can be seen from Figures 2–5 where the ~1-Mev electrons take significantly longer to attain equilibrium than do the ~300-kev electrons. In fact, Figure 4 shows a case where all 300-kev electrons are well into a decay mode along with the equatorial ~1-Mev electrons. However, the low-altitude ~1.2-Mev electrons continue to increase.

The conclusion drawn here is that diffusion effects and decay times show a strong pitch-angle dependence for ~1-Mev electrons because pitch-angle diffusion mechanisms are not as effective in moving ~1-Mev electrons down a flux tube as they are for ~300-kev electrons.

Among possible pitch-angle diffusion mechanisms, *Roberts* [1966, 1968] has discussed the scattering of relativistic electrons along a flux tube using cyclotron-resonance scattering by whistler-mode disturbances and bounce-resonance scattering by perturbations having electric or magnetic field components parallel to the local field. In particular, Roberts has considered these mechanisms operating with irregular, wide-band noise-like field fluctuations. Irregular whistler-mode disturbances with rms magnetic field fluctuations of order $>10^{-3}$ γ or bounce resonance scattering from irregular electric field fluctuations of the order of $\geq$0.01 v/km rms or magnetic intensity fluctuations of the order of $>10^{-5}$ rms of B_{eq} yield pitch-angle diffusion rates in rough agreement with observed outer-zone electron lifetimes [*Roberts*, 1968]. However, the power spectral density functions that

characterize the strength of the mechanism and determine the diffusion coefficients are not yet well known.

Both bounce-resonance and cylotron-resonance scattering may be important in pitch-angle diffusion since there may not be enough power available in the high-frequency whistler region for the cyclotron-resonance interaction to effectively move particles with $\alpha_{eq} \sim \pi/2$ away from the equator.

If the above mechanisms are of major importance in pitch-angle diffusion along a flux tube, then the fact that they apparently act more effectively for ~300-kev electrons than ~1-Mev electrons yields information concerning the respective power spectral density function.

We shall assume that these mechanisms are the dominant ones causing pitch-angle diffusion for relativistic electrons. The less effective pitch-angle diffusion for ~1-Mev electrons may be due to (*a*) a reduced effectiveness of the bounce-resonance interaction in removing the electrons away from $\alpha_{eq} \sim \pi/2$ or (*b*) a reduced efficiency for the whistler mode cyclotron-resonance interaction in lowering pitch angles ultimately into the loss cone. If case (*a*) prevailed and cyclotron-resonance scattering remained effective, then the low-altitude electron intensities would closely follow equatorial intensities, and there would be no buildup of electron intensities at small pitch angles. This is not the case for the ~1-Mev particles and thus, case (*b*) seems applicable. Since the ~1-Mev electrons can take several days to reach equilibrium while the ~300-kev electrons take only a small fraction of a day, it seems that the power spectra density function for the wide band whistler mode noise interaction during a magnetic storm decreases in magnitude as those frequencies are approached which are responsible for the scattering of ~1-Mev electrons.

While whistler mode scattering is a strong function of $\cos \alpha_{eq}$, the index of refraction, and the propagation direction of the wave relative to the local field direction, the following discussion may give certain limits concerning the power spectral density. The electrons not being scattered are ~1-Mev electrons mirroring at low altitude, $\cos \alpha_{eq} \sim 1$. Using $\cos \alpha_{eq} = 1$, an index of refraction $n \sim 10$, and assuming that the irregular whistler waves propagate nearly parallel to the field line, then the frequencies responsible for scattering an ~1-Mev electron in the cyclotron-resonance interaction are those in the region of 1 kHz at $L = 3$ and 200 Hz at $L = 5$.

The power spectral density function for the wide band whistler mode noise thus appears to have significantly less power at $\omega \approx 1$ kHz (corresponding to ~1-Mev electrons) than it has at $\omega \approx 2$ kHz (corresponding to ~300-kev electrons) at $L = 3$. The respective values at $L = 5$ are ~200 Hz (1-Mev electrons) and ~500 Hz (~300-kev electrons). While spatial dependencies in the power spectral density function will be important in determining equilibrium conditions over a wide range of altitudes, the present results indicate that the power spectral density function may decrease significantly in the region $\lesssim 1$ kHz.

Figure 18 displays the measured decay times for the equatorially mirroring electrons at

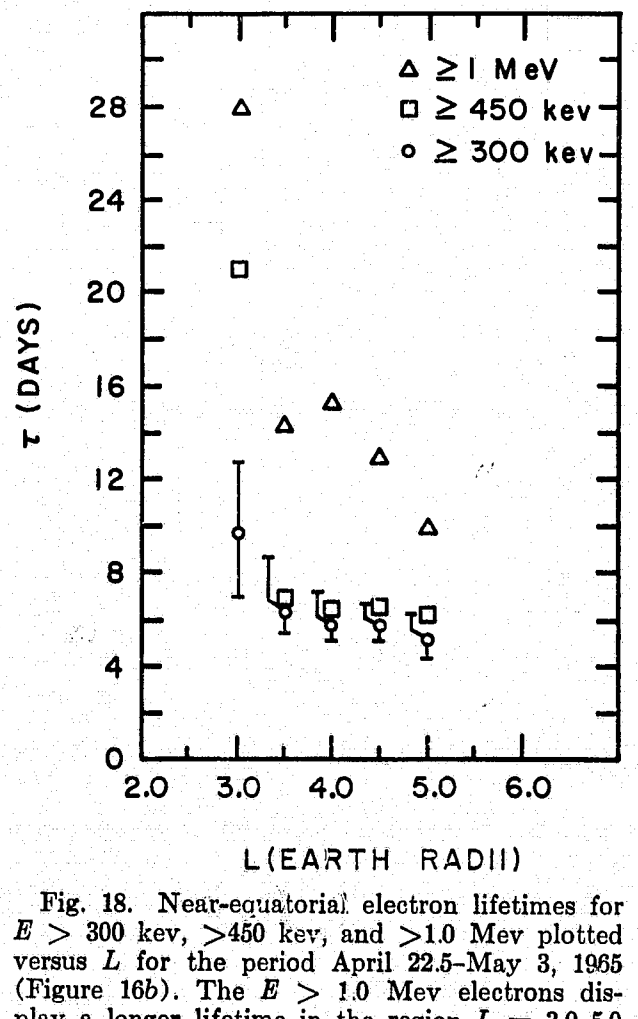

Fig. 18. Near-equatorial electron lifetimes for $E > 300$ kev, >450 kev, and >1.0 Mev plotted versus L for the period April 22.5–May 3, 1965 (Figure 16*b*). The $E > 1.0$ Mev electrons display a longer lifetime in the region $L = 3.0$–5.0 during this time period.

$\geq$300 kev, $\geq$450 kev, and $\geq$1 Mev after the April 18, 1965, storm. The decays are measured during the long-term post-storm period, April 22.5–May 3, 1965. It is seen that the $\gtrsim$1-Mev electrons display a longer lifetime throughout the $3 \leq L \leq 5$ region after this storm. In general, it was found that, during the period under study, January 1–June 29, 1965, whenever a persistent long-term decay could be obtained for both electron energies, the $\geq$1 Mev electrons displayed the longer lifetime (e.g., Figure 4). The low-altitude $\geq$1.2 Mev decay times are more difficult to obtain but where available show slightly longer lifetimes than the $\geq$230-kev electrons in the region $3 \leq L \leq 5$. Similar results have been observed for the period October 1–10, 1963 [*Williams and Smith,* 1965].

It thus appears that even during times well removed from major storms loss mechanisms in the $3 \lesssim L \lesssim 5$ region are less effective when operating on ~1-Mev electrons than on ~300-kev electrons.

It should be noted that the data of Figure 18 along with the $\geq$450-kev electron pitch-angle data, Figure 17, indicate that the transitional energy region in the preceding discussions is between 450 kev and 1 Mev. However, since we only have low-altitude data at $\geq$280 kev and $\geq$1.2 Mev, we shall continue to use $\gtrsim$300 kev and $\gtrsim$1.0 Mev as our reference energies.

Sources. It has been suggested that a source of energetic outer-zone electrons is the cross-L diffusion, under conservation of the first two adiabatic invariants, of a low-energy population initially located at the magnetospheric boundary [*Parker,* 1960; *Tverskoy,* 1964]. Such a process has been effectively employed in an attempt to arrive at an equilibrium outer-zone proton distribution [*Nakada and Mead,* 1965]. Observations indicating that such diffusion occurs for outer-zone electrons have also been reported [*Frank,* 1965*b*; *Craven,* 1966]. The initial appearance of energetic electrons well within the trapping regions and their subsequent diffusion toward lower and higher L shells shows that the above cross-L diffusion process need not be the major source of energetic electrons in the outer zone. The position at which energetic electrons are first seen within the trapping region and the variation of this position with the size of the storm (Figure 15) qualitatively can explain the dependence of outer-zone electron intensity maxima on magnetic activity [*McDiarmid and Burrows,* 1967]. In addition, the appearance of 1-3 Mev electrons at L values of ~8 R_E may be explained without requiring electrons of a few hundred kilovolts at the boundary. These high L energetic electrons could be due to the outward diffusion of energetic electrons initially appearing at lower L shells.

The source of the energetic electrons initially appearing within the trapping region is unknown. The possible sources are (1) acceleration of the local plasma and (2) acceleration of a low-energy population, which is somehow transported in from other regions (e.g., the magnetotail).

Carpenter [1963, 1966] has interpreted ground-based whistler data as indicating the existence of a sharp knee, the plasmapause, in the radial profile of electron concentration. The plasmapause, located at ~4 R_E during periods of light magnetic activity, is thought to separate an inner region of ~100 electrons/cm^3 from an outer region of ~1 electron/cm^3.

In discussing the distribution of electric fields in the magnetosphere, *Block* [1966] has reported that space charge effects will develop a central field free region within the magnetosphere and distribute the field toward the outer regions. He identifies the field free region with the above high-density region within the plasmapause and considers that the possible low-density region results from the electric fields in the outer magnetosphere sweeping away the local thermal plasma.

Carpenter [1966] has further observed an inward motion of the plasmapause during two periods of enhanced magnetic activity in July 1963. At this time the quiescent location of the whistler knee was at ~5–5.5 R_E. The plasmapause was observed to move to the region 2.8–3.8 R_E during the magnetic activity present on July 21, 22, and 30, 1963. The respective maximum D_{st} values were -23 γ, -30 γ, and -20 γ [*Suguira and Hendricks,* 1966]. The trapped electron data in Figure 15 indicate that for D_{st}^{max} of -20 γ to -30 γ, energetic electrons are first seen at $L > 5$ R_E. The appearance of energetic electrons during small magnetic disturbances is thus seen to occur well above the region to which the whistler knee is observed to move. That is, the energetic electron population is observed in the low-density region as

discussed by *Carpenter* [1963] or, equivalently, in the field region as described by *Block* [1966].

Bauer and Krishnamurthy [1968*a*] have suggested an alternative explanation for the existence of a whistler cutoff, i.e., plasmapause, during magnetic storms. They argue that the absence of whistler propagation above a certain altitude (L shell) may be due to the absorption of these waves via Landau damping by intense energetic electron fluxes appearing within the ring current region during a storm.

The present energetic electron observations are consistent with this possibility in that for the -20 γ to -30 γ storms reported [*Carpenter*, 1966], the whistler knee was observed to move to lower altitudes from an ambient value that is coincident, within the allowable errors, with the initial appearance of energetic electrons. The appearance of energetic electrons may damp the waves and cause the observed lowering of the knee.

If during quiet times, the ambient plasma density on the high-altitude side of the plasmapause is $\sim$1 cm^{-3} [*Carpenter*, 1963], then it is not possible to obtain from the local plasma the low-energy particle intensities thought to be responsible for the ring current [*Hoffman and Bracken*, 1965; *Frank*, 1967]. It is possible, however, with these low plasma densities to support the energetic ($\gtrsim$280 kev) electron population found in these regions during storms. Therefore, the primary acceleration mechanism responsible for the freshly observed energetic electrons during a main phase storm, which seems to reside within the trapping regions but above the whistler knee, can use both local plasma and transported plasma as a major source of particles.

The response of the topside ionosphere during the April 17, 1965, magnetic storm has been reported by *Bauer and Krishnamurthy* [1968*b*]. Both enhancements and depletions of topside ionization were observed and were found to depend on the phase of the storm. In particular, a large depletion in the maximum electron density $Nm\ F_2$ was associated with the main phase expansion of the field at the time of the symmetric phase of the ring current. The peak depletion was observed to occur at $L = 3$, in excellent agreement with the initial appearance of energetic electrons at 1100 km and the location of their maximum intensity (Figure 11). *Bauer and Krishnamurthy* [1968*b*] suggest that this depletion represents an upward flux of plasma caused by reduced plasma densities at high altitudes due to either the main phase field expansion or to the acceleration of the local thermal plasma. The present results indicate that a major acceleration mechanism can operate within the stable trapping regions and initially at high altitudes.

If the local plasma were energized, a local low-energy depletion could result owing to the energization and to field expansion caused by the energized particles. This in turn could cause an upward flow of ionospheric plasma to these regions and yield the $Nm\ F_2$ depletions observed in the ionosphere [*Bauer and Krishnamurthy*, 1968*b*]. The spatial correlation of the equatorial and low-altitude energetic trapped electron results and the simultaneous $Nm\ F_2$ depletion results during the April 17, 1965, magnetic storm are consistent with such a process. The equivalent low-altitude and equatorial regions may be obtained roughly from Figures 11, 14, and 15.

Thus the creation of intense energetic particle populations within the magnetosphere may stem from a variety of sources (e.g., local plasma, a low-energy population from the magnetotail, or ionospheric effects).

Many of these effects (decay, cross-L diffusion, pitch-angle diffusion, acceleration, etc.) may well be storm-dependent. The power spectral density function, for example, may vary from storm to storm and may also have a different shape during quiet times. This would have the effect of varying the energy at which pitch-angle diffusion would become effective as a function of some as yet unknown storm parameter. Simultaneous particle-wave-field observations over many storms are required in order to identify the more significant sources and losses throughout the outer zone. The difficulty of these identifications is emphasized by the iterative nature of these mechanisms; i.e., sufficient particle intensities and anisotropies may trigger instabilities that produce the diffusion leading to the loss of the initial particles [*Kennel and Petchek*, 1966].

Similar particle-field-wave-plasma observations for a variety of storms will be invaluable in furthering understanding of the relation between magnetospheric plasma and energetic

particles associated with the stable trapping region.

Summary

Simultaneous data have been presented for trapped electrons at energies $\gtrsim$280 kev and $\gtrsim$1 Mev as observed throughout much of the outer zone at 1100 km by the satellite 1963 38C and in the near-equatorial regions by the Explorer 26 satellite. These observations were obtained during the time period January 1 through June 29, 1965, for the L values 3.0, 3.5, 4.0, 4.5, 5.0, and 5.5 R_E. The behavior of the trapped electron intensities was studied and discussed during five well-defined magnetic storms, which were accompanied by electron intensity increases throughout much of the region of observation. The following results and conclusions were obtained:

(1) The $\gtrsim$300-kev trapped electrons on a given *L shell* (Figure 2) rapidly ($\lesssim$1–2 days) come to equilibrium after a large magnetic disturbance, thereby causing the entire *L shell* to behave uniformly over extended periods of time.

(2) Pitch-angle data for near equatorially mirroring $\gtrsim$450-kev electrons during the April 18, 1965, storm indicate that these electrons rapidly ($\lesssim$0.1 day) come to equilibrium within a given *flux tube*.

(3) It is thus concluded that the $\gtrsim$300-kev electrons also come to equilibrium within a given *flux tube* within ~0.1 days and that the longer (~1–2 day) nonuniform behavior on a given *L shell* (Figure 2) is due to field expansion during the storm (see number 10 below).

(4) It is further concluded that the longer term (many day) cross-L diffusion and decay processes acting on $\gtrsim$300-kev electrons appear to be pitch-angle independent owing to the rapidity of the pitch-angle diffusion mechanisms that strongly couple >300-kev electron intensities all along the line of force.

(5) Such an apparent pitch-angle independence for the long-term cross-L diffusion and decay processes is *not* observed for the $\gtrsim$1-Mev electrons.

(6) It is thus concluded that pitch-angle diffusion mechanisms are not as effective in lowering the mirror points of $\gtrsim$1-Mev electrons as they are for $\gtrsim$300-kev electrons. It is this energy dependence of the pitch-angle scattering mechanisms that allows the observation of a strong pitch-angle dependence for cross-L diffusion and decay effects at $\gtrsim$1 Mev.

(7) Using the cyclotron and bounce-resonance interactions with wide band irregular field fluctuations, as described by *Roberts* [1968], as major loss mechanisms, it is found that the power spectral density function characterizing the cyclotron-resonance interaction may decrease significantly in magnitude as the frequency is lowered from ω ~1000–2000 Hz to $\omega \sim$ 200–1000 Hz.

(8) Longer lifetimes are observed for $\gtrsim$1-Mev electrons than for $\gtrsim$300-kev electrons, indicating that either cross-L diffusion or the bounce-resonance interaction may be less effective at higher energies.

(9) Shorter lifetimes for both low- and high-altitude trapped $\gtrsim$300-kev electrons were observed immediately ($\lesssim$5 days) after the April 17 storm than during the long-term (5–16 days) post-storm period (Figure 16). This effect was seen in the region $L \sim 3\ R_E$ where the storm produced its largest energetic particle effects. The shorter lifetime in the immediate post-storm period may be due to an enhancement of loss processes during disturbed periods.

(10) Measuring the time required for the electron intensities to reach one-half their maximum value, $t_{m/2}$, after the start of a storm has led to the result that energetic ($\geq$300 kev, $\gtrsim$1 Mev) electrons associated with a main phase magnetic disturbance may initially appear well within the trapping regions and subsequently diffuse both in toward lower L values and out toward higher L values. A case of a possible double appearance of energetic electrons was found in the April 17, 1965, storm.

(11) It was also observed that the minimum $t_{m/2}$ and maximum intensity at both low and high altitude occurred at lower L values as the maximum D_{tt} of the storm increased. This is in agreement with previous low-altitude results [*Arens and Williams*, 1967]. It was further observed that the equatorial and low-altitude minimum $t_{m/2}$ values fell on separate curves (Figure 15) on an L versus D_{tt}^{max} plot. This is interpreted as a measure of field expansion during the storm and yields $\Delta R \gtrsim 0.2\ R_E$ at $R \sim 5\ R_E$ for $D_{tt}^{max} = -30\ \gamma$ and $\Delta R \sim 0.5\ R_E$ at $R \sim 3.2\ R_E$ for $D_{tt}^{max} = -140\ \gamma$. The latter value agrees well with the $\Delta R \sim 0.5\ R_E$ at

$R = 3.5\ R_E$ obtained by L. R. Davis (personal communication) during the same April 17, 1965, storm included in this study.

(12) The appearance of energetic electrons within the trapping regions and its variation with D_{st}^{max}, coupled with the subsequent transport of these electrons, can qualitatively explain the dependence of outer-zone electron intensity maxima on magnetic activity (*McDiarmid and Burrows*, 1967]. These observations can also explain the appearance of several Mev electrons at L values of $\sim 8\ R_E$ without requiring a several hundred kilovolt population at the magnetospheric boundary.

(13) Preliminary evidence indicates that the energetic electrons initially appear on the high-altitude side of the whistler knee, i.e., on the low density side of the plasmapause as discussed by *Carpenter* [1963]. The motion of the whistler knee to lower altitudes during small magnetic storms [*Carpenter*, 1963], coupled with the region of appearance of energetic ($\gtrsim$300 kev) electrons during similar size storms, lends support to the suggestion of *Bauer and Krishnamurthy* [1968*a*] that, during storms, the whistler cutoff and the apparent motion of the whistler knee is due to the appearance of energetic electrons associated with the storm ring current that absorbs the waves via Landau damping.

(14) The depletion in the topside ionosphere maximum electron concentration, $Nm\ F_2$, was observed to peak at $L = 3$ during the April 17, 1965, magnetic storm [*Bauer and Krishnamurthy*, 1968*b*]. This region of peak $Nm\ F_2$ depletion agrees very well with the region of minimum $t_{m/2}$ and maximum intensity observed for the low-altitude energetic electrons during this same storm (Figure 11). The energetic electrons during the April 17, 1965, magnetic storm appeared initially well within the trapping regions ($L = 3$ at 1100 km) and were thus produced by an acceleration mechanism acting in these regions on either the local low-energy population or on a low-energy population transported in from elsewhere.

Acknowledgments. It is a pleasure to acknowledge the stimulating and helpful discussions held with Drs. C. S. Roberts, S. J. Bauer, A. Eviatar, and M. Schulz.

We wish to express our appreciation to Drs. S. Hendricks and M. Sugiura for making the hourly D_{st} averages for 1965 available to us and to Dr. D. H. Fairfield for the *AE* indices.

The help of Miss C. G. Maclennan in analyzing the Explorer 26 pitch-angle data is greatly appreciated.

REFERENCES

Arens, J. F., and D. J. Williams, Long-term time history of outer zone trapped electrons at 1100 km (abstract), Trans. Am. Geophys. Union, 48, 169, 1967.

Arens, J. F., D. J. Williams, L. J. Lanzerotti, and C. S. Roberts, Comparison of outer zone trapped electron behavior at 1100 km and at 3-5 R_E during the April 18, 1965, magnetic storm (abstract), Trans. Am. Geophys. Union, 48, 169, 1967.

Bauer, S. J., and B. V. Krishnamurthy, Possible relationship between the stormtime whistler cutoff and the magnetospheric ring current, J. Geophys. Res., 73, 1853, 1968a.

Bauer, S., and B. V. Krishnamurthy, Behavior of the topside ionosphere during a great magnetic storm, Planetary Space Sci., 1968b.

Block, L. P., On the distribution of electric fields in the magnetosphere, J. Geophys. Res., 71, 855, 1966.

Bostrom, C. O., J. W. Kohl, and D. J. Williams, The February 5, 1965, solar proton event, 1, Time history and spectrums observed at 1100 kilometers, J. Geophys. Res., 72, 4487, 1967.

Brown, W. L., and C. S. Roberts, Observations of outer zone electrons on April 18, 1965, by the Explorer 26 satellite (abstract), Trans. Am. Geophys. Union, 47, 135, 1966.

Buck, T. M., G. H. Wheatley, and J. W. Rodgers, Silicon p-n junction radiation detectors for the Telstar satellite, IEEE Trans. Nucl. Sci., NS-11, 294, 1964.

Cahill, L. J., Jr., Inflation of the inner magnetosphere during a magnetic storm, J. Geophys. Res., 71, 4505, 1966.

Carpenter, D. L., Whistler evidence of a "knee" in the magnetospheric ionization density profile, J. Geophys. Res., 68, 1675, 1963.

Carpenter, D. L., Whistler studies of the plasmapause in the magnetosphere, 1, Temporal variations in the position of the knee and some evidence on plasma motions near the knee, J. Geophys. Res., 71, 693, 1966.

Craven, J. D., Temporal variations of electron intensities at low altitudes in the outer radiation zone as observed by satellite Injun 3, J. Geophys. Res., 71, 5643, 1966.

Fälthammer, C. G., Effects of time-dependent electric fields on geomagnetically trapped radiation, J. Geophys. Res., 70, 2503, 1965.

Forbush, S. E., G. Pizzella, and D. Venkatesan, The morphology and temporal variations of the Van Allen radiation belt, October 1959 to December 1960, J. Geophys. Res., 67, 3651, 1962.

Frank, L. A., A survey of electrons E>40 kev beyond 5 earth radii with Explorer 14, J. Geophys. Res., 70, 1593, 1965a.

Frank, L. A., Inward radial diffusion of electrons greater than 1.6 million electron volts in the outer radiation zone, J. Geophys. Res., 70, 3533, 1965b.

Frank, L. A., On the extraterrestrial ring current during geomagnetic storms, J. Geophys. Res., 72, 3753, 1967.

Freeman, J. W., Jr., The morphology of the electron distribution in the outer radiation zone and near the magnetospheric boundary as observed by Explorer 12, J. Geophys. Res., 69, 1691, 1964.

Hoffman, R. A., and P. Bracken, magnetic effects of the quiet time proton belt, J. Geophys. Res., 70, 3541, 1965.

Kennel, C. F., and H. E. Petschek, Limit on stably trapped particle fluxes, J. Geophys. Res., 71, 1, 1966.

Lanzerotti, L. J., Outer zone electron fluxes during the February 5, 1965, solar proton event, Chapter 9, this report.

Lincoln, J. V., Geomagnetic and solar data, J. Geophys. Res., 70, 5953, 1965.

Lincoln, J. V., Geomagnetic and solar data, J. Geophys. Res., 71, 1477, 1966.

McDiarmid, I. B., and J. R. Burrows, Dependence of the position of the outer radiation zone intensity maxima on electron energy and magnetic activity, Can J. Phys., 45, 2873, 1967.

Nakada, M. P., and G. D. Mead, Diffusion of protons in the outer radiation belt, J. Geophys. Res., 70, 4777, 1965.

O'Brien, B. J., A large diurnal variation of the geomagnetically trapped radiation, J. Geophys. Res., 68, 989, 1963.

O'Brien, B. J., High-latitude geophysical studies with satellite Injun 3, 3, Precipitation of electrons into the atmosphere, J. Geophys. Res., 69, 13, 1964.

Parker, E. N., Geomagnetic fluctuations and the form of the outer zone of the Van Allen radiation belt, J. Geophys. Res., 65, 3117, 1960.

Roberts, C. S., On the relationship between the unidirectional and omnidirectional flux of trapped particles on a magnetic line of force, J. Geophys. Res., 70, 2517, 1965.

Roberts, C. S., Electron loss from the Van Allen zones due to pitch-angle scattering by electromagnetic disturbances, Chapter 4, this report.

Roberts, C. S., Cyclotron resonance and bounce resonance scattering of electrons trapped in the earth's magnetic field, Chapter 5, this report.

Rose, D. C., The Alouette satellite results, in Proc. Advan. Study Inst., Radiation Trapped in the Earth's Magnetic Field, edited by B. M. McCormac, p. 191, D. Reidel Publishing Company, Dordrecht, Holland, 1966.

Sugiura, M., and S. Hendricks, Provisional hourly values of equatorial D_{st} for 1961, 1962, and 1963, NASA/GSFC Document X-612-66-355, August, 1966.

Tverskoy, B. A., Dynamics of the radiation belts of the earth, 2, Geomagnetism and Aeronomy, 3, 351, 1964.

Williams, D. J., Outer-zone electrons, in Proc. Advan. Study Inst., Radiation Trapped in The Earth's Magnetic Field, edited by B. M. McCormac, p. 263, D. Reidel Publishing Company, Dordrecht, Holland, 1966.

Williams, D. J., and A. M. Smith, Daytime trapped electron intensities at high latitudes at 1100 kilometers, J. Geophys. Res., 70, 541, 1965.

CHAPTER 11

Drift Mirror Instability in the Magnetosphere: Particle and Field Oscillations and Electron Heating

L. J. LANZEROTTI, A. HASEGAWA, AND C. G. MACLENNAN

Bell Telephone Laboratories, Murray Hill, New Jersey 07974

The published $L = 5$ equatorial magnetosphere particle and field data from the April 18, 1965, geomagnetic storm are reanalyzed in the context of the drift mirror instability theory developed by Hasegawa. These data, together with previously unpublished electron pitch-angle data, are shown to satisfy the requirements and consequences of the instability. Additional particle data observed during a 1967 substorm by an experiment on ATS 1 are also presented to show that the observation of the April 18 instability was not an isolated occurrence in the magnetosphere. The data also contain evidence for electron heating during the time of the instability.

INTRODUCTION

A number of papers have been published describing and discussing the many geophysical observations made during the time period including the large April 17–18, 1965, geomagnetic storm [*Cahill*, 1966; *Houston and Earhard*, 1966; *Gosling et al.*, 1967; *Meng and Akasofu*, 1967; *Lanzerotti*, 1968*a*; *Brown et al.*, 1968; *Hoffman and Cahill*, 1968; *Sonnerup et al.*, 1969]. In addition to the fact that this was a large storm following a long period of relatively quiet geomagnetic conditions, perhaps the most important feature of the event was that the satellite Explorer 26 was fortuitously located at apogee and remained at an essentially stationary position in the magnetosphere long enough to observe the beginning of large proton and electron flux enhancements and modulations at the start of a polar substorm on April 18. It has seemed likely that the particle and field observations made by Explorer 26 were indicative of a fundamental magnetosphere process.

Recently, a breakthrough in the theoretical understanding of the April 18 satellite observations was made possible by the development of a new theory of the mirror instability by one of the authors [*Hasegawa*, 1969*a*], hereafter denoted as paper 1. By extending the theory of the mirror instability [*Chandrasekhar et al.*, 1958] to consider gradients in both the magnetic field B and the hot plasma density n, a coexisting cold plasma, and the effect of finite cyclotron radius, Hasegawa has observed that the particle and field phenomena seen by Explorer 26 at $L = 5$ on April 18 after the first large proton enhancements can be explained by the occurrence of a mirror instability in the magnetosphere. He has called this instability the drift mirror instability because of the coupling with the drift waves produced by ∇B and ∇n.

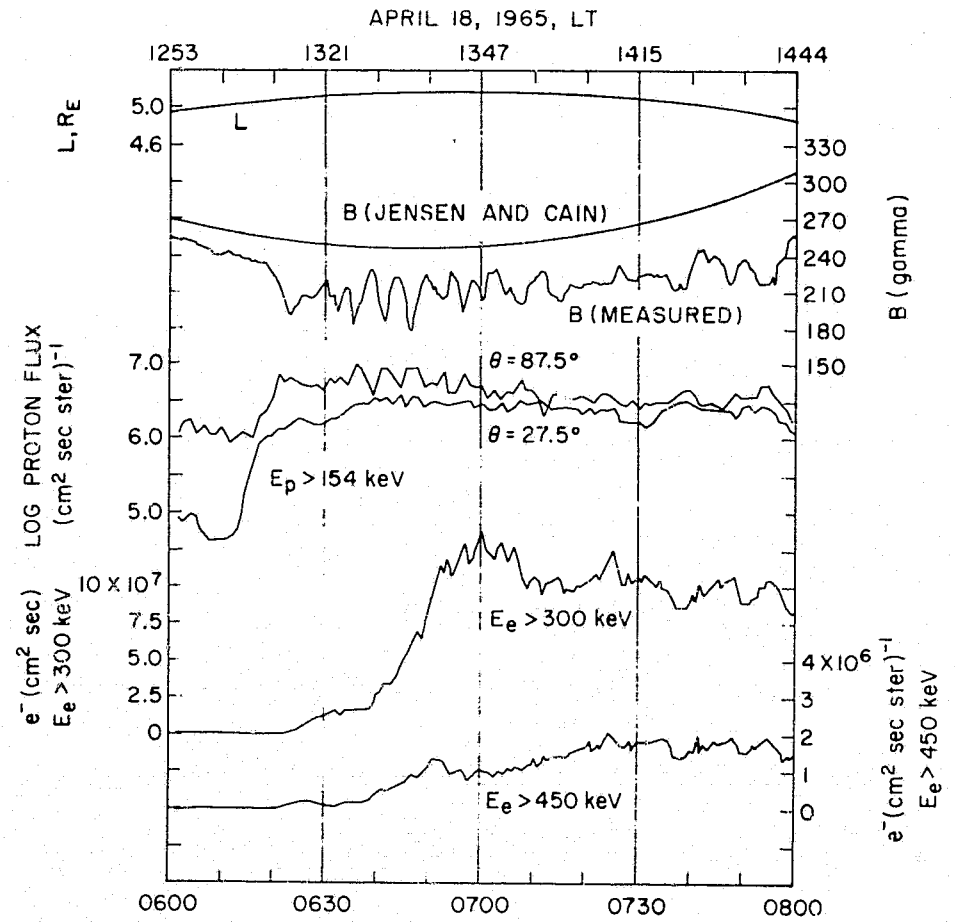

Fig. 1. Over-all plot of the magnetic field intensity and proton and electron observations measured during the second Explorer 26 apogee pass of April 18, 1965 (taken from Figure 2 of *Brown et al.* [1968]).

In this paper the previously published data from the April 17–18 storm period are reanalyzed in the context of this theory to substantiate the relevance of the mirror instability to the proton and field oscillations observed by Explorer 26. In addition, unpublished electron pitch-angle data obtained during the electron flux enhancement are presented and shown to be consistent with the consequences of the instability. To indicate that indeed such an instability is active during other substorms in the magnetosphere, electron, and proton data during a 1967 substorm observed by the BTL experiment on ATS 1 are presented. Finally, it is shown from both the Explorer 26 and ATS 1 data that electron heating occurs in the magnetosphere during the time period following the onset of instability. A possible heating mechanism is presented.

The Explorer 26 experiment, consisting of six partially depleted, solid-state *p-n* junction detectors, has been described previously [*Brown et al.*, 1968; *Williams et al.*, 1968]. In addition to the spin-averaged flux data from the experiment published in those papers, the E6 ($E_e >$ 450 kev) electron detector was also sampled more frequently to give a pitch-angle distribution approximately once each twenty seconds.

The ATS 1 experiment, consisting of a six-element solid-state detector telescope has also been previously described in the literature [*Lanzerotti et al.*, 1967; *Lanzerotti*, 1968*b*]. This experiment measures the spin-averaged flux of particles mirroring near the magnetic equator at synchronous altitude (6.6 R_E, 150°W, 0°N).

Results

Explorer 26 Observations

A composite view of the magnetic field observations and several proton and electron flux

observations during the second Explorer 26 apogee pass on April 18 as presented by *Brown et al.* [1968] is reproduced here as Figure 1. During the 0600–0800 UT time interval, the local time of the satellite changed from ~1250 to ~1440, and the geomagnetic latitude changed from ~4.5° to ~8.3°. The general features of the temporal observations have been well described previously [*Brown et al.*, 1968].

Important experimental observations from Figure 1 that will be discussed in detail are the sudden 'kink' in the increase (decrease) of the proton fluxes (magnetic field intensity) at ~0622 and the general anticorrelation between the magnitude oscillations of the magnetic field intensity and the proton flux intensity subsequent to this 'kink.' In addition, the electron flux variations are discussed in terms of the observed acceleration and oscillations. It is noted that the oscillations observed in the two electron flux channels are not well-correlated with either the field or proton oscillations. The lack of such correlations could be due to the fact that all local pitch-angle electrons (from ~25° to 90°) were measured during each sample period plotted in this figure. Between 0730 and 0800, however, several large pulsations in both electron flux channels correspond to decreases in the field magnitude.

An expanded view of the magnetic field fluctuations from 0620 to 0650 UT is plotted in Figure 2. This figure indicates very clearly the anticorrelation between the field intensity and the near-local 90° proton fluxes plotted from three different energy channels at the time of the three large field decreases.

The $E_e > 450$-kev electron fluxes for two separate pitch-angle intervals are also shown in Figure 2. The time periods when the fluxes were not a maximum at a pitch angle near 90° are indicated by shaded horizontal bars on the data plot. Below the electron data are plotted the fractional differences between the 90° and non-90° electron fluxes compared with the 90° fluxes. One-half the fractional differences are plotted for the first 10 minutes. The gaps in this pitch-angle data result from the mode sequencing of the experiment.

From the data of Figure 2 it is clearly evident that, even though there are large simultaneous electron flux increases, at the time of the magnetic field decreases the tendency is for the local 90° pitch-angle electron fluxes to decrease below the values of the fluxes at a smaller local pitch angle. It should also be pointed out that prior to the large field oscillations, accompanied by the major electron increases, an initial, smaller electron enhancement was observed in the electron fluxes between 0620 and 0625. Between 0625 and 0630 the electron fluxes were highly anisotropic, with the local pitch angle (LPA) distribution strongly peaked near 90° [*Brown and Roberts*, 1966; *Williams et al.*, 1968].

ATS 1 Observations

The satellite ATS 1, being in a synchronous circular orbit, is an experimental platform that is always in a stationary observing position, as Explorer 26 was during its apogee passes. A particularly striking case of phenomena similar to the April 18 observations in Figure 1 was observed by ATS 1 during a magnetic storm on June 26, 1967. Proton and electron data from several channels of the BTL experiment on ATS 1 during this time period are plotted in Figure 3. The local time of these observations spans 1300–1600.

Unfortunately, neither proton nor electron pitch-angle data were obtained here, nor were protons of energies less than 600 kev measured. Nevertheless, these data show clearly that after the electron 'wipeout' during hour 2300 UT, large electron oscillations (~4-min periods; equatorial pitch angle near 90°) were superimposed upon the electron increases during hour 00 UT. Simultaneously with the electron oscillations, the proton fluxes oscillated *out of phase* with the electrons during most of the two hours after the 'wipeout.' The auto- and cross-correlation analyses of the 1-minute average $E > 400$ kev electron channel and the 1-minute average $0.6 < E < 1.0$ Mev proton channel shown in Figure 4 confirm this out-of-phase relationship between the equatorial 90° pitch-angle electron and proton fluxes. It has been reported that during hour 00 large oscillations of ~30 γ amplitude were observed in the magnetic field intensity and that these oscillations were *in phase* with the electron oscillations [*Barfield et al.*, 1968].

40

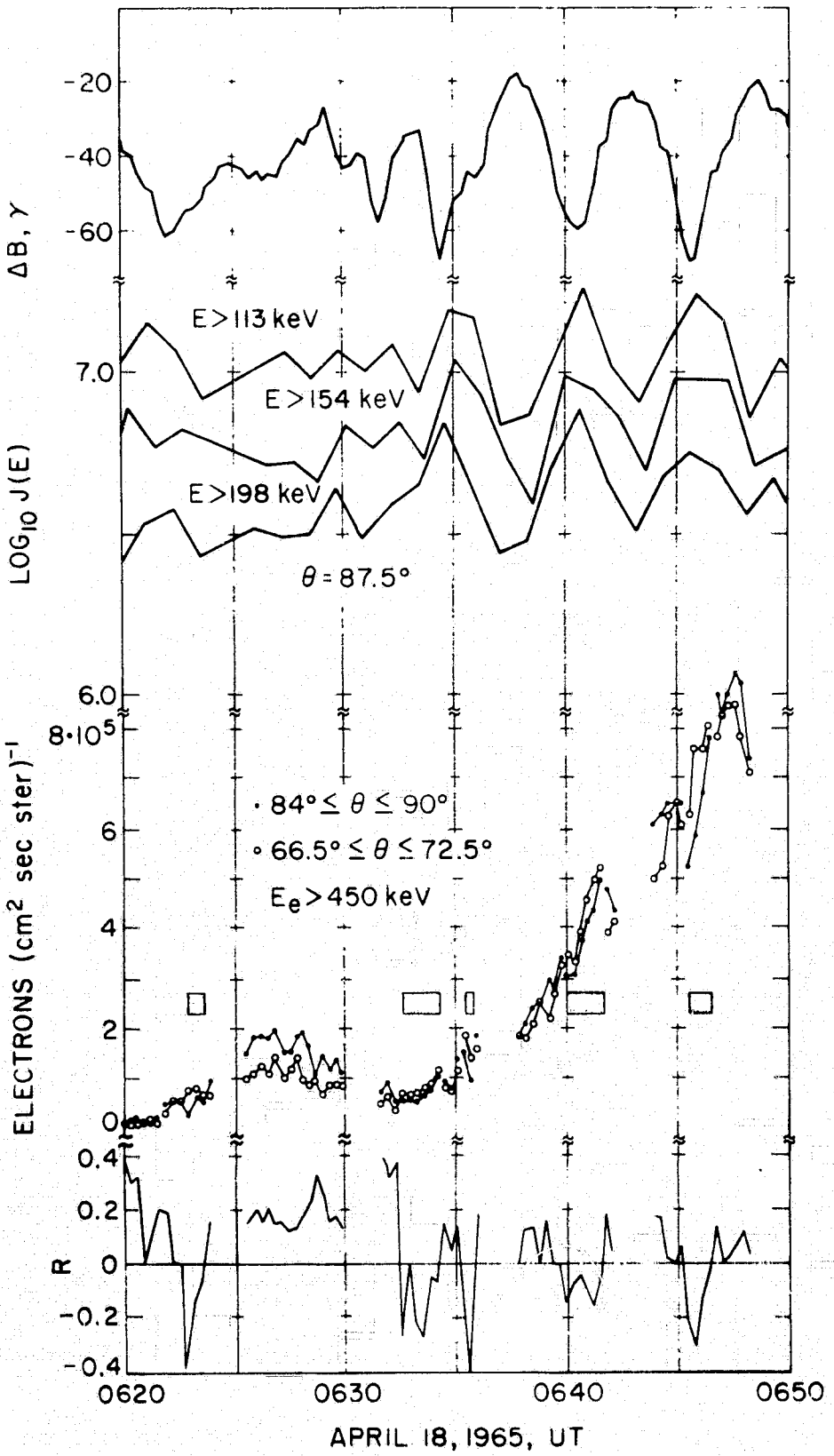

Fig. 2. Plot of the magnetic field oscillations and three of the proton energy channels of LPA ~90° [*Sonnerup et al.*, 1969]. Also plotted are $E_e > 450$ kev electron data at two different pitch angles as well as the fractional differences between the LPA ~90° and LPA ~70° fluxes. One-half the fractional differences are plotted for 0620–0630.

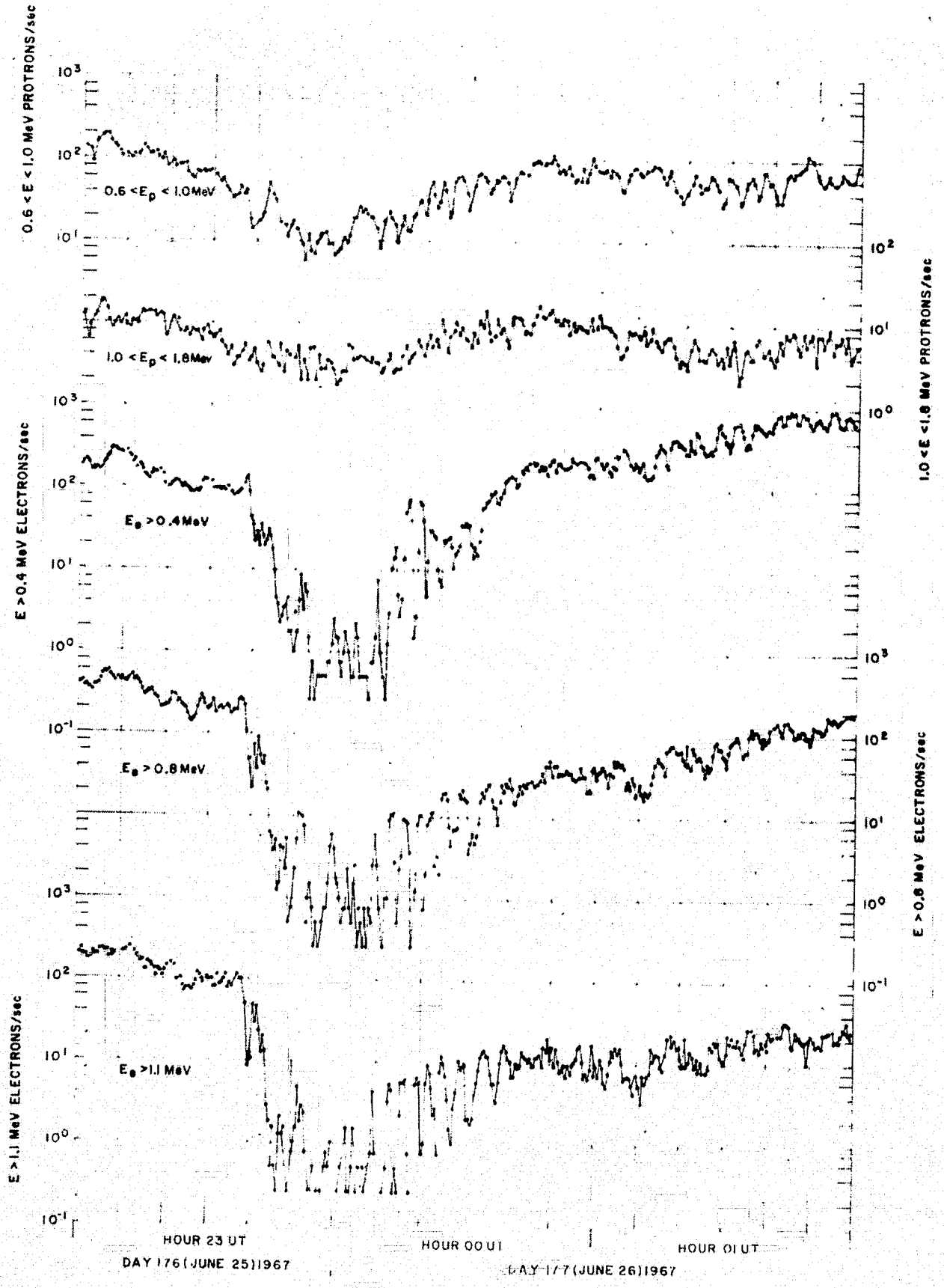

Fig. 3. Two proton and three electron energy channels of ATS 1 data during June 25–26, 1967. Each data point corresponds to a 3.9-sec spin-averaged flux measurement. The separation between successive measurements of a given particle energy channel is ~27 sec.

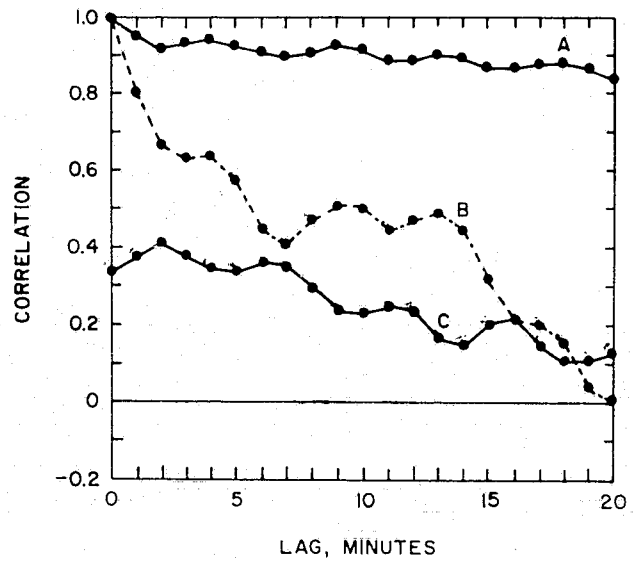

Fig. 4. Curve A: Autocorrelation of the 1-minute average $E > 400$ kev electron fluxes. Curve B: Autocorrelation of the 1-minute average $0.6 < E < 1.0$ Mev proton fluxes. Curves C: Cross-correlation between these two particle fluxes.

Discussion

Proton Observations

As is shown in Figures 1 and 2, the proton fluxes began to increase sharply and the magnetic field intensity began to decrease sharply at approximately 0618 UT on April 18. After the sharp 'kink' in the proton flux increase and the magnetic field decrease at ~0622, the proton fluxes underwent small oscillations about their enhanced values for approximately 10 minutes. The amplitudes of the small oscillations increased until three large oscillations appeared in the fluxes, definitely out of phase with corresponding oscillations of the magnetic field.

Sonnerup et al. [1969], comparing these oscillations with four different models, concluded that protons 'sloshing back and forth in the acoustic mode' were the 'most attractive' explanation for the observations. Although the conclusions of this paper agree that the oscillations are caused by a wave phenomenon, it is well known [*Fried and Gould*, 1961], and has also been pointed out in paper 1, that the acoustic mode is subject to heavy ion Landau damping if $T_i > T_e$, a condition which holds for the magnetosphere plasma. Thus, it is difficult to account for such sharp oscillations by invoking the acoustic mode.

To compare the proton observations made by Davis on Explorer 26 [*Soraas and Davis*, 1968] and reported by *Brown et al.* [1968], with the theory of drift mirror instability, a functional representation for the fluxes at a given pitch angle θ and above a given energy threshold E_s was assumed. This fit of an assumed function to the data was necessary to obtain the hot proton plasma density and average energy since proton fluxes below 113 kev were not measured. The theoretical representation was then fit to the data kindly furnished to us by Dr. Leo Davis (personal communication). Davis' 10° interval proton pitch-angle observations at four different energies were fit to the function

$$J(E > E_s) = 2.2 \cdot 10^6 n_0 E_T \left(1 + \frac{E_s}{2E_T}\right) \cdot \exp\left(-\frac{E_s}{2E_T}\right)(\sin^2\theta - \sin^2\theta_c)^s \cdot \frac{\Gamma(s + 3/2)}{2\pi(\cos^2\theta_c)^{2s+1}\Gamma(\frac{1}{2})\Gamma(s+1)} \cdot (\text{cm}^2\ \text{ster sec})^{-1} \qquad (1a)$$

where a distribution function consisting of a product of a pitch-angle function and a Boltzmann distribution function in velocity space

$$df(\theta, v) = \frac{n_0\Gamma(s + 3/2)}{2\pi(\cos^2\theta_c)^{2s+1}\Gamma(\frac{1}{2})\Gamma(s+1)} \cdot (\sin^2\theta - \sin^2\theta_c)^s(2\pi \sin\theta\, d\theta) \cdot \left[\frac{1}{(2\pi)^{1/2}v_T}\right]^3 4\pi v\, dv \exp\left(\frac{-v^2}{2v_T^2}\right) \qquad (1b)$$

was assumed. In the above equations, n_0 and E_T are the hot proton density (cm^{-3}) and the average energy ($=(\frac{1}{2})m_i v_T^2$, ev), respectively, and θ_c is the loss cone angle.

Assuming the separable function (equation 1a), the fit of the pitch-angle distribution for each energy was obtained. The average s value obtained from these four pitch-angle fits for each measurement interval was then used to obtain n_0 and E_T from the energy fit. Three examples of these fits used to derive values of n_0, E_T, and the asymmetry parameter s are shown in Figure 5 for three measurement intervals around the proton 'kink.' To avoid confusion only three different proton pitch-angle intervals are shown in the figures. The broken

lines correspond to the fit to the 45° pitch-angle protons. The values of n_0, E_T, and s for each set of data were obtained by averaging the values obtained for all pitch-angle intervals.

These averaged values of the total energy, density, and asymmetry parameter were then used to derive parallel and perpendicular proton pressure representations (cf. paper 1)

$$p_{\parallel} \propto n_0 E_T \frac{1}{2s + 3} \tag{2a}$$

$$p_{\perp} \propto n_0 E_T \frac{s + 1}{2s + 3} \tag{2b}$$

and were used to determine if the instability criterion required by the theory was met. In deriving equation 2, the loss cone angle θ_c was taken to be zero (a good approximation at $L = 5$). It was shown in paper 1 that the requirement for the instability to set in is that the asymmetry parameter s satisfy the relationship

$$s > \frac{B_M^2}{1.21 E_T n_0} \frac{2s + 3}{2s + 2} \tag{3}$$

where B_M is the equatorial magnetic field intensity in gammas.

The parameters n_0, E_T, and s obtained from the fits are shown in Figure 6, together with the quantities $p_{\perp}$ and $p_{\parallel}$ derived from equation 2. The parameters plotted in Figure 6 were used to evaluate the right-hand side of equation 3. These results and the asymmetry parameter s are plotted in Figure 7 for the 0610–0730 UT time interval.

The parameters obtained from the fitting the procedure never satisfy the instability criterion. For example, at the 'kink' in the proton and field data just after the large proton increases (~0622 UT, where it is presumed that the instability first occurred) it is found that $n_0 \sim 0.9$, $s \sim 0.9$, and $E_T \sim 25$ kev. Since B is ~192 γ, the right-hand side of equation 3 becomes 2.1, which is larger than s.

One of the more likely reasons for the failure to satisfy the instability criterion is an inadequacy of the fitting procedure used to determine n_0 and E_T. The measured proton fluxes, all of energies $\gtrsim$100 kev, are extrapolated to lower energies to estimate n_0 and E_T (the latter of which is ~25 kev). In addition, as indicated in Figure 5, the fitting was done to data, log $J(E_p > E_s)$, which are of the order of 6 ~ 7. A 10% error in the experimental log(fluxes)

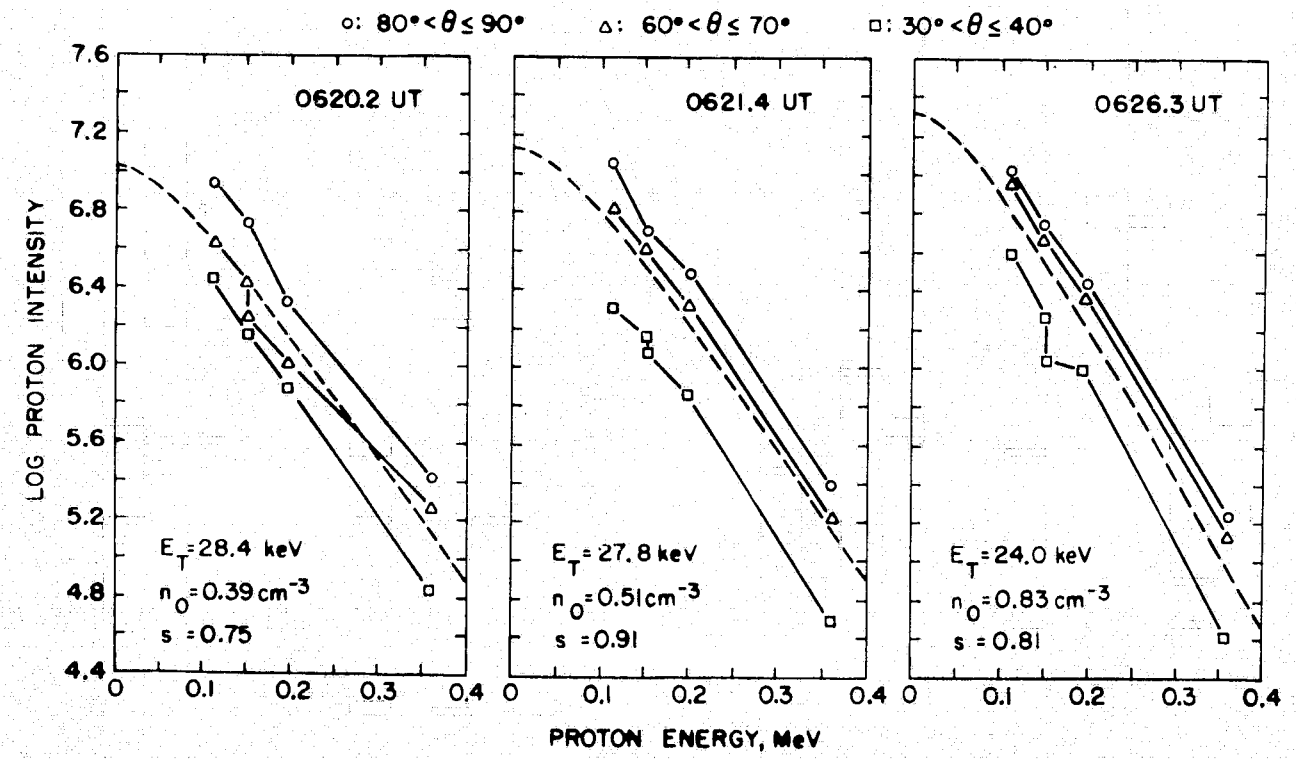

Fig. 5. Three examples of the fits to the proton pitch-angle data using equation 1. The dotted lines correspond to the fits to LPA 45° protons.

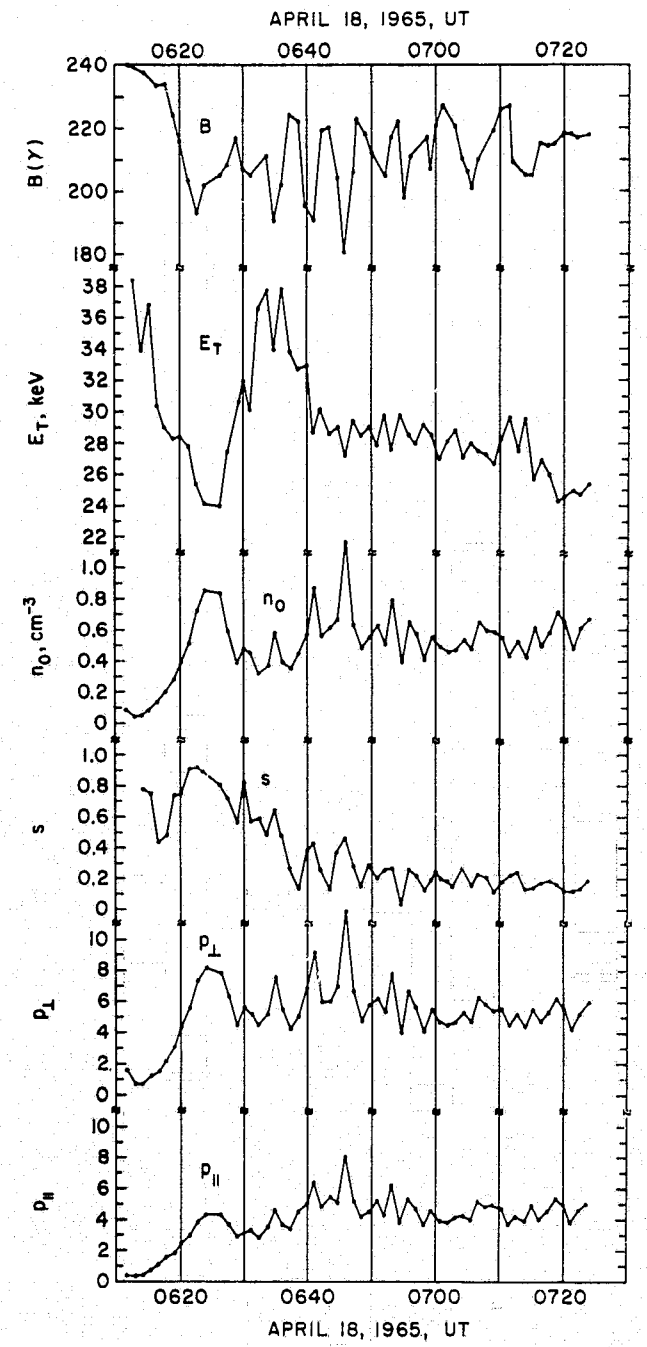

Fig. 6. The magnetic field intensity and the parameters n_0, E_T, and s obtained from the fitting procedure. Plotted at the bottom of the figure are $p_\perp$ and $p_{||}$ for protons obtained from equation 2.

could give rise to an error in log n_0 of $\sim$ log 0.7, or an error in n_0 of a factor of 2 or more.

Two other aspects of the experimental measurements tend to give slightly lower than actual values to s and/or n_0 during periods of large flux pitch-angle asymmetries. The first of these is the fact that the average efficiency over the entire detector opening angle was used in computing the particle fluxes. During the period of large anisotropies, the fluxes near LPA 90° would tend to be underestimated and the fluxes near LPA 0° overestimated.

The second of these is due to the fact that the satellite rotated through an angle of approximately 11° (also approximately the full opening angle of the detector) during each pitch-angle sample period. Because of the orientation of the detector to the satellite spin axis, this average over the spin (or detector) was most severe for local pitch angles ~35°–90°, where individual measurements were averages over ~15° in local pitch angles. Taken together both of the above experimental measurement effects amount to an approximately 10% increase in s and indicate that near 0622 UT, $s \sim 1.0$, and the right-hand side of equation 3 ~2.0.

To confirm that the estimates of the energy density as obtained from the data are in fact lower than the actual values, the proton energy densities obtained from the fits were compared with the energy density deduced by *Hoffman and Cahill* [1968] from the magnetic field data during the storm. They deduced the energy density from magnetic field measurements made during an Explorer 26 pass early on April 19, during the symmetric phase of the event. Unfortunately, no similar determinations were made during the more asymmetric period on April 18.

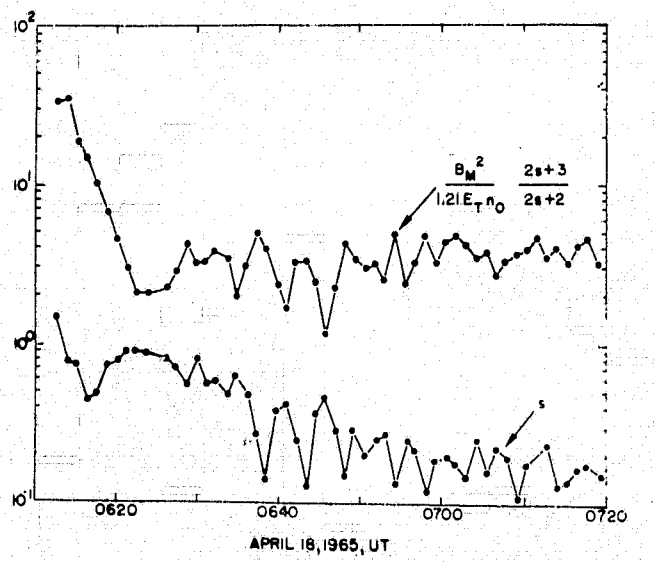

Fig. 7. Plot of the instability criterion and the pitch-angle asymmetry parameter, s, as a function of time.

Using equation 1*a* an expression for the total energy density of protons can be obtained in terms of n_0 and E_T

$$\bar{E} = 4.8 \cdot 10^{-12} n_0 E_T \text{ erg/cm}^3 \qquad (4)$$

If the fitted values of n_0 and E_T at 0622 UT are used, it is found that $\bar{E} \sim 8.7 \times 10^{-8}$ erg/cm^3. This is ~4 times smaller than the energy density of 3.2×10^{-7} erg/cm^3 obtained by Hoffman and Cahill on April 19. However, judging from the larger *Dst* depression on April 18 than on April 19, it would certainly be expected that the energy density on the 18 would be at least as large as that on the 19 (implying a larger proton density or average energy or both). If the energy density that Hoffman and Cahill computed for April 19 held also on April 18, then the instability criterion would easily have been met, given the fitted *s* values.

In addition, the energy density of 8.7×10^{-8} erg/cm^3 is also ~3 times less than the actual ring current proton energy density (~2.2×10^{-7} erg/cm^3) measured at $L = 5$ by *Frank* [1967] during a substantially smaller storm period in 1966 (*Dst* maximum of ~40 γ during the 1966 storm compared with a maximum of ~150 γ for the 1965 storm). Hence, although the direct measurements made on Explorer 26 at the time do not demonstrate it, there is strong evidence for believing the mirror instability criterion is met at the time of the ~0622 UT proton flux and magnetic field 'kink' and that the subsequently observed oscillations are consequences of the instability.

The observed frequency of the three large field and proton oscillations can be considered in the context of the theoretical predictions. As was shown in paper 1, the real part of the angular frequency is given by the drift wave frequency, ω^*, where

$$\omega^* = k_\perp \kappa v_{\parallel i}^2 / \omega_{ci} \qquad (5)$$

In equation 5, $k_\perp$ is the perpendicular wave number, κ is a measure of the particle density and magnetic field gradients, $v_{\parallel i}$ is the ion (proton) parallel thermal velocity, and ω_{ci} is the proton cyclotron frequency.

As is indicated in paper 1, $k_\perp$ can be taken as ~1 over the proton cyclotron radius. This then allows the frequency to be written as

$$\omega^* = \frac{\kappa v_{\parallel i}}{3} \left(\frac{T_\parallel}{T_\perp}\right)^{1/2} (2\Delta)^{1/2} \qquad (6a)$$

where Δ is a measure of the overshooting of the instability condition and is expected to be ~0.1 (cf, paper 1). $T_\perp$ and $T_\parallel$ are the perpendicular and parallel proton temperatures, respectively. Since κ is found to be $3/R$ in a dipole field varying as R^{-3}, it follows that

$$\omega^* = 0.098 \frac{(E_{\parallel i})^{1/2}}{L} \left(\frac{T_\parallel}{T_\perp}\right)^{1/2} (\Delta)^{1/2} \qquad (6b)$$

where $R = LR_E$ and $E_{\parallel i}$ (kev) is the average proton kinetic energy in the parallel direction. According to equation 6*b*, the condition $T_\parallel/T_\perp \sim 0.5$ at $L = 5$ yields $\omega \sim 0.015$ to ~0.04 rad/sec for Δ between 0.1 and 1. The observed frequency during the April 18 storm was ~0.02 rad/sec, in good agreement with the theoretical predictions.

For a given value of Δ, there is a one-to-one correspondence between the maximum growth rate of the instability and the real part of the angular frequency, ω. As can be obtained from paper 1, for $\beta_\perp \sim 1$, the growth rate can be written as

$$\text{Im}(\omega) \sim \omega^* \frac{R_E}{\rho_i} \Delta^{3/2} \qquad (7)$$

where ρ_i is the ion (proton) gyroradius. For the values of Δ taken above, $\text{Im}(\omega) \sim \omega^*$. This is of the order of the time period observed from the instability onset to the large, periodic oscillations (Figure 7).

The phase relationship of the proton and field oscillations must also be considered. As is shown in paper 1, the variation of the proton density associated with the drift mirror instability can be written as

$$\frac{n_1}{n_0} = \frac{B_{z1}}{B_{z0}} \left(1 - \frac{T_\perp}{T_\parallel}\right) \qquad (8)$$

B_z is the horizontal component of the magnetic field and the subscripts zero and 1 denote the unperturbed and perturbed quantities, respectively.

The variations in the empirically fitted density data plotted in Figure 6 indicate that the oscillations are consistent with $T_\perp > T_\parallel$ if the following relations derived in paper 1 are considered

$$\frac{p_{\perp 1}}{p_{\perp 0}} \propto 2 \frac{B_{z1}}{B_{z0}} \left(1 - \frac{T_\perp}{T_\parallel}\right) \qquad (9a)$$

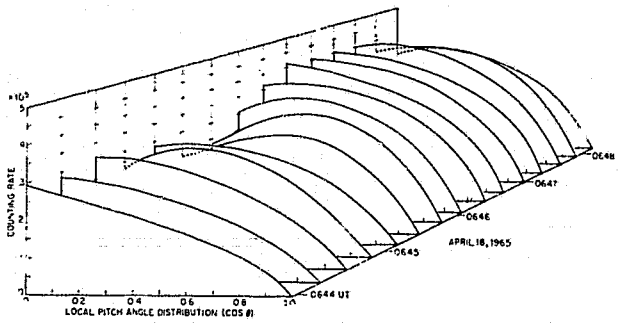

Fig. 8. A perspective graph of the fits to the $E_e > 450$ kev electron flux LPA distributions during the period ~0643–0650, April 18, 1965.

$$\frac{p_{\parallel 1}}{p_{\parallel 0}} \propto \frac{B_{s1}}{B_{s0}}\left(1 - \frac{T_\perp}{T_\parallel}\right) \qquad (9b)$$

and

$$\frac{p_{\perp 1}}{p_{\parallel 1}} = 2\frac{T_\perp}{T_\parallel} = 2(s+1) \qquad (9c)$$

Furthermore, not only do $p_\perp$ and $p_\parallel$ oscillate out of phase with the magnetic field (Figure 6) but also the amplitude of the oscillations in $p_\perp$ are predicted by equation 9 to be $2(1 + s)$ times that of $p_\parallel$, which is in quantitative agreement with the values of Figure 6, derived from the fitted data.

As was noted in the previous section, the proton oscillations measured by the ATS 1 experiment on June 26 were observed to be out of phase with the large magnetic field intensity oscillations. However, owing to the lack of both pitch angle information and lower energy measurements, it is impossible to theoretically treat these proton observations as the April 18 observations were treated above. Nevertheless, the phase characteristics of the proton flux oscillations and reported magnetic field oscillations, as well as the electron observations discussed below, strongly imply that the same instability also existed in the magnetosphere during this substorm. For this instability period an oscillation frequency ~0.023 rad/sec is observed at $L = 6$ (Figure 3). This frequency also lies in the theoretically predicted frequency range as shown by equation (6*a*).

Electron Observations

1. Oscillations. As was evident in Figures 1 and 2, large increases in the electron population were observed to occur at approximately the same time as the onset of the largest magnetic field oscillations during the April 18 storm period. Any $E_e > 300$ kev electron flux oscillations superimposed upon the large increases would tend to be obscured because the detector measured LPA from ~25°–90° during one sample period.

It has generally been observed in the $E_e > 450$ kev electron pitch-angle data that during the April 18 electron oscillations, the local electron pitch-angle distributions tend to be peaked at an angle smaller than 90°. This is clearly seen in Figure 2 for the period during the electron increases. In addition, analytical fits to the $E_e > 450$ kev electron pitch-angle distributions during 0643–0650 are plotted in perspective view in Figure 8 to give a more graphic display of some of the changes observed in the pitch-angle distributions. The functional fit to the data was an extension of the normal pitch-angle distribution as in equation 1 [*Roberts*, 1965; *Williams et al.*, 1968]

$$J(E > E_e) \propto [A + Bx^n - (A + B)x^{2n}]^s$$

where $x = (1 - B_0/B)^{1/2}$.

A functional form for the behavior of the electron fluxes above a given threshold energy (E_e) as a function of pitch angle can be

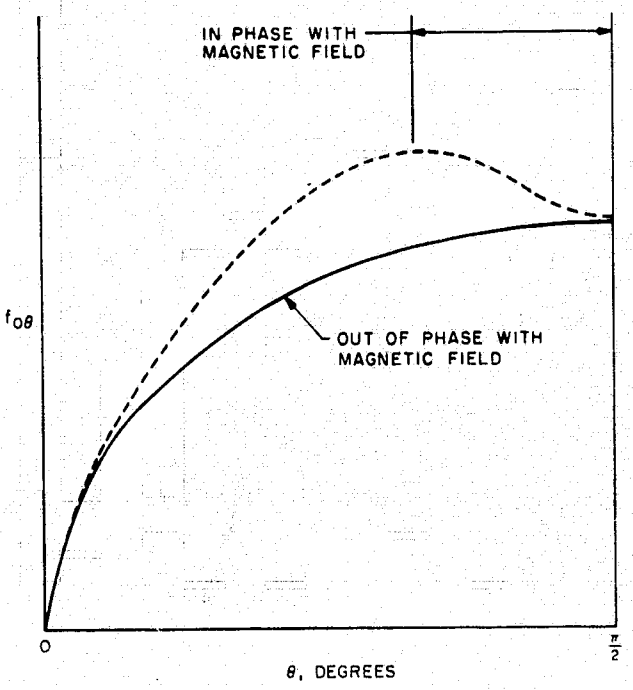

Fig. 9. Electron pitch-angle sketch showing the relationship of the electron oscillation phase to the magnetic field oscillation phase (equation 10).

derived using the perturbed distribution function obtained in paper 1 and transforming the variables from (u, v_s) to (v, θ)

$$\frac{dJ(v > v_s, \theta)}{d\Omega} = n_0 \int_{v_s}^{\infty} vf(v)\, dv$$

$$= -\frac{B_s}{2B_0} \int_{v_s}^{\infty} 4\pi v^3 f_{0s}(v)\, dv$$

$$\cdot \sin^2 \theta (\cot \theta + \tan \theta) \frac{df_{0\theta}(\theta)}{d\theta} \qquad (10)$$

where Ω is the solid angle, v is the electron velocity, and θ is the electron pitch angle. Referring to the sketch in Figure 9, it is seen that when the pitch-angle distribution has a peak at other than 90°, $df/d\theta$ will be negative, and an in-phase oscillation of the electrons with the magnetic field will occur. This is exactly the phenomena observed during the large electron increases shown in Figures 2 and 3. It should be noted that electron and proton oscillations that are out of phase cannot be accounted for by an acoustic mode model of the phenomena.

The electron oscillations observed on ATS 1 during the June 26, 1967, event were much larger than those observed during the April 18, 1965, storm period (Figure 3). However, as has been mentioned above, during both the June 26 and April 18 events, the electron oscillations were out of phase with the proton oscillations and in phase with the reported magnetic field oscillations [*Barfield et al.*, 1968]. Again large increases in the electron population were observed to occur at approximately the time of the largest proton oscillations (which also corresponded approximately to the time of the largest field oscillations).

Electron Observations

2. Heating. The characteristic electron heating time, assuming an exponential increase, during the first forty minutes of June 26 has been plotted in Figure 10, together with data from four electron energy channels ($E_e > 10$ kev, > 300 kev, > 450 kev, and > 1000 kev) from the April 18 storm. The heating would appear to be slightly faster during the April 18 storm for the three 'relativistic' energy channels. Although the heating time as plotted in this figure is more rapid for the 300-kev electrons than for the 1.9-Mev electrons, the nonrelativistic 10-kev electron heating, taken from data presented by *Brown et al.* [1968], is quite slow.

Although a complete theoretical treatment has not yet been carried out, the accelerations during the oscillations can be attributed to transit time damping, which heats the electrons in the parallel direction. In this case, for $T_\parallel > T_\perp$ the in-phase relationship with the magnetic fields is accounted for (cf. equation 9).

The rate of electron heating during the oscillations may be roughly computed as follows. The rate of change of the electron energy, W_e, due to transit time damping can be expressed as

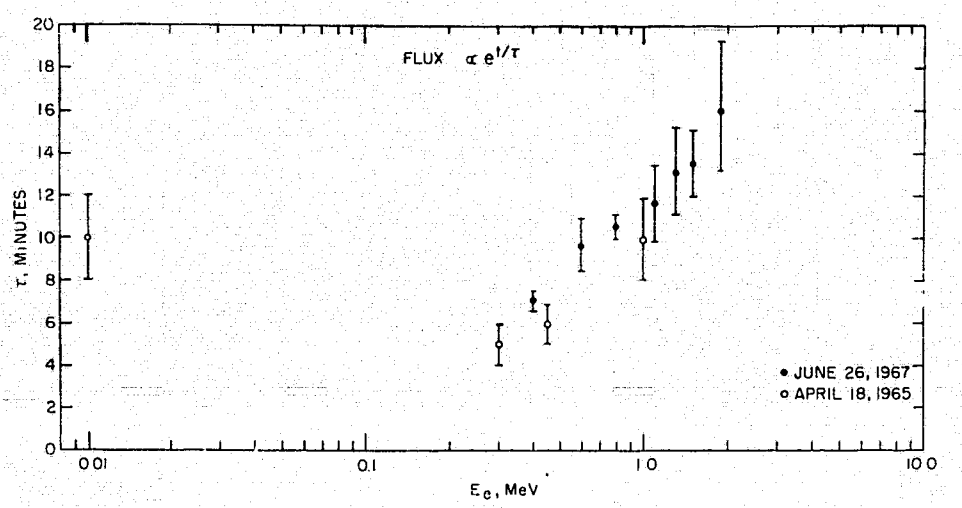

Fig. 10. Plot of the rate of electron heating during the initial large heatings observed on both Explorer 26 and ATS 1. Note the data point at 10 kev.

$$\frac{\partial W_{\|e}}{\partial t} = -\omega \operatorname{Im} \langle E \cdot \epsilon \cdot E \rangle$$

$$= -\frac{\omega \epsilon_0 E_y^2}{2} \operatorname{Im} (\epsilon_{yy}) \qquad (11)$$

where E_y is the electric field in the direction normal to both the magnetic field and the wave vector (denoted by the direction y). $\operatorname{Im}(\epsilon_{yy})$ is the yy component of the imaginary part of the equivalent dielectric constant. This term of the dielectric constant has been given in paper 1 as

$$\operatorname{Im} (\epsilon_{yy}) = -\frac{k_\perp^2 v_{\perp e}^2 \omega_{pe}^2}{\omega^2 \omega_{ce}^2} \frac{T_{\perp e}}{T_{\|e}} \operatorname{Im} Z' \left(\frac{\omega}{k_\| v_{\|e}} \right) \qquad (12)$$

where Z' is the plasma dispersion function [*Fried and Conte*, 1961]. In equation 12, ω_{pe} and ω_{ce} are the electron plasma frequency and cyclotron frequency, respectively; $v_{\perp e}$ and $v_{\|e}$ are the electron velocities in the perpendicular and parallel directions (to the magnetic field), respectively; and $T_{\perp e}$ and $T_{\|e}$ are the perpendicular and parallel electron temperatures, respectively.

Because of the nonuniformity of the magnetic field, either the wave or the electron may be reflected (mirrored) at some local point along the line of force. At the mirror point, either $k_\|$ or $v_{\|e}$ will go to zero in the dispersion relation of equation 12 (depending upon whether the wave or the electron mirrored closer to the equator) causing a resonant interaction between the electron and wave.

In the case of the resonant interaction, Im $Z \sim 1$ because $\omega \sim k_\| v_{\|e}$. In the nonrelativistic limit $W_{\|e} \sim 1/2\ m_e n_{e0} v_{\|e}^2$ and since $E_y = \omega B_z / k_\perp$, equation 11 can be expressed as

$$\frac{1}{W_{\perp e}} \frac{\partial W_{\|e}}{\partial t} = \left(\frac{B_z}{B_{z0}} \right)^2 \omega \qquad (13)$$

or

$$W_e \sim W_{e0} \exp \left[\left(\frac{B_z}{B_{z0}} \right) \right]^2 \omega t$$

if it is assumed $W_{\|e} \sim W_{\perp e} \sim W_e$.

The rate of heating is thus equal to $(B_z/B_{z0})^2 \omega$ in the nonrelativistic limit, where ω is the wave frequency seen by the electrons; i.e., higher energy electrons see a higher frequency wave because of the Doppler shift (a larger drift velocity and opposite in direction to that of the very nonrelativistic protons). For the case of $\omega \sim 0.02$ rad/sec and $(B_z/B_{z0})^2 \sim (25/200)^2 \sim 1/64$, the heating time, t, is found to be ~5 minutes for ~300 kev electrons (Doppler-shifted wave ω ~10 times that of the observed ω), in good agreement with the observations.

This prediction of a faster heating rate for higher energy electrons appears to be borne out in the Explorer 26 April 18 observations (Figure 10) where the 10-kev electrons (nonrelativistic) have a slower heating rate than the 300-kev electrons (almost relativistic). It is clear, however, that this nonrelativistic calculation does not predict the heating rate for the electron data plotted in Figure 10. For these relativistic electrons, the rate of heating becomes smaller for higher energy electrons. The breakdown of the nonrelativistic estimate is probably due to a combination of the increased synchroton radiation energy loss and the increased mass of the relativistic electrons.

Unsolved Problems

Although the above analyses and discussions have shown quite conclusively that the drift mirror instability exists on occasion in the magnetosphere and that electron heating apparently accompanies the occurrence of the instability, there remain a number of unsolved problems concerning the observations in general and the April 18 storm in particular. The first of these problems concerns the initial large proton increases observed by Explorer 26 at ~0620 UT on April 18. *Houston and Earhart* [1966] have reported that, after the peak of solar activity on April 16, 1965 [*Meng and Akasofu*, 1967], there was unusual riometer absorption beginning at ~0604 and ~0612 recorded at Bedford, Massachusetts ($L = 3.1$), and Durham, New Hampshire ($L = 3.2$), respectively. Combining riometer measurements and neutron monitor measurements, they concluded that 'the April 18 event must be at least partially attributable to protons.'

It is possible that at least the higher energy protons observed on Explorer 26 at ~0620 could result from the rapid penetration of solar protons deep into the magnetosphere. It has been shown that during the several days around

the June 26 observations reported here, the solar proton fluxes measured on ATS 1 and outside the magnetosphere on Explorer 34 were approximately the same and that both sets of measurements had approximately the same energy spectra to energies as low as ~600 kev [*Lanzerotti*, 1968*c*].

Although, as has been seen, it is necessary for the proton fluxes to be highly anisotropic as well as to have an increased energy density for the onset of instability, it is interesting that these two distinct examples of the mirror instability occurred when there were enhanced solar particle fluxes present in interplanetary space. Since the mirror instability is not always seen when an enhanced ring current is present or when enhanced interplanetary fluxes are present, there must exist some mechanism that suddenly causes a large anisotropy in the fluxes or that momentarily diffuses or accelerates the protons in a preferentially perpendicular direction. One possible mechanism may be cyclotron heating by the electromagnetic waves generated at the magnetosheath and transmitted across the magnetosphere [*Hasegawa*, 1969*b*].

Another unsolved problem concerns the heating of the electrons. As is evident from Figure 2 of *Brown et al.* [1968] and has been explicitly pointed out [*Lanzerotti*, 1968*a*], during the third pass of Explorer 26 through $L = 5$ on April 18, the enhanced electron fluxes were substantially depleted and did not increase above the 0600–0900 UT values until 12–24 hours later. If the electrons heated by the mirror instability decayed away, this decay was much faster than the 5–6 day decay normally associated with 450-kev electrons at $L = 5$ [*Williams et al.*, 1968; *Roberts*, 1969]. This fact, and the fact that this type of relativistic electron heating apparently has not been observed on ATS 1 as frequently as the type reported by *Lanzerotti and Maclennan* [1969] suggest that heating associated with the mirror instability, while being a fundamental magnetosphere process, does not contribute appreciably to the energetic outer-zone electron population.

During both of these events the electron population was severely depleted before the instability onset. It is possible to speculate that the process that causes the proton pitch-angle anisotropy, resulting in the instability, could also cause the high-energy electron losses.

Conclusions

It has been shown that the particle and field oscillations that occasionally occur in the magnetosphere in the presence of enhanced proton fluxes with strongly anisotropic pitch-angle distributions may be attributed to the drift mirror instability model of *Hasegawa* [1969*a*]. In particular, the phenomena at $L = 5$ observed during the April 18, 1965, storm and the particle measurements on June 26, 1967, at $L \sim 6$ both are consistent with the instability theory. It has also been shown that electron flux depletions and subsequent electron heating apparently accompany the occurrence of the drift mirror instability.

Acknowledgments. We gratefully acknowledge many profitable discussions with Drs. M. Schulz and W. L. Brown. We express our appreciation to Dr. L. Davis for the use of his Explorer 26 proton data, and for numerous discussions concerning his experiment. We also thank Drs. B. Sonnerup, W. D. Cummings, J. Barfield, and G. K. Parks for useful discussions.

REFERENCES

Barfield, J. N., W. D. Cummings, and P. J. Coleman, Jr., Storm related wave phenomena observed at synchronous equatorial orbit (abstract), Trans. Am. Geophys. Union, 49, 743, 1968.

Brown, W. L., L. J. Cahill, Jr., L. R. Davis, C. E. McIlwain, and C. S. Roberts, Acceleration of trapped particles during a magnetic storm, J. Geophys. Union, 47, 135, 1966.

Brown, W. L., and C. S. Roberts, Observations of outer zone electrons on April 18, 1965, by the Explorer 26 satellite (abstract), Trans. Am. Geophys. Union, 47, 15, 1966.

Cahill, L. J., Jr., Inflation of the inner magnetosphere during a magnetic-storm, J. Geophys. Res., 71, 4505, 1966.

Chandrasekhar, S., A. N. Kaufman, and K. M. Watson, The stability of the pinch, Proc. Roy. Soc. (London), 245A, 435, 1958.

Frank, L. A., On the extraterrestrial ring current during geomagnetic storms, J. Geophys. Res., 72, 3753, 1967.

Fried, B. D., and R. W. Gould, Longitudinal ion oscillations in a hot plasma, Phys. Fluids, 4, 139, 1961.

Fried, B. D., and S. D. Conte, The Plasma Dispersion Function, Academic Press Inc., New York, 1961.

Gosling, J. T., J. R. Asbridge, S. J. Bame, A. J. Hundhausen, and I. B. Strong, Measurement of the interplanetary solar wind during the large geomagnetic storm of April 17-18, 1965, J. Geophys. Res., 72, 1813, 1967.

Hasegawa, A., Drift mirror instability in the magnetosphere, Phys. of Fluids, 12, 2642, 1969a.

Hasegawa, A., Heating of the magnetospheric plasma by electromagnetic waves generated in the magnetosheath, J. Geophys. Res., 74, 1763, 1969b.

Hoffman, R. A., and L. J. Cahill, Jr., Ring current particle distributions derived from ring current magnetic field measurements, J. Geophys, Res., 73, 6711, 1968.

Houston, R. E., and J. R. Earhart, Some observations of the cosmic ray event of April 18, 1965, J. Geophys. Res., 71, 5762, 1966.

Lanzerotti, L. J., Comparison of the electron response in the magnetosphere at L = 5 with the solar wind during the April 17-18, 1965, magnetic storm, J. Geophys. Res., 7, 438, 1968a.

Lanzerotti, L. J., Calibration of a semiconductor telescope for space experiments, Nucl. Instr. and Methods, 61, 99, 1968b.

Lanzerotti, L. J., Penetration of solar protons and alpha particles to the geomagnetic equator, Phys. Rev. Letters, 21, 929, 1968c.

Lanzerotti, L. J., C. S. Roberts, and W. L. Brown, Temporal variations in the electron flux at synchronous altitudes, J. Geophys. Res., 72, 5893, 1967.

REFERENCES (continued)

Lanzerotti, L. J., and C. G. Maclennan, The Magnetosphere substorm of August, 1967, 2, Relativistic electron accelerations at synchronous altitudes, EOS, Trans. Am. Geophys. Union, 50, 287, 1969.

Meng, C. I., and S. I. Akasofu The geomagnetic storm of April 17-18, 1965, J. Geophys. Res., 72, 4905, 1967.

Roberts, C. S., On the relationship between the unidirectional and omnidirectional flux of trapped particles on a magnetic line of force, J. Geophys. Res., 70, 2517, 1965.

Roberts, C. S., Pitch angle diffusion of electrons in the magnetosphere, Rev. Geophys., 7, 1969.

Sonnerup, B. U. O., L. J. Cahill, Jr., and L. R. Davis, Resonant vibration of the magnetosphere observed from Explorer 26, J. Geophys. Res., 74, 1969.

Soraas, F., and L. R. Davis, Temporal variations of the 100 kev to 1700 kev trapped protons observed on satellite Explorer 26 during first half of 1965, GSFC X-612-68-328, 1968.

Williams, D. J., J. F. Arens, and L. J. Lanzerotti, Observations of trapped electrons at low and high altitudes, J. Geophys. Res., 73, 5673, 1968.

CHAPTER 12

Radial Diffusion of Outer-Zone Electrons: An Empirical Approach to Third-Invariant Violation

L. J. LANZEROTTI AND C. G. MACLENNAN

Bell Telephone Laboratories, Murray Hill, New Jersey 07974

MICHAEL SCHULZ

Space Physics Laboratory, Aerospace Corporation
El Segundo, California 90045

The near-equatorial fluxes of outer-zone electrons ($E > 0.5$ Mev and $E > 1.9$ Mev) measured by an instrument on the satellite Explorer 15 following the geomagnetic storm of December 17–18, 1962, are used to determine the electron radial diffusion coefficients and electron lifetimes as functions of L for selected values of the conserved first invariant μ. For each value of μ, the diffusion coefficient is assumed to be time-independent and representable in the form $D = D_n L^n$. The diffusion coefficients and lifetimes are then simultaneously obtained by requiring that the L-dependent reciprocal electron lifetime, as determined from the Fokker-Planck equation, deviate minimally from a constant in time. Applied to the data, these few assumptions yield a value of D that is smaller by approximately a factor of 10 than the value recently found by Newkirk and Walt in a separate analysis of 1.6-Mev electron data obtained during the same time period on another satellite. The electron lifetimes are found to be strong functions of L, with 4- to 6-day lifetimes observed at the higher L values (4.6–4.8).

Of the dynamical processes that account for sources and sinks of radiation belt particles in the earth's magnetosphere, one of the processes most extensively studied at the theoretical level is charged particle diffusion across L by violation of the third adiabatic invariant. Although the theoretical work has been quite extensive [*Kellogg*, 1959; *Parker*, 1960; *Davis and Chang*, 1962; *Tverskoy*, 1964, 1965; *Dungey*, 1965; *Nakada and Mead*, 1965; *Nakada et al.*, 1965; *Fälthammar*, 1965, 1966; *Ershkovich et al.*, 1967; *Conrath*, 1967; *Newkirk and Walt*, 1968*a*, *b*; *Schulz and Eviator*, 1969; *Fälthammar and Walt*, 1969; *Roederer and Schulz*, 1969], comparatively little experimental information has been obtained in the outer zone to conclusively establish the role of radial diffusion as a common process applicable to a wide range of particle energies. (See, e.g., *Newkirk and Walt* [1968*a*] and *Farley* [1969] for discussions of inner-zone electron radial diffusion and the supporting data.)

For many authors the study of radial diffusion was originally motivated by the desire to explain the source of outer-zone protons and electrons. While radial diffusion of solar wind particles by third-invariant violation seems satisfactory to explain the presence of high-energy outer-zone protons [*Davis et al.*, 1964; *Nakada and Mead*, 1965], the presence of high-energy electrons at large L (~6–8) has proved a stumbling block to the complete acceptance of such a simple mechanism for electron transport and energization.

Some recent outer-zone [*Williams et al.*, 1968] and inner-zone [*Pfitzer and Winkler*, 1968] studies strongly suggest that rather energetic electrons can be produced deep within the trapping regions during magnetic storms, probably by acceleration mechanisms that violate two or more adiabatic invariants. These electrons could subsequently diffuse radially inward and outward from an intense high-energy source nearby, rather than from the boundary.

An extremely simplified view of magnetospheric electron dynamics could consist of two parts. First, during a magnetic storm, energetic electrons would be produced within the trapping regions by nonadiabatic processes. After the storm, the subsequent time history of the

fluxes would be determined by the third-invariant violating diffusion and first-invariant violating loss processes. The spirit of this paper is to treat observed post-storm electron fluxes in the context of radial diffusion and to determine the diffusion coefficients and lifetimes that would best summarize the observations.

The earliest experimental evidence that cross-L diffusion might play a significant role in the dynamics of outer-zone electrons was obtained by *Frank et al.* [1965] from the time dependence of the L profiles of 1.6-Mev electron fluxes, measured near the equator on Explorer 14 in December 1962 and January 1963. These data, as well as the data from another event in April-May 1963, were later examined in more detail by *Frank* [1965]. In both of the cases examined by Frank, the 'leading edge' of a flux profile was observed to move radially inward with time. *Craven* [1966] studied high-latitude electron data from Injun 3. Following several storm periods, Craven examined the position of the peak of the outer-zone electron intensity (at 1.6 Mev) as this peak apparently moved radially inward across L. By studying this feature of an enhanced flux distribution, he obtained a diffusion velocity an order of magnitude lower than that of *Frank* [1965].

Paolini et al. [1968] discussed high-latitude measurements of 1- to 4-Mev electrons observed during July and August 1963. Since their data suggest an e-folding energy that is independent of L, they concluded that during 'quiet' times the diffusion process is bimodal for $L > 4$. *Theodoridis* [1968] and *Theodoridis et al.* [1968] considered the implications of such a diffusion process by constructing elaborate computer models to predict electron distributions in the radiation belts. One of the big disadvantages of these models is their neglect of the finite electron loss cone.

Of published outer-belt electron data, *Frank et al.* [1964] has certainly been the most widely quoted evidence for radial diffusion in the outer magnetosphere. Not until the quantitative analysis of these data by *Newkirk and Walt* [1968*b*] (here denoted by NW), however, was it possible to positively state that the data indicated a diffusive, rather than a convective, inward movement. NW numerically solved the one-dimensional Fokker-Planck diffusion equation given by *Fälthammar* [1966] for appropriately selected boundary and spectral conditions. By using a temporally constant lifetime of 20 days at all L values and a temporally constant diffusion coefficient $D = 1 \times 10^{-8} L^{10}$ day^{-1}, they were able to obtain satisfactory visual agreement with the data.

No comparable studies of electron radial diffusion at low energy (e.g., 0.3–1.0 Mev) have appeared in the literature. Because of the possible importance of outer-zone radial diffusion and the perhaps unique set of geophysical conditions producing the L profiles of *Frank et al.* [1964], it is of interest to reexamine the outer-zone electron fluxes of December 1962 and January 1963. Near-equatorial fluxes of locally mirroring electrons at energies $E > 0.5$ Mev and $E > 1.9$ Mev, measured by a Bell Laboratories instrument package on Explorer 15, are analyzed here, in an effort to evaluate the diffusion coefficient and lifetimes of outer-zone electrons.

The method of analysis requires no assumptions concerning either the L dependence or the magnitude of the particle lifetime τ against pitch angle scattering. Since two energy channels are available, an electron energy spectrum is obtainable by interpolation and need not be postulated a priori. Equatorial fluxes are obtained from off-equatorial measurements by means of an observationally determined pitch-angle distribution that is assumed to have a time-independent functional form. The analysis does not require that the differential diffusion equation be solved, and thus no arbitrary constants appear in the solution as boundary conditions.

The diffusion coefficient is assumed to be time-independent and representable in the form $D = D_n L^n$. Its optimum functional form and magnitude are then determined from the observational data by requiring that the L-dependent reciprocal lifetime, as determined from the Fokker-Planck equation, deviate minimally from a constant in time. This one major assumption is compatible with the viewpoint that the solution of a diffusion equation, with a temporally constant diffusion coefficient and lifetime function, should closely describe the physical observations. The method of solution circumvents several of the assumptions that previous workers found necessary (see discussion above). In particular, the present approach

yields *both* a diffusion coefficient and an L-dependent lifetime against pitch-angle scattering.

Instrumentation

The data from the two electron energy channels discussed here were provided by two detectors flown as part of a complement of six on board the nearly equatorial satellite Explorer 15. Explorer 15 was launched October 27, 1962, into an elliptical orbit of 18° inclination with an apogee of 17300 km, a perigee of 310 km, and an orbital period of 312 min. The satellite spin rate was ~73 rpm.

The detectors were shielded p-n junction semiconductor devices similar to those flown on the Telstar satellite and developed by *Buck et al.* [1964]. The low-energy electron detector ($E > 0.5$ Mev) had a full aperture of 20° and an effective geometrical factor for electrons of 6.5×10^{-4} cm² ster. The high-energy electron detector ($E > 1.9$ Mev) had a full aperture of 20° and an effective electron geometrical factor of 5.5×10^{-4} cm² ster. The count accumulation time was 1.46 sec, or slightly more than one complete satellite spin period.

Analytical Technique

The function $F \equiv L^3\Phi(L, t)$ satisfies the diffusion equation

$$\frac{\partial F}{\partial t} = -\frac{F}{\tau} + L^2 \frac{\partial}{\partial L}\left(\frac{D}{L^2}\frac{\partial F}{\partial L}\right) \qquad (1)$$

given by *Fälthammar* [1966], where Φ is the differential unidirectional flux at constant μ, and $J = 0$. (See appendix A for a proof for the case of relativistic electrons.) The traditional approach to third-invariant diffusion is that equation 1 should be solved for $F(L, t)$, subject to certain assigned initial and boundary conditions, under the assumptions that τ is a known function of L and a constant in time, while D is a constant in time and a function of L that can be represented as $D_n L^n$. The values of n and D_n are then adjusted until the solution of (1) resembles the observed function $F = L^3\Phi(L, t)$ in spatial structure and temporal evolution. The result is called a determination of D.

Another procedure consists of treating (1) as a differential equation for D. When the partial derivatives $(\partial F/\partial t)$ and $(\partial F/\partial L)$ are determined from the observational data, D may be expressed as a numerical quadrature involving a single arbitrary constant. This constant can be evaluated by requiring, for example, that D approach zero for very small L. As in the traditional approach, τ is specified as a known function of L that is constant in time and independent of F.

Both of the above techniques are potentially sensitive to choices of constants and functions of L that are arbitrary in a mathematical sense. No provision is made for an independent determination of τ, so the resulting D is partially determined by the specification of τ. In addition, if only one energy channel is available, an energy spectrum must be introduced arbitrarily to permit the representation of $\Phi(L, t)$ for constant first invariant μ. Finally, the imposition of boundary conditions that are not easily verified by the physical measurements may influence the determination of D.

The analytic approach used here involves a significant departure from the above methods. The spirit of (1) is preserved by requiring that the reciprocal lifetime function

$$\lambda_n(L, t) \equiv -\frac{1}{F}\frac{\partial F}{\partial t} + D_n \frac{L^2}{F}\frac{\partial}{\partial L}\left(L^{n-2}\frac{\partial F}{\partial L}\right) \qquad (2)$$

deviate minimally from a constant in time. This constant, the temporal mean value of $\lambda_n(L, t)$, is denoted by $\langle\lambda_n(L, t)\rangle$ and depends on n and D_n. These are the variables with respect to which the L-averaged variance

$$G_n(D_n) \equiv \iint (\lambda_n^2 - \langle\lambda_n\rangle^2)\, dt\, dL \qquad (3)$$

is to be minimized. Both n and D_n are assumed to be constant in time, as in the other approaches to the problem. The validity of this assumption is open to question; the same question can be raised concerning the temporal constancy of $\tau(L)$ in (1). All methods of obtaining time-independent transport coefficients for magnetospheric particles are equally deficient in this respect.

The physical meaning of G is as follows. The temporal evolution of F is attributed to a combination of diffusion across L and pitch-angle scattering into the loss cone. To the extent that radial diffusion is accounted for by properly choosing a diffusion coefficient, only the decay

of F through pitch-angle scattering remains. Thus, the function G is a measure of the failure to eliminate the time variations of F that are attributable to radial diffusion; G would vanish if $D = D_nL^n$ were chosen so that F exactly satisfied the diffusion equation. Since G never vanishes in practice, the 'best' evaluation of D can be achieved by minimizing the extent to which D fails to account for all radial diffusion.

The function G is rather ad hoc, in the sense that G cannot be derived from some set of mathematical postulates. For example, the integration over L could be weighted by any arbitrarily chosen function of L. The constant weighting factor (unity) was chosen here for lack of any compelling reason to do otherwise. The need to integrate over L at all arises from the need to define a single function over the entire L range being analyzed, since the resulting D_n applies to this entire range.

The variational principle used here is more closely related to the least-squares criterion (weighted or unweighted) commonly used in data analysis than to the variational principles of Lagrangian or Hamiltonian mechanics. As noted above, however, $G_n(D_n) = 0$ if and only if F satisfies (1) for the correct choice of time-independent transport coefficients. The possibility remains that magnetospheric transport coefficients fluctuate widely in time. For such an eventuality an intractable problem, invalidating all current analyses of the data, would exist. It is more optimistic to suppose that the evolution of particle fluxes in the radiation belts can be described *approximately* by assigning an appropriate set of time-independent transport coefficients. The present approach is one of several designed to implement this optimistic viewpoint.

Initial minimization of $G_n(D_n)$ is achieved by requiring that

$$\frac{\partial G_n}{\partial D_n} = 2 \cdot \iint \left(\lambda_n \frac{\partial \lambda_n}{\partial D_n} - \langle \lambda_n \rangle \frac{\partial \langle \lambda_n \rangle}{\partial D_n} \right) dt\, dL = 0 \tag{4}$$

for a fixed n. This linear equation for D_n yields a value of D_n uniquely determined by the data. The result is

$$D_n = \iint \left\{ \frac{\partial \ln F}{\partial t} \left[(n-2) \frac{L^{n-1}}{F} \left(\frac{\partial F}{\partial L} \right) + \frac{L^n}{F} \frac{\partial^2 F}{\partial L^2} \right] - \Delta \ln F \left\langle (n-2) \frac{L^{n-1}}{F} \left(\frac{\partial F}{\partial L} \right) + \frac{L^n}{F} \frac{\partial^2 F}{\partial L^2} \right\rangle \right\} dt\, dL \div \iint \left\{ \left[(n-2) \frac{L^{n-1}}{F} \left(\frac{\partial F}{\partial L} \right) + \frac{L^n}{F} \frac{\partial^2 F}{\partial L^2} \right]^2 - \left\langle (n-2) \frac{L^{n-1}}{F} \left(\frac{\partial F}{\partial L} \right) + \frac{L^n}{F} \frac{\partial^2 F}{\partial L^2} \right\rangle^2 \right\} dt\, dL \tag{5}$$

The integrals in equations 3–5 are definite and extend over the range of L (L_1 up to L_2) and time (t_1 up to t_2) covered by the data. The difference in a quantity between times t_2 and t_1 is denoted by Δ, and the angle brackets denote a time average over the interval $t_1 \leq t \leq t_2$. The symmetric partial derivatives of F are obtained from the data by a standard technique of numerical analysis (first differences). The integrals over time and L were computed by means of the trapezoidal rule in the present work.

The procedure outlined above is repeated for many value of n, e.g., $n = 1, 2, 3, \ldots, 20$. Insertion of the G_n -minimizing D_n, called $D_n{}^*$, in (2) allows the decay constant $\lambda_n(L) \equiv \langle \lambda_n(L, t) \rangle$ to be determined. Plotting $G_n(D_n{}^*)$ against n is a procedure that, at least in principle, allows the best-fitting functional form of $D = D_n{}^* L^n$ to be identified. If $G_n(D_n{}^*)$ has a sharp minimum for some $n = N$, then this identification is virtually unique. In this case the lifetime $\tau(L)$ is identified as the reciprocal of $\lambda_N(L)$.

Observations

Electron profile at constant energy. Explorer 15 did not necessarily measure electrons at the same magnetic field value on each pass through a given L shell. Since the pitch-angle distributions were anisotropic, it was necessary to convert the raw data at each L to equivalent equatorial data. The details of obtaining the generally small corrections associated with this conversion are given in appendix B. All data treated in this paper have been 'corrected' in this manner.

The corrected data are plotted in Figure 1 at four L values for the outer zone electrons (E

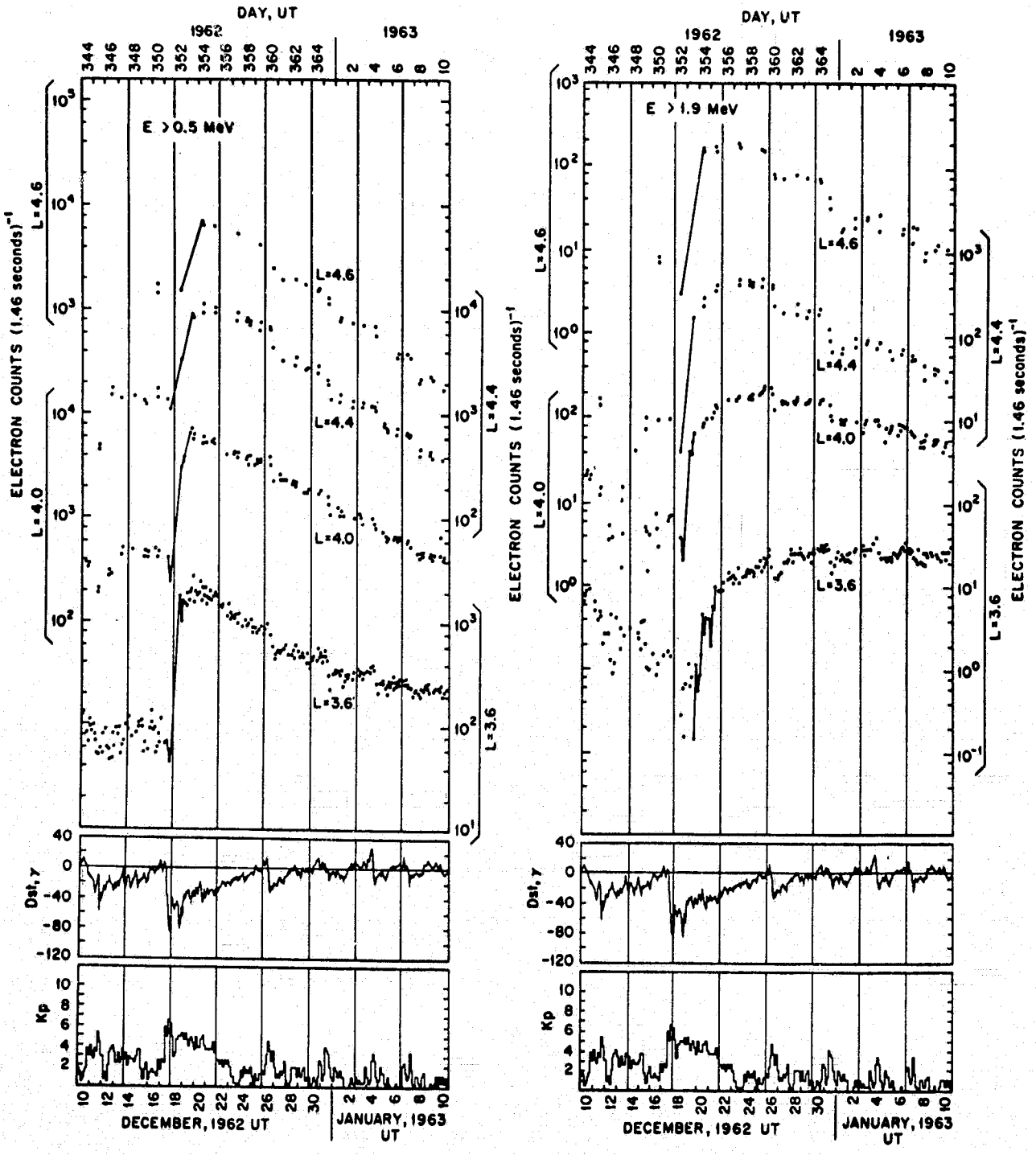

Fig. 1. Explorer 15 electron data from two energy channels for the time period around the magnetic storm of December 17–18, 1962. Large increases in the electron counting rates were observed in both energy channels and at all L values following the storm. The 3-hour-average Kp index and the hourly D_{st} value are plotted at the bottom of the figure.

$>$ 0.5 Mev and $E > 1.9$ Mev) during 32 days in 1962–1963. The D_{st} values and the 3-hour averaged Kp indices are plotted at the bottom of the figure.

The data shown in the figure indicate that the magnetic storm of December 17–18 produced large increases in both the low-energy and high-energy particle fluxes measured by Explorer 15. After the storm, the lower energy electrons on all L shells decayed steadily away, but the higher energy fluxes at lower L did not undergo discernable decay. Such stormlike

enhancements and subsequent decays of electron fluxes in the outer zone have been studied and discussed by many people [e.g., *Williams et al.*, 1968].

After the decay of the storm-produced ring current, only small geomagnetic disturbances were observed during the remainder of the time plotted in Figure 1. Although no new high-energy electrons were introduced into the radiation belts, the decaying fluxes underwent apparent adiabatic changes [*McIlwain*, 1966*b*] owing to the enhanced ring current (as measured by D_{st}) on December 26 and 31 and January 4 and 7.

The median observed data values for both energy channels on December 7, 20, 23, and 29 and January 8 are plotted as a function of L in Figure 2. These are the same days for which *Frank et al.* [1964] presented data points. The L profiles of the electron data at 1.9 Mev indicate very clearly the inward movement of the front edge of the electron profile. With the major exception of the data of January 8 (excluded from the analysis of NW) the 1.9-Mev electron profiles from Explorer 15 are similar at the leading edge to the 1.6-Mev electron flux profiles of *Frank et al.* [1964] (see inset, Figure 2). It should be noted, however, that the ratio between the maximum and minimum electron count rates measured by Explorer 15 after the storm is approximately 100 times the ratio measured by *Frank et al.* [1964].

A most striking feature of the lower energy data plotted in Figure 2 is the absence of an inward-moving leading edge. Rather, the fluxes appear to decay away rather steadily. It is interesting to note that, if only these lower energy data were available, discussions of radial diffusion would probably not arise. It is important to attempt to reconcile these two seemingly dissimilar profiles with the concept of radial diffusion.

Electron profile at constant μ. The diffusion process considered by NW in their analysis of the data of *Frank et al.* [1964] violates only the third adiabatic invariant. In this case, the first and second invariants, μ and J, are conserved. Since the Explorer 15 instrument measured the electron fluxes in two energy channels, it is possible to obtain L profiles at various times at constant μ by interpolating to find electron energy spectra. For particles mirroring at the equator it can easily be shown that

$$\gamma^2 = 1 + 2\mu B/m_0c^2 \tag{6}$$

and

$$\mu = [2 + (E/m_0c^2)](E/2B) \tag{7}$$

where E and m_0c^2 are the electron kinetic energy and rest energy respectively, B is the local (equatorial) magnetic field intensity, and γ is the usual relativistic mass factor.

The daily median electron fluxes in the two energy channels at each L value were used to obtain power-law and exponential representations of the particle spectra. These spectra were then used to construct flux versus time plots of the electron data for selected values of μ (300, 550, 750, and 1000 Mev/gauss). The flux versus time plots resulting from the exponential spectral representation for $\mu = 300$ and 750 Mev/gauss are shown in Figure 3, beginning after the storm on December 20. The e-folding energies as a function of time for $L = 3.6$ and 4.0 are shown at the top of the figure. The ordinate of each data plot is $L^3\Phi$, where Φ is the electron flux (cm^2 sec ster Mev)$^{-1}$, corrected to the equator. The general decay characteristics of the electron fluxes after the magnetic storm enhancement show up quite clearly, as do the presumably adiabatic decreases in the fluxes on December 26 and 31 and January 4 and 7.

The daily median electron fluxes from the power-law spectral representation are not shown but appear much as the data plotted in Figure 3. The results obtained in this paper were found to be very similar for the two spectral representations, so they will be discussed interchangeably.

The median flux profiles of the constant μ data using the power law spectral representation are shown in Figure 4 for the same days as the data of Figure 2 and *Frank et al.* [1964]. When viewed at constant μ, the data no longer exhibit a distinct leading edge that moves radially inward. Rather, at $\mu = 750$ Mev/gauss, the fluxes at the higher values of L decay steadily away, while the fluxes at the lower values of L (3.4 — 4.0) tend to increase. This behavior suggests a widening of the electron spatial distribution, but since the complete flux versus L distribution was not accessible to

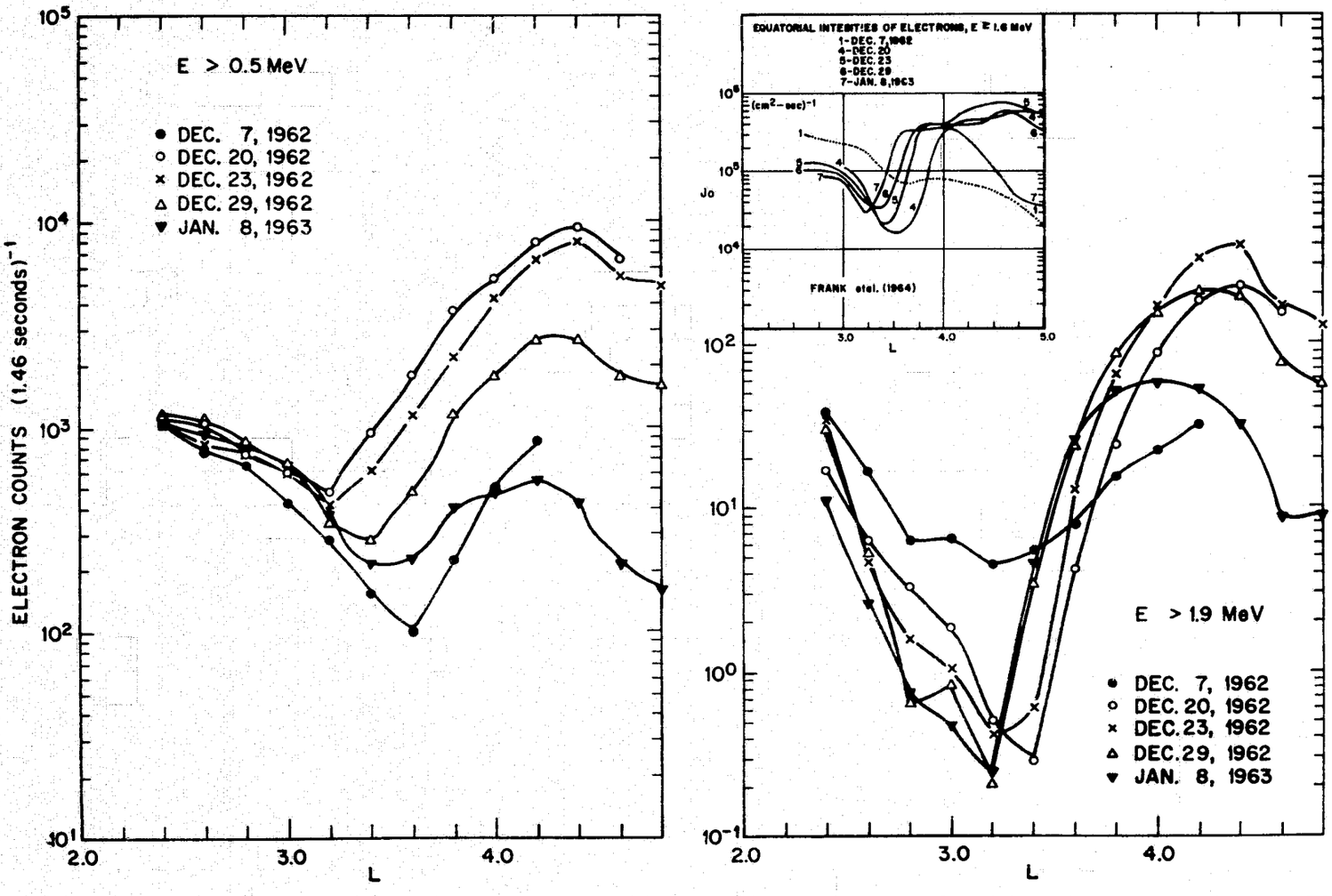

Fig. 2. Radial profile of the daily median electron fluxes measured in both energy channels on several selected days after the magnetic storm. The electron fluxes ($E > 1.6$ Mev) measured on the same days by *Frank et al.* [1964] with an instrument on the Explorer 14 satellite are shown in the inset.

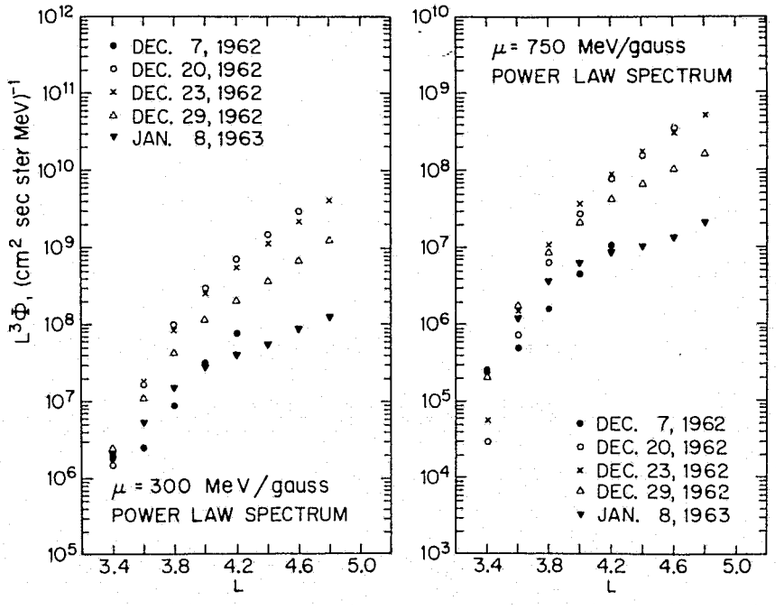

Fig. 3. Electron data at constant first invariant μ for an exponential spectral representation of the fluxes. At the top of the figure the spectral parameters E_0 are plotted as a function of time for $L = 3.6$ and 4.0.

Explorer 15, it is not possible to measure the increasing half-width. (The widening of an initially narrow shell of enhanced electron fluxes enabled *Brown* [1966] and NW to estimate the radial diffusion coefficient for 1.9-Mev electrons at $L = 1.765$.) Only at $L = 3.4$ was there a hint of an increase in the fluxes at $\mu = 300$ Mev/gauss. At the higher values of L the fluxes steadily decayed away.

One additional manipulation of the data merits comment. Diffusion coefficients were determined not only from constant-μ data such as those shown in Figure 3, but also from constant-μ data after removal of the presumed adiabatic variations. The adiabatic variations were removed by identifying several isolated days on which $D_{st} \approx 0$. The 5 days on which $|D_{st}| \lesssim 8\ \gamma$ were December 23, 25, and 30 and January 4 and 10. 'Adiabatically corrected' data points for the intervening days of comparatively large D_{st} were manufactured by fitting a cubic polynomial in the time variable to the data obtained on the 5 days during which ring current effects could not have been significant. The data thus 'smoothed' for $\mu = 300$ and 750 Mev/gauss are plotted in Figure 5. Data points for the 5 reference ($D_{st} \approx 0$) days are denoted by crosses.

The adiabatic variations were not easily removed by using ring current models. The method of interpolation summarized in Figure 5 circumvents the need to assume a particular model for the ring current. It seems, moreover, that the variations in the 1.9-Mev electron fluxes apparently are not always purely adiabatic, since the decreases are generally larger than would be predicted by a reasonable ring current model. This phenomenon was originally noted by *McIlwain* [1966*b*].

Results

Both the unsmoothed and the smoothed electron data for $\mu = 300$, 550, 750, and 1000 Mev/gauss were analyzed by the technique outlined earlier. The electron lifetimes and diffusion coefficients were obtained for both the power-law and exponential representations of the spectral fit between the two energy channels. The results for both spectral representations were very similar; only the power law results will be graphically presented here.

Unsmoothed data. Plots of $G_n(D_n^*)$ as a

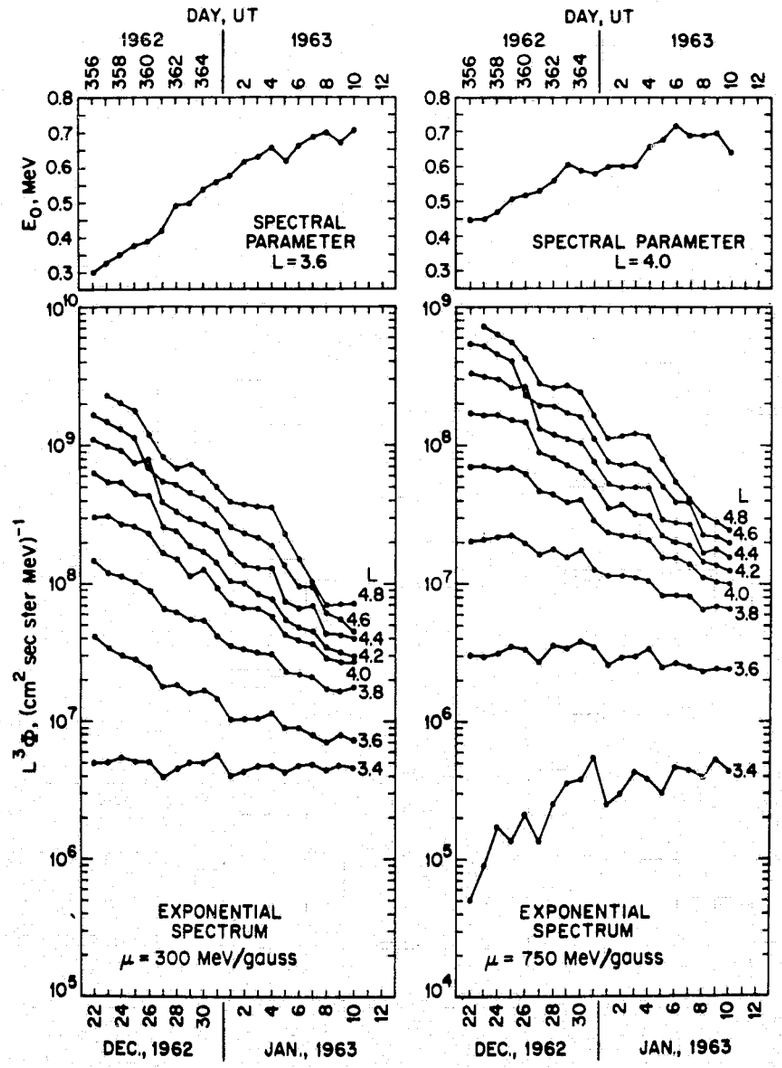

Fig. 4. Radial profiles of the daily median flux values at two values of μ. The data are from a power law representation of the electron spectra and are for the same days as the data of Figure 2. Note the lack of leading-edge profiles when the data are presented at constant μ.

function of the index n resulting from the analysis of the unsmoothed data are presented in Figure 6. No minimum in G with respect to n is found for any μ. Thus, the analytical technique introduced here fails to uniquely define an optimum value of n when applied to the Explorer 15 data. Each value of n, however, yields a rather well-defined value of D_n. This is evident from Figure 7, where $G_n(D_n)$ is plotted for $n = 6$, 8, 10, and 12 with $\mu = 750$ Mev/gauss. Similar results hold for the other μ-values, except that the minima of $G_n(D_n)$ are broader and the values of D_n* are more poorly defined for $\mu = 300$ Mev/gauss than for the three higher values of μ.

The appropriate electron lifetime τ (equation 2) for each of several values of n and μ is plotted as a function of L in Figure 8. The variation of τ with the choice of index n is generally small, particularly at the higher L values. The lifetimes in Figure 8 vary from several tens of days at $L = 3.4$ to approximately five days at $L = 4.8$.

The corresponding diffusion coefficients (equation 5) obtained simultaneously as functions of L are shown (divided by L^{10}) in Figure 9.

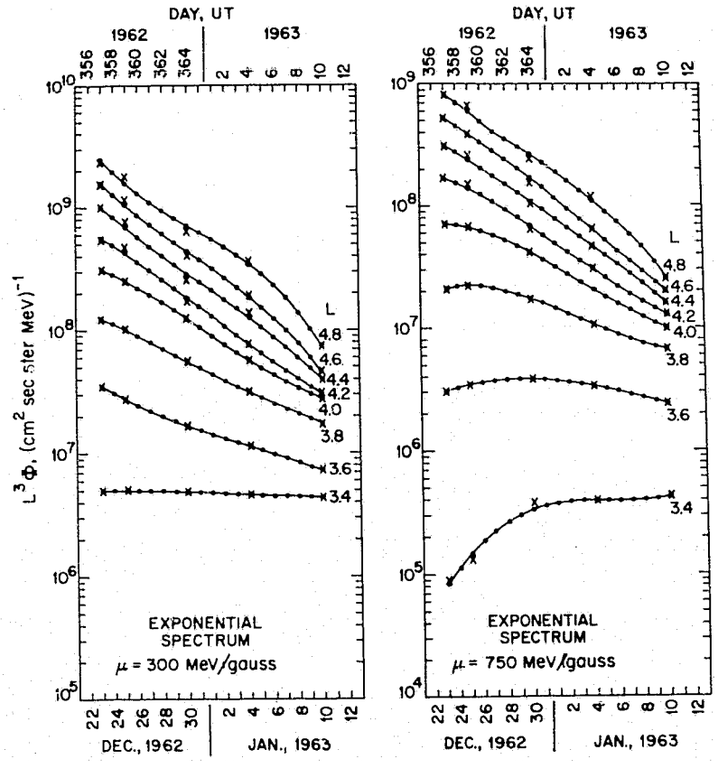

Fig. 5. Data at constant μ after artificially removing the adiabatic variations. The data are from an exponential representation of the electron spectra. The 5 days of $|D_{st}| \lesssim 8\ \gamma$ used for the least-squares cubic fit are denoted by crosses.

Although the optimal values of n were not determined by this analysis, there are valid theoretical reasons for believing that n should fall roughly between 6 and 12 [*Tverskoy*, 1965; *Nakada and Mead*, 1965; *Fälthammar*, 1966]. Accordingly, the values of $D_n{}^*L^{n-10}$ for $n = 6$, 8, 10, and 12 are plotted for the four μ values. In each plot the shaded region includes those values of D/L^{10} that satisfy the requirement $6 \leq n \leq 12$ and $G < G_{max}$ for some reasonably chosen maximum value (see Figures 6 and 7). The shaded area thus specifies the total limits of uncertainty acknowledged in the present evaluation of D. The cross-hatching in Figure 9 indicates the corresponding result obtained by NW from the electron data of *Frank et al.* [1964]. The results obtained here are smaller than those found by NW by approximately a factor of 10. The scale at the top of each portion of Figure 9 indicates the variation of electron energy with L at constant μ.

Smoothed data. To test the sensitivity of the analytical technique to adiabatic variations (which may well be coincident in time with nonadiabatic effects), the procedure for calculating G, τ, and D was repeated, using the smoothed daily median data.

The values of $G_n(D_n{}^*)$ for the four μ values are plotted in Figure 10 as functions of n. The values of $G_n(D_n)$ in Figure 10 are smaller than those in Figure 6, as might have been expected from the lack of adiabatic scatter in the smoothed data. Only a weak minimum is found in G for the three higher μ values; no minimum at all is found for $\mu = 300$ Mev/gauss. The plot of $G_n(D_n)$ versus D_n that corresponds to Figure 7 is not shown for the smoothed data but does reveal well-defined minima for G for the several values of n.

The values of τ extracted from the smoothed data are plotted in Figure 11 for the four μ values. The electron lifetimes are seen to be similar to those obtained from the unsmoothed data; again there is an inverse variation of τ with L.

The values of D_nL^{n-10} obtained from the

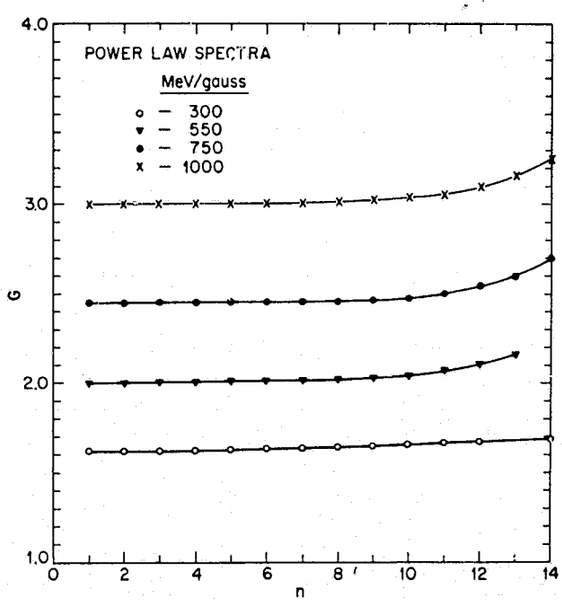

Fig. 6. Plots of the variance $G_n(D_n^*)$ as a function of n for 4 values of μ, using the unsmoothed data and power-law spectral representations of the fluxes.

smoothed data are plotted in Figure 12 for the same indices n as in Figure 9. The error estimates are indicated by the shaded regions and were made, as in Figure 9, by referring to Figure 10 and the appropriate plots of $G_n(D_n)$ versus D_n (not shown). The value of a reasonably chosen G_{max} is indicated on each plot. The results for D/L^{10} are again well below those of NW, also indicated in Figure 12.

Discussion

Electron measurements from two separate energy channels of an experiment on Explorer 15 have been used to obtain the equivalent fluxes of equatorially mirroring electrons at constant first-invariant μ as a function of L and time, following a magnetic storm on December 17–18, 1962. By using these fluxes at selected values of μ and a variational principle, the electron lifetimes and radial diffusion coefficient were obtained as functions of L.

The electron lifetimes show a strong dependence on L. The L dependences and magnitudes are in general agreement with 0.5-Mev electron lifetime data compiled by *Roberts* [1969] and are in disagreement with the 20-day lifetime postulated at all L values beyond $L = 2.1$ by NW. Visually measured lifetimes in the outer zone following the April 18, 1965, storm have been published by *Williams et al.* [1968]. Their lifetime values and L dependences are also in general agreement with the results obtained here.

The values of D published by NW and those found here by using different data obtained during the same time period are the only ones in this energy range obtained from analytical techniques based on a diffusion equation. (The value of D obtained by *Kavanagh* [1968] for 50- to 100-kev electrons had a complicated L dependence and was ~100 times larger than the value obtained by NW at $L = 5$.) The diffusion coefficients obtained here are smaller by approximately a factor of 10 than those obtained by NW.

As is stated above, NW treated the diffusion problem by assuming initial spectral conditions and boundary conditions on the diffusion equation. They also assumed an electron lifetime independent of L and substantially larger than the lifetimes found here for $L \gtrsim 4$. Finally, NW

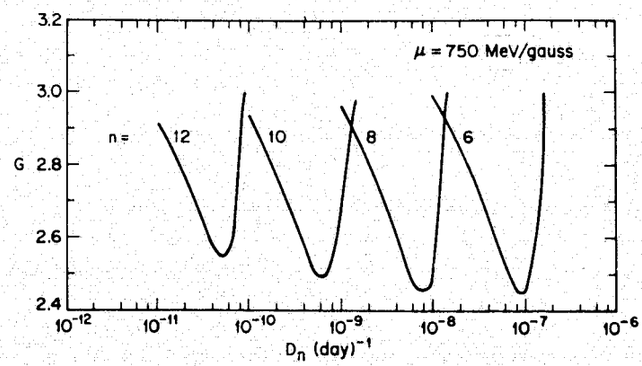

Fig. 7. The function $G_n(D_n)$ for 4 values of n at $\mu = 750$ Mev/gauss, using the unsmoothed data and power-law spectral representations of the fluxes.

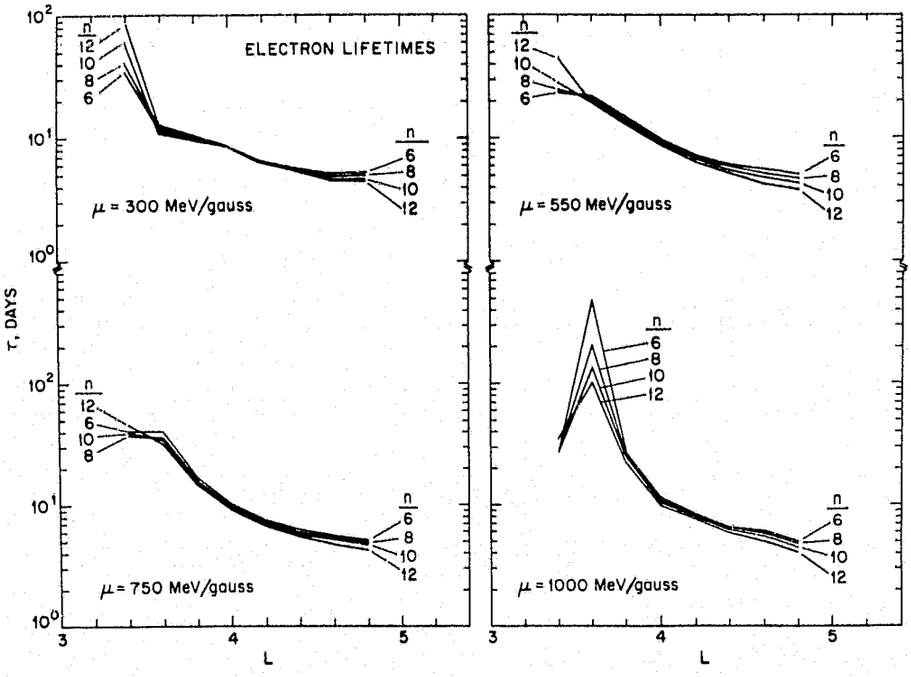

Fig. 8. Electron lifetimes τ as a function of L for 4 values of μ and several values of n. The lifetimes are extracted from the unsmoothed data with power-law representation of the spectra.

obtained their mean values of D by a visual comparison of their computer results with the observations reported by *Frank et al.* [1964].

The present results are obtained without recourse to the imposition of boundary conditions, since the diffusion equation is exploited in its differential form. This procedure is consistent with the objective of placing maximum significance on the observational data and minimum reliance on assumptions not readily verified by physical measurements. The present approach is so different in philosophy from the methods employed by previous investigators that a proper comparison may be difficult. It is claimed here that, if the correct boundary conditions can be found, the combination of D and τ obtained above will more nearly predict the evolution of F than any other combination of $D = D_n L^n$ and $\tau(L)$.

NW have stated that their results in the region $4 < L < 5$ were quite sensitive to their boundary conditions at $L \sim 6$ and to the source spectrum. To insure that the results presented here were not being unduly influenced by the inclusion of the data at high L, the analysis was repeated using only data up to and including $L = 4.4$. Although the n dependence of $G_n(D_n^*)$ changed somewhat for each μ, the values of D_n^* were in general only ~5–10% larger.

The results presented above were obtained for a 20-day time period after the large magnetic storm. In Figure 13 we present values of D_n for $n = 6$, 8, 10, and 12 obtained from analyses of 12- and 15-day segments of unsmoothed data (power-law spectral interpolation) after the storm. The values of D for the segments in the latter portion of the original 20-day period are found to be approximately three times larger than for the entire period. The values of D obtained from the data in the initial part of the period are approximately the same as those found for the entire 20-day interval.

The results for D and τ were found to be relatively insensitive to several other modifications of the basic procedure. These modifications, which usually changed D by at most a factor of 2 and left τ virtually unchanged, involved details of numerical differentiation and integration at the endpoints of the temporal and spatial intervals, the replacement of all derivatives in (5) by logarithmic derivatives (numerical derivatives of ln F), and the insertion

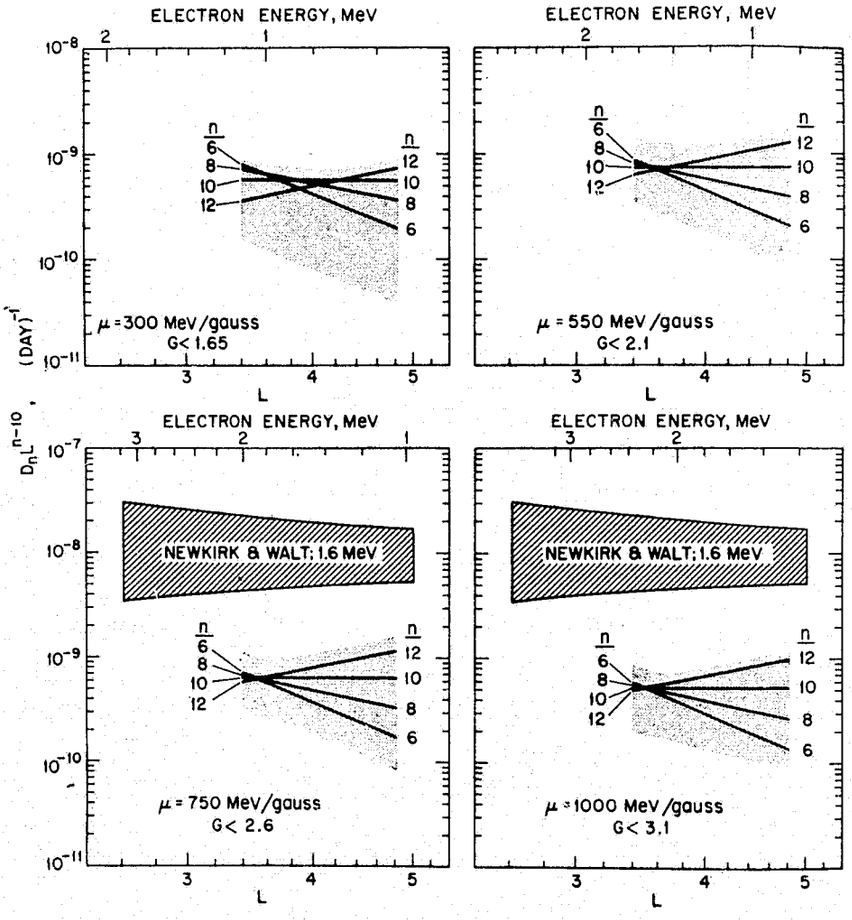

Fig. 9. Electron diffusion coefficients for 4 values of μ and several values of n. These diffusion coefficients are extracted from the unsmoothed data with power-law representations of the spectra. The results obtained by *Newkirk and Walt* [1968*b*] from Explorer 14 data during the same time period are so denoted in the figure.

of a weighting function proportional to L^{-3} in both numerator and denominator of (5).

The L dependence of D was not successfully obtained by using the variational technique employed here. This was a significant disappointment. No hint of an optimum value of n is apparent in Figure 6 (unsmoothed data). The results for the smoothed data suggest that n becomes larger as μ increases, but no special confidence should be placed in this interpretation. NW suggest that $n = 10 \pm 1$ is a good representation of their results, although the uncertainties in their value of D (see Figures 9 and 12) are often as large as those acknowledged in this paper.

The small range of L analyzed in this paper could be one reason why n was so poorly determined. The L range of NW extended from $L = 2.6$ to 5.0. It should be noted, however, that the movement of the enhanced flux profiles as presented by *Frank et al.* [1964] and as presented in this paper (Figure 2) did not extend over such a large L range. In fact, when *Frank* [1965] presented values of the diffusion velocity for this data, he quoted values only from $L = 3.4$ to 4.7.

The diffusion coefficient $D = D_n L^n$ can be written [*Fälthammar*, 1966; *Schulz and Eviatar*, 1969] as

$$D_n L^n \sim 3 \times 10^{-8} (\bar{\omega}/b)^2 S(\bar{\omega}) L^{10} \qquad (8)$$

where b is the stand-off distance of the magnetopause, $S(\omega) \equiv d\langle(\Delta b)^2\rangle/d\omega$ is a spectrum characterizing the magnetospheric disturbance producing the diffusion, and $\bar{\omega}/2\pi$ is the mean longitudinal drift frequency of an electron. For steplike

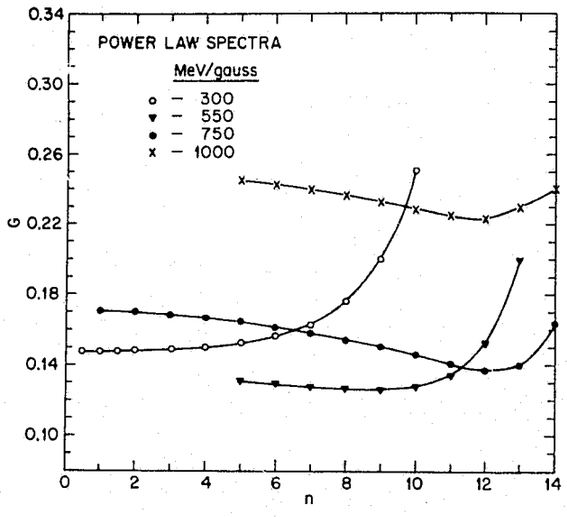

Fig. 10. Plots of the variance $G_n(D_n^*)$ as a function of n for 4 values of μ, using the smoothed data and power-law spectral representations of the fluxes.

disturbances that have a duration long compared with $2\pi/\bar{\omega}$, $S(\bar{\omega})$ is inversely proportional to $\bar{\omega}^2$, so the energy dependence in (8) disappears. However, *Fälthammar* [1966] has noted, for example, that for impulses of duration less than $2\pi/\bar{\omega}$ the diffusion coefficient varies as $\mu^2 L^6$ in the nonrelativistic limit. Thus, for actual geomagnetic conditions, the L dependence of the diffusion coefficient might not be expected to be precisely L^{10} nor independent of μ. The results presented in Figures 9 and 12 suggested a weakly inverse variation of D with μ, particularly at the higher values of n. This behavior would correspond to impulses that have a finite rise time on the drift time scale.

The values of D derived in this paper are of the same order at the higher L values as the diffusion coefficient caused by pitch-angle scattering in the presence of drift-shell splitting, as recently calculated by *Roederer and Schulz* [1969] and by *Fälthammar and Walt* [1969]. Since this type of radial diffusion probably occurs at constant energy, it must be handled by an equation [*Fälthammar and Walt*, 1969] that differs somewhat from (1). A variational analysis of the present data in the context of constant-energy diffusion is currently in progress.

The diffusion results for $\mu = 300$ Mev/gauss seem anomalous in that, for both the unsmoothed and the smoothed data, $G_n(D_n^*)$ increases steadily as n increases. Although this may reflect an inadequacy of the analytical procedure, it is noteworthy that the 0.5-Mev

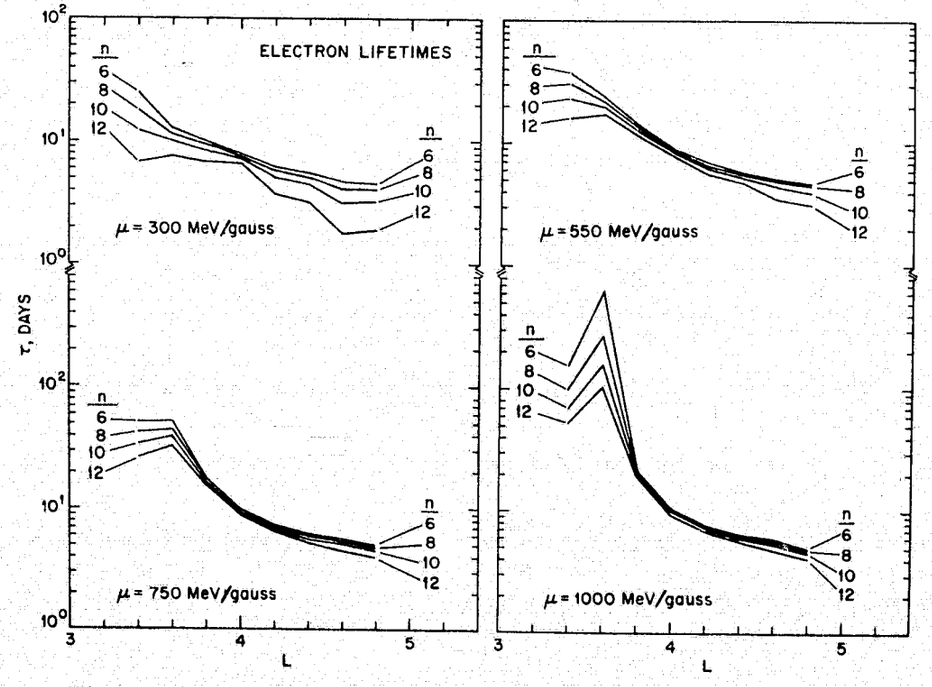

Fig. 11. Electron lifetimes τ as a function of L for 4 values of μ and several values of n. These lifetimes are extracted from the smoothed data with power-law representations of the spectra.

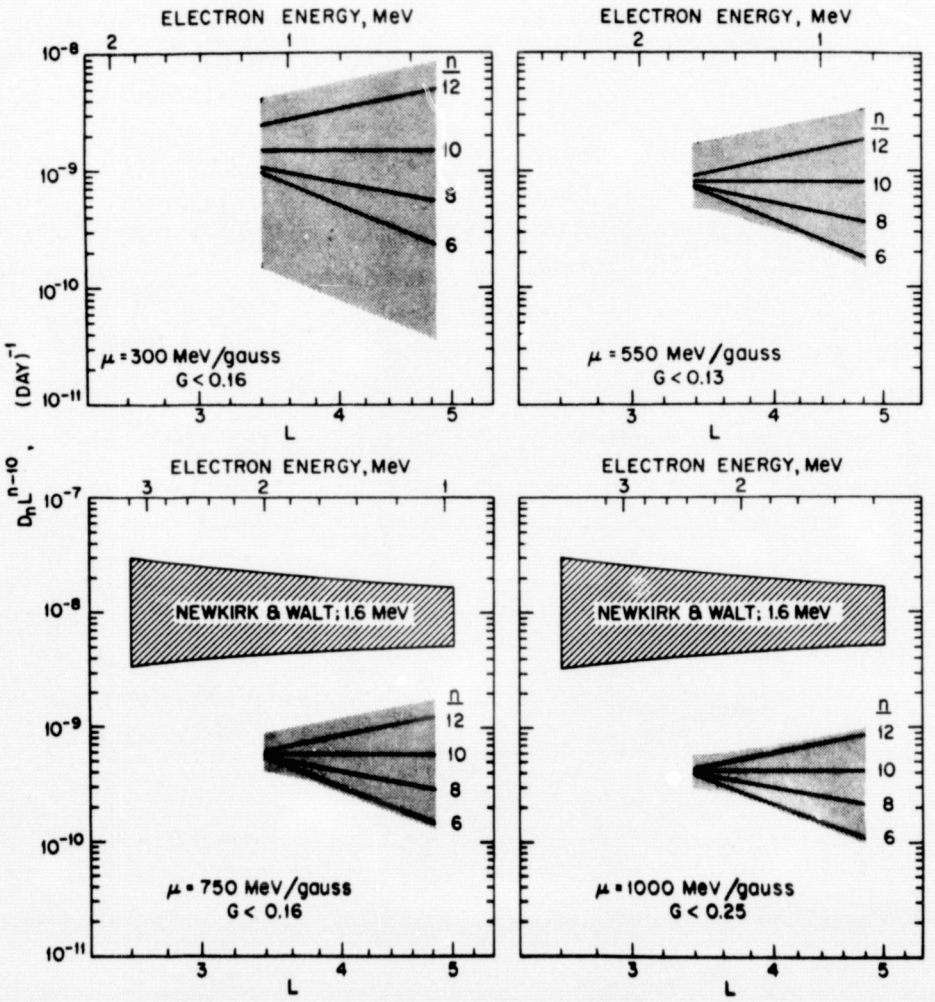

Fig. 12. Electron diffusion coefficients for 4 values of μ and several values of n. These diffusion coefficients are extracted from the smoothed data with power-law representations of the spectra. The results obtained by *Newkirk and Walt* [1968*b*] from Explorer 14 data during the same time period are so denoted in the figure.

data (Figure 2) and the $\mu = 300$ Mev/gauss data (Figure 4) seem to exhibit a straight decay that apparently obscures any diffusive features of the type evident at the larger values of E and μ. The reasons for the different temporal evolution of weakly relativistic and extremely relativistic electrons is not known but certainly deserves further study before anyone can claim that post-storm radiation-belt dynamics are well understood.

Several past determinations by various observational methods of an outer-zone diffusion coefficient are listed in Table 1. The results reported by *Tverskoy* [1964, 1965] and *Nakada and Mead* [1965] were obtained by using sudden commencement and sudden impulse data, as recorded on ground-based magnetograms. *McDiarmid and Burrows* [1967] obtained an estimate of the diffusion coefficient from their measurements by following the peak (crest) of the electron outer belt, as did *Craven* [1966]. *Frank* [1965] and *Vernov et al* [1966, 1968] measured the velocity of a 'leading edge' in a single energy channel, but did not thereby preserve the first invariant. This procedure leads to a 'diffusion velocity' larger in magnitude than the true $(\partial D/\partial L)_\mu$.

The results obtained here are intermediate in magnitude between the estimates of *Nakada and Mead* [1965] and the computations of NW. Thus, the intensity and number of magnetic perturbations required for the electron diffusion are not as large as would be required by NW.

The spectral parameter E_0 (e-folding energy), of which two time history plots are shown in Figure 3, were plotted as a function of L for a

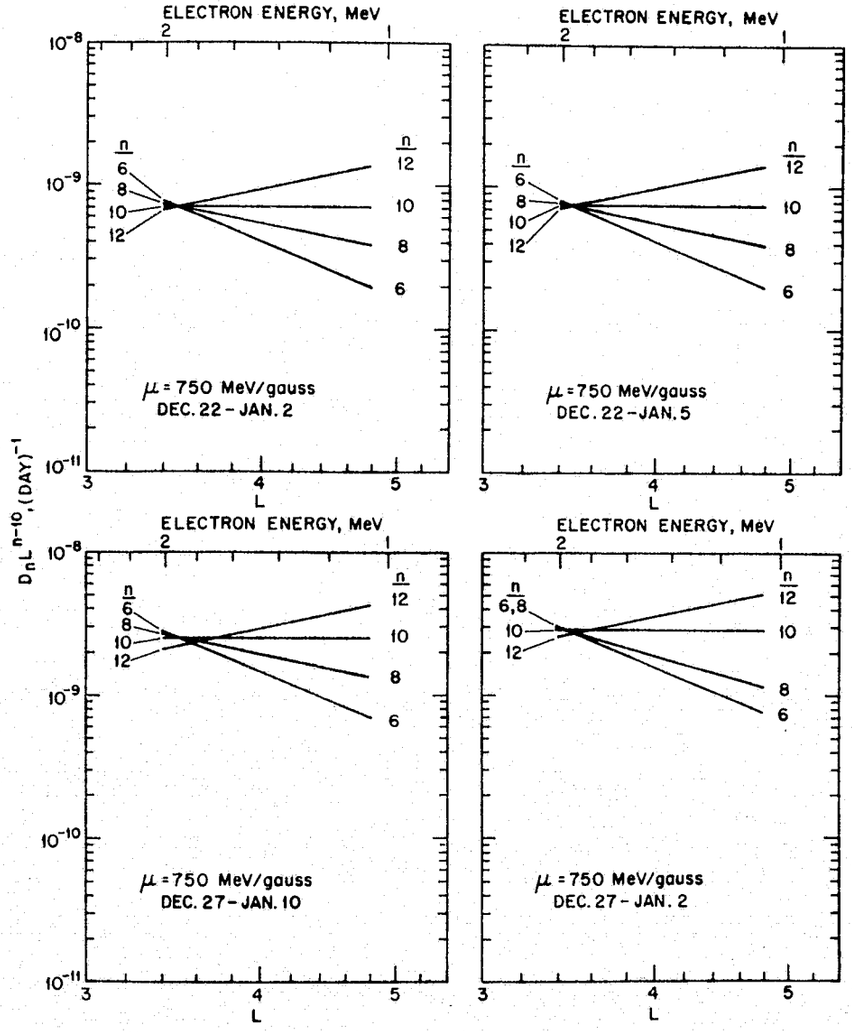

Fig. 13. Electron diffusion coefficients for $\mu = 750$ Mev/gauss obtained by processing several subsets of the total 20-day period of unsmoothed data (power-law spectral representation).

number of consecutive days following the December storm. During the entire post storm period analyzed, it was found that $(\partial E_0/\partial L) < 0$ from $L \sim 3.8$ to ~ 4.8. This negative radial gradient of E_0 suggests constant-μ diffusion. *Paolini et al.* [1968], apparently observing a nearly vanishing derivative of E_0 with respect to L after other storms, hypothesized a bimodal diffusion mechanism to explain their results.

During the course of this study, a number of intriguing possibilities for future investigations of radial diffusion and other magnetospheric processes have suggested themselves. In addition to an investigation of the present data in the context of constant-energy diffusion, a study is being made of ATS 1 electron longitudinal-drift echoes [*Lanzerotti et al.*, 1967; *Brewer et al.*, 1969] in an attempt to determine the power spectrum $S(\omega)$ of the magnetic disturbances. Another interesting possibility is a study of the power spectra of several ground-based magnetograms during the time interval discussed here in an attempt to determine $S(\bar{\omega})$. Since $2\pi/\bar{\omega} \sim$ 10–30 min for electrons of these energies, the 2.5-min digitized data might well suffice for this study. Finally, it seems highly important to examine electron data (with perhaps better spectral information) from other time periods by using the variational technique introduced here.

TABLE 1. Outer-Zone Radial Diffusion Coefficients

Reference	DL^{-10} (day^{-1})	L Range	Constant	Method	Comments
Tverskoy [1964]	$2\text{–}4 \times 10^{-11}$	$\lesssim 7$	μ	Magnetogram (sc)	
Tverskoy [1965]	$4\text{–}13 \times 10^{-9}$	$\lesssim 7$	μ	Magnetogram (sc, si)	
Nakada and Mead [1965]	$1\text{–}2 \times 10^{-10}$	$\lesssim 7$	μ	Magnetogram (sc, si)	
Vernov et al. [1966]	$\sim 7 \times 10^{-9}$	5.0–6.0	E	Diffusion velocity	$E > 2$ Mev, $\theta \sim 41° \pm 5°$
Vernov et al. [1968]	$3\text{–}4 \times 10^{-8}$	4.0–6.0	E	Diffusion velocity	$E > 100$ kev
Frank [1965]	$\sim 5 \times 10^{-7}$	3.4–4.7	E	Diffusion velocity	$E \sim 1.6$ Mev
Craven [1966]	$\sim 3 \times 10^{-8}$	3.5–6.5	E	Crest velocity	$E \sim 1.6$ Mev
McDiarmid and Burrows [1967]	$5\text{–}8 \times 10^{-9}$	4.4–4.6	E	Crest velocity	$E \sim 0.25$, 3.9 Mev
Kavanagh [1968]	$\sim 1 \times 10^{-6}$	~ 5	μ	Quadrature for D	$E \sim 50$, 100 kev
Newkirk and Walt [1968*b*]	$\sim 1 \times 10^{-8}$	2.6–5.0	μ	Solution of (1) for Φ	$E \sim 1.6$ Mev
Present result	$4\text{–}8 \times 10^{-10}$	3.4–4.8	μ	Variational principle	$E \sim 0.5$, 1.9 Mev

Appendix A: Relativistic Diffusion Equation

By considering nonrelativistic particles mirroring at and diffusing in the equatorial plane of a magnetic dipole field, *Nakada and Mead* [1965] and *Fälthammar* [1966] have deduced that the equation

$$\frac{\partial F}{\partial t} = L^2 \frac{\partial}{\partial L}\left(\frac{D}{L^2}\frac{\partial F}{\partial L}\right) - \frac{F}{\tau} \qquad \text{(A-1)}$$

describes the evolution of the function $F = L^3\Phi$, where Φ is the unidirectional particle flux per unit energy, averaged over the azimuthal drift path at constant μ (first invariant) and J (second invariant) in the limit $J = 0$. For the present work it is essential to verify the validity of (A-1) for relativistic particles; for other applications [*Schulz and Eviatar*, 1969] it is of interest to extend the relativistic result to the equatorial plane of a more general magnetic field.

Since particles that mirror at the equator follow paths of constant field intensity B under adiabatic motion, it is convenient to define L by the relation

$$L^3 = (B_d/B) \qquad \text{(A-2)}$$

where $B_d = 0.31$ gauss is the equatorial field strength at the surface of the earth. This definition corresponds to that given by *McIlwain* [1966*a*] and *Schulz and Eviatar* [1969]. As a general rule, the flux $\Phi(p, \alpha; \mathbf{r})$ per unit energy and solid angle Ω at pitch angle α is related to the distribution function $f(p_\parallel, p_\perp; \mathbf{r})$ that satisfies Liouville's theorem by the relation

$$\iint \Phi(p, \alpha; \mathbf{r})\, dE\, d\Omega = \iint f(p_\parallel, p_\perp; \mathbf{r})(p/m)p^2\, dp\, d\Omega \qquad \text{(A-3)}$$

where $m = \gamma m_0$ is the relativistic mass. The total energy $mc^2 = E + m_0c^2$ is related to the scalar momentum p by the equation

$$(E + m_0c^2)^2 = p^2c^2 + m_0{}^2c^4 = p_\parallel{}^2c^2 + p_\perp{}^2c^2 + m_0{}^2c^4 \qquad \text{(A-4)}$$

where $p_\parallel = p\cos\alpha$ and $p_\perp = p\sin\alpha$. From (A-4) it follows that $mdE = p\,dp$. Since (A-3) applies to any general domain of energy and pitch angle, the integrands are necessarily equal, so that

$$\Phi(p, \alpha; \mathbf{r}) = p^2 f(p_\parallel, p_\perp; r, \theta, \lambda) \qquad \text{(A-5)}$$

This equation is specialized to the case of equatorially mirroring particles by requiring that $p_\parallel = 0$, $\alpha = \pi/2$, and $\theta = \pi/2$. The first invariant is then given by

$$\mu = p^2/2m_0B = p^2L^3/2m_0B_d \qquad \text{(A-6)}$$

and it follows that

$$L^3\Phi(p, \pi/2; \mathbf{r}) = 2\mu m_0 B_d f(0, p_\perp; r, \pi/2, \lambda) \qquad \text{(A-7)}$$

Since $df/dt = 0$ along any dynamical trajectory,

the detailed behavior of $L^3\Phi$ is completely deterministic. Diffusion occurs only in the sense that the phase variable φ of *Brewer et al.* [1969] (defined so that under adiabatic motion a particle drifts at a constant rate in φ) is suppressed. Any particle detector having a nonvanishing drift-frequency bandwidth automatically averages over this phase in a temporally asymptotic situation. Thus, diffusion is observed to occur in the radial variable conjugate to φ. Since the drift-shell geometry is independent of μ in the absence of static electric fields, this radial variable is a function only of L for a given magnetic field configuration.

Because $F \equiv L^3\Phi$ is related by the constant factor $2\mu m_0 B_d$ to the distribution function f that satisfies Liouville's theorem, this function appears to the right of all differential operators in the diffusion equation. The remaining structure of the diffusion equation depends on the Jacobian of the transformation of variables that relates $(r, \theta, \lambda, p_\perp, p_\parallel)$ to (L, φ, μ, J). *Brewer et al.* [1969] have shown that

$$r\, dr\, d\lambda = (c\mu/\gamma\bar{\omega}qB)\, dB\, d\varphi = -(3c\mu/\gamma\bar{\omega}qL)\, dL\, d\varphi \tag{A-8}$$

where $\bar{\omega}/2\pi$ is the drift frequency, q is the charge, and $(\mu/q\gamma\bar{\omega})$ depends only on L for $J = 0$. In the present case it is possible to identify

$$2\pi p_\perp\, dp_\perp = 2\pi m_0 B\, d\mu = 2\pi m_0 B_d L^{-3}\, d\mu \tag{A-9}$$

It thus remains to be shown that

$$r \sin\theta\, d\theta\, dp_\parallel = (4/\pi)\, dJ \tag{A-10}$$

at $J = 0$ without the assumption of a dipole field. This is done by representing the bounce motion as a harmonic oscillation of frequency $\Omega/2\pi$, while noting that $ds = r \sin\theta\, d\theta$ for the limiting case of equatorially mirroring particles. *Roederer and Schulz* [1969] have shown that, in this limit, $J = (\pi/m\Omega)p_{\parallel m}{}^2 = |\pi p_{\parallel m} s_m|$, where $p_{\parallel m}$ is the equatorial value of $p_\parallel$, and s_m is the maximum excursion of the guiding center from the equator. Since either value can be positive or negative, it follows that $dp_\parallel = 2|p_{\parallel m}|$, and that $ds = 2|s_m|$ for particles with second invariants between zero and dJ. In other words, it follows that $dJ = (\pi/4)dp_\parallel ds = (\pi/4)r \sin\theta\, d\theta\, dp_\parallel$ in the limit $J = 0$. The net result of (A-8) through (A-10) is that

$$r^2 \sin\theta\, dr\, d\theta\, d\lambda\, 2\pi p_\perp\, dp_\perp\, dp_\parallel = -(24\mu c m_0 B_d/q)(1/\gamma\bar{\omega}L^4)\, dL\, d\varphi\, d\mu\, dJ \tag{A-11}$$

From this follows the diffusion equation

$$\frac{\partial F}{\partial t} = \gamma\bar{\omega}L^4 \frac{\partial}{\partial L}\left(\frac{D}{\gamma\bar{\omega}L^4}\frac{\partial F}{\partial L}\right) \tag{A-12}$$

which reduces to (A-1) in the limit of a dipole field and on inclusion of a phenomenological loss term $-F/\tau$.

This loss term is a simplified representation of the loss via pitch-angle diffusion of the set of particles that have conserved μ and J $(=0)$. This loss-term representation is valid in practice only if the pitch-angle distribution at each L is approximately constant in time and if shell-splitting effects [*Roederer*, 1968; *Roederer and Schulz*, 1969; *Fälthammar and Walt*, 1969; *Pfitzer et al.*, 1969] are comparatively unimportant to the over-all picture.

It may be of interest to note that $F \equiv L^3\,\Phi$ is related to the function $n^*(\mu, L, J = 0; t)$, which appears in the radial-diffusion analysis of *Schulz and Eviatar* [1969], by the equation $F = (cq/24\pi)\gamma\bar{\omega}L^4 n^*$. A universal formalism for the construction of diffusion equations applicable

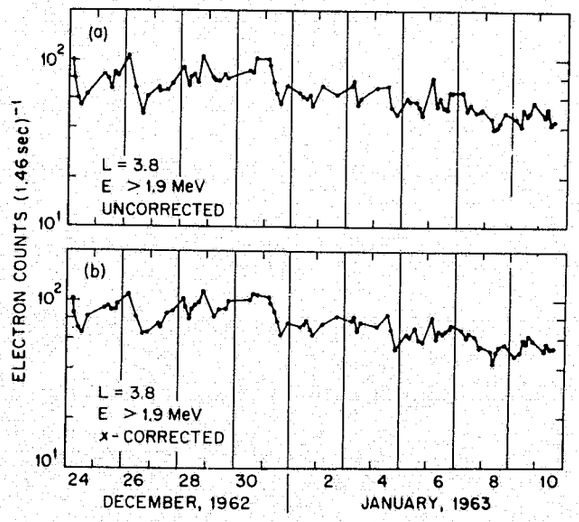

Fig. 14. (*a*) Uncorrected $L = 3.8$ electron data ($E > 1.9$ Mev) following the December magnetic storm. (*b*) The same data after pitch-angle correction to the equator.

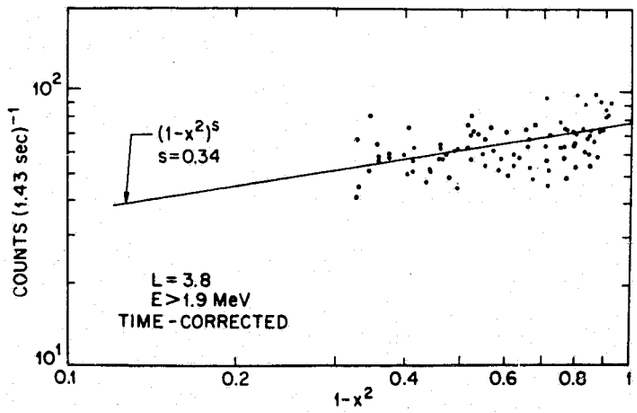

Fig. 15. Plot of the data of Figure 14 ($L = 3.8$, $E > 1.9$ Mev) as a function of $(1 - x^2)$ on a logarithmic scale. The solid line indicates the x correction after removal of the steady decay seen in Figure 14.

to more general dynamical processes has been given by *Haerendel* [1968]. The equation derived above constitutes a special case of the more general equation.

Appendix B: Pitch-Angle Corrections

Since the analyses in the foregoing text have been performed for electron fluxes corrected to the equator, it is of interest to see how severe the pitch-angle corrections were. Figure 14*a* shows the counting rates at $L = 3.8$ for the 1.9-Mev electron channel during the period of analysis. Figure 14*b* shows the electron counts versus time after they were pitch-angle corrected to the equator. A small reduction in the spread of the points is noted, as is a general over-all increase in the average counting rate.

The pitch-angle corrections were made by assuming that the pitch-angle distribution was constant in time. The data points were then least-squares fitted to the function

$$R = \xi\{\exp[\eta(t - t_0)]\}(1 - x^2)^s \qquad \text{(B-1)}$$

where ξ, η, and s are the constants to be determined from the fit, and the variable

$$x = (1 - B_0/B)^{1/2}$$

has been defined and discussed by *Roberts* [1965]. The constant η removes the steady decay (assumed exponential), and s defines the pitch-angle distribution.

In Figure 15, logarithmic data corrected only for η are plotted as a function of $(1 - x^2)$ on a logarithmic scale. The solid line in the figure is the best fit to the data after removal of the scatter attributable to the steady decay. The maximum x correction, at $x \sim 0.8$, was $\sim$22% in this case ($L = 3.8$). The x correction ranged from $\sim$1% at the higher L values to $\sim$20–25% at $L = 3.6$–3.8. At $L = 3.4$, the correction was $\sim$75% at $x = 0.8$.

Acknowledgments. We thank Drs. M. Walt, L. L. Newkirk, L. A. Frank, J. M. Cornwall, T. A. Farley, C. E. McIlwain, and J. G. Roederer for enthusiastic and profitable discussions. We also thank Drs. W. L. Brown, A. Hasegawa, and C. S. Roberts for commenting on the manuscript and for stimulating discussions.

The work of one author (M.S.) was performed under U. S. Air Force Space and Missile Systems Organization (SAMSO) contract no. F04701-69-C-0066.

* * *

The Editor wishes to thank T. J. Birmingham and another referee for their assistance in evaluating this paper.

References

Brewer, H. R., M. Schulz, and A. Eviatar, Origin of drift-periodic echoes in outer-zone electron flux, *J. Geophys. Res., 74,* 159, 1969.

Brown, W. L., Observations of the transient behavior of electrons in the artificial radiation belts, in *Radiation Trapped in the Earth's Magnetic Field,* edited by B. M. McCormac, D. Reidel, Dordrecht, Holland, 1966.

Buck, T. M., G. H. Wheatley, and J. W. Rodgers, Silicon *p-n* junction radiation detectors for the Telstar satellite, *IEEE Trans. Nucl. Sci., NS-11,* 294, 1964.

Conrath, B. J., Radial diffusion of trapped parti-

cles with arbitrary pitch angle, *J. Geophys. Res., 72,* 6069, 1967.
Craven, J. D., Temporal variations of electron intensities at low altitudes in the outer radiation zone as observed with satellite Injun 3, *J. Geophys. Res., 71,* 5643, 1966.
Davis, L., Jr., and D. B. Chang, On the effect of geomagnetic fluctuations on trapped particles, *J. Geophys. Res., 67,* 2169, 1962.
Davis, L. R., R. A. Hoffman, and J. M. Williamson, Observations of protons trapped above 2 R_E (abstract), *Trans. Amer. Geophys. Union, 45,* 84, 1964.
Dungey, J. W., Effects of electromagnetic perturbations on particles trapped in the radiation belts, *Space Sci. Rev., 4,* 199, 1965.
Ershkovich, A. I., V. D. Pletner, G. A. Skuridin, L. S. Chesalin, and V. P. Shalimar, Motion of a charged particle in the magnetosphere under the action of sudden geomagnetic impulse, *J. Atmos. Terr. Phys., 29,* 454, 1967.
Fälthammar, C. -G., Effects of time-dependent electric fields on geomagnetically trapped radiation, *J. Geophys. Res., 70,* 2503, 1965.
Fälthammar, C. -G., On the transport of trapped particles in the outer magnetosphere, *J. Geophys. Res., 71,* 1487, 1966.
Fälthammar, C. -G., and M. Walt, Radial motion resulting from pitch-angle scattering of trapped electrons in the distorted geomagnetic field, *J. Geophys. Res., 74,* 4184, 1969.
Farley, T. A., Radial diffusion of electrons at low L values, *J. Geophys. Res., 74,* 377, 1969.
Frank, L. A., Inward radial diffusion of electrons greater than 1.6 million electron volts in the outer radiation zone, *J. Geophys. Res., 70,* 3533, 1965.
Frank, L. A., J. A. Van Allen, and H. K. Hills, A study of charged particles in the earth's outer radiation zone with Explorer 14, *J. Geophys. Res., 69,* 2171, 1964.
Haerendel, G., Diffusion theory of trapped particles and the observed proton distribution, in *Earth's Particles and Fields,* edited by B. M. McCormac, Reinhold, New York, 1968.
Kavanagh, L. D., Jr., An empirical evaluation of radial diffusion coefficients for electrons of 50–100 kev from $L = 4$ to $L = 7$, *J. Geophys. Res., 73,* 2959, 1968.
Kellogg, P. J., Van Allen radiation of solar origin, *Nature, 183,* 1295, 1959.
Lanzerotti, L. J., C. S. Roberts, and W. L. Brown, Temporal variations in the electron flux at synchronous altitudes, *J. Geophys. Res., 72,* 5893, 1967.
McDiarmid, I. B., and J. R. Burrows, Dependence of the position of the outer radiation zone intensity maxima on electron energy and magnetic activity, *Can. J. Phys., 45,* 2873, 1967.
McIlwain, C. E., Magnetic coordinates, in *Radiation Trapped in the Earth's Magnetic Field,* edited by B. M. McCormac, D. Reidel, Dordrecht, Holland, 1966*a*.
McIlwain, C. E., Processes acting upon outer zone electrons, 1, Adiabatic perturbations, preprint, University of California at San Diego, *UCSD-SP-66-5,* September, 1966*b*.
Nakada, M. P., and G. D. Mead, Diffusion of protons in the outer radiation belt, *J. Geophys. Res., 70,* 4777, 1965.
Nakada, M. P., J. W. Dungey, and W. N. Hess, On the origin of outer belt protons, 1, *J. Geophys. Res., 70,* 3529, 1965.
Newkirk, L. L., and M. Walt, Radial diffusion coefficient for electrons at low L values, *J. Geophys. Res., 73,* 1013, 1968*a*.
Newkirk, L. L., and M. Walt, Radial diffusion coefficient for electrons at $1.76 < L < 5$, *J. Geophys. Res., 73,* 7231, 1968*b*.
Paolini, F. R., G. C. Theodoridis, S. Frankenthal, and L. Katz, Radiation diffusion processes of relativistic outer-belt electrons, *Ann. Geophys., 24,* 1968.
Parker, E. N., Geomagnetic fluctuations and the form of the outer zone of the Van Allen radiation belt, *J. Geophys. Res., 65,* 3117, 1960.
Pfitzer, K. A., and J. R. Winckler, Experimental observation of a large addition to the electron inner radiation belt after a solar flare event, *J. Geophys. Res., 73,* 5792, 1968.
Pfitzer, K. A., T. W. Lezniak, and J. R. Winckler, Experimental verification of drift shell splitting in the distorted magnetosphere, *J. Geophys. Res., 74,* 4687, 1969.
Roberts, C. S., On the relationship between the unidirectional and omnidirectional flux of trapped particles on a magnetic line of force, *J. Geophys. Res., 70,* 2517, 1965.
Roberts, C. S., Pitch angle diffusion of electrons in the magnetosphere, *Rev. Geophys., 7,* 305, 1969.
Roederer, J. G., Shell splitting and radial diffusion of geomagnetically trapped particles, in *Earth's Particles and Fields,* edited by B. M. McCormac, Reinhold, New York, 1968.
Roederer, J. G., and M. Schulz, Effect of shell splitting on radial diffusion in the magnetosphere, *J. Geophys. Res., 74,* 4117, 1969.
Schulz, M., and A. Eviatar, Diffusion of equatorial particles in the outer radiation zone, *J. Geophys. Res., 74,* 2182, 1969.
Theodoridis, G. C., Bimodal diffusion in the earth's magnetosphere, 1, An acceleration mechanism for trapped particles, *Ann. Geophys., 24,* 944, 1968.
Theodoridis, G. C., F .R. Paolini, and S. Frankenthal, Bimodal diffusion in the earth's magnetosphere, 2, On the electron belts, *Ann. Geophys., 24,* 1015, 1968.
Tverskoy, B. A., Dynamics of the radiation belts of the earth, *Geomagn. Aeron., 3,* 351, 1964.
Tverskoy, B. A., Transport and acceleration of charged particles in the earth's magnetosphere, *Geomagn. Aeron., 5,* 517, 1965.
Vernov, S. N., S. N. Kuznetsov, Yu.I. Logachev, G. B. Lopatina, E. N. Sosnovets, and V. G.

Stolpovsky, Radial diffusion of electrons of energy >100 kev in the outer radiation belt, *Space Res., 8,* p. 120, 1968.

Vernov, S. N., I. A. Savenko, M. V. Tel'tsov, and P. I. Shavrin, Observations of a diffusion wave of relativistic electrons in the outer radiation belt, *Geomagn. Aeron., 6,* 503, 1966.

Williams, D. J., J. F. Arens, and L. J. Lanzerotti, Observations of electrons at low and high altitudes, *J. Geophys. Res., 73,* 5673, 1968.

Chapter 13

PARTICLE DETECTION EQUIPMENT AND PARTICLE DATA PROCESSING

PARTICLE DETECTION EQUIPMENT

The particle detection equipment carried by Explorer XV and Explorer XXVI was designed to measure the spatial and angular distributions and energy spectra of electrons and protons in the radiation zones of the earth. The equipment for each satellite consisted of six diffused silicon p-n junction particle detectors, a bias power supply, and the associated electronics all packaged to form a flight unit. The flight unit was mounted in the satellite so that the detectors were oriented perpendicular to the satellite spin axis.

The six detectors permitted measurements to be made of the integral flux of electrons and protons above energies established by a combination of absorbers and pulse height discriminators. Each detector had two pulse height discrimination levels which were provided by a single discriminator and a switched gain amplifier. In each case, the lower pulse height level had a high efficiency for counting both electrons and protons; the higher pulse height level had a very low efficiency for counting electrons but a high efficiency for counting protons. In this way, the proton contamination of the lower pulse height level could be extracted.

As an additional check on the separation of electrons and protons, the electrical bias supplied to the detectors was reduced from 100 volts to 5 volts for approximately 100 seconds every 400 seconds (320 telemetry frames in each 1280). The bias reduction reduced the active thickness of the detector by a factor of approximately four and reduced the efficiency of the detector for electrons by a factor of 50 to 100 without a corresponding decrease in the efficiency for protons.

Since the particle detection equipment for the two satellites was fabricated at the same time, the description included in the final report on Explorer XV, dated June 30, 1964, is largely applicable to the Explorer XXVI equipment. However, the equipment for Explorer XXVI was modified to broaden the scope of the experimental program started with Explorer XV. The modification of the equipment allowed comprehensive studies to be made of protons in an energy range which fell between and

joined the low energy measurements of L. R. Davis and the high energy measurements of C. E. McIlwain.

The approximate energies and the angular aperture sizes of the six electron an and proton detectors on Explorer XXVI are listed in Table I below in order of increasing particle energy. All of the detectors accumulated data on a time-sharing basis in the 18-bit scaler of the cosmic ray logic box provided in the satellite. The accumulation was in each case 5 telemetry frames (approximately 1.6 seconds, and comparable to the rotational period of the satellite). The read-out time for the register was three telemetry frames, so a sequence of accumulation and read-out occupied eight frames. Table I shows, in parenthesis, the time base on which each discrimination level of each detector had access to the register.

Table I

DETECTOR CHARACTERISTICS

Detector	Electron Threshold	Proton Threshold	Aperature (Full Angles)
1	0.3 MeV (8/128)	1.5 MeV (8/128)	10°Cone
2	0.45 MeV (8/128)	5 MeV (8/128)	Ellipitcal 10° x 30°
3	1.0 MeV (8/64)	10 MeV (8/64)	Scatter Dome, 20° Cone
4	1.7 MeV (8/128)	16 MeV (8/128)	Elliptical 15° x 34°
5	2.5 MeV (8/64)	21 MeV (8/64)	Scatter Dome, 50° Cone
6	3.5 MeV (8/128)	27 MeV (8/128)	Scatter Dome, 50° Cone

Detectors 2 and 4 not only added detail to the electron energy distribution but also were designed to provide information on the angular distribution of the electrons as viewed from the spinning satellite. The detectors fed pulses into log ratemeter circuits in the cosmic-ray logic package. The sampling time was half a telemetry frame (approximately 0.16 seconds). At a satellite spin rate of 25 rpm, this time corresponded to a rotation of about 24 degrees. This angle limited the accuracy in determining the angular distribution, but since the sampling time was not, in general, commensurate with the rotational rate of the satellite, the measurements were overlapping and permitted determination of the distribution to a resolution of about 10 degrees. Each of the log rate meters were read in one analog word of the telemetry frame.

The dynamic ranges of all the detectors were approximately as follows. In each detector the maximum counting rate was at least 200 kilocycles. The minimum counting rate was limited by the counting time. In the digital channels this corresponds to 1 count in 1.6 seconds. In the analog channels this corresponds to 1 count in .16 seconds. This dynamic range was approximately 3×10^5 for the digital channels and approximately 1.5×10^4 for the analog channels. The effective detector area of each detector was approximately 3×10^{-2} cm^2. The efficiency of Detector (1) for counting electrons in the fission beta spectrum was approximately 0.4 for the low discrimination level, and 0.2, 0.1, 0.06, 0.03, and 0.01 for the low discrimination level of Detectors (2) through (6).

PARTICLE DATA PROCESSING

Computer programs were devised to reduce the particle data obtained from the Bell Laboratories particle detection equipment on the Explorer satellites. The process used to reduce the data is outlined below. Following the reduction, analysis of the data was planned and performed along lines considered most effective for extracting significant scientific information from the data. The preceding chapters illustrate the approaches used in analyzing the data.

Data Reduction Process

Particle data originating in the Bell Laboratories particle detection equipment on the satellite was telemetered to the ground and recorded on magnetic tape. These "data tapes" were sent by NASA/GSFC to Bell Laboratories, Murray Hill, New Jersey for processing. NASA/GSFC also furnished orbital information on "master orbit tapes" which provided pertinent orbital information and other information such as temperature and voltages on the satellite, and spin rate and orientation of the detectors in the earth's magnetic field. The data tapes and master orbit tapes were put through a data reduction process as follows:

I. A blocked and packed orbit tape was produced from the master orbit tapes furnished by NASA/GSFC. To do this the NASA/GSFC master orbit tapes (eight day nominal length) were reblocked on a 1460 computer and packed into a compact digital form on a 7094 computer.

II. Data tapes (one orbit each) were copied from 556 bits/inch to 800 bits/inch for running in the high density mode on a 7094 computer.

III. With six of the data tapes (II above) and the appropriate orbit tapes (I above) on a 7094 computer, the data was merged with the orbital information and processed through the initial stage of the data reduction program which yielded the following:

A. Reduced data tapes.

B. Stromberg Carlson 4020 microfilm plots of the digital data as a function of Satellite Position L by half orbits.

C. If desired, a complete print-out of the reduced data tapes in microfilm form.

D. A short diagnostic and bookkeeping print-out of the run.

IV. The reduced data tapes were reprocessed in the second stage of the data reduction program to provide three highly compact digital library tapes. Together, three such library tapes contained all of the significant reduced data for a period of one-half month or approximately 45 orbits of the satellite.